ANTI-MICROBIAL IMMUNITY AND INFLAMMATION IN HERMANSKY-PUDLAK SYNDROME TYPE 1



Athena Cavounidis

Lincoln College

A thesis submitted for the degree of

Doctor of Philosophy in Clinical Medicine

Trinity Term 2021

Abstract

Inflammatory bowel disease (IBD) is caused by a breakdown in tolerance of the immune system to the gut microbiota in genetically predisposed individuals. The mechanisms underlying IBD are complex and multifactorial. Monogenic diseases with intestinal inflammation provide important puzzle pieces in identifying key mechanisms of barrier function. Hermansky-Pudlak Syndrome type 1 (HPS-1) features defective vesicle trafficking and can include complications such as Crohn's-like intestinal inflammation and pulmonary fibrosis. In this thesis, I pinpoint aberrant immunometabolism in HPS-1 patient macrophages using transcriptomics and functional assays. Following bacterial infection, HPS-1 macrophages feature an augmented *TNF/OSM* signature, which underlies polygenic IBD. I validate the deregulated immunometabolism in HPS1 knockout HAP1 cells, which have defective cholesterol metabolism and enhanced low density lipoprotein uptake. Using lysosomal immunoprecipitation and proteomics, I identify increased mTOR levels on HPS1 knockout lysosomes, which translates into enhanced mTORC1 signaling. The amplified mTORC1 signaling in HPS1 deficiency is mediated by Rab32. The alterations in metabolism and mTORC1 activation cause impaired anti-bacterial immunity in HPS1 knockout cells and HPS-1 patient macrophages. Mass cytometry of HPS-1 peripheral blood reveals an expansion of inflammatory monocytes, while serum proteomics uncovers a TNF/IL-1α signature in HPS-1. Suppression of mTORC1 signaling through rapamycin treatment rescues the bacterial clearance defect in HPS-1 patient macrophages, providing a novel therapeutic target for HPS-IBD. These findings have implications beyond HPS, since augmented mTOR signaling and derailed metabolism can trigger inflammation in several diseases, such as lysosomal storage disorders.

To my parents and Johannes – my rock solid support team

Acknowledgments

I would like to thank everyone who has made my time as a DPhil student special and who has enriched this journey. Thanks to Holm for believing in me as a Master's student and welcoming me into the laboratory. I am grateful to Holm and Fiona for their supervision throughout these years. I feel privileged to have worked in such a stimulating environment, on several fascinating projects, and to have had the chance to present my project to various audiences during my DPhil. Melania and Sumeet, two talented postdoctoral scientists in the lab, have been a major part of this journey and two friends I have learned so much from. I thank them for shaping the scientist I am today and for teaching me resilience. I consider myself as incredibly fortunate to have been in the lab at the same time as past and present members of the Uhlig lab, including Dominik, Hebe, Zoe, Hannah, Joanneke, Aline, Maria, Tom, Lisa, Arian, Boryana, Mastura and Alex.

I would like to thank the MRC-DTP and the Nuffield Department of Medicine for funding this DPhil. The MRC-DTP provided a wonderfully collegial environment under the leadership of Prof. Ester Hammond and stewardship of Aga Bush, which I have very much appreciated over the last few years. I have also relished being at Lincoln College, where I made some great friendships, met my brilliant mentor, Sabine Jaccaud, and my great college advisor, Alessandra Geremia. Additionally, I feel immense gratitude for the Hermansky-Pudlak Syndrome Network for making me feel at home in this rare disease community. It is magnificently rewarding to feel that my research can have real impact on patients' lives. Specifically, I would like to acknowledge Prof. Louis Cohen, Dr. Bernadette Gochuico, Prof. William Gahl, Donna Appell and Valerie Friedman for being superb collaborators, providing research samples and making me feel part of this unique community from the start. I would

also like to acknowledge Prof. David Sims, Dr. Charlie George and Dr. Devika Agarwal, who provided bioinformatic training on the Biomedical Data Science training program, as well as my outstanding and friendly cohort. This 10-week program was a terrific learning experience and a highlight of my DPhil. I would also like to thank Prof. Alison Simmons and Prof. Nadine Cerf-Bensussan for examining this thesis and providing valuable suggestions for the project.

Massive thanks to my dear friends Ayako, Jonny, Angela and Ioanna for always being there for me and propping me up. I am grateful to Juli, Lea, Ron, Cornelia, Ester, Phil, Jana, Vivian, Elena, Armin, Felix and Sarah for shaping this path and for making my time in Oxford so enjoyable. They were all influential in myriads of ways and I am delighted to have gone through this DPhil with them by my side. I also really appreciate the time and effort taken by Ioanna, Johannes, Jonny and Angela to read my thesis, making many valuable comments and suggestions.

I am forever indebted to my beloved parents, brother and sister-in-law for their unwavering love and support, which have been instrumental throughout this DPhil but also in the steps that led me here. Last but certainly not least, thanks to my partner, Johannes. I am immeasurably lucky to have been able to share this time with him. My family and Johannes are the reason I have made it to this stage, so I would like to thank them once again for always believing in me.

COVID-19 statement

During the Coronavirus disease 2019 (COVID-19) pandemic, my experiments, along with those of colleagues all over the world, were disrupted. My work was paused for several months and restrictions affected my experimental work beyond departmental closures. I am listing a few of these disruptions here, since many of the experiments that I would have been able to perform in normal times would have been part of this thesis. First of all, I was not able to obtain additional patient blood samples to further validate the mechanism I identified in a cell line. Additionally, the Translational Gastroenterology Unit, where the laboratory is based, was closed from March 2020 until October 2020. Other departments, where some experiments were to be performed, still have restrictions that do not allow for easy access, delaying experiments involving microscopy and metabolic measurements. Following the recruitment of HPS-1 patients with IBD in Puerto Rico, I was delayed in obtaining gut samples. These samples will be used for spatial transcriptomics in order to pinpoint tissue changes in HPS-IBD and identify relevant cellular interactions. This is work that I hope to start but will unfortunately not form part of this thesis. However difficult this time may have been, our laboratory meetings continued and the interactions with my colleagues did not cease, which I am very grateful for.

Contributions

I have been fortunate to have great collaborators during my DPhil. I am listing the experiments or analyses that have not been performed by me.

Experiment	**Contributor**	**Contribution**
RNA-sequencing	Oxford Genomics Center, Wellcome Trust Center for Human Genetics	Performed library preparation and sequencing run. I performed the biological experiment and the analysis.
Lysosomal proteomics	Dr. Georgina Berridge, Dr. Roman Fischer and Prof. Benedikt Kessler, Target Discovery Institute	Performed the proteomic sample processing and run as well as the initial analysis. I performed the experiment and the last part of the analysis.
Patient samples	Dr. Louis Cohen, Icahn School of Medicine at Mount Sinai	Collected patient samples.
Patient-derived cell assays	Dr. Sumeet Pandey and Dr. Melania Capitani	Provided experimental help when we received patient samples (once in 2017 and once in 2018).
Seahorse assay	Dr. Sumeet Pandey	Performed the experiment. I analyzed the results.
Mass cytometry	Dr. Louis Cohen, Icahn School of Medicine at Mount Sinai	Performed and analyzed the experiment.
Olink proteomics	Dr. Louis Cohen, Icahn School of Medicine at Mount Sinai	Performed the experiment. I analyzed the results.

Research Output and Publications

The results presented in this thesis will form an original research article on Hermansky-Pudlak Syndrome type 1 but this has not been published yet. The title and author list of the manuscript are provided below.

Title: Hermansky-Pudlak syndrome type 1 causes impaired anti-microbial immunity and inflammation due to dysregulated immunometabolism

Author list: Athena Cavounidis, Sumeet Pandey, Melania Capitani, Dominik Aschenbrenner, Seunghee Kim-Schulze, Esther A. Torres, Georgina Berridge, Dermot P.B. McGovern, Benedikt Kessler, Roman Fischer, Fiona Powrie, Bernadette R. Gochuico, William A. Gahl, Louis Cohen and Holm H. Uhlig

During my DPhil, I have contributed to several other projects, some of which have been published, and to three editorials.

Research articles:

1. Hong, Y., M. Capitani, C. Murphy, S. Pandey, **A. Cavounidis**, H. Takeshita, S. Nanthapisal, T. Yasuda, B. Bader-Meunier, D. McCreary, E. Omoyinmi, A. Rao, C. Booth, K. Gilmour, N. Sebire, N. Shah, N. Klein, A.N. Bullock, D. Eleftheriou, H.H. Uhlig, and P. Brogan. 2020. Janus kinase inhibition for autoinflammation in patients with DNASE2 deficiency. J Allergy Clin Immunol. 145:701-705 e708.
2. Serra, E.G., T. Schwerd, L. Moutsianas, **A. Cavounidis**, L. Fachal, S. Pandey, J. Kammermeier, N.M. Croft, C. Posovszky, A. Rodrigues, R.K. Russell, F. Barakat, M.K.H.

Auth, R. Heuschkel, M. Zilbauer, K. Fyderek, C. Braegger, S.P. Travis, J. Satsangi, M. Parkes, N. Thapar, H. Ferry, J.C. Matte, K.C. Gilmour, A. Wedrychowicz, P. Sullivan, C. Moore, J. Sambrook, W. Ouwehand, D. Roberts, J. Danesh, T.A. Baeumler, T.A. Fulga, M. Karaminejadranjbar, A. Ahmed, R. Wilson, J.C. Barrett, A. Elkadri, A.M. Griffiths, C.i.I.g. investigators, I.B.D.c.s.i. Oxford, I. Study, I.B.D.c.i. Swiss, U.I.G. Consortium, N.I.G. Consortium, S.B. Snapper, N. Shah, A.M. Muise, D.C. Wilson, H.H. Uhlig, and C.A. Anderson. 2020. Somatic mosaicism and common genetic variation contribute to the risk of very-early-onset inflammatory bowel disease. Nat Commun. 11:995.

3. Swan, D.J., D. Aschenbrenner, C.A. Lamb, K. Chakraborty, J. Clark, S. Pandey, K.R. Engelhardt, R. Chen, **A. Cavounidis**, Y. Ding, N. Krasnogor, C.D. Carey, M. Acres, S. Needham, A.J. Cant, P.D. Arkwright, A. Chandra, K. Okkenhaug, H.H. Uhlig, and S. Hambleton. 2019. Immunodeficiency, autoimmune thrombocytopenia and enterocolitis caused by autosomal recessive deficiency of PIK3CD-encoded phosphoinositide 3-kinase delta. Haematologica. 104:e483-e486.

Editorials:

1. **Cavounidis, A.**, J. Alderson, and M. Quastel. 2020. Multisystem inflammatory syndrome in children: getting to the heart of the matter. Nat Rev Immunol. 20:520.
2. **Cavounidis, A.**, and E.H. Mann. 2020. SARS-CoV-2 has a sweet tooth. Nat Rev Immunol. 20:460.
3. **Cavounidis, A.**, and H.H. Uhlig. 2018. Crohn's Disease in Niemann-Pick Disease Type C1: Caught in the Cross-Fire of Host-Microbial Interactions. Dig Dis Sci.

Abbreviations

4EBP	4E-binding protein
AIEC	Adherence Invasive Escherichia coli
AMPK	AMP-activated protein kinase
AP3B1	AP-3 complex subunit beta-1
AP3D1	AP-3 complex subunit delta-1
ATG16L1	Autophagy related protein 16 like 1
ATP	Adenosine triphosphate
BLOC	Biogenesis of lysosome-related organelle complex
BLOC1S	Biogenesis of lysosome-related organelle complex 1 subunit
bp	Base pair
CASTOR1	Cytosolic arginine sensor for mTORC1 subunit 1
CCL	C-C motif chemokine ligand
CCR	C-C chemokine receptor type
CD	Cluster of differentiation
cDNA	Complementary DNA
CHI3L1	Chitinase 3 like protein 1
CLN	Ceroid lipofuscinosis neuronal
COVID-19	Coronavirus disease 2019
CRISPR/Cas9	Clustered regularly interspaced short palindromic repeats/CRISPR-associated protein 9
CRTH2	Chemoattractant receptor homologue expressed on Th2 cells
CTL	Cytotoxic T lymphocyte
CTSC	Cathepsin C
CXCL	C-X-C motif ligand
CXCR	C-X-C motif chemokine receptor 1
CyTOF	Cytometry by time of flight
DAPI	4’,6-diamidino-2-phenylindole
DC	Dendritic cell
DEPTOR	DEP domain-containing mTOR-interacting protein
DMEM	Dulbecco's Modified Eagle Medium
DSS	Dextran sodium sulfate
DTNBP1	Dysbindin
EEA1	Early endosome antigen 1
EPCAM	Epithelial cell adhesion molecule
ER	Endoplasmic reticulum
FDR	False discovery rate
FFA	Free fatty acids
fgsea	Fast gene set enrichment analysis
FKBP12	12-kDa FK506-binding protein
FlowSOM	Flow self-organizing map
FOXP3	Forkhead box P3

FSB	Flow staining buffer
FSC-A	Forward sideward scatter
GAPDH	Glyceraldehyde 3-phosphate dehydrogenase
GATOR	Gap activity toward Rags 1
GDP	Guanosine diphosphate
GFP	Green fluorescent protein
GM-CSF	Granulocyte macrophage colony-stimulating factor
GO-seq	Gene ontology analyzer for RNA-seq
gp130	Glycoprotein 130
GPR65	G protein-coupled receptor 65
GTP	Guanosine triphosphate
GWAS	Genome-wide association studies
HA	Hemagglutinin
HIF1α	Hypoxia-inducible factor 1 α
HPS	Hermansky-Pudlak Syndrome
HPS-1	Hermansky-Pudlak Syndrome type 1
HPS-PF	Hermansky-Pudlak Syndrome pulmonary fibrosis
HRP	Horseradish peroxidase
IBD	Inflammatory bowel disease
IBDu	Inflammatory bowel disease unclassified
IFN-γ	Interferon γ
Ig	Immunoglobulin
IGF2	Insulin-like growth factor 2
IL	Interleukin
IL-1R	Interleukin 1 receptor
IL12RB1	Interleukin 12 receptor beta 1 subunit
IL13Rα2	IL-13 receptor α2
IPEX	Immune dysregulation, polyendocrinopathy, enteropathy, X-linked
IPF	Idiopathic pulmonary fibrosis
IRGM	Immunity-related GTPase family M protein
KEGG	Kyoto Encyclopedia of Genes and Genomes
KIF13A	Kinesin Family Member 13A
LACC1	Laccase domain containing 1
LAL	Lysosomal acid lipase
LAMP	Lysosomal-associated membrane protein
LC3	Microtubule-associated protein light chain 3
LDL	Low density lipoprotein
LIMP2	Lysosomal integral membrane protein 2
LOX-1	Lectin-type oxidized LDL receptor 1
LPS	Lipopolysaccharide
LRO	Lysosome-related organelle
LRRK2	Leucine-rich repeat kinase 2
LTOR	Late Endosomal/Lysosomal Adaptor, MAPK And MTOR Activator

LysoIP	Lysosomal immunoprecipitation
LYST	Lysosomal trafficking regulator
M-CSF	Macrophage colony-stimulating factor
MDP	Muramyl dipeptide
MHC	Major histocompatibility complex
mLST8	mammalian lethal with SEC13 protein 8
MOI	Multiplicity of infection
mRNA	Messenger RNA
mSIN1	stress-activated map kinase interacting protein
mTOR	Mechanistic target of rapamycin
mtROS	Mitochondrial reactive oxygen species
NADPH	Nicotinamide adenine dinucleotide phosphate
NFκB	nuclear factor kappa-light-chain-enhancer of activated B cells
NOD2	Nucleotide-binding oligomerization domain-containing protein 2
NPC	Niemann-Pick Type C
ORP	Oxysterol binding related protein
OSBP	Oxysterol-binding protein
OSM	Oncostatin M
PAGE	Polyacrylamide gel electrophoresis
PBMC	Peripheral blood mononuclear cell
PBS	Phosphate Buffered Saline
PBS-T	PBS with Tween-20
PF	Pulmonary fibrosis
PPARγ	Peroxisome proliferator-activated receptor γ
PRAS40	Proline-rich Akt substrate of 40 kDa
PROTOR	Proline-rich protein
PRR	Pattern recognition receptor
pS6	Phosphorylation of S6
PTGS2	Prostaglandin-endoperoxide synthase 2
qPCR	quantitative polymerase chain reaction
RAPTOR	Regulatory-associated protein of mTOR
RGS1	Regulator of G-protein signaling-1
RHEB	Ras-homolog enriched in brain
RICTOR	Rapamycin-insensitive companion of mammalian target of rapamycin
RIPK2	Receptor-interacting serine/threonine-protein kinase 2
RISK	Risk Stratification and Identification of Immunogenetic and Microbial Markers of Rapid Disease Progression in Children with Crohn's Disease
RNA	Ribonucleic acid
RNA-seq	RNA sequencing
RORγT	RAR-related orphan receptor γ
ROS	Reactive oxygen species
RPMI	Roswell Park Memorial Institute medium
S6K1	Ribosomal protein S6 kinase 1

SAM	S-adenosylmethionine
SAMTOR	S-adenosylmethionine sensor upstream of mTORC1
SDS	Sodium dodecyl sulfate
siRNA	Small interfering RNA
SLC38A9	Solute carrier family 38, member 9
SNE	Distributed Stochastic Neighbor Embedding
SQSTM1	Sequestosome 1
SREBP	Sterol regulatory element-binding protein
STAT3	Signal transducer and activator of transcription 3
TFEB	Transcription factor EB
TGF	Transforming growth factor
Th	T helper
TLR	Toll-like receptor
TMEM192	Transmembrane protein 192
TNF	Tumor Necrosis Factor
Treg	T regulatory
TSC	Tuberous sclerosis
tSNE	t-distributed stochastic neighbor embedding
TYRP	Tyrosinase-related protein
UC	Ulcerative colitis
ULK1	Unc-51 like autophagy activating kinase 1
UMAP	Uniform Manifold Approximation and Projection
V-ATPase	Vacuolar-type ATPase
VAMP	vesicle-associated membrane protein
VAP	vesicle-associated membrane protein-associated protein
VTI1B	vesicle transport through interaction with t-SNAREs homolog 1B
XIAP	X-linked inhibitor of apoptosis protein

Table of contents

ABSTRACT **1**

ACKNOWLEDGMENTS **3**

COVID-19 STATEMENT **5**

CONTRIBUTIONS **6**

RESEARCH OUTPUT AND PUBLICATIONS **7**

ABBREVIATIONS **9**

CHAPTER 1 - INTRODUCTION **17**

1.1 INFLAMMATORY BOWEL DISEASE 17
1.1.1 Genetics *18*
1.1.1.1 Polygenic IBD & autophagy 19
1.1.1.2 Monogenic diseases that present with intestinal inflammation 21
1.1.2 Cell types *23*
1.1.2.1 Epithelial and stromal cells 23
1.1.2.2 Innate immune cells 25
1.1.2.3 Adaptive immune cells 29
1.1.3 Microbiota *32*
1.1.4 Therapies *33*
1.2 LYSOSOMES AND LYSOSOME-ASSOCIATED DISORDERS 35
1.2.1 Lysosomes *35*
1.2.1.1 Organelle structure and functions 35
1.2.1.2 mTOR signaling and metabolism 39
1.2.1.3 Lysosome-related organelles 44
1.2.2 Hermansky-Pudlak Syndrome *45*
1.2.2.1 Genetics of Hermansky-Pudlak Syndrome 46
1.2.2.2 Intestinal inflammation in Hermansky-Pudlak Syndrome 47
1.2.2.3 Lung fibrosis in Hermansky-Pudlak Syndrome 48
1.2.2.4 Vesicle trafficking in Hermansky-Pudlak Syndrome 50
1.2.2.5 The BLOC-3 pathway in host defense and lipid metabolism 54
1.2.2.6 Treatments for Hermansky-Pudlak Syndrome 56
1.2.3 Other lysosome-associated disorders *57*
1.3 AIMS OF THE PROJECT 60

CHAPTER 2 - MATERIALS & METHODS **62**

2.1 PATIENTS AND ETHICS 62
2.2 CELL CULTURE 63
2.2.1 PBMC isolation and monocyte differentiation into macrophages *63*
2.2.2 HAP1 cell culture *63*
2.2.3 CRISPR/Cas9 gene editing and validation *64*
2.2.4 siRNA transfections *65*
2.2.5 Lentiviral production and transduction *65*
2.3 BIOCHEMICAL AND MOLECULAR BIOLOGY METHODS 66
2.3.1 Western blotting *66*

2.3.2 RNA extraction, reverse transcription and quantitative polymerase chain reaction (qPCR) *68*
2.3.3 Gentamicin protection assay *69*
2.3.4 Lysosome Immunoprecipitation *69*
2.3.5 Lysosomal proteomics *70*
2.4 FLOW CYTOMETRY 72
2.4.1 Monocyte MDP/LPS stimulation assay *72*
2.4.2 S6 phosphorylation flow cytometry *73*
2.4.3 TMEM192-HA staining *74*
2.4.4 Autophagy flux *74*
2.4.5 LDL uptake *74*
2.4.6 Phagocytosis of E. coli Bioparticles *75*
2.4.7 Lysosomal function measurement *75*
2.4.8 Neutral lipid flow cytometry *75*
2.4.9 Mitochondrial reactive oxygen species measurement *76*
2.4.10 Flow cytometry of lysosomes *76*
2.4.11 Sorted immune cells *76*
2.5 MICROSCOPY 77
2.6 SEAHORSE ASSAY 77
2.7 PATIENT PHENOTYPING 78
2.7.1 Cytometry by time of flight (CyTOF) processing and analysis *78*
2.7.2 Olink serum proteomics *81*
2.8 TRANSCRIPTOMIC ANALYSIS 82
2.8.1 RNA-seq of HPS-1 macrophages *82*
2.8.1.1 Sample preparation 82
2.8.1.2 RNA extraction, library preparation and RNA-seq 82
2.8.1.3 Pre-processing 83
2.8.1.4 Differential expression analysis 84
2.8.1.5 Pathway analysis 84
2.8.1.6 Weighted Gene Correlation Network Analysis 84
2.8.2 Publicly available datasets *85*
2.8.2.1 STRING analysis of IBD risk loci and Mendelian diseases 85
2.8.2.2 Transcriptomics of small intestinal myeloid subsets 85
2.8.2.3 Single cell RNA-seq of monocyte-derived macrophages 86
2.8.2.4 Single cell RNA-seq of peripheral blood mononuclear cells 86
2.8.2.5 Human protein atlas 86
2.8.2.6 HPS1 knockout epithelial cell transcriptomics 87
2.9 STATISTICAL ANALYSES AND FIGURE PREPARATION 87
2.10 DATA ACCESS 88

CHAPTER 3 - HPS-1-ASSOCIATED GENE SIGNATURES AND PATHWAYS 89

3.1 INTRODUCTION 89
3.2 RESULTS 90
3.2.1 IBD risk loci and monogenic diseases with IBD do not overlap with the BLOC-3 pathway *90*
3.2.2 BLOC-3 is strongly expressed in myeloid cells *91*
3.2.2.1 BLOC-3 pathway expression in the blood 91

3.2.2.2 BLOC-3 myeloid expression is homogeneous in the small intestine 96
3.2.2.3 Macrophage single cell RNA-seq shows uniform expression of BLOC-3 across subsets 98
3.2.3 HPS-1 patient macrophage transcriptomics 100
3.2.3.1 Principal Component Analysis 101
3.2.3.2 Differential expression analysis uncovers an inflammatory gene signature in HPS-1 102
3.2.3.3 Pathway analysis 104
3.2.3.4 Correlation network analysis reveals an LDL metabolism module in HPS-1. 108
3.2.4 HPS1 knockout lung organoid transcriptomics 110
3.3 Discussion 114

CHAPTER 4 - THE ROLE OF LIPID METABOLISM AND MTORC1 SIGNALING IN HPS1 DEFICIENCY 118

4.1 Introduction 118
4.2 Results 119
4.2.1 Generation of an HPS1 deficiency model system in HAP1 cells 119
4.2.2 LDL uptake and cholesterol metabolism are perturbed in HPS1-deficient HAP1 cells 120
4.2.3 Lysosomal proteolytic activity in HPS1 deficiency is intact 122
4.2.4 HPS1-deficient cells have higher levels of lysosomal mTOR 123
4.2.5 mTORC1 signaling is amplified in HPS1 deficiency and is mediated by Rab32 129
4.2.6 Oxidative phosphorylation is reduced in HPS1 deficiency 132
4.2.7 HPS1 deficiency causes hampered bacterial clearance 133
4.3 Discussion 138

CHAPTER 5 - DEFECTIVE ANTI-MICROBIAL ACTIVITY AND INFLAMMATION IN HPS-1 PATIENTS 144

5.1 Introduction 144
5.2 Results 145
5.2.1 Cholesterol metabolism is deregulated in macrophages from HPS-1 patients 145
5.2.2 HPS-1 patient macrophages have impaired bacterial handling 146
5.2.3 HPS-1 and NPC1 bacterial handling defects rescued by rapamycin 147
5.2.4 HPS3 deficiency causes impaired bacterial clearance but does not affect mTORC1 signaling 149
5.2.5 HPS-1 patient peripheral blood mass cytometry identifies inflammatory monocytes 151
5.2.6 HPS-1 patient serum proteomics reveals a TNF/IL-1α signature 156
5.2.7 NOD2 and TLR4 signaling are intact in HPS-1 159
5.3 Discussion 160

CHAPTER 6 - DISCUSSION 165

6.1 Inflammation in HPS-1 166
6.2 The distinct functions of BLOC-2 and BLOC-3 171
6.3 The intersection of lipid metabolism and bacterial clearance in intestinal inflammation 172
6.4 mTORC1 inhibition as a metabolic checkpoint 175
6.5 Is HPS-1 an immunodeficiency? 177
6.6 Future directions 179

6.7 CONCLUSION..... 181
CHAPTER 7 - REFERENCES 183

Chapter 1 - Introduction

1.1 Inflammatory bowel disease

Inflammatory bowel disease (IBD) is a group of chronic disorders resulting in intestinal inflammation. IBD is caused by the complex and intricate interplay between the microbiota and the immune system within the context of genetic predisposition. The three main categories to clinically describe the pathology of IBD are Crohn's disease, Ulcerative Colitis (UC) and IBD unclassified (IBDu). Crohn's disease affects the entire digestive tract and is characterized by patchy inflammation, which is asymmetrical and transmural (Torres et al., 2017). On the other hand, UC is restricted to the colonic mucosa and is continuous, starting at the rectum (Ungaro et al., 2017). IBDu is used to describe IBD symptoms that do not meet the criteria for a Crohn's disease or UC diagnosis. The prevalence of IBD is approximately 0.3 % in westernized countries such as North American and most European nations (Ng et al., 2018). At the same time, newly westernized countries are observing a steady increase in IBD incidence, indicating that adopting patterns associated with industrialization may predispose to IBD (Ng et al., 2018). These epidemiological studies accentuate the rising incidence of IBD on a global scale, reinforcing the need to investigate the factors involved in the development and maintenance of the disease.

IBD is a complex disease, and numerous players contribute to its development. These varied factors include genetics, the immune system, diet and the microbiome. In a healthy individual, these features act in concert to preserve homeostasis in the gastrointestinal tract. However, upon changes in one of these elements, the dynamic interplay can be perturbed, resulting in intestinal inflammation. Genetics is a major participant in determining risk to develop IBD, which has become increasingly understood in recent decades, owing to

Genome-Wide Association Studies (GWAS). Furthermore, Mendelian diseases with IBD-like inflammation emphasize disease-relevant pathways and inform our mechanistic understanding of complex IBD. The integrity of the epithelium, which acts as a barrier between the lumen where the microbes reside and where the immune cells are located, is crucial for gut health. Moreover, immune cells that fall into the innate or adaptive arm have key roles to play at the interface of host-microbial interactions (Uhlig and Powrie, 2018). Other cell types, such as stromal cells, have recently been appreciated for their multifaceted and commandeering roles in pathogenesis (West et al., 2017).

Our understanding of gastrointestinal health and disease stems from human studies to some extent, but largely originates from murine models of disease. Cellular crosstalk and host-microbe interactions will be considered in the following sections, with a special focus on the role of autophagy and microbial clearance in intestinal health and disease. Lastly, current therapies used for the treatment of IBD will be interrogated.

1.1.1 Genetics

GWAS have underlined the role of different risk loci in polygenic IBD. In other words, multiple single nucleotide polymorphisms affect the risk to develop intestinal inflammation. These variants may on their own have low IBD penetrance (Uhlig and Schwerd, 2016). However, Mendelian diseases, which typically feature mutations affecting one gene, may present with IBD-like symptoms, providing valuable clues to disentangle individual pathways playing a role in IBD (Uhlig, 2013). Different cell types may be affected by polymorphisms or mutations in specific genes such as the epithelial barrier, stromal cells, innate immune cells including neutrophils, monocytes and macrophages, as well as effector and T regulatory cells (Uhlig and Powrie, 2018).

1.1.1.1 Polygenic IBD & autophagy

GWAS relies on the comparison of single nucleotide polymorphisms between disease and healthy controls, providing an unbiased view into disease genetics (Verstockt et al., 2018). Prior to GWAS, the first gene to be described as a susceptibility locus for IBD is Nucleotide-binding Oligomerization Domain-containing protein 2 (NOD2) (Hugot et al., 2001; Ogura et al., 2001). NOD2, a Pattern Recognition Receptor (PRR) within the NOD-like receptor family, is the receptor for the bacterial component muramyl-dipeptide (MDP) (Inohara et al., 2003). PRRs are innate immune receptors that recognize structural patterns that are conserved among pathogens, orchestrating the sensing of pathogens (Medzhitov, 2007). NOD2 is localized on endosomes, mediating signal transduction through X-linked inhibitor of apoptosis protein (XIAP) and Receptor-interacting serine threonine-protein kinase 2 (RIPK2) (Nakamura et al., 2014). The downstream signaling involves nuclear factor kappa light chain enhancer of activated B cells (NF-κB) activation, the transcription of pro-inflammatory cytokines (Damgaard et al., 2012; Hasegawa et al., 2008) and bacterial clearance (Cooney et al., 2010; Homer et al., 2010). Following the identification of NOD2, multiple other risk loci have been identified for IBD.

To date, over 230 single nucleotide polymorphisms are associated with the development of IBD (de Lange et al., 2017; Jostins et al., 2012; Liu et al., 2015). These risk loci have been attributed to certain candidate genes in several cases but are sometimes intronic, and their effect on gene expression may rely on context-dependent gene regulation patterns (Fairfax et al., 2014; Uhlig and Schwerd, 2016). Multiple IBD risk loci fall within the autophagy pathway, which is intricately linked to bacterial elimination **(Figure 1.1)** (Graham and Xavier, 2020). Autophagy is a conserved catabolic process involving the degradation of intracellular

material, such as damaged organelles or microbes (Gatica et al., 2018). Autophagy involves the recruitment of microtubule-associated protein light chain 3 (LC3) to phagophores, which is converted to LC3-II, marking autophagosomes (Dikic and Elazar, 2018). The gene *ATG16L1* is an IBD risk locus (Hampe et al., 2007). *ATG16L1* encodes autophagy-related protein 16 like 1 (ATG16L1), which participates in autophagy, and is downstream of NOD2, engaging the autophagy machinery to promote the degradation of the microbes sensed (Cooney et al., 2010; Homer et al., 2010). The Crohn's disease-associated T300A *ATG16L1* variant results in its degradation by caspase 3 at a higher rate, dampening autophagy flux and stymying macrophage bacterial elimination (Murthy et al., 2014). Additionally, the gene *IRGM*, which encodes an autophagy pathway protein, falls into an IBD locus (Parkes et al., 2007). In the presence of MDP, immunity-related guanosine triphosphate (GTP)ase family M protein (IRGM) interacts with NOD2, enhancing autophagosome formation (Chauhan et al., 2015). More recently, the function of an IBD risk variant in *GPR65* was elucidated (Lassen et al., 2016). Specifically, G protein-coupled receptor 65 $(Gpr65)^{-/-}$ mice were more susceptible to colitis in the *Citrobacter rodentium* model of colitis and lysosomal function was impaired in HeLa cells expressing the GPR65 variant I231L. Interestingly, a leucine-rich repeat kinase 2 (LRRK2) variant that increases its kinase activity, is associated with both Crohn's and Parkinson's disease (Hui et al., 2018). LRRK2 phosphorylates several Rab GTPases and pathogenic variants enhance this phosphorylation (Steger et al., 2016). A study has revealed that LRRK2 permits the survival of *Mycobacterium tuberculosis* by regulating phagosome maturation (Hartlova et al., 2018). These studies illustrate the critical role of autophagy and lysosomal function in intestinal health.

Polygenic IBD is a complex disorder, where genetic determinants play a major but not complete role in the development and penetrance of disease. A key module emerging from

IBD GWAS is the autophagy pathway. While unraveling the mechanisms underlying IBD pathogenesis can be challenging, monogenic diseases with IBD-like intestinal inflammation provide vital insights and will be discussed further in the next section.

1.1.1.2 Monogenic diseases that present with intestinal inflammation

Mendelian disorders that can lead to the development of IBD have allowed for increased understanding of the pathways crucial for gut homeostasis (Charbit-Henrion et al., 2021). The genes implicated in Mendelian IBD have been divided into several categories to underscore their function and relevance in different cell types (Uhlig, 2013). These classes include barrier integrity, phagocytic function, adaptive immune defects, immune regulatory defects and hyper-inflammation. A few monogenic diseases relevant for phagocyte function, innate immunity and auto-inflammation will be highlighted.

Phagocyte function is fundamental for host-microbial interactions, intracellular signal transduction and interfacing with other immune cell types. The nicotinamide adenine dinucleotide phosphate (NADPH) oxidase complex is involved in bacterial clearance through a respiratory burst and release of reactive oxygen species (ROS) (Uhlig, 2013). Mutations in all five genes involved in the NADPH oxidase complex, namely *CYBA, CYBB, NCF1, NCF2* and *NCF4*, result in Chronic Granulomatous Disease (Arnold and Heimall, 2017). The NADPH oxidase complex, in addition to generating ROS, induces efficient autophagy of *Salmonella enterica* serovar Typhimurium, starting with LC3 coating of phagosomes (Huang et al., 2009). Phagocyte functions are pivotal to maintain the innate barrier in the gastrointestinal tract **(Figure 1.1)**.

Niemann-Pick Type C1 (NPC1), a neurodegenerative disease and lysosomal storage disorder (Vanier, 2010), also presents with intestinal inflammation (Schwerd et al., 2016).

NPC1 patients have granulomatous colitis and phagocytes from NPC1 patients are less able to eliminate microbes, pointing to a microbial clearance defect (Schwerd et al., 2016).

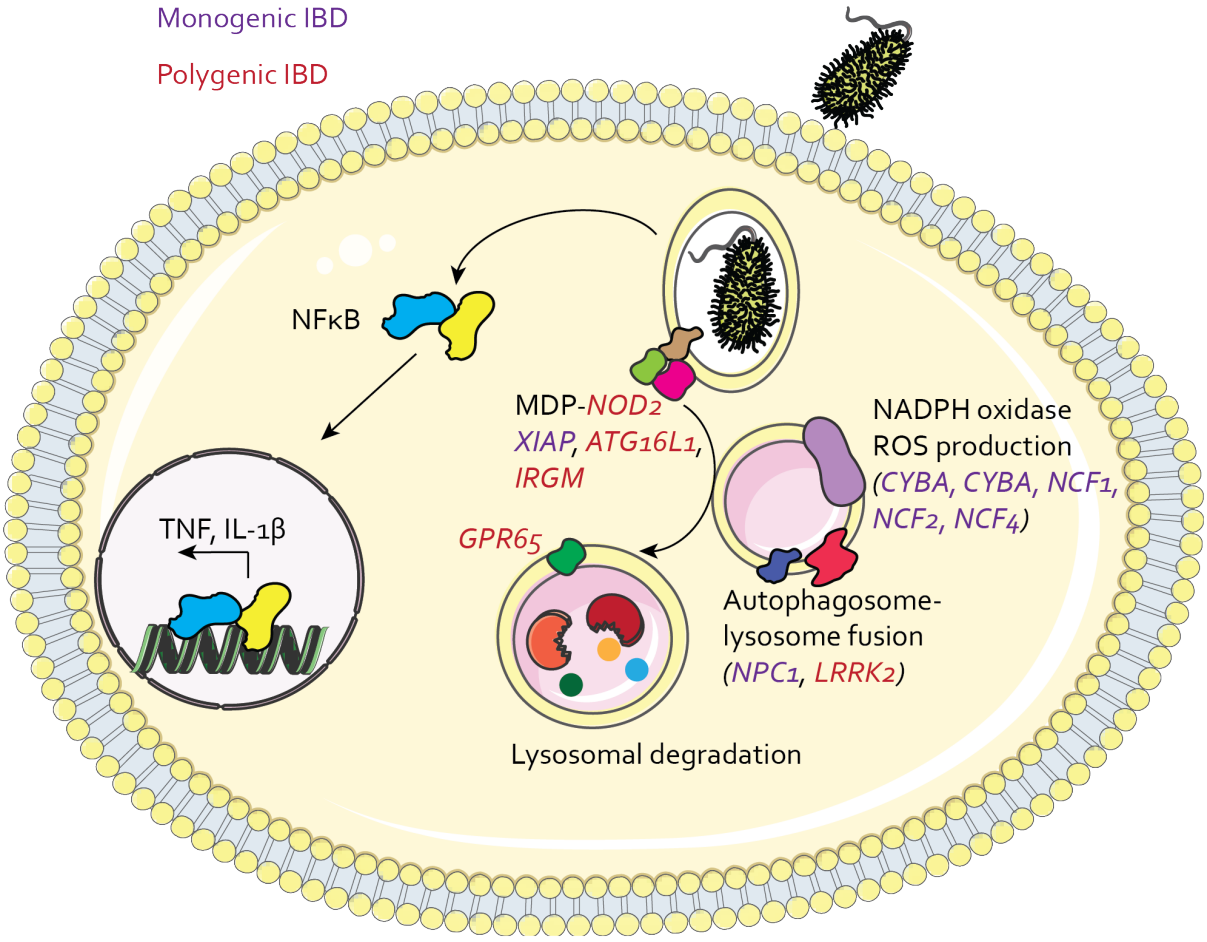


Figure 1.1. Bacterial degradation defects in polygenic and monogenic IBD. Following infection with a bacterium, NOD2/XIAP signaling results in NF-κB activation and the transcription of pro-inflammatory cytokines. At the same time, NOD2/XIAP cooperation with ATG16L1 and IRGM results in autophagy, which involves autophagosome-lysosome fusion. LRRK2 and NPC1 defects abrogate this fusion step, while GPR65 is required for lysosomal acidification. On certain endosomes, the NADPH oxidase complex, whose components might be mutated in chronic granulomatous disease, results in reactive oxygen species production.

Hyper-inflammatory disorders can also present with IBD-like symptoms. For instance, XIAP deficiency results in hemophagocytic lymphohistiocytosis (Rigaud et al., 2006) and

Crohn's disease in some cases (Aguilar et al., 2014). XIAP is involved in signal transduction downstream of NOD2, where it ubiquitylates RIPK2 and mediates NF-κB activation (Damgaard et al., 2012). On the other hand, mevalonate kinase deficiency presents with auto-inflammation, periodic fever and intestinal inflammation (Favier and Schulert, 2016). Mevalonate kinase deficiency results in excessive IL-1 production (Galeotti et al., 2012) and the gastrointestinal symptoms can be treated with the IL-1R antagonist recombinant protein anakinra (Levy et al., 2013). These inflammatory disorders underscore the importance of metabolism, cytokine production and bacterial sensing signal transduction in the gut.

Mendelian diseases that feature IBD-like inflammation emphasize the different layers of complexity in maintaining homeostasis. These pathways are broadly categorized into epithelial barrier, phagocyte, adaptive, immunoregulatory and hyper-inflammatory diseases, and help focus the lens on specific pathways that become awry in disease.

1.1.2 Cell types

Multiple cell types orchestrate the dynamic interactions taking place in the gastrointestinal tract. These cell types include but are not limited to epithelial cells, stromal cells and immune cells. Immune cells comprise phagocytes, such as monocytes, macrophages and neutrophils, and adaptive immune cells, including T cells and B cells. The understanding of these interactions and the variegated roles and phenotypes of these cells in health and disease has recently been strongly reinforced by single cell technologies.

1.1.2.1 Epithelial and stromal cells

The intestinal epithelium maintains a physical barrier between the gut lumen, where the microbiome is present, and the lamina propria, which is inhabited by immune cells. The

intestinal epithelial cells that line this barrier originate from stem cell crypts (Snippert et al., 2010) and acquire diverse functions to maintain barrier integrity and relay signals to the immune system. The intestinal stem cells found at the base of the crypts are denoted by the expression of *Lgr5* (Barker et al., 2007). On the other hand, stromal cells, mostly comprised of fibroblasts and endothelial cells, are recently being recognized as key players in driving intestinal inflammation.

One of the first layers of defense against invading pathogens is the epithelial barrier, which is protected by specialized types of epithelial cells. Specifically, goblet cells express *MUC19* and *MUC3A*, which help produce mucus, and have been implicated in IBD pathogenesis through GWAS (McCole, 2014). Within the mucus layer, immunoglobulin A (IgA) is secreted by plasma cells, resulting in the reduced mobility of bacteria (Johansson and Hansson, 2016). Mucins create a layer to maintain a certain distance to microbes, and goblet cells are also able to produce anti-microbial peptides. Paneth cells in the small intestine are tasked with anti-microbial peptide production in the defense against microbes (Bevins and Salzman, 2011). Through single cell sequencing of epithelial cells in UC and controls, novel epithelial subtypes are being identified in the gut (Parikh et al., 2019). For instance, a novel goblet cell type that expresses *WFDC2*, a protease inhibitor that is depleted in UC, is crucial in maintaining the mucus layer. Epithelial cells in the intestine therefore have a wide functional spectrum, preserving barrier integrity and commencing immune responses.

On the other hand, stromal cells have recently emerged as inflammatory drivers in the intestine. A leukocyte-derived cytokine, Oncostatin M (OSM), has gained traction since its receptor, primarily expressed on stromal cells, has been identified in IBD GWAS (Liu et al., 2015). High *OSM* and *OSMR* expression correlates with TNF non-response in human IBD (West et al., 2017). These results have been further supported by single cell sequencing, which has

identified a subset of inflammation-associated fibroblasts, enriched in TNF non-responders, that may interact with the myeloid compartment (Smillie et al., 2019). These results are in keeping with previous findings suggesting that fibroblasts may be a key target in anti-TNF therapies since the TNF produced is directed towards mesenchymal cells in various chronic inflammatory disorders (including arthritis and Crohn's-like inflammation) (Armaka et al., 2008). A different study identified a cluster of fibroblasts, which produced pro-inflammatory cytokines and the alarmin IL-33, that was greatly expanded in UC (Kinchen et al., 2018). Intestinal epithelial cells and stromal cells provide structural integrity through upholding barrier function in the gut. Both cell types are now emerging as important interactors with immune cells and provide insights into additional pathological mechanisms of disease.

1.1.2.2 Innate immune cells

Following the single columnar layer of epithelial cells, innate immune cells reside in the lamina propria, forming the second barrier in the gut. Innate immune cells include neutrophils, monocytes, macrophages and dendritic cells (DCs). These innate cells have important roles in both the first response to barrier breach, the maintenance and resolution of inflammation.

Neutrophils are one of the first cell types recruited to the site of injury. Neutrophil recruitment occurs through C-X-C Motif Chemokine Ligand 8 (CXCL8), which is secreted by a variety of cell types including macrophages, epithelial cells and fibroblasts (Russo et al., 2014). CXCL8 binds to C-X-C Motif Chemokine Receptor 1 (CXCR1) and CXCR2 expressed on neutrophils, mediating their chemotaxis to the gut. Using colonic biopsies, $CXCR1^{+}CXCR2^{+}$ neutrophils have been identified as major producers of the pro-inflammatory cytokine IL-23, which perpetuates the IL-23/Th17 axis described in IBD and other chronic inflammatory

diseases (Kvedaraite et al., 2016). Additionally, in the T cell transfer colitis model, where T cells are transferred into the T and B cell-depleted $Rag1^{-/-}$ mouse, neutrophils accumulate in the inflamed intestine (Griseri et al., 2015). Neutrophils are thought to elicit inflammatory responses through the secretion of pro-inflammatory cytokines and the generation of reactive oxygen species.

Macrophages have been characterized as belonging to two main classes based on their phenotype: M1 and M2. M1 macrophages correspond to a pro-inflammatory cytokine-producing subset, activated by lipopolysaccharide (LPS) and Interferon γ (IFN-γ) while producing TNF, IL-1β, IL-12, IL-23 and IL-6 (Martinez and Gordon, 2014). M2 are tolerogenic and anti-inflammatory, and can be subdivided further based on their activation molecules and the generation of different cytokines, but all M2 macrophages are potent IL-10 producers (Martinez and Gordon, 2014). M2a macrophages are activated by IL-4 and IL-13, while M2b by Toll-like receptor (TLR) or IL-1R ligands, and M2c by IL-10 itself. However, macrophages have been found to be plastic, changing and acquiring new features based on environmental cues, challenging the concept of distinct classes.

Tissue-resident macrophages in the gastrointestinal tract are replenished from cycling monocytes, rather than originating from the yolk-sac during embryogenesis, as in most other tissues (Bain et al., 2014). Under homeostatic conditions in the gut, macrophages favor the expansion of Treg cells through the production of IL-10. In IL-10R-deficient patients, M1 macrophages are expanded and secrete large amounts of pro-inflammatory cytokines (Shouval et al., 2014). In the anti-IL10R/*helicobacter hepaticus*-driven model of intestinal inflammation, major histocompatibility complex (MHC)-II^{+} monocytes and macrophages were shown to be significant producers of IL-23 in the gut during inflammation (Arnold et al., 2016). Recent single cell technologies have highlighted the existence of an inflammatory

monocyte/macrophage and inflammatory fibroblast module in IBD (Martin et al., 2019; Smillie et al., 2019). Specifically, these subsets correlate with anti-TNF non-response in IBD and are thought to revolve around pathogenic OSM signaling. In subsets of Crohn's disease patients, ileal macrophages highly express *TNF*, *IL1B*, *IL6* and *IL23* (Martin et al., 2019), which can drive inflammation **(Figure 1.2)**. Other studies have found that IL-23 production in monocytes is regulated by an autocrine and paracrine signaling network of IL-10 and IL-1α/β, which can predict TNF responsiveness in patients (Aschenbrenner et al., 2020). At the same time, the myeloid compartment, and macrophages in particular, are tasked with the clearance of microbes, which can involve autophagy and the ligation of PRRs (Lassen and Xavier, 2018). In conclusion, monocytes and macrophages need to balance cytokine generation and bactericidal function to preserve homeostasis in the gastrointestinal tract.

Dendritic cells (DCs) are professional antigen presenting cells at the interface of the innate and adaptive immune systems, acting on environmental cues and eliciting adaptive immune responses. One study found that *B. fragilis* outer membrane vesicles contribute to Treg responses, which is dependent on the autophagy pathway in dendritic cells (Chu et al., 2016). Specifically, CD11c-restricted $Nod2^{-/-}$ or $Atg16l1^{-/-}$ mice were unable to prime Tregs to produce IL-10 following outer membrane vesicle treatment, driving colitis. Moreover, the requirement for NOD2 and ATG16L1 in human DC autophagy has been probed (Cooney et al., 2010; Homer et al., 2010). Immature DCs were not able to induce autophagosome formation when DCs lacked NOD2 and ATG16L1. Cytokine responses in DCs are also crucial for intestinal homeostasis. For instance, in IL10RA-deficient patients, DCs generate high levels of IL-1β, which then stimulate an IFN-γ response by CD4 T cells, which is thought to drive inflammation (Veenbergen et al., 2019). In summary, DC function depends on both autophagy and cytokine responses to control antigen presentation and aberrant cytokine responses in T cells.

The phagocytes explored in this section are fundamental for intestinal homeostasis, where dysregulation results in inflammation. Innate immune cells receive information from the intestinal milieu, which is then translated into cytokine responses, chemotaxis of different cell types and conveying of information to the adaptive immune system.

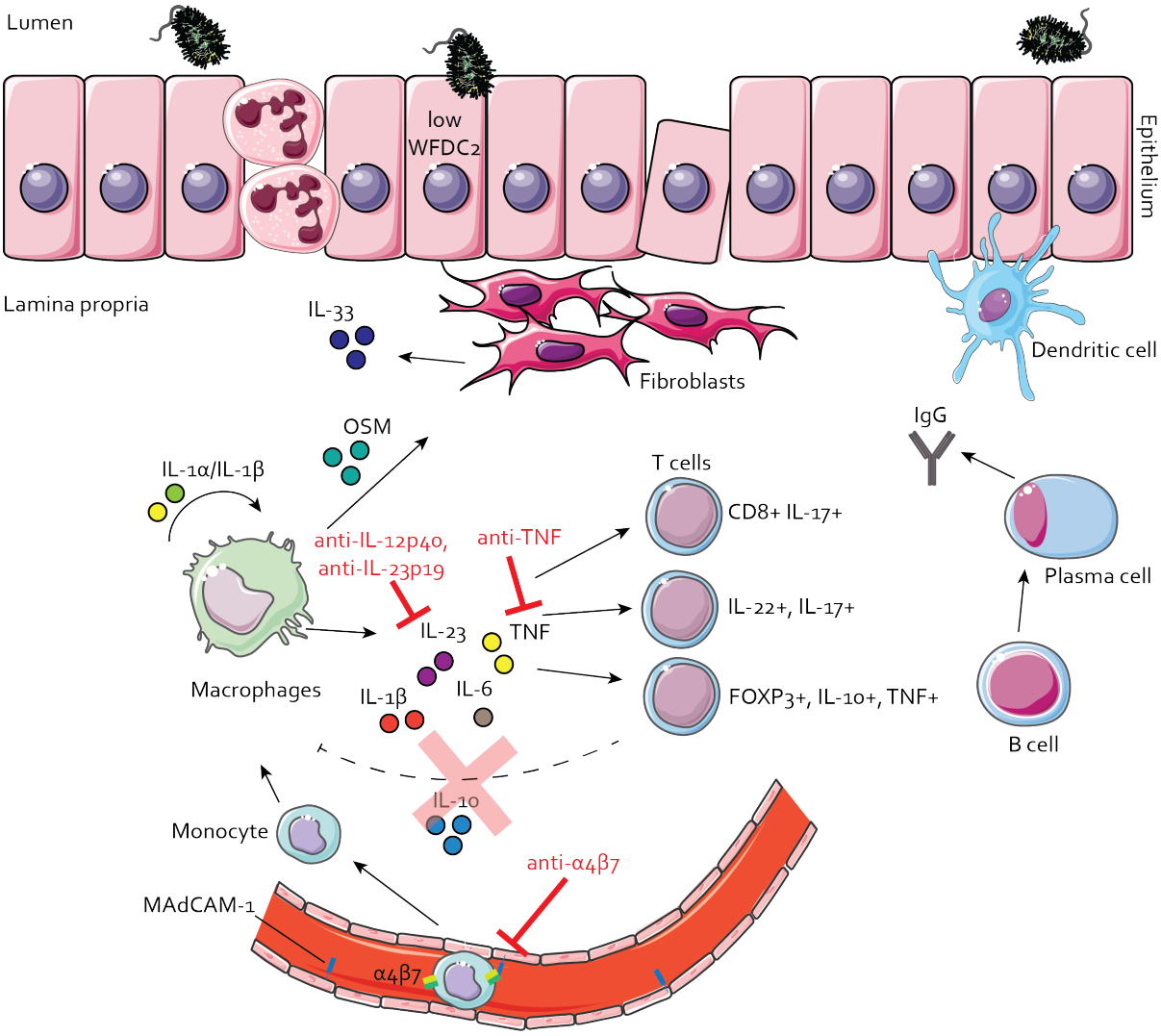


Figure 1.2. Mechanisms underlying inflammatory bowel disease and approved monoclonal antibody therapies. Following the breakdown of the intestinal barrier, multiple factors contribute to inflammation. Monocytes recruited from the blood through the $\alpha_4\beta_7$ integrin differentiate into macrophages or dendritic cells. Macrophages are maintained through a pathogenic IL-1α/IL-1β autocrine loop and secrete pro-inflammatory cytokines such as TNF, IL-1β, IL-23, OSM and IL-6, acting on diverse cell types, but lose responsiveness to anti-

inflammatory IL-10 during inflammation. IgG^+ plasma cells are also implicated in disease, while fibroblasts interact with macrophages and potentially neutrophils, exacerbating inflammation. Pro-inflammatory cytokine-producing T cells expand in IBD, while T regulatory cells are not as able to exert their anti-inflammatory effects. Leukocytes recruited from the blood through $\alpha_4\beta_7$ can be targeted through depletion of this integrin. Anti-TNF therapies are in widespread clinical use. The pro-inflammatory cytokine IL-23 is targeted through the anti-IL-12p40 subunit or anti-IL-23p19 monoclonal antibodies.

1.1.2.3 Adaptive immune cells

The adaptive immune system in the gut includes T cells, humoral immunity and innate-like lymphocytes. Following barrier insult or translocation of invading microbes into the lamina propria, innate immune cells take up antigens and produce pro-inflammatory cytokines that steer the adaptive immune response **(Figure 1.2)**. In this section, I will discuss the adaptive immune system in the context of IBD pathogenesis.

The study of the IL-23/T helper 17 (Th17) axis has taken center stage in IBD research, as well as other chronic inflammatory diseases, in the last two decades. IL-23 plays a major role in IBD pathology, as evidenced through GWAS and functional assays. IL-23, composed of the p19 and p40 subunits, binds the IL-23R, which cooperates with interleukin 12 receptor beta 1 subunit (IL12RB1) to signal through signal transducer and activator of transcription 3 (STAT3) (Uhlig and Powrie, 2018). IL-23 is secreted by myeloid cells and neutrophils, and acts on subsets expressing the core transcription factor RAR-related orphan receptor γ (RORγT), namely Th17, γδ T cells and type 3 innate lymphoid cells (Stockinger and Omenetti, 2017). While Th17 cells confer a host-protective role during homeostasis through the secretion of IL-17 and IL-22, IL-23 drives the pathogenicity of Th17 cells as suggested by studies in experimental allergic encephalomyelitis (Ghoreschi et al., 2010). These pathogenic Th17 cells that also accumulate in IBD produce granulocyte macrophage colony-stimulating factor (GM-

CSF) and IFN-γ, activating myeloid cells (Griseri et al., 2012; Uhlig and Powrie, 2018). Furthermore, using Il23r$^{-/-}$ mice, it has been shown that IL-23 signaling can block the expansion of forkhead box P3 (FOXP3)$^{+}$ Treg cells and suppress IL-10 production (Ahern et al., 2010). Murine studies have demonstrated that innate lymphoid cells are inflammation drivers and major responders to IL-23, through the generation of IL-17 and IFN-γ (Buonocore et al., 2010). In humans, the high levels of IL-23 produced by lamina propria mononuclear cells can be greatly reduced by treatment with monoclonal antibodies targeting IL-12p40 (Ahern et al., 2008; Feagan et al., 2016; Fuss et al., 2006). These studies showcase the emerging role of a pathogenic IL-23/Th17 node in IBD pathogenesis.

Treg cells have been in the spotlight in IBD due to their crucial immunosuppressive functions in the intestine. Tregs are demarcated by the surface markers CD4 and CD25 and the transcription factor FOXP3, and secrete large amounts of IL-10 (Newton et al., 2016). The importance of these cells in the immune response are evidenced by immune dysregulation, polyendocrinopathy, enteropathy, X-linked (IPEX) syndrome, which is caused by defects in *FOXP3* (Bennett et al., 2001). In mice, it has been shown that transfer of CD4^{+}CD25^{+} Tregs resolves inflammation (Mottet et al., 2003). Nevertheless, one study found that Tregs from inflamed regions of ulcerative colitis patients expressing both IL-10 and TNF are expanded (Smillie et al., 2019). To conclude, Tregs are essential for gut homeostasis and may become perturbed in disease, although more investigations are required to address this question.

B cells have been implicated in IBD, especially plasma cells that produce antibodies such as IgA and IgG. IgA is found at mucosal sites, where it coats microbes that are associated with high susceptibility to colitis in mice (Palm et al., 2014). At the same time, disease-associated antibodies have been identified towards various self or bacterial antigens, which may contribute to disease severity. For instance, in ileal CD, increased levels of anti-GM-CSF

antibodies were identified in both adult and pediatric patients (Gathungu et al., 2013). Bacterial antigens that have been found to stimulate antibody production against them in CD are flagellin (Lodes et al., 2004) and the *E. coli* outer membrane porin C (Mow et al., 2004). A recent study showcased that a subset of Crohn's disease patients have an inflammatory module that includes IgG-producing plasma cells (Martin et al., 2019). Whether the production of antibodies by B cells is a major contributor to disease pathogenesis remains elusive.

Studying immune cells individually in the context of IBD can be useful to tease apart specific pathways but is limiting in a complex disease. A recent analysis illustrated the complex interplay between various immune cell types in active Crohn's disease (Martin et al., 2019). Specifically, ileal biopsy single cell ribonucleic acid (RNA)-sequencing identified a module that correlated with TNF-non-response. This inflammatory module comprises IgG plasma cells, activated fibroblasts, T cells and inflammatory macrophages. A different study has highlighted that $CD8^{+}IL\text{-}17^{+}$ T cells are expanded in UC, indicating a role for CD8 T cells in disease (Smillie et al., 2019). Additionally, alterations in $CD8^{+}$ T cells such as their activation ($CD69^{+}$, $Eomesodermin^{+}$) (Boland et al., 2020) or imbalance between effector and immunoregulatory states may underlie ulcerative colitis (Corridoni et al., 2020). These investigations highlight the multi-factorial nature of intestinal inflammation, highlighting the need to understand emerging networks that involve a wide array of cell types.

Adaptive immune cells play a crucial role in the development, maintenance and resolution of intestinal inflammation. While extensive studies have probed the role of specific cytokines and cell types, recent technological advances such as single cell analysis are shedding light on cellular networks in IBD. These cell-cell interactions and disease-associated

signatures will allow for careful examination of the causes of response or non-response to certain therapies.

1.1.3 Microbiota

Environmental factors are key contributors to the pathogenesis of IBD, and while there are ample factors to consider, the microbiome in the gastrointestinal tract plays an important role. Microbiome changes characterize IBD (Ni et al., 2017) and these alterations are influenced by diet, lifestyle, exposure to antibiotics (especially early in life) (Lewis et al., 2015) and the method of delivery (Bager et al., 2012), to name a few. Microbial dysbiosis is a common occurrence in disease pathology, which broadly corresponds to a loss in microbial diversity, but whether this is a cause or consequence remains elusive.

Certain microbes have been associated with inflammation or health, even though what comprises a healthy microbiome remains challenging to define. For instance, IBD patients have a higher abundance of *Enterobacteriaceae*, which includes Adherent Invasive *E. coli* (Baumgart et al., 2007; Halfvarson et al., 2017). Specifically, the abundance of *E. coli* appears to correlate with a reduction in *Clostridiales* in studies (Baumgart et al., 2007; Gevers et al., 2014), showcasing the complex dynamics of the microbiome. At the same time, *Firmicutes* are decreased in patients with IBD and this reduction correlates with ileal recurrence of the disease following surgical intervention (Sokol et al., 2008). Lastly, the relationship between bacterial metabolites and immune cells has been investigated in mouse models. Specifically, short chain fatty acids secreted by *Clostridium* species result in the expansion of Tregs and contribute to resistance to colitis (Atarashi et al., 2011; Smith et al., 2013). These examples are far from exhaustive but illustrate the convoluted forces at work in microbial composition, which contribute to host-pathogen interactions in the gut.

Apart from bacterial communities in the gastrointestinal tract, fungi and viruses have been appreciated as contributors to homeostasis or inflammation. The viral composition or virome has been investigated in the context of IBD, revealing an association with amplified *Caudovirales* bacteriophages in the gut (Norman et al., 2015). However, whether the virome drives microbiota changes or vice versa has not been elucidated. Moreover, studies of fungal composition in IBD exposed an augmented abundance of *Candida albicans* and a diminished abundance of *Saccharomyces cerevisiae* compared to healthy controls (Sokol et al., 2016). These findings depict the large diversity of influences on microbial ecology in the intestine.

In summary, several studies over recent years have emphasized the importance of microbial composition in the gut. While multiple reports draw on associations of particular phyla or species with IBD, decreased bacterial diversity seems to correlate with dysbiosis and inflammation.

1.1.4 Therapies

Therapies in IBD have evolved with increased research in the field. The first line and more conventional treatments will be discussed followed by monoclonal antibody therapies, which include cytokine or leukocyte trafficking treatments. Lastly, perturbations to the microbiome will be considered.

Anti-inflammatory and immunosuppressive drugs have been widely used for the treatment of Crohn's disease and UC, representing classical, first-line treatments. The anti-inflammatory drug mesalazine used in UC impairs cytokine production through NF-κB inhibition (Bantel et al., 2000) and prostaglandin synthesis (Neurath, 2017). On the other hand, azathioprine and methotrexate mediate broader immunosuppression (D'Haens et al., 1997; Feagan et al., 2000). In patients with severe disease that do not respond to treatments,

surgical intervention is an option (Neurath, 2017). In diseases that involve a known gene defect affecting blood cells, especially in monogenic diseases such as IL-10 signaling defects or XIAP deficiency, hematopoietic stem cell transplantation provides a viable strategy to ameliorate disease pathology (Chellapandian et al., 2016; Engelhardt et al., 2013; Kotlarz et al., 2012; Tsuma et al., 2015).

In light of the fundamental role of cytokines in IBD pathogenesis and the recruitment of leukocytes to the gut, cytokine- and leukocyte-targeting therapies have been used in IBD **(Figure 1.2)**. Anti-TNF therapies are used for both Crohn's disease and UC treatment with great efficacy, but not all patients respond, while others develop resistance to the drugs (Neurath, 2017; Rutgeerts et al., 2005; Sands et al., 2004). A newer monoclonal antibody therapy for IBD targets the shared IL-23/IL-12 p40 subunit and has proven effective in a subset of patients (Feagan et al., 2016; Sands et al., 2019b). Additionally, the IL-23 p90 subunit, which is unique to IL-23, has been targeted therapeutically, leading to improvement in clinical symptoms and inducing remission in some cases (Feagan et al., 2017; Sands et al., 2017). A different class of antibodies targets the recruitment of leukocytes to inflamed sites in the intestine through blocking the $\alpha_4\beta_7$ integrin (Sands et al., 2019a). Since these drugs are relatively new therapies, a biomarker-based classification of patients for different treatments may help improve response rates in the future and decrease healthcare costs.

Given that microbial composition and diversity in the gut are important for homeostasis, microbial perturbations may deliver novel therapies. Fecal microbiota transfer has been considered as a treatment option, but results are not conclusive as to its efficacy in maintaining remission (Moayyedi et al., 2015; Rossen et al., 2015). IBD therapies are administered primarily based on clinical symptoms. However, with increased mechanistic

understanding and molecular classification of pathologies, personalized medicine is on the horizon for IBD treatment.

1.2 Lysosomes and lysosome-associated disorders

1.2.1 Lysosomes

The lysosome is a central organelle for the degradation of intracellular and extracellular components. The lysosome is characterized by a low pH, which activates lysosomal hydrolases that mediate lysosomal degradative capacity. Additionally, the lysosome is emerging as a key organelle in metabolic and transcriptional regulation. In this section, lysosomal biology and its regulation by mechanistic target of rapamycin (mTOR) will be explored.

1.2.1.1 Organelle structure and functions

The lysosome provides a recycling hub within the cell: a place to degrade macromolecules, organelles and pathogens. The lysosome is composed of a limiting bilayer, transmembrane proteins such as lysosomal-associated membrane protein (LAMP) 1 and LAMP2 that maintain lysosomal integrity, a lumen-facing glycocalyx and luminal proteins such as hydrolases (Lubke et al., 2009; Perera and Zoncu, 2016). These act in concert to degrade incoming material following lysosomal fusion with late endosomes or autophagosomes. In the last decade, the lysosome has been recognized as a crucial signaling and metabolic center in the cell, mediating these actions through inter-organellar membrane contacts in certain instances (Lawrence and Zoncu, 2019). Lysosomal degradation results in the availability of material such as amino acids and lipids that can then be used for anabolic reactions by the cell.

The lysosome fuses with mature autophagosomes or late endosomes, both of which encompass material destined for degradation. The acidic pH in lysosomes is controlled by the multi-subunit vacuolar type (V)-ATPase rotary pump, which translocates protons into the lumen of the lysosome following adenosine triphosphate (ATP) hydrolysis (Kane, 1995; Zhao et al., 2015). In this acidic environment, the lysosomal hydrolases are active and degrade molecules into their constituent parts. The hydrolases are sorted to the lysosome as they acquire a mannose-6-phosphate tag in the Golgi, recognized by the mannose-6-phosphate receptor (Saftig and Klumperman, 2009). However, mannose-6-phosphate receptor-independent pathways have been reported as well, such as the sorting of β-glucocerebrosidase by lysosomal integral membrane protein 2 (LIMP2) (Reczek et al., 2007). Sorting to the lysosome is critical for lysosomal function in degrading macromolecules, organelles and pathogens.

In response to stress, cells react with the catabolic process of autophagy to produce nutrients and degrade harmful material. Autophagy initiation occurs at the phagophore assembly site, where autophagy (ATG) proteins are recruited to an isolation membrane (Dikic and Elazar, 2018) **(Figure 1.3)**. Unc-51 like autophagy activating kinase 1 (ULK1) is recruited and the isolation membrane buds off from ER protrusions under the control of the phosphatidylinositol 3-kinase complex 3 (PI3KC3) (Dikic and Elazar, 2018; Karanasios et al., 2013). The phagophore elongates to enclose a part of the cytoplasm that contains the material to be degraded, forming a double membrane structure. The elongation process requires the actions of ATG7, ATG5, ATG12 and ATG16L1, resulting in the lipidation of LC3 (LC3-I to LC3-II conversion) and its insertion into the double membrane (Dooley et al., 2014). Autophagosome maturation is the final process prior to autophagosome-lysosome fusion and involves the recruitment of proteins needed for fusion. Syntaxin (STX) 17 and synaptosomal-

associated protein (SNAP) 29 are enlisted to the autophagosome and interact with vesicle-associated membrane protein (VAMP) 8 on lysosomes, mediating fusion (Itakura et al., 2012). The autophagy machinery orchestrates phagophore initiation, elongation and autophagosome maturation to propel autophagosome-lysosome fusion.

An alternate route to the lysosome involves late endosomes, carrying cargo destined for degradation, fusing with lysosomes. The fusion of late endosomes with lysosomes is controlled by Rab7, which is required for exit from the late endosomal compartment (Vanlandingham and Ceresa, 2009) **(Figure 1.3)**. Fusion of late endosomes and lysosomes depends on STX7, vesicle transport through interaction with t-SNAREs homolog 1B (VTI1B) and STX8 on the endosome and VAMP7 or VAMP8 on the lysosome or another late endosome (Pryor et al., 2004). Autophagy and late endosome-lysosome fusion represent two primary methods of directing cargo to the degradative compartment.

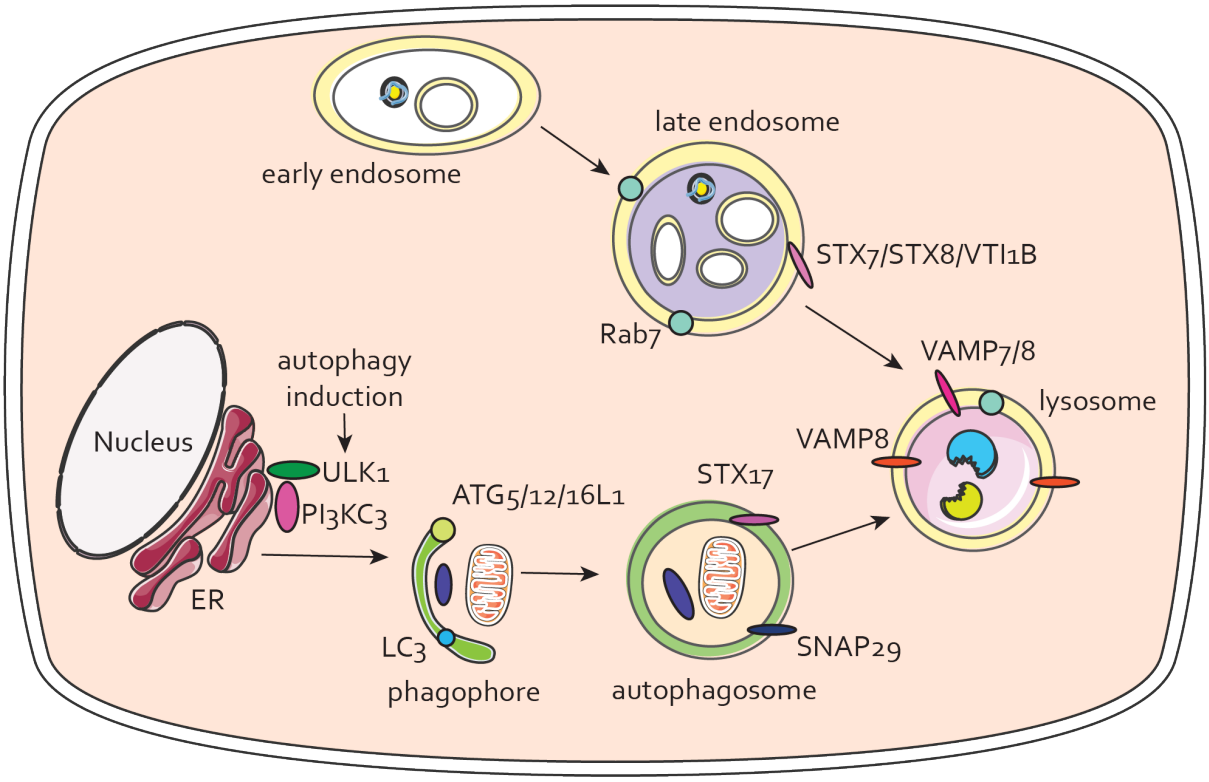


Figure 1.3. Autophagy and endosome-lysosome fusion. The early endosome fuses with the late endosome, which is decorated by Rab7. The late endosome can then fuse with the lysosome through VAMP7/8 and STX7/STX8/VTI1B. At the same time, autophagy can be initiated in the cell, which involves ULK1 and the PI3KC3 complex. The phagophore is joined by the ATG5/12/16L1 complex and LC3 and engulfs material for degradation. Once the material is enclosed, the autophagosome is formed, which fuses with the lysosome through protein interactions involving STX17/SNAP29 on the autophagosome and VAMP8 on the lysosome.

Transmembrane transporters of the lysosome are dedicated to exporting material into the cytoplasm for eventual reuse. The reuse depends on appropriate localization, which is in part dictated by the inter-organelle contacts the lysosome establishes, which are also crucial for lipid homeostasis (Lawrence and Zoncu, 2019; Thelen and Zoncu, 2017). For instance, NPC2 shuttles cholesterol within the lysosomal lumen, depositing cholesterol to NPC1, which carries it out of the lysosomal compartment (McCauliff et al., 2019). Through lysosome-endoplasmic reticulum (ER) contacts, mediated by oxysterol binding related protein (ORP) 5, among others, cholesterol makes its way to the ER, where it is esterified by acetyl-CoA acetyltransferase (Du et al., 2011; Hoglinger et al., 2019). Cholesterol can also be transported from the ER to the lysosome, mediating mTOR complex 1 (mTORC1) activation through oxysterol-binding protein (OSBP) on the lysosome and vesicle-associated membrane protein-associated protein (VAP) A/B on the ER (Lim et al., 2019). Furthermore, the efflux of amino acids, which occurs through the concerted actions of specialized transporters, is controlled by mTORC1 and the V-ATPase pump (Abu-Remaileh et al., 2017). The trafficking of lipids and amino acids to and from the lysosome are integral mechanisms to maintain lipid homeostasis.

The lysosome is also tasked with mediating plasma membrane repair and performing lysosomal exocytosis to secrete its contents, highlighting the importance of positioning within the cell. Neuraminidase 1 deficiency results in the over-sialylation of LAMP1 and amplified lysosomal clustering near the plasma membrane, leading to increased lysosomal exocytosis (Yogalingam et al., 2008). Lysosomal exocytosis-like processes help *Salmonella enterica* Typhimurium-infected cells to combat infection (Roy et al., 2004). Specifically, the Type III Secretion System of *Salmonella* induces pore formation in phagosomes, which can be mended by the fusion of lysosomes with the newly formed phagosomes, which requires Synaptotagmin 7 and a Ca^{2+} influx. These examples illustrate that the position of lysosomes within the cell is crucial to carry out its functions. Lysosomes are highly motile organelles, owing to their attachment to microtubules and association with kinesins, through biogenesis of lysosome-related organelles complex 1 (BLOC-1) related complex and Arl8 (Pu et al., 2015). Lysosome positioning is crucial for fusion with late endosomes and autophagosomes, as well as for the transport of lysosomes and lysosome-related organelles (LROs) to the plasma membrane.

The lysosome is able to eliminate incoming material earmarked for degradation, which can include defective organelles, macromolecules or invading pathogens. At the same time, the lysosome forms homeostatic contacts with other organelles. Lastly, lysosomal exocytosis aids in plasma membrane repair and provides an additional mechanism for pathogen defense. Despite these wide-ranging functions, the lysosome also shares features with other organelles, LROs, and can act as a metabolic signaling platform in the cell.

1.2.1.2 mTOR signaling and metabolism

The lysosome has recently taken center stage as an important metabolic hub within the cell. In response to different stressors or nutrients, and the changing needs of the cell, the lysosome adapts through a tightly regulated, baroque signaling network **(Figure 1.4)**.

mTOR is a serine/threonine kinase and a subunit of the two major complexes mTORC1 and mTORC2 (Lawrence and Zoncu, 2019; Liu and Sabatini, 2020; Perera and Zoncu, 2016). mTORC1 is composed of mTOR, mammalian lethal with SEC13 protein 8 (mLST8), regulatory associated protein of mTOR (RAPTOR) and the mTORC1-inhibiting proteins proline-rich Akt substrate of 40 kDa (PRAS40), DEP domain-containing mTOR-interacting protein (DEPTOR) and 12-kDa FK506-binding protein (FKBP12). Ras homolog enriched in brain (RHEB) is required for the catalytic activity of mTORC1, which is in turn inhibited by tuberous sclerosis (TSC) 1 and TSC2. mTORC2, on the other hand, contains rapamycin-insensitive companion of mammalian target of rapamycin (RICTOR) instead of RAPTOR, which is activated by stress-activated map kinase interacting protein (mSIN1) and proline-rich protein (PROTOR) 1/2, while also lacking PRAS40 and FKBP12. Rapamycin, through which mTOR acquired its name, inhibits mTORC1 but not mTORC2, through the binding of FKBP12-rapamycin to mTOR.

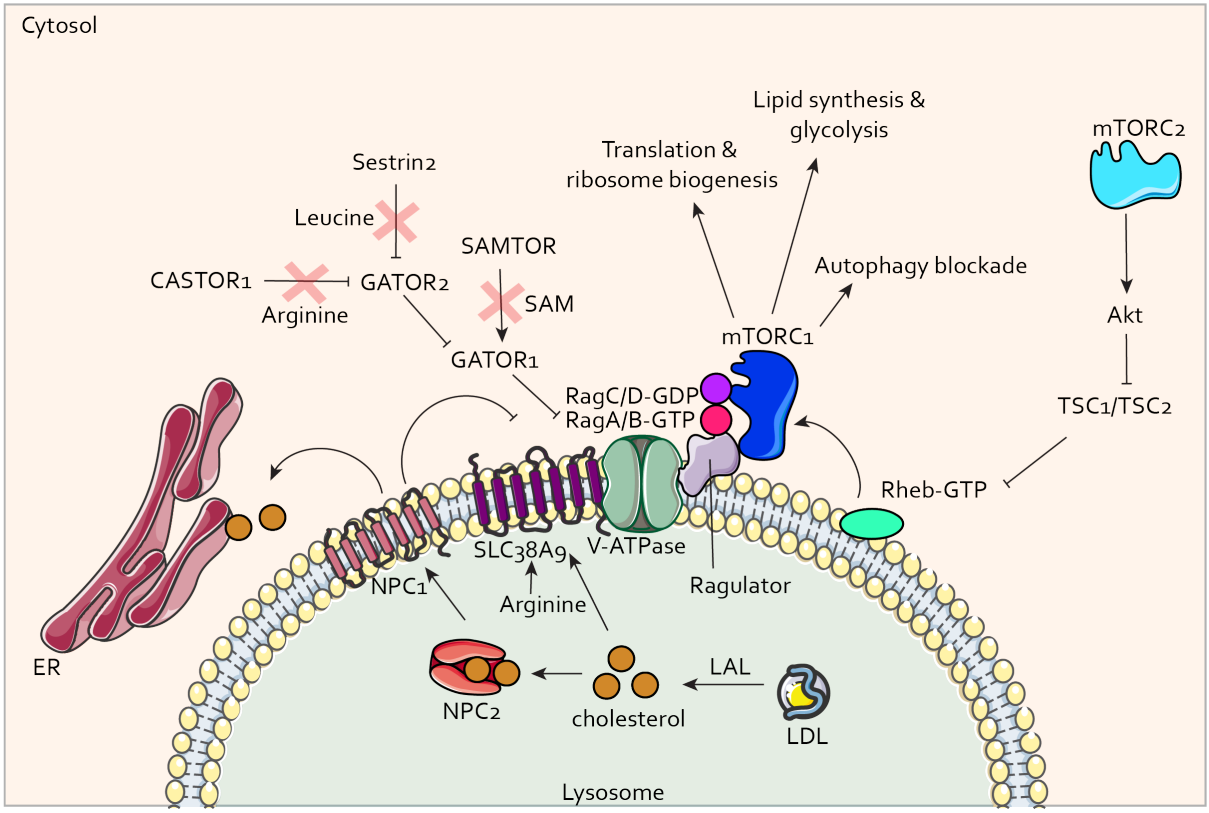


Figure 1.4. mTORC1 regulation and signaling from the lysosomal surface. mTORC1 localizes to the lysosome during nutrient-rich conditions. Intra-lysosomal arginine and cholesterol stimulate solute carrier family 38, member 9 (SLC38A9), which interacts with the V-ATPase pump and the mTORC1 machinery. The cytosolic amino acid sensors signal the presence of their respective amino acid through GATOR1 to RagA/B, which is crucial for mTORC1 lysosomal association. Specifically, arginine is sensed through CASTOR1, leucine through Sestrin2 and SAM through SAMTOR. mTORC2 can also activate mTORC1 signaling through the inhibition of the TSC complex, which inhibits RHEB-GTP. The consequences of mTORC1 activation include translation and ribosome biogenesis, lipid synthesis and uptake, a switch to glycolytic metabolism and autophagy blockade.

mTORC1 receives its environmental cues from the concerted actions of RHEB and Rag GTPases. The Rag GTPases recruit mTORC1 to the lysosomal surface only under amino acid-rich conditions (Sancak et al., 2010), a process that takes place within a few minutes (Manifava et al., 2016). The heterodimeric Ras-related GTP-binding protein (Rag) C/D or RagA/B are anchored at mTORC1 through the Ragulator complex, which is fed cues from

amino acid sensors (Sancak et al., 2010). When the cytosol is rich with nutrients, RagC/D undergoes GTP hydrolysis to guanosine diphosphate (GDP) and RagA/B is GTP-loaded, a process mediated by the guanine nucleotide exchange factor activity of Ragulator, and the V-ATPase pump (Bar-Peled et al., 2012). The presence of growth factors then allows mTORC1 to associate with RHEB-GTP, which stimulates its kinase activity (Long et al., 2005). Amino acid sensing is crucial for mTORC1 activation. Sestrin2 senses leucine (Saxton et al., 2016b; Wolfson et al., 2016), cytosolic arginine sensor for mTORC1 subunit 1 (CASTOR1) senses arginine (Chantranupong et al., 2016; Saxton et al., 2016a) and S-adenosylmethionine sensor upstream of mTORC1 (SAMTOR) senses S-adenosylmethionine (SAM) (Gu et al., 2017), feeding this information to gap activity toward Rags 1 (GATOR1), directly in the case of SAMTOR and through GATOR2 in the case of Sestrin2 and CASTOR1. Amino acids and other metabolites are not only sensed in the cytosol, but also from within the lysosomal lumen, a process dependent upon intact lysosomes and the V-ATPase pump (Zoncu et al., 2011). For instance, SLC38A9 senses arginine and cholesterol within the lysosome, leading to the stimulation of mTORC1 (Castellano et al., 2017; Wang et al., 2015). Furthermore, there is a strong and complex cooperation between the signals that feed into the activation of mTORC1. Specifically, arginine is able to stimulate mTORC1 through inhibiting TSC2 binding to RHEB with the help of growth factors (Carroll et al., 2016). Purines also appear to promote mTORC1 activation through RHEB-GTP, as purine biosynthesis inhibitors suppress mTORC1 (Emmanuel et al., 2017). These wide-ranging, synergistic and antagonistic signals team up to determine the activation status of mTORC1, while research into additional cues and sensors is underway.

The two mTOR complexes have extensive functions that govern cellular survival. mTORC1 affects protein translation and ribosomal biogenesis through the phosphorylation of 4E-binding protein (4EBP) and ribosomal protein S6 kinase 1 (S6K1) (Liu and Sabatini, 2020).

Furthermore, mTORC1 hinders autophagy and lysosomal biogenesis through mechanisms including ULK1 and transcription factor EB (TFEB) phosphorylation. ULK1 phosphorylation by mTORC1 disrupts its association with AMP-activated protein kinase (AMPK), abrogating autophagy induction (Kim et al., 2011).

TFEB phosphorylation keeps this transcription factor out of the nucleus, but when mTORC1 is inactive, TFEB translocates to the nucleus and transcribes genes involved in autophagy and lysosomal biogenesis (Settembre et al., 2011; Settembre et al., 2012). When mTORC1 is active, it impacts metabolism via the transcription factors sterol regulatory element-binding protein (SREBP) 1, SREBP2, peroxisome proliferator-activated receptor γ (PPARγ) and hypoxia-inducible factor 1 α (HIF1α), and sways the cellular metabolic state from oxidative phosphorylation to glycolysis (Duvel et al., 2010; Liu and Sabatini, 2020; Thelen and Zoncu, 2017). Oxidative phosphorylation is a crucial pathway for cellular metabolism and ATP production (O'Neill and Pearce, 2016). Enhanced mTORC1 signaling in myeloid-specific $Tsc1^{-/-}$ mice can result in attenuated M2 macrophage polarization and heightened pro-inflammatory cytokine production (Byles et al., 2013). These results are consistent with studies showing that oxidative phosphorylation suppression impairs the re-polarization of M1 macrophages into the M2 phenotype, unless nitric oxide synthase is inhibited (Van den Bossche et al., 2016).

On the other hand, mTORC2 influences apoptosis and glucose uptake through Akt, which results in proliferation. Furthermore, Akt can inhibit TSC2 in response to insulin, therefore releasing RHEB and stimulating mTORC1 (Menon et al., 2014). Consequently, mTORC1 and mTORC2 can communicate and cooperate in carrying out their diverse functions.

To conclude, cellular needs are integrated into signals through amino acid and cholesterol sensing by mTOR on the lysosomal surface. mTORC1 and mTORC2 signaling together lead to changes in transcription, translation, metabolic regulation, catabolism, growth and proliferation.

1.2.1.3 Lysosome-related organelles

Lysosomes are degradative organelles that are found across most cell types. LROs share multiple features with lysosomes but are cell-type specific, with functions that are distinct from conventional lysosomes (Luzio et al., 2014). The formation of LROs depends on complex machinery that includes endosomal/membrane trafficking while using filaments and motor proteins for transport and GTPases, BLOCs, SNAP receptors (SNAREs) and vacuolar protein sorting (VPS) proteins (among others) for sorting, targeting, trafficking and fusion events (Huizing et al., 2008).

LROs are typically specialized secretory lysosomes, releasing their contents into the extracellular space. These LROs are usually restricted to certain cell types, and some examples include melanosomes in melanocytes, lytic granules in cytotoxic T lymphocytes, delta granules in platelets, lamellar bodies in alveolar epithelial cells, the azurophil granule in neutrophils and the MHC-II organelle in antigen-presenting cells (Huizing et al., 2008). For instance, melanosomes mature in four distinct phases prior to exocytosis, leading to the uptake of melanosomes by keratinocytes (Raposo et al., 2007). The first stage has the characteristic appearance with intra-luminal vesicles, while the second stage exhibits striations, marked by pre-melanosome protein 17, which is required for melanin deposition (Bowman et al., 2019; Huizing et al., 2008). In the third stage, melanin starts to become present in the melanosomes, while stage four is complete with melanin deposits. The

melanogenic enzymes tyrosinase (TYR), tyrosinase-related protein 1 (TYRP1) and TYRP2 are required for melanin synthesis and are routed to developing melanosomes through the endosomal system with the help of the complexes adaptor related protein complex 3 (AP-3), BLOC-1, BLOC-2 and BLOC-3 and the GTPases Rab32 and Rab38 (Marks et al., 2013).

Defects in the formation and trafficking of LROs and lysosomes result in LRO disorders that include Hermansky-Pudlak Syndrome, Griscelli Syndrome and Chediak-Higashi Syndrome (Luzio et al., 2014). Lysosomal function is not only crucial in monogenic disorders, but also in complex IBD, where GWAS have identified multiple polymorphisms in autophagosomal and lysosomal genes such as *ATG16L1*, *GPR65* and *IRGM* (Lassen et al., 2016). These examples point to the necessity for a functional lysosomal compartment for homeostasis in a wide variety of organs and cell types.

1.2.2 Hermansky-Pudlak Syndrome

Hermansky-Pudlak Syndrome (HPS) is an autosomal recessive condition, first described in 1959 by Czechoslovakian physicians Hermansky and Pudlak (Hermansky and Pudlak, 1959). HPS presents with oculocutaneous albinism, platelet aggregation, ceroid lipofuscin accumulation and in some instances, intestinal inflammation and lung fibrosis (Gahl et al., 1998; Garay et al., 1979; Hermansky and Pudlak, 1959; Mahadeo et al., 1991). The albinism results in hypopigmentation of the skin and eyes and low visual acuity. On the other hand, the platelet aggregation, which causes an increased propensity to bleed, originates from the absence of platelet granules. Ceroid lipofuscin is composed of autofluorescent lipid-protein aggregates that may impede lysosomal degradation (Huizing et al., 2000; Huizing et al., 2008; Thelen and Zoncu, 2017). Diagnosis of HPS is established through the observation of oculocutaneous albinism and a tendency to bleed (Yokoyama and Gochuico, 2021).

Additionally, genomic approaches can identify variants in one of the HPS genes and confirm the diagnosis.

1.2.2.1 Genetics of Hermansky-Pudlak Syndrome

On a genetic level, HPS is caused by mutations in 11 different genes. Specifically, the genes mutated include *HPS1, AP3B1, HPS3, HPS4, HPS5, HPS6, DTNBP1, BLOC1S3, BLOC1S6, AP3D1* and *BLOC1S5* (Huizing et al., 2020; Pennamen et al., 2020). The encoded proteins of these genes form different complexes **(Table 1.1)**. Specifically, AP-3 complex subunit delta-1 (AP3D1) and AP-3 complex subunit beta-1 (AP3B1) are part of the AP-3 complex; Dysbindin (DTNBP1), Biogenesis of lysosome-related organelle complex 1 subunit (BLOC1S) 3, BLOC1S6 and BLOC1S5 compose the Biogenesis of lysosome-related organelle complex (BLOC)-1; HPS3, HPS5 and HPS6 form the BLOC-2 complex; HPS1 and HPS4 shape the BLOC-3 complex.

Table 1.1. HPS types are caused by mutations in eleven different genes, whose encoded proteins form four distinct complexes. The table below lists the HPS type, corresponding gene affected and which complex the encoded protein belongs to. Additionally, the table describes the HPS types that develop immunodeficiency, pulmonary fibrosis (PF) and inflammatory bowel disease (IBD).

HPS type	Gene affected	Complex	Immunodeficiency	PF	IBD
HPS-1	*HPS1*	BLOC-3	No	Yes	Yes
HPS-2	*AP3B1*	AP-3	Yes	Yes	No
HPS-3	*HPS3*	BLOC-2	No	No	Yes
HPS-4	*HPS4*	BLOC-3	No	Yes	Yes
HPS-5	*HPS5*	BLOC-2	No	No	No
HPS-6	*HPS6*	BLOC-2	No	No	Yes
HPS-7	*DTNBP1*	BLOC-1	No	No	No
HPS-8	*BLOC1S3*	BLOC-1	No	No	No
HPS-9	*BLOC1S6*	BLOC-1	No	No	No
HPS-10	*AP3D1*	AP-3	Yes	No	No
HPS-11	*BLOC1S5*	BLOC-1	No	No	No

The prevalence of HPS is estimated to be 1:500,000, but is amplified in Puerto Rico, where the prevalence is 1:1,800 individuals due to founder effects (Anikster et al., 2001; Oh et al., 1996). Specifically, a 16 bp duplication in *HPS1* is prominent in northwestern Puerto Rico, whereas a deletion in *HPS3* is more prevalent in central Puerto Rico (Santiago Borrero et al., 2006). The frequency of the *HPS1* mutation is 1:21 in northwestern Puerto Rico and the *HPS3* mutation 1:32 in central Puerto Rico. A minimum of two variants have been reported in each of the 11 genes causing HPS (Huizing et al., 2020; Pennamen et al., 2020).

1.2.2.2 Intestinal inflammation in Hermansky-Pudlak Syndrome

Colitis is only present in certain HPS subtypes (O'Brien et al., 2021). Specifically, 15 % of HPS-1 and 8 % of HPS-4 patients develop IBD (Anderson et al., 2003; Felipez et al., 2010; Gahl et al., 1998; Hazzan et al., 2006; Hussain et al., 2006; Ito et al., 2005; Kouklakis et al., 2007; O'Brien et al., 2021; Yoshiyama et al., 2009). HPS-1 and HPS-4 patients have a distinct gut inflammation reminiscent of Crohn's disease, as granulomata, abscesses, ulcerations and fistulizing disease are some of the intestinal observations. On the other hand, 17 % HPS-3 and 14 % HPS-6 patients have developed IBD, although it is milder in comparison to the BLOC-3-specific types (O'Brien et al., 2021). Therefore, HPS1 and HPS4, which as a complex control the Rab GTPases Rab32 and Rab38 (Gerondopoulos et al., 2012), can serve as examples of Mendelian disorders that can provide useful information into the pathways involved in IBD.

A limited number of studies has been conducted to examine HPS-IBD. A study on Hps1-deficient mice indicated that Paneth cells have decreased secretion of lysozyme in the intestine (Yu et al., 2020b). At the same time, three HPS-1 patients and $Hps1^{-/-}$ mice had an enhanced abundance of *Prevotellaceae* bacteria compared to controls. In order to interrogate the role of the BLOC-3/Rab32 pathway in colitis, one study used CD11c-specific $Rab32^{-/-}$ mice

treated with dextran sodium sulfate (DSS) to induce colitis (Xie et al., 2018). The authors found that the CD11c-specific Rab32$^{-/-}$ mice had a more severe disease course, featuring the expression of the pro-inflammatory cytokines *Il6, Il1a* and *Il1b,* and greater neutrophil infiltration. These two studies point to alterations in Paneth and myeloid cells in HPS-IBD. However, the cellular mechanisms involved and immune alterations have not been elucidated.

1.2.2.3 Lung fibrosis in Hermansky-Pudlak Syndrome

The etiology of lung fibrosis in HPS, particularly present in HPS-1, HPS-2 (caused by *AP3B1* mutations) and HPS-4 patients, has been extensively studied. Specifically, both cell extrinsic and intrinsic mechanisms have been proposed to contribute to the development of lung fibrosis in HPS.

Different cytokines and chemokines have been implicated in HPS pulmonary fibrosis (HPS-PF). The pro-fibrotic cytokine IL-11 is upregulated in HPS1-deficient lung organoids, HPS-1 patient lung fibrosis and idiopathic pulmonary fibrosis (IPF) patients (Strikoudis et al., 2019). The authors also showed that in HPS4/IL-11 double knockout lung organoids, the pro-fibrotic expression pattern was diminished, highlighting the crucial role of IL-11 in HPS lung fibrosis. Hps1$^{-/-}$/Hps2$^{-/-}$ mice spontaneously develop lung fibrosis, featuring surfactant protein accumulation and increased cleaved caspase 3 (indicative of apoptosis) in alveolar epithelial type II cells (Mahavadi et al., 2010). Following endotoxin administration, Hps2$^{-/-}$ and Hps1$^{-/-}$ mice had increased expression of CCL3, and the Hps2$^{-/-}$ mice investigated in more detail had higher TNF in bronchoalveolar lavage fluid (Young et al., 2006). In the same study, isolated alveolar macrophages of Hps2$^{-/-}$ and Hps1$^{-/-}$ mice had higher TNF production following LPS stimulation. Increased CCL2 and CCL3 levels in HPS-1 patient lungs have also been reported,

and their secretion by alveolar macrophages could be normalized by *in vitro* treatment with the anti-fibrotic drug pirfenidone (Rouhani et al., 2009). Furthermore, HPS-1-PF patients have enhanced TNF and IFN-γ levels in the serum compared to familial pulmonary fibrosis patients, highlighting an inflammatory component in HPS-1-PF (El-Chemaly et al., 2018).

Additionally, a pathogenic epithelial/macrophage crosstalk has been suggested to drive HPS lung fibrosis (Young et al., 2016). Specifically, murine $Hps1^{-/-}$ or $Hps2^{-/-}$ alveolar epithelial type II cells secrete CCL2, leading to macrophage recruitment through CCR2 and production of transforming growth factor (TGF)-β, which appears to induce apoptosis in alveolar epithelial type II cells. The lung fibrosis in HPS patients is therefore driven by an intricate array of cellular interactions.

On the other hand, cell intrinsic mechanisms have also been suggested to play large roles in HPS lung fibrosis. $Hps1^{-/-}$ mice have a higher amount of p62 in the lung, suggesting autophagy flux blockade (Ahuja et al., 2016). Small interfering ribonucleic acid (siRNA)-mediated knockdown of HPS1 in the lung epithelial A549 cell line resulted in increased p62 and LC3-II levels, which could be reduced with LC3B overexpression (Ahuja et al., 2016). Consistent with these findings, autophagy flux impairment has been observed in IPF and rapamycin, which is an mTORC1 inhibitor, can reduce the severity of lung fibrosis, measured by collagen content, in bleomycin-treated mice (Patel et al., 2012). Moreover, the role of chitinase 3 like protein 1 (CHI3L1) in HPS lung fibrosis has been elucidated in two studies. Firstly, CHI3L1 levels were higher in the plasma of HPS-1 lung fibrosis patients and in the lungs of $Hps1^{-/-}$ mice (Zhou et al., 2015). On a tissue level, CHI3L1 is thought to contribute to inflammatory and tissue repair processes. The localization of the CHI3L1 receptor IL-13 receptor α2 (IL13Rα2) was impaired in $Hps1^{-/-}$ mice, which resulted in apoptosis following bleomycin-induced fibrosis. However, the fibrotic effects of CHI3L1 occur through binding to

chemoattractant receptor homologue expressed on Th2 cells (CRTH2). This study highlights that BLOC-3 is required for the localization of IL13Rα2, through which anti-apoptotic pathways act, and that fibrosis was mediated through CHI3L1/CRTH2 signaling. In a subsequent study, galectin-3 was found to mediate the effects of CHI3L1 in Hps1$^{-/-}$ bleomycin-treated mice through the inhibition of the CHI3L1 anti-apoptotic effects (Zhou et al., 2018b). Specifically, galectin-3 augments M2 macrophages and pro-fibrotic fibroblasts in the Hps1$^{-/-}$ lung, potentially through its binding to both CHI3L1 and IL13Rα2. In summary, lower autophagy levels and perturbations in intracellular signaling contribute to HPS lung fibrosis in addition to cytokine production, epithelial apoptosis and enhanced leukocyte recruitment.

1.2.2.4 Vesicle trafficking in Hermansky-Pudlak Syndrome

AP-3, BLOC-1, BLOC-2 and BLOC-3 are involved in melanosome biogenesis, with roles in membrane fusion, vesicle transport and directing proteins to LROs (Huizing et al., 2008). In this section, I will highlight the known functions of these complexes in vesicle trafficking.

Patients with AP-3 deficiency have immunodeficiency, distinguishing AP3B1 defects in terms of clinical manifestations (Ammann et al., 2016; Jung et al., 2006). Affected individuals suffer from bacterial (Wenham et al., 2010) and viral (Jones et al., 2013) infections, particularly of respiratory nature, and have neutropenia (Ammann et al., 2016; de Boer et al., 2017). AP-3 deficiency results in high cell surface expression of lysosomal proteins such as CD63, LAMP1 and LAMP2, hinting at a function in lysosomal membrane protein trafficking (Dell'Angelica et al., 1999). Further studies have interrogated the interaction between BLOC-1 and BLOC-2 or AP-3, finding that BLOC-1 and AP-3 deficiencies result in increased cell surface CD63 expression, indicating its impaired trafficking (Di Pietro et al., 2006). At the same time, BLOC-1 and BLOC-2/AP-3 mediate the trafficking of TYRP1, with their absence resulting

in increased TYRP1 internalization. The cytotoxic T lymphocyte (CTL) activity of AP-3 deficient cells is hampered, and the cytotoxic granules display an abnormal distribution within cells (Clark et al., 2003). However, deficiencies in BLOC-1, BLOC-2 and BLOC-3 do not affect CTL activity (Bossi et al., 2005), suggesting differential functions. Furthermore, TLR9 stimulation of plasmacytoid dendritic cells with defects in AP-3, BLOC-1 and BLOC-2 does not elicit type I interferon production in mice (Blasius et al., 2010). BLOC-3-deficient mice were not tested in this study. In addition, AP-3 deficiency results in dampened Toll-like receptor (TLR)4- and myeloid differentiation primary response 88 (MyD88)-positive phagosomes following particulate stimulation in dendritic cells and consequently, reduced signaling (Mantegazza et al., 2012). Interestingly, AP-3 deficient dendritic cells hypo-secreted IL-1β following *Salmonella* Typhimurium infection (Mantegazza et al., 2017). Moreover, mesenteric lymph nodes and the spleen had a higher bacterial load in AP-3-deficient mice at 5 days (but not 3 days) post-infection compared to controls. In summary, AP-3 defects result in aberrant vesicle trafficking, impaired CTL function and hampered anti-microbial responses.

BLOC-1 has emerged as an important complex in recycling endosomes while certain BLOC-1 components play a role in lysosomal positioning. A study has shown that BLOC-1 deficiency results in TYRP1 being mistargeted to syntaxin 13-positive early endosomes, near early endosome antigen 1 (EEA1)-stained endosomes (Setty et al., 2007). BLOC-1 is required for the elongation of endosomal tubules, in cooperation with kinesin family member 13A (KIF13A) and actin (Delevoye et al., 2016). Additionally, BLOC-1 shares components with BLOC-1 related complex, which allows lysosomes to move towards the cell periphery and contribute to cell migration (Pu et al., 2015).

BLOC-2 defects result in a mild form of inflammatory bowel disease compared to BLOC-3 deficiency (O'Brien et al., 2021). Research has revealed that BLOC-2 deficiency leads

to an increase in transferrin receptor at the cell surface, with augmented endocytosis rates (Dennis et al., 2015). On the other hand, BLOC-2 deficiency results in amplified cell surface delivery of TYRP1, where its endocytosis rate is enhanced, and it accumulates in the Golgi. The authors suggest that BLOC-2 is involved in redirecting melanosomal cargo to the melanosome and its deficiency results in mistargeting to the Golgi and plasma membrane. Furthermore, Rab22a appears to recruit BLOC-1 and BLOC-2 to the early endosome, where they regulate the formation of recycling endosomes (Shakya et al., 2018). Therefore, BLOC-1 and BLOC-2 act to mediate the formation of tubular endosomes that can interact with melanosomes and potentially deliver cargo.

The HPS1 and HPS4 proteins interact divalently to form BLOC-3, which is involved in melanosome formation (Carmona-Rivera et al., 2013; Nazarian et al., 2003). BLOC-3 has been described to act as a guanine nucleotide exchange factor for Rab32 and Rab38, activating these proteins (Gerondopoulos et al., 2012) **(Figure 1.5)**. The same study also demonstrated that BLOC-3 determines the localization of Rab32. The frequency of perinuclearly-distributed lysosomes in BLOC-3-deficient fibroblasts was lower compared to controls, with fewer movements both towards and away from the nucleus (Falcon-Perez et al., 2005). BLOC-3 appears to choreograph the recycling of VAMP7 from melanosomes, following its recruitment using BLOC-1 and tubulovesicular carriers (Dennis et al., 2016). VAMP7 is involved in autophagosome fusion with lysosomes and trafficking to melanosomes. VAMP7 departs melanosomes with Vps9 domain and ankyrin-repeat-containing protein (VARP) (which keeps VAMP7 in an inactive conformation) and Rab38, and BLOC-3 is needed to restore tubules emanating from melanosomes (Schafer et al., 2012). Therefore, BLOC-3 deficiency might result in excess VAMP7 on LROs, mediating increased fusion and impacting the delivery of cargo through the unavailability of a factor involved in trafficking to the lysosome.

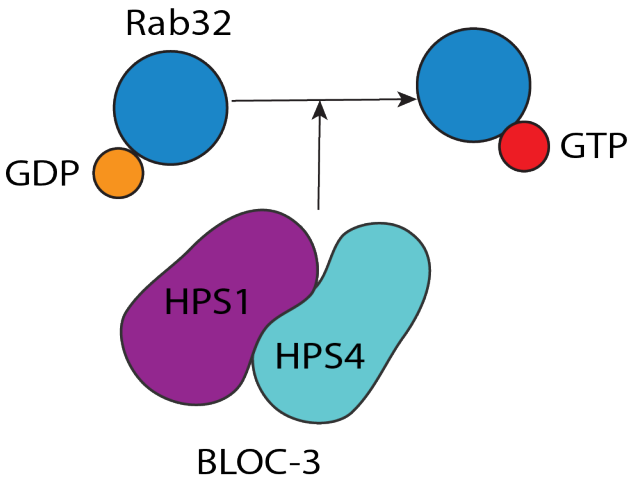


Figure 1.5. BLOC-3 is a guanine nucleotide exchange factor for Rab32 and Rab38. BLOC-3 is composed of HPS1 and HPS4 and acts as a guanine nucleotide exchange factor for Rab32 and Rab38, helping to exchange GDP for GTP on these G-proteins.

Additionally, BLOC-3 immunoprecipitates with Rab9a in the GTP-bound form (Kloer et al., 2010). The BLOC-3-Rab9a interaction is mediated by HPS4, while a mutant form of HPS4 that does not bind Rab9a results in the correct localization of Rab32 and immunoprecipitates with it (Ohishi et al., 2019). These results suggest that Rab32 targeting is dependent on BLOC-3 but not Rab9a binding to BLOC-3. Therefore, Rab9a might mediate other functions of BLOC-3, which may be cell-type specific. For instance, Rab9a has been found to orchestrate Atg5-independent autophagy in mouse embryonic fibroblasts, where silencing of Rab9a results in increased isolation membranes (Nishida et al., 2009). These studies highlight the role of BLOC-3 in recycling VAMP7 from melanosomes and allow for the speculation that the involvement of BLOC-3 in autophagy may be through Rab9a.

The intricate role of Rab32 and Rab38 in the context of melanosome biogenesis has been elucidated. The actin-based motor myosin Vc interacts with Rab32 and Rab38 to aid in trafficking of TYRP1 and VAMP7 to melanosomes (Bultema et al., 2014). Knockdown of

myosin Vc causes the accumulation of melanosomes within melanocytes, suggesting an additional role in secretion. Rab32 and Rab38 co-immunoprecipitate with BLOC-2, AP-3 and AP-1, and Rab38 was shown to colocalize with clathrin (Bultema et al., 2012). Combined Rab32 and Rab38 deficient cells were unable to transport TYRP1 to the melanosome and led to decreased abundance of tyrosinase and TYRP2. Furthermore, BLOC-2 depletion decreases Rab38 levels but does not have a strong effect on Rab32. The GTPase activating protein (GAP) RUN and TBC1 domain-containing protein 1 (RUTBC1) inactivates Rab32 and Rab38, and its knockdown leads to reduced expression of tyrosinase and TYRP1 (Marubashi et al., 2016). Surprisingly, the Rab32 and Rab38 constitutively active variants also result in reduced expression of these melanogenic enzymes. Rab32 has recently been shown to bind to sorting nexin 6 and mediate trafficking of retromer cargo to the Golgi (Waschbusch et al., 2019). Specifically, Rab32 constitutively active and inactive variants resulted in a dispersed mannose-6-phosphate receptor staining within the cell, suggesting the necessity for a balance in its expression pattern. Therefore, Rab32 appears to act beyond melanosome biogenesis and the expression of Rab32 and Rab38 must be tightly regulated.

1.2.2.5 The BLOC-3 pathway in host defense and lipid metabolism

BLOC-3 is involved in endosomal trafficking, particularly studied in the case of the melanosome, but appears to act more broadly in the lysosomal compartment aiding in cell intrinsic immunity. Rab32 or HPS4 deficiency in mice led to an inability to combat the pathogen *Salmonella typhi* and *Salmonella enterica* serovar Typhimurium (Spano et al., 2016). An invasive *Salmonella enterica* serovar Typhimurium strain has effectors (SopD2 and GtgE) which can antagonize the functions of Rab32. Additionally, in a GTPase interactome study, Rab32 was shown to restrict *Listeria monocytogenes* in a dendritic cell line (Li et al., 2016b).

GWAS have also shed light on the role of Rab32 in host defense, since the Rab32 locus is associated with leprosy, caused by *Mycobacterium leprae* (Zhang et al., 2011). In addition, Rab32 interacts with LRRK2, and they colocalize at recycling or late endosomes (McGrath et al., 2019; Waschbusch et al., 2014). LRRK2 has been shown to aid *Mycobacterium tuberculosis* in macrophages, and given its interaction with Rab32, it is possible that Rab32 cooperates with or inhibits other molecules to mediate bacterial elimination (Hartlova et al., 2018). While these findings all point to a crucial role for Rab32 and BLOC-3 in host defense, the function and mechanism of Rab32-mediated host protection and relevance to patients remain unclear.

Rab32 appears to act in lipid metabolism and controls lipid droplet number, as evidenced by its effective role in reprogramming induced pluripotent stem cells (Pei et al., 2015). Specifically, overexpressing Rab32 amplified the amount of $LC3^{+}$ autophagosomes in cells and resulted in an increased expression of lipid synthesis genes. Interestingly, the authors reported an increase in the expression of *TSC1* and *TSC2*, two negative regulators of mTORC1, following overexpression of Rab32. A different study found that Rab32 mutants reduced the size of lipid droplets in *Drosophila*, surrounded LysoTracker stained lysosomes and colocalized with autophagy-related protein 8 $(ATG8)^{+}$ autophagosomes (Wang et al., 2012). At the same time, knockdown of Rab32 resulted in increased lipolysis and concomitant decrease in lipid content in hepatocytes (Li et al., 2016a). The authors suggested that autophagy regulates the size of lipid droplets.

Recently, Rab32 was found to associate with mTORC1 in hepatocytes and stimulate its phosphorylation of S6K1 and S6, but not ULK1, in the presence of amino acids (Drizyte-Miller et al., 2020). In Rab32 knockdown cells, TFEB translocation to the nucleus was enhanced, but surprisingly, autophagy was reduced. Furthermore, Rab32 appears to be required for the formation of autophagic vacuoles derived from the ER, where Rab32 was

localized (Hirota and Tanaka, 2009). Moreover, Rab32 has been found on the ER and mitochondria, affecting the mitochondrial-associated membrane through calcium signaling and protein kinase A anchoring (Bui et al., 2010). Lastly, Rab32 is induced upon ER stress, and Rab32 overexpression or its dominant-active mutant result in a larger number of mitochondria (Haile et al., 2017).

The lipidome of HPS1-deficient mice is characterized by the atherosclerotic-like accumulation of certain lipids (Ma et al., 2019). Specifically, in the plasma of $Hps1^{-/-}$ mice, phosphatidic acid, sphingomyelin, cholesterol, triacylglycerol and lysophosphatidylserine were amplified. The authors also found an increase in lipid droplet number in the liver of $Hps1^{-/-}$ mice. It is tempting to speculate that lipophagy might be defective, or that lipid metabolism is impaired in $Hps1^{-/-}$ mice.

In conclusion, Hermansky-Pudlak Syndrome can present with lung fibrosis and IBD in certain subtypes. The mechanisms of disease are likely complex, as defects in the BLOC-3 pathway reduce autophagy flux, result in easier replication of microbial pathogens and disrupt lipid metabolism. However, how these distinct pathways are tied together and the underlying mechanisms that produce the clinical manifestations in HPS are not clear.

1.2.2.6 Treatments for Hermansky-Pudlak Syndrome

The treatment for HPS is based on remedying the symptoms and there is no cure for the disease. For instance, lung fibrosis is treated with the small molecule pirfenidone or lung transplantation, which are similar therapeutic options to IPF, a severe interstitial lung disease (El-Chemaly and Young, 2016; O'Brien et al., 2011; O'Brien et al., 2018). Pirfenidone inhibits TGF-β, and has been used for experimental treatment in HPS although its efficacy has not yet been determined (Yokoyama and Gochuico, 2021). The bleeding diathesis can be managed

using desmopressin, but blood transfusions might be required following extensive blood loss (El-Chemaly and Young, 2016).

The BLOC-3-specific emergence of Crohn's-like inflammation has been treated with TNF-targeting therapies (Felipez et al., 2010; Girot et al., 2019; Grucela et al., 2006; Hussain et al., 2006; Ishihara et al., 2019; Kouklakis et al., 2007; Sofia et al., 2017). In a cohort of 13 HPS-IBD patients treated with anti-TNF, 7 responded, 2 did not respond, one lost response with time and 3 had to discontinue the treatment (O'Brien et al., 2021). Therefore, anti-TNF therapies have had some success in HPS-1, but additional treatment options are needed for the disease. Lastly, gene editing technologies may provide a novel avenue for therapies in HPS, where microhomology-mediated end joining has corrected the *HPS1* 16 bp frameshift mutation in B lymphoblastoid cells (Iyer et al., 2019).

1.2.3 Other lysosome-associated disorders

Other lysosome-related organelle or lysosomal storage disorders provide important insights into shared mechanisms of action. In this section, I examine several relevant diseases, which share features with HPS.

Chediak-Higashi Syndrome is caused by mutations in the *LYST* gene and results in albinism, bleeding diathesis and immune dysregulation (Bowman et al., 2019; Nagle et al., 1996). Specifically, lysosomal trafficking regulator (LYST) acts in the exocytosis of LROs such as lytic granules, diminishing the ability of natural killer cells and CTLs to secrete granules (Chiang et al., 2017). Furthermore, fewer LPS beads reached $Rab7^{+}$ organelles in Lyst-deficient mice bone marrow DCs, suggesting that phagosomal maturation and cytokine production downstream of TLR4 was abrogated (Westphal et al., 2017). A different study illustrated that while autophagy was not impaired in LYST siRNA-treated cells, the lysosomes were fewer and

larger (Holland et al., 2014). The part that LYST plays in different cell types suggests multiple functions for this protein that are crucial for various aspects of the immune response.

Griscelli Syndrome is caused by mutations in the *RAB27A, MLPH* or *MYOVA* genes, leading to hypopigmentation (Menasche et al., 2003; Menasche et al., 2000). The encoded proteins act to attach melanosomes onto the actin cytoskeleton for secretion (Bossi et al., 2005; Hume et al., 2002). Similar to LYST, Rab27a is required for the secretion of CTL granules containing granzyme A and hexosaminidase and perform target cell lysis (Stinchcombe et al., 2001). Both Chediak-Higashi Syndrome and Griscelli Syndrome have defects in LRO biogenesis, similar to HPS, however, the precise roles of these genes is still being uncovered.

Niemann-Pick Type C1 (NPC1) and NPC2 are lysosomal storage disorders with neurological involvement and detrimental lipid accumulation (Vanier, 2010). Once low density lipoprotein (LDL) is transported to the lysosome, acid lipase breaks down LDL, and cholesterol is then transferred to NPC2 within the lumen, and handed over to the sterol-binding pocket of NPC1 (Kwon et al., 2009). NPC1 deficiency results in dampened autophagy, measured by p62 and LC3-II levels (Sarkar et al., 2013). Rapamycin can boost autophagy flux and cyclodextrin can ameliorate the extensive cholesterol accumulation. These findings can be explained by an investigation showing that NPC1 interacts with the transporter SLC38A9 and inhibits mTORC1 activation (Castellano et al., 2017). Therefore, in NPC1 deficiency, the balance is shifted to an active mTORC1 complex and reduced autophagy. NPC1 patients, consistent with dampened autophagy, are not able to degrade certain bacteria, which could offer clues towards the IBD-like intestinal inflammation observed in some patients (Schwerd et al., 2016). Another study has attributed the initiating factor of the storage disorder to sphingosine accumulation, which drives the accrual of cholesterol and other sphingolipids (Lloyd-Evans et al., 2008). The lipid-transporting functions of NPC1 and NPC2 within the

lysosome ensure appropriate lipid localization, and dysregulation results in augmented mTORC1 signaling, stalled autophagy flux and lipid storage.

Neuronal ceroid lipofuscinosis is a neurodegenerative disorder, also called Batten disease, and is caused by mutations in one of 13 genes with the most common ones being *CLN1, CLN2* and *CLN3* (Mole and Cotman, 2015). The genes implicated in neuronal ceroid lipofuscinosis are lysosomal enzymes or lysosomal membrane proteins. For example, ceroid lipofuscinosis neuronal (CLN) 3 deficiency has been shown to reduce autophagy flux in a mouse model of the disease, measured by LC3-II accumulation (Cao et al., 2006). Defective autophagosome maturation has also been observed in CLN5 and CLN6 deficiencies, with aberrant accumulation of α-synuclein or autofluorescent storage material, respectively (Adams et al., 2019; Thelen et al., 2012). The induction of autophagy through TFEB activation reduced the storage material in $CLN3^{-/-}$ mice (Palmieri et al., 2017).

A different lysosomal storage disorder, Gaucher's disease, results from a deficiency in glucocerebrosidase, encoded by the *GBA1* gene (Kinghorn et al., 2017). Subsequently, glucosylceramide accumulates in lysosomes, resulting in autophagy blockade in a *Drosophila* model of disease (Kinghorn et al., 2016). Short hairpin RNA-mediated knockdown of glucocerebrosidase 1 in cortical neurons resulted in lipid and α-synuclein accumulation (Mazzulli et al., 2011). Therefore, neuronal ceroid lipofuscinosis and Gaucher's disease are also intricately linked with the autophagy pathway.

Furthermore, the storage disease mucopolysaccharidosis type VII is caused by β-glucuronidase deficiency and subsequently glycosaminoglycan degradation is attenuated (Montano et al., 2016). In a chondrocyte β-glucuronidase-deficient cell line, mTORC1 signaling was enhanced and autophagy flux was impaired, which could be rescued by autophagy induction or mTOR downregulation (Raptor depletion) (Bartolomeo et al., 2017). This study

highlights the involvement of autophagy in lysosomal storage diseases, delineating the possibility for autophagy induction to treat these disorders (Seranova et al., 2017).

Lysosomal acid lipase (LAL) deficiency is caused by mutations in the *LIPA* gene, leading to Wolman's disease (early childhood) or a cholesteryl ester storage disease (late childhood and adults) (Burton et al., 2015). Specifically, symptoms can include hepatomegaly, liver fibrosis and abnormal lipid levels. LAL resides in the lysosome and breaks down triglycerides and cholesteryl esters and its deficiency results in their accumulation (Meng et al., 2020).

Lysosomal storage disorders present an interesting interaction between lipid accumulation and autophagy. The study of lysosomal biology has been aided by these diseases, resulting in the delineation of required lysosomal proteins in lysosome maturation, acidification and degradation. However, while these disorders result in the accumulation of material within the lysosome, the triggers can be different and distinguishing between primary and secondary causes of disease is a complex task.

1.3 Aims of the project

Hermansky-Pudlak Syndrome type 1 is a lysosome-related organelle disorder that involves defective vesicle trafficking. HPS-1 patients can develop pulmonary fibrosis and intestinal inflammation. This thesis aims to delineate the cellular and molecular mechanisms underlying tissue inflammation in Hermansky-Pudlak Syndrome type 1. Additionally, the role of the BLOC-3 pathway in bacterial elimination and lipid metabolism will be elucidated. Specifically, in this thesis, I aim to:

1. Identify relevant cell types in which HPS1 and HPS4 might act to focus functional studies on the cell types affected by pathogenic variants in the BLOC-3 pathway.

2. Reveal transcriptional signatures in HPS-1 patient cells at baseline and after stimulation to gain greater insight into specific pathways that might be significant for HPS-1 pathology.
3. Investigate patient-derived primary cells and cell lines to understand the molecular mechanism underlying HPS1 deficiency-associated inflammation.
4. Evaluate the peripheral blood and serum proteome of HPS-1 patients to pinpoint potential inflammatory drivers.
5. Establish a model highlighting how HPS1 deficiency causes organ pathology by integrating the evidence from different 'omics' and functional approaches.

Chapter 2 - Materials & Methods

2.1 Patients and ethics

The study was approved by the institutional review boards (Oxford IBD cohort study and a subproject to investigate rare diseases; 11/YH/0020, 16/YH/0247). Written informed consent was provided by all HPS-1 and HPS-3 patients through Mount Sinai (IRB 11-01669). Only anonymous patient information was processed. A sample from an NPC1 patient was obtained through the Oxford IBD cohort rare disease subproject. The HPS-1, HPS-3 and NPC1 patients showed typical phenotypic features of their respective diseases and carried pathogenic mutations. A summary of patient characteristics is provided **(Table 2.1)**. Control peripheral blood mononuclear cells (PBMCs) were obtained from healthy volunteers recruited via the Oxford GI biobank.

Table 2.1. Patient population used in this thesis. IBD: inflammatory bowel disease; PF: pulmonary fibrosis; HPS-1: Hermansky-Pudlak Syndrome type 1; HPS-3: Hermansky-Pudlak Syndrome type 3; NPC1: Niemann-Pick type C1.

Experiment	**Group**	**N; (Male/Female)**	**Age (years ± standard deviation)**	**Phenotype (% IBD; % lung fibrosis)**
CyTOF	HPS-1	8 (4/4)	44 ± 12	25 % PF
	Controls	12 (5/7)	47 ± 14	
Serum proteomics	HPS-1	11 (3/8)	39 ± 14	18 % PF; 36 % IBD
	Controls	50 (26/24)	35 ± 9	
Transcriptomics	HPS-1	4 (2/2)	36 ± 8	25 % PF
	Controls	4 (2/2)	26 ± 1	
Functional experiments	HPS-1	10 (7/3)	41 ± 11	10 % PF
	Controls	12 (8/4)	37 ± 12	

HPS-3	4 (1/3)	32 ± 19.6	
NPC1	1 (0/1)	10	100 % IBD

2.2 Cell culture

2.2.1 PBMC isolation and monocyte differentiation into macrophages

Blood was added dropwise to a tube containing 15 mL Lymphoprep (Axis-Shield, catalog number 1114545) to perform gradient centrifugation at 800 g for 30 minutes with no deceleration. The buffy coat was extracted and washed with Phosphate Buffered Saline (PBS) (Sigma) twice. Cells were counted in Trypan Blue (Sigma) and 50 million PBMCs were plated. Monocytes were obtained using the adherence method in Roswell Park Memorial Institute medium (RPMI) 1640 (Sigma, catalog number R8758) following 2 hours of incubation at 37 °C and 5 % CO_2. Subsequently, adherent cells were treated with 100 ng/mL macrophage colony-stimulating factor (M-CSF) (Peprotech, catalog number 300-25) in RPMI 1640 (Sigma), 10 % fetal bovine serum (FBS) (Sigma, catalog number F7524) and 1 % Penicillin/Streptomycin (Sigma, catalog number P4333) for 5 days to differentiate them into macrophages. Macrophages were scraped in versene (Thermo Fisher, catalog number 15040066), counted and plated for subsequent experiments.

2.2.2 HAP1 cell culture

HAP1 cells (Horizon Discoveries, catalog ID C631) were maintained in Dulbecco's Modified Eagle Medium (DMEM) (Sigma, catalog number D5796) with 10 % fetal bovine serum at 37 °C and 5 % CO_2. Cells were detached with 0.05 % Trypsin-EDTA (Sigma, catalog number T4049) and washed with PBS. HAP1 cells were frozen in 90 % medium and 10 % dimethyl sulfoxide. Cells were regularly checked for mycoplasma.

2.2.3 CRISPR/Cas9 gene editing and validation

The guide RNA sequence for clustered regularly interspaced short palindromic repeats (CRISPR)/CRISPR-associated protein 9 (Cas9) gene editing of the *HPS1* gene was obtained from a previous publication (Doench et al., 2016). Cas9:gRNA ribonucleoprotein complexes were generated according to the manufacturer's protocol using High Fidelity Cas9 (IDT, catalog number 1081060) with the crRNA sequence 5' GGACGGTCATCTTATCCGAA 3' and tracrRNA (IDT, catalog number 1072533). Specifically, to prepare the oligo mix, 1 µL 100 µM crRNA was mixed with 1 µL 100 µM tracrRNA and 98 µL nuclease-free duplex buffer. The mix was incubated at 95 °C for 5 minutes and allowed to cool to room temperature. Ribonucleoprotein complexes were generated by combining 24 µL 1 µM oligo mix, 24 µL 1 µM Cas9 and 352 µL Opti-MEM (Gibco, Fisher Scientific, catalog number 10149832), and incubating at room temperature for 5 minutes. 400 µL ribonucleoprotein complexes, 19.2 µL lipofectamine 2000 (ThermoFisher, catalog number 11668019) and 380.8 µL Opti-MEM were mixed and incubated for 20 minutes at room temperature. Transfection mix was added onto 800,000 HAP1 cells at low passage, which had been plated the day before. 48 hours post-transfection, cells were single-cell diluted and expanded in conditioned medium, consisting of 20 % used HAP1 cell medium, 10 % FBS and 70 % DMEM-FBS medium. The cells were allowed to grow for 14 days with medium supplementation every 3-4 days, followed by expansion prior to screening.

Screening for clones was performed following DNA extraction (DNeasy Blood and Tissue kit, QIAGEN, catalog number 69504), using polymerase chain reaction (PCR) with Phusion polymerase (New England Biolabs, catalog number M0531S) and according to the manufacturer's protocol. The following forward (5' CAATGGTGACCACACCGAGA 3') and

reverse (5’ GCTGGGGGCAGTATGTGAAA 3’) primers were used for PCR. Gel electrophoresis using 50 mL of 1.5 % agarose (Bioline, catalog number BIO-41025) in 1x TAE (AppliChem, catalog number A4686) buffer and 5 µL GelRed (Biotium, catalog number 41003) dye. 1 kb and 100 bp HyperLadder (New England Biolabs, catalog numbers N3232L and N3231L, respectively) was used to determine approximate DNA sizes. Gels were visualized under UV light and desired bands were excised with a scalpel. Gel extraction was achieved using the QIAquick Gel Extraction kit (QIAGEN, catalog number 28115). Sanger sequencing was performed by Source Bioscience and using the same forward primer as for the PCR (5’ CAATGGTGACCACACCGAGA 3’).

2.2.4 siRNA transfections

For siRNA transfections, the Rab32 siGENOME (Horizon Discovery, SMARTPool, catalog number M-009920-02-0005) and the non-targeting siRNA pool #1 (Horizon Discovery, catalog number D-001206-13-05) were used. Cells were transfected with 40 nM siRNA and INTERFERin (Polyplus transfection, catalog number 409-10) according to the manufacturer’s protocol. Specifically, 200,000 HAP1 cells were plated in 6-well plates overnight. 40 nM siRNA in 200 µL serum-free DMEM was mixed with 12 µL INTERFERin and incubated for 10 minutes prior to addition to cells. Experiments were performed 72 hours following transfection.

2.2.5 Lentiviral production and transduction

Plasmids used for lentiviral transduction were pLJC5-Tmem192-3xHA (a gift from David Sabatini, Addgene plasmid 102930), psPAX2 (a gift from Didier Trono, Addgene plasmid 12260) and pMD2.G (a gift from Didier Trono, Addgene plasmid 12259). Transformed bacteria were grown in LB with ampicillin (Sigma, catalog number A5354) at 100 µg/mL overnight.

Plasmid isolation was performed using the EndoFree Plasmid Maxi Kit (QIAGEN, catalog number 12362) and concentrations were determined on a Nanodrop.

Human embryonic kidney 293 T-antigen cells (ATCC) were transfected at 60-80 % confluence in a 15 cm dish using lipofectamine 2000 and Opti-MEM. Specifically, 1.5 µg pLJC5-Tmem192-3xHA, 1.5 µg psPAX2 and 0.5 µg pMD2.G were mixed with 1.5 mL Opti-MEM. At the same time, 1.5 mL Opti-MEM was mixed with 56 µL lipofectamine and incubated at room temperature for 5 minutes. Mixtures were combined for 20 minutes at room temperature and added to the dish containing 10 mL DMEM with 10 % FBS. Viral supernatant was collected after 48 and 72 hours, pooled and filtered through a 0.45 µm filter. 100,000 HAP1 cells in a 24-well plate were used for transduction. 2 mL of viral supernatant was combined with 6 µg/mL polybrene (catalog number TR-1003-G, Sigma) and added to cells. After 48 hours, cells were positively selected with 0.5 µg/mL puromycin and kept in puromycin-containing medium until 1 day before each experiment (catalog number P8833, Sigma).

2.3 Biochemical and molecular biology methods

2.3.1 Western blotting

Cells were lysed in pH 7.5 buffer containing 50 mM Tris, 150 mM NaCl, 2 mM EDTA, 50 mM NaF, 1 % Nonidet-P40 and 2 mM $Na_4P_2O_7$ plus cOmplete protease inhibitors (Roche, catalog number 04693159001). Cell lysates were loaded on NuPAGE Novex 4-12 % Bis-Tris Protein Gels, 1.0 mm, 10 well (Thermo Fisher, catalog number NP0321BOX) and NuPAGE 2-(N-morpholino)ethanesulfonic acid sodium dodecyl sulfate (SDS) running buffer (Life Technologies, catalog number NP0002) using standard protocols. Blotting was done on a polyvinylidene fluoride membrane (Invitrolon, Thermo Fisher, catalog number LC2005) using NuPAGE transfer buffer (Life Technologies, catalog number NP00061) and 10 % methanol.

Membranes were blocked in 5 % skimmed milk (Sigma, catalog number 70166) or 5 % bovine serum albumin (Sigma, catalog number A7906-1KG) in PBS with 0.05 % Tween-20 (Sigma, catalog number P2287-500ML) (PBS-T) for 1 hour if probing for phosphorylated proteins (pS6). Membranes were then incubated in 2 % milk or bovine serum albumin with antibodies for 1 hour at room temperature or overnight at 4 °C.

The antibodies used are listed here and in **Table 2.2**: anti-LAMP2 (clone H4B4, Santa Cruz Biotechnology, catalog number sc-18822), anti-hemagglutinin (HA) (clone C29F4, Cell Signaling, catalog number 3724S), anti-cathepsin C (CTSC) (clone D-6, Santa Cruz Biotechnology, catalog number sc-74590), anti-mTOR (polyclonal, Cell Signaling, catalog number 2972), anti-S6 (clone 5G10, Cell Signaling, catalog number 2217S), anti-pS6 Ser235/236 (polyclonal, Cell Signaling, catalog number 2211S), anti-glyceraldehyde 3-phosphate dehydrogenase (GAPDH) (clone 14C10, horseradish peroxidase (HRP) conjugate, Cell Signaling, catalog number 3683S) and anti-β-actin (clone 8H10D10, HRP conjugate, Cell Signaling, catalog number 12262S). Membranes were washed three times in PBS-T prior to incubation with HRP-conjugated secondary antibodies in 2 % milk or bovine serum albumin for 1 hour at room temperature. Specifically, anti-mouse IgG HRP-linked (Cell Signaling, catalog number 7076S) and anti-rabbit IgG HRP-linked (Cell Signaling, catalog number 7074S) were used. Membranes were washed three times in PBS-T.

Lastly, enhanced chemiluminescence (GE Healthcare Life Science, catalog number RPN2106) was used for detection and results were recorded on a Biorad Chemidoc imaging system. For analysis of S6 protein levels, pS6 bands were stripped using Restore Western blot stripping buffer (Thermo Fisher, catalog number 21059) for 30 minutes, washed in PBS-T and re-blocked. For densitometry analysis, Fiji (ImageJ) was used to quantify the density of bands

in the pS6-to-GAPDH ratio and the iBright Analysis software (Thermo Fisher) was utilized for the mTOR-to-LAMP2 ratio calculation.

Table 2.2. Antibodies used for Western blotting in this thesis. The antibody clone, manufacturer, catalog number and dilution used are specified.

Antibody	Clone	Manufacturer	Catalog number	Dilution
LAMP2	H4B4	Santa Cruz Biotechnology	sc-18822	1:1000
HA	C29F4	Cell Signaling	3724S	1:1000
CTSC	D-6	Santa Cruz Biotechnology	sc-74590	1:1000
mTOR	polyclonal	Cell Signaling	2972	1:1000
S6	5G10	Cell Signaling	2217S	1:1000
pS6 pS235/pS236	polyclonal	Cell Signaling	2211S	1:1000
GAPDH (HRP conjugate)	14C10	Cell Signaling	3683S	1:1000
β-actin (HRP conjugate)	8H10D10	Cell Signaling	12262S	1:1000

2.3.2 RNA extraction, reverse transcription and quantitative polymerase chain reaction (qPCR)

RNA extraction was performed using RNeasy mini kit (QIAGEN, catalog number 74104) according to the manufacturer's protocol. Complementary DNA (cDNA) synthesis was performed using 1 µg RNA and High Capacity cDNA Reverse Transcription Kit (Applied Biosystems, catalog number 4368814). 100 ng cDNA, PrecisionPLUS qPCR master mix (Primer Design, catalog number Z-PPLUS-iC-20ML) and Taqman probes (Life Technologies, **Table 2.3**) were used to obtain the relative gene expression to the housekeeping gene, *RPLP0*. Expression was determined by the 2ΔCt method (Livak and Schmittgen, 2001).

Table 2.3. Taqman probes used in this thesis. The probes were supplied by Life Technologies and the identifier for each is listed.

Probe	Identifier
RPLPO	Hs00420895_gH
HPS1	Hs00945781_g1
HPS4	Hs01031019_m1
LDLR	Hs01092524_m1
FASN	Hs01005622_m1
HMGCR	Hs00168352_m1

2.3.3 Gentamicin protection assay

80,000 macrophages or 40,000 HAP1 cells were plated per well in 96-well plates the day before for HAP1 cells or 1 hour before the experiment for macrophages. Prior to infection, macrophages or HAP1 cells were treated with 50 µM rapamycin (Cayman Chemical, catalog number 13346), lipid mixture 1 as free fatty acids (Sigma, catalog number L0288) at 1:10, 50 µM cholesterol (Cholesterol, catalog number C8667, Sigma) for 2.5 hours or 50 µM etomoxir overnight (Sigma, catalog number E1905). HAP1 cells were infected at 1:100 multiplicity of infection (MOI), meaning 1 cell per 100 bacteria, and macrophages at 1:10 MOI for 1 hour. Infections with different bacterial species and strains included green fluorescent protein (GFP)-*Salmonella* Typhimurium (NCTC 12023), Adherent Invasive *E. coli* strain LF82 and *Staphylococcus aureus* (NCTC 657). Cells were then treated with 100 µg/mL gentamicin (Sigma, catalog number G1397) for 2 hours to kill extracellular bacteria and subsequently lysed with 1 % Triton X-100 (Sigma, catalog number T8787). Lysates were then plated in 1:10 or 1:100 dilutions on Luria broth agar plates and incubated at 37 °C overnight and quantified on the following day.

2.3.4 Lysosome Immunoprecipitation

The protocol described has been adapted from the first publication of this technique (Abu-Remaileh et al., 2017). 20 million HAP1 cells were plated the day before the experiment in 15 cm dishes. Cells were rinsed with PBS and then scraped in 1 mL KPBS (136 mM KCl and 10 mM KH_2PO_4 at pH 7.25, adjusted using KOH). A whole cell sample was kept aside while the rest was homogenized with 25 strokes of the dounce glass tissue homogenizer (VWR, catalog number 71000-516) on ice. The homogenate was centrifuged at 600 g for 2 minutes at 4 °C and the supernatant was applied onto 50 µL Pierce anti-HA magnetic beads (Thermo Fisher, catalog number 88836), mixed and put onto a gentle rotator for 5 minutes at 4 °C. The tubes were placed onto a magnet, washed in KPBS 3 times and dry pellets of beads-lysosomes were frozen at -80 °C. A small sample was taken during the last KPBS wash for Western blot analysis.

A standard curve was created with different concentrations of cells to yield different amounts of LAMP2, which were then used to quantify the amount of lysosomes extracted. This method was adapted from a previously published mitochondrial immunoprecipitation study (Chen et al., 2017). Specifically, 250,000 cells per 15 µL were used that would be loaded in the SDS-polyacrylamide gel electrophoresis (PAGE) gel and serially diluted 1:1 to obtain 7 standard curve samples. Additionally, in order to quantify the lysosome equivalents, 1,920,000 cells per 15 µL (following lysosome extraction) were used, with the expectation that the yield would be low. 15 µL were loaded per well in the SDS-PAGE and the percent of lysosomes extracted was calculated by interpolating from the standard curve of band intensities.

2.3.5 Lysosomal proteomics

The HAP1 cell bead-lysosomes were thawed from -80 °C for proteomic analysis. Proteomics was performed by Dr. Georgina Berridge and Dr. Roman Fischer from the Benedikt Kessler

group at the Target Discovery Institute, University of Oxford. Proteins phosphorylated *in vitro* were subjected to SMART Trypsin digest (Thermo Fisher) treatment according to the manufacturer's instructions, desalted using SepPak reversed phase columns (Waters), and injected into an LC-MS/MS platform (Dionex Ultimate 3000 nano LC and Q-Exactive). Sample separation was undertaken using a 50-cm-long EasySpray column (ES803; Thermo Fisher) with a 75-µm inner diameter and a gradient of 2 to 35 % acetonitrile in 0.1 % formic acid and 5 % dimethyl sulfoxide with a 250 nL/min flow rate for 60 minutes. MS1 spectra with a resolution of 70,000 and an ion target of 3e6 were acquired for a maximum of 100 ms. MS/MS data were acquired after isolation with a mass window of 1.6Th and fragmentation at 28 % normalized collision energy (HCD, Resolution 17,500). PEAKS V.8.5 (Bioinformatics Solutions) and a Uniprot/Trembl database (UP000005640 [homo sapiens] and UP000054420 [salmonella enterica]) were used to analyze the LC-MS/MS data set to identify phosphorylation (S, T, Y), as well as oxidation (M) and deamidation (N, Q). Mass tolerance was 10 ppm for precursor and 0.05 Da for fragment mass, 3 missed cleavages with a peptide level false discovery rate set to 1 %. Freestyle 1.3 (Thermo Fisher) was used to generate extracted ion chromatograms of relevant peptides that were quantified after Gaussian smoothing (five data points). Progenesis QI (Waters) based label-free quantitation results were imported into Perseus 1.5.2.4 (Tyanova et al., 2016). Quantitative data was log2 transformed and normalized by median subtraction and missing values were imputed based on normal distribution. The proteomics data have been deposited to the ProteomeXchange Consortium via the PRIDE partner repository (Perez-Riverol et al., 2019) with the dataset identifier PXD024435 and 10.6019/PXD024435. gProfiler (Raudvere et al., 2019) was used to investigate the Kyoto Encyclopedia of Genes and Genomes (KEGG) pathways (Kanehisa and Goto, 2000)

in our proteomics samples enriched in the most abundant proteins, as previously described for isolated peroxisomes (Ray et al., 2020).

2.4 Flow cytometry

All antibodies and dyes used in this thesis are listed with their methods and in **Table 2.4**.

Table 2.4. Antibodies and dyes used for flow cytometry in this thesis. The antibody clone, manufacturer, catalog number and dilution or concentration used are specified.

Antibody	Clone	Manufacturer	Catalog number	Dilution or concentration
Fixable Viability Dye eFluor 780	-	eBioscience	65-0865-14	1:1000
HLA-DR PerCP/Cy5.5	L243	BioLegend	307629	1:100
CD14 BV650	M5E2	BioLegend	301835	1:100
TNF eFluor 450	MAb11	eBioscience	48-7349-42	1:50
pS6 pS235/pS236 AF488	N7-548	BD Biosciences	560434	1:10
pS6 pS235/pS236 AF647	N7-548	BD Biosciences	560435	1:10
LC3 FITC	4E12	Millipore	FCCH100171	1:20
HA AF488	16B12	Thermo Fisher	A21287	1:200
LDL-BODIPY	-	Thermo Fisher	L3483	25 µg/mL
pHrodo Red E. coli Bioparticles	-	Thermo Fisher	P35361	100 µg/mL
DQ-Ovalbumin	-	Thermo Fisher	D12053	10 µg/mL
BODIPY 493/503	-	Thermo Fisher	D3922	1 µg/mL
MitoSOX Red	-	Thermo Fisher	M36008	5 µM
LysoTracker Deep Red	-	Thermo Fisher	L12492	1:1000

2.4.1 Monocyte MDP/LPS stimulation assay

Monocytes were stimulated with 100 ng/mL LPS (Enzo Life Sciences, catalog number ALX-581-013-L001) or 200 ng/mL lipidated MDP (L-18 MDP) (Sigma, catalog number A0936) with

1:1000 Golgi plug (BD Biosciences, catalog number 555029) for 2.5 hours. Cells were scraped and washed in flow staining buffer (FSB), consisting of PBS with 0.5 % FCS. Cells were stained for live-dead using the Fixable Viability Dye eFluor 780 (eBioscience, catalog number 65-0865-14, 1:100 dilution) and antibodies against HLA-DR (PerCP/Cy5.5, clone L243, BioLegend, catalog number 307629, 1:100 dilution) and CD14 (Brilliant Violet 650, clone M5E2, BioLegend, catalog number 301835, 1:100 dilution) were incubated on ice for 20 minutes. For fixation and permeabilization, Cytofix/Cytoperm (BD Biosciences, catalog number 554714) was used and cells were incubated on ice for 20 minutes. Cells were washed in perm/wash (BD Biosciences, catalog number 554723), which was diluted 1:10 in water. Cells were then resuspended in perm/wash with anti-TNF (eFluor 450, clone MAb11, eBioscience, catalog number 48-7349-42, 1:50 dilution) on ice for 30 minutes. Monocytes were washed twice with perm/wash solution and re-suspended in FSB for flow cytometric analysis. Data were plotted as ΔTNFα (%) from the unstimulated to the stimulated condition.

2.4.2 S6 phosphorylation flow cytometry

40,000 HAP1 cells were plated in 96-well plates the day prior to the experiment. HAP1 cells were treated with 50 µM rapamycin (Cayman Chemical, catalog number 13346) for 2 hours, 25 µg/mL LDL (Thermo Fisher, catalog number L3483) for 1 hour or lipid mixture 1 as free fatty acids for 2 hours at 1:10 (Sigma, catalog number L0288). For phosflow, the Fixable Viability Dye eFluor 780 (eBioscience, catalog number 65-0865-14) was used prior to detachment with trypsin and fixation with Cytofix (BD Biosciences, catalog number 554655) for 10 minutes at 37 °C. Cells were permeabilized with perm buffer III (BD Biosciences, catalog number 558050) for 30 minutes on ice and stained with pS6 pS235/pS236 (AF488, clone N7-548, BD Biosciences, catalog number 560434, 1:10 dilution or AF647, clone N7-548, BD

Biosciences, catalog number 560435, 1:10 dilution) for 1 hour at room temperature. Cells were then washed in FSB two times prior to acquisition.

2.4.3 TMEM192-HA staining

40,000 HAP1 cells were plated in 96-well plates the day prior to the experiment. Cells were detached and fixed and permeabilized using Cytofix/Cytoperm (BD Biosciences, catalog number 554714) for 20 minutes on ice. Cells were washed in FSB and then stained with an anti-HA AF488 antibody (Thermo Fisher, clone 16B12, catalog number A21287, 1:200 dilution) for 30 minutes on ice. HAP1 cells were washed with FSB twice prior to acquisition.

2.4.4 Autophagy flux

Autophagy was measured using the FlowCellect Autophagy LC3 Antibody-based Assay Kit (Millipore, catalog number FCCH100171) and according to the manufacturer's instructions with some adaptations. Specifically, cells were treated with 10 nM bafilomycin A1 (Merck, catalog number SML1661) for 2 hours. Cells were then washed in Hanks' Balanced Salt Solution (Thermo Fisher, catalog number 14175095) and detached with trypsin. Following centrifugation, cells were washed in 1 X assay buffer. Next, cells were resuspended in 1 X reagent B solution to permeabilize cells and spun down immediately. Kit-based 1 X LC3-FITC staining was performed at room temperature for 30 minutes. Cells were washed in assay buffer twice prior to resuspending in assay buffer for flow cytometric analysis. Autophagy flux was calculated as: (bafilomycin A1 – untreated) / untreated, as described previously (Alsaleh et al., 2020).

2.4.5 LDL uptake

For LDL internalization, 40,000 HAP1 cells were serum-starved overnight and stimulated with 10 µg/mL, 25 µg/mL LDL-BODIPY (Thermo Fisher, catalog number L3483) or unlabeled LDL (Thermo Fisher, catalog number L3486) for indicated time points. Cells were stimulated with 50 µM rapamycin (Cayman Chemical, catalog number 13346) for 2 hours, where indicated, prior to LDL treatment.

2.4.6 Phagocytosis of *E. coli* Bioparticles

For phagocytosis measurements, 40,000 HAP1 cells were plated the day prior to the experiment. Cells were kept under fed (DMEM + 10 % FCS) or starved (DMEM only) conditions. Cells were treated with pHrodo Red *E. coli* Bioparticles (Thermo Fisher, catalog number P35361, 100 µg/mL) for indicated time points according to the manufacturer's protocol. Cells were then trypsinized, washed in FSB two times and acquired on a flow cytometer.

2.4.7 Lysosomal function measurement

For lysosomal function, DQ-Ovalbumin was used to measure peptide cleavage. 40,000 HAP1 cells were plated the day prior to the experiment under fed or starved conditions. On the day of the experiment and where indicated, cells were treated with 25 µg/mL LDL for 1 hour under serum-starvation. Cells were treated with 10 µg/mL DQ-Ovalbumin (ThermoFisher, catalog number D12053) for 2 hours. Cells were washed in FSB two times prior to acquisition.

2.4.8 Neutral lipid flow cytometry

For cholesterol stimulation and BODIPY staining, macrophages were treated with 5 X cholesterol or HAP1 cells with 1 X cholesterol (Cholesterol lipid concentrate 250 X, Thermo

Fisher, catalog number 12531018) for 2 hours. Cells were stained with 1 µg/mL BODIPY 493/503 (Thermo Fisher, catalog number D3922) for 20 minutes at 37 °C. Cells were detached with trypsin, washed with FSB and re-suspended in it for acquisition.

2.4.9 Mitochondrial reactive oxygen species measurement

In order to measure mitochondrial ROS, the MitoSOX Red mitochondrial superoxide indicator (Thermo Fisher, catalog number M36008) was used according to the manufacturer's instructions. Specifically, 40,000 HAP1 cells were plated the day prior to the experiment. On the day of the experiment, cells were treated with 5 µM MitoSOX Red in Hanks' Balanced Salt Solution for 15 minutes at 37 °C. Cells were detached with trypsin and washed in Hanks' Balanced Salt Solution. Cells were re-suspended in FSB prior to acquisition.

All of the above flow cytometry experiments were run on an LSRFortessa, and data were analyzed using FlowJo (Treestar) software.

2.4.10 Flow cytometry of lysosomes

For flow cytometry analysis of lysosomes, the 'Lysosome Immunoprecipitation' protocol was adapted to 10 µL anti-HA magnetic beads, in order to capture more lysosomes per bead. Next, lysosomes with beads were washed in KPBS after homogenization and the lysosome extraction was stained with LysoTracker Deep Red (catalog number L12492, Thermo Fisher, 1:1000 dilution) for 1 hour. Lysosome samples were washed in FSB and acquired on a Cytek Aurora.

2.4.11 Sorted immune cells

In order to quantify the gene expression of *HPS1* and *HPS4* in immune cells using a qPCR, the cDNA of immune cells from a previously published study was used (Schulthess et al., 2019). Therefore, the immune cell sorting was not performed as part of this thesis. All cells were sorted using an Aria III flow cytometer (BD Biosciences). $CD14^+$ monocytes were obtained by CD14 bead enrichment, and subsequently differentiated into macrophages with 100 ng/mL M-CSF for 5 days.

2.5 Microscopy

100,000 macrophages were seeded on tissue culture slides (Sarstedt, catalog number 94.6170.802) and infected with GFP-*Salmonella* Typhimurium, MOI 1:20, for 1 hour. Cells were supplemented with 100 µg/mL gentamicin for 1 hour prior to fixation for 10 minutes at 37 °C in 4 % paraformaldehyde (Thermo Fisher, catalog number 28906).

Similarly, 80,000 HAP1 cells were stained with LysoTracker (Thermo Fisher, catalog number L12492, 1:2000) for 1 hour at 37 °C. Cells were stained with an anti-HA AF488 (Thermo Fisher, clone 16B12, catalog number A21287) antibody for 1 hour following fixation for 10 minutes at 37 °C in 4 % paraformaldehyde and permeabilization with 0.01 % Triton (Sigma, catalog number T8787) in PBS for 10 minutes at room temperature.

Cells were washed in PBS and sealed with vecta shield containing 4',6-diamidino-2-phenylindole (DAPI) (Vector labs, catalog number H-1200-10). Images were acquired on a Zeiss LSM 880 microscope using a 63 X/1.4 oil objective lens. Results were analyzed using Fiji (ImageJ). In order to quantify the state of bacteria, they were classed as GFP^+DAPI^+ (replicating/alive), $GFP^{dim}DAPI^+$ (being degraded) and GFP^-DAPI^+ (already degraded).

2.6 Seahorse assay

This assay was performed by Dr. Sumeet Pandey at the WIMM thanks to Prof. Alison Simmons providing access for this experiment. Oxygen consumption rate of the HAP1 cells was quantified on a XF96 extracellular flux analyzer (Seahorse Bioscience) using the Seahorse XF Cell Mito Stress kit (Agilent, catalog number 103015-100) and according to previous studies (Schulthess et al., 2019). The Seahorse XFe96 FluxPak (Agilent, catalog number 102601-100) was used and 50,000 cells were plated in Seahorse base media (Seahorse XF base medium (Agilent, catalog number 102353-100) in 12 replicates per condition with 1 % FBS, 1 mM glutamine (Sigma, catalog number 59202C-100ML) and 2 mM sodium pyruvate (Sigma, catalog number S8636-100ML). Plates were incubated in a CO_2-free incubator at 37 °C for 1 hour prior to acquisition on the Seahorse analyzer.

2.7 Patient phenotyping

2.7.1 Cytometry by time of flight (CyTOF) processing and analysis

The recruitment of patients, CyTOF experiment and analysis was performed by Dr. Louis Cohen at the Icahn School of Medicine at Mount Sinai. Prior to CyTOF, previously optimized antibody mixtures were prepared in cell staining media (CSM, Fluidigm). Whole blood was collected from patients into a sodium heparin vacutainer and processed within one hour. 1.2 ml of blood was mixed with 3 ml of Thaw-Lyse buffer (Smart Tube) and incubated for 10 minutes at room temperature. Samples were centrifuged and resuspended in 10 ml Thaw-Lyse buffer and incubated for 10 minutes at room temperature. Samples were again centrifuged and washed in CSM. Each sample was then resuspended in 800 µl of 1 X Barcode Perm Buffer (Fluidigm). Compatible Pd-barcodes were thawed, resuspended in 100 µL of 1 X Barcode Perm Buffer and added to the samples, followed by 30 minutes on ice and washing in CSM and pooled together. Each barcoded set of samples was resuspended in 100 µL CSM

containing 100 U ml^{-1} heparin (Sigma) to block non-specific MaxPar Antibody binding. A titrated surface antibody panel **(Table 2.5)** designed to allow identification of all major immune subsets was prepared in 100 µl CSM, filtered through a 0.1 µm spin filter (Amicon) and added to the sample. Samples were stained for 30 minutes on ice, washed with CSM and fixed with 2 % formaldehyde (Electron Microscopy Sciences) in PBS. The samples were washed and permeabilized with 1 ml ice-cold 100 % methanol. Samples were incubated on ice for 30 minutes (or transferred to −80 °C for long term storage), washed twice with CSM and resuspended in 100 µL CSM with heparin. Samples were washed with CSM and incubated for 30 minutes in 2 % formaldehyde in PBS containing 0.125 nM Ir nucleic acid intercalator (Fluidigm). The samples were washed and stored as pellets in CSM until CyTOF acquisition.

Immediately prior to acquisition, samples were washed with PBS and deionized water, counted and resuspended at a concentration of 1 million cells ml^{-1} in water containing a 1:20 dilution of EQ 4 Element Beads (Fluidigm). Samples were acquired on a CyTOF2 Mass Cytometer equipped with a SuperSample fluidics system (Victorian Airships) to facilitate bulk sample acquisitions. Samples were acquired at a flow rate of 0.045 mL min^{-1} and an event rate of < 400 events per second. CyTOF FCS files were concatenated and normalized using the bead-based normalization tool in the Helios software (Fluidigm), the barcoded samples were automatically deconvoluted and cross-sample doublets were filtered using a Matlab-based debarcoding tool (Glassberg et al., 2018) and the resulting files were uploaded to the Cytobank software (Chen and Kotecha, 2014). Cell events were identified as Ir191/193 positive events, and residual Ce140+ normalization beads were excluded.

All analyses of CyTOF samples were performed using Cytobank. High-dimensional analysis used to map the multi-dimensional data into 2-dimensional space include a self-organizing map (SOM, FlowSOM) and t-distributed stochastic neighbor embedding (SNE) (Van

Gassen et al., 2015). All high-dimensional analyses were performed on singlets and the data files were analyzed together to ensure cell clusters are stable across experiments. In all analyses, cells were clustered using surface antibody markers. For vi-distributed SNE and FlowSOM analysis all samples were set to equal sampling at 30,000 events per sample and run per default parameters for the software. For FlowSOM metacluster number was optimized to minimize metaclusters composed of a single cluster. Major immune populations were identified based on canonical marker expression patterns. Principal component analysis of FlowSOM metaclusters was performed using SPSSv26 based on eigenvalue > 1 without rotation. A heatmap of surface marker expression was generated using the heatmap.2 package in R 3.5.1.

Table 2.5. CyTOF antibodies used for immune phenotyping of peripheral blood. 35 surface markers were used to identify cell types in HPS-1 and control blood.

Channel	Target	Clone	Manufacturer	Catalog number
113In	CD57	HNK-1	Biolegend	359602
115In	CD45	HI30	Biolegend	304002
141Pr	Va7.2	3C10	Biolegend	351702
142Nd	CD19	REA675	Miltenyi	130-122-301
143Nd	CD45RA	REA562	Miltenyi	130-122-292
144Nd	CD62L	DREG-56	Biolegend	304802
145Nd	CD4	REA623	Miltenyi	130-122-283
146Nd	CD8	REA734	Miltenyi	130-122-281
147Sm	CD49d	9F10	Biolegend	304302
148Nd	CD16	REA423	Miltenyi	130-108-027
149Sm	CD127	A019D5	Fluidigm	3149011B
150Nd	CD1c	REA694	Miltenyi	130-122-298
151Eu	CD123	REA918	Miltenyi	130-122-297

152Sm	CD66B	REA306	Miltenyi	130-108-019
153Eu	PD-1	EH12.2H7	Biolegend	329926
154Sm	CXCR4	12G8	Biolegend	306512
155Gd	CD27	REA499	Miltenyi	130-122-295
156Gd	PD-L1	29E.2A3	Biolegend	329711
158Gd	BTLA	MIH26	Biolegend	344504
159Tb	CD103	Ber-Act8	Biolegend	350202
160Gd	CD14	REA599	Miltenyi	130-122-290
161Dy	CD56	REA196	Miltenyi	130-108-016
162Dy	CD64	10.1	Biolegend	305016
163Dy	CCR4	205410	R&D	MAB1567
164Dy	CCR9	L053E8	Biolegend	358902
165Ho	CCR6	G034E3	Biolegend	353402
166Er	CD25	REA570	Miltenyi	130-114-541
167Er	NKG2D	1D11	Biolegend	320810
168Er	CD3	REA613	Miltenyi	130-122-282
169Tm	Beta7	REA441	Miltenyi	130-122-309
170Er	CD38	REA671	Miltenyi	130-122-288
171Yb	CD161	HP-3G10	Biolegend	339902
172Yb	CD11b	M1/70	Biolegend	101202
173Yb	CXCR3	REA232	Miltenyi	130-108-022
174Yb	HLADR	REA805	Miltenyi	130-122-299
175Lu	ÇD29	TS2/16	Biolegend	303021

2.7.2 Olink serum proteomics

The recruitment of patients and serum proteomics was performed by Dr. Louis Cohen at the Icahn School of Medicine at Mount Sinai. The Olink assay was performed according to the protocol of the Olink Inflammation (Olink, 11-00866) panel, which consists of 92 paired oligonucleotide antibody-labeled probes (Olink, 2019).

1 µl of patient plasma was mixed with 3 µl Olink incubation mix and incubated at 4 °C overnight. The next day the Olink extension reagent mix was added to each well, vortexed, spun down and placed into a thermal cycler for pre-amplification over 1.5 hours. 2.8 µl from each well was then mixed with 7.2 µl of detection mix and placed on a 96-96 Dynamic Array Integrated Fluidic Circuit chip along with the oligonucleotide pairs. The chip was processed through the Fluidigm BioMark qPCR reader per the supplier's protocol. Sample data quality was normalized using Olink's Normalized Protein eXpression Manager software. A heatmap was generated using the heatmap.2 package in R and a principal component analysis plot using the online tool ClustVis (Metsalu and Vilo, 2015).

2.8 Transcriptomic analysis

2.8.1 RNA-seq of HPS-1 macrophages

2.8.1.1 Sample preparation

Monocyte-derived macrophages were infected at 1:10 MOI with *Salmonella* Typhimurium for 1 hour. Cells were then treated with 100 µg/mL gentamicin for 2 hours to kill extracellular bacteria. Next, cells were washed in PBS and frozen at -80 °C after adding 200 µL RLT (from RNeasy mini kit) with β-mercaptoethanol. Baseline samples were not infected and collected at the same time.

2.8.1.2 RNA extraction, library preparation and RNA-seq

RNA extraction was performed using RNeasy mini kit (QIAGEN, catalog number 74104) according to the manufacturer's protocol. Library preparation and RNA sequencing was performed at the Wellcome Trust Center for Human Genetics, University of Oxford. Total RNA quantity and integrity were assessed, using Quant-IT RiboGreen RNA Assay Kit (Thermo

Fisher, catalog number R11490), Tapestation 2200 (Agilent, catalog number G2964AA) and RNA Screentape (Agilent, catalog number 5067-5576). Purification of mRNA, generation of double stranded cDNA and library construction were performed using TruSeq® Stranded mRNA HT (Illumina, catalog number RS-122-2103) with minor modifications to manufacturer specifications. Minor modifications included the following custom primers (25 µM each) that were used for the PCR enrichment step:

Multiplex PCR primer 1.0

5'-AATGATACGGCGACCACCGAGATCTACACTCTTTCCCTACACGACGCTCTTCCGATCT-3'

Index primer

5'-

CAAGCAGAAGACGGCATACGAGAT[INDEX]CAGTGACTGGAGTTCAGACGTGTGCTCTTCCGATCT-3'

Indices were according to the eight base tags developed by the Wellcome Trust Center for Human Genetics (Lamble et al., 2013). Amplified libraries were analyzed for size distribution using the Agilent Tapestation 2200 D1000 (Agilent, catalog number 5067-5582). Libraries were quantified using Picogreen and relative volumes were pooled accordingly. Sequencing was performed as 75 bp paired end reads on a HiSeq4000 according to Illumina specifications.

2.8.1.3 Pre-processing

The pre-processing of the RNA-seq data was performed through a python 3.6 pipeline using ruffus and cgatcore (CGAT developers, 2019). Firstly, md5sums were checked following the file transfer protocol. For the initial quality control of samples, fastqc was performed on all fastq files and the files were aligned to hg38 using hisat2 (Kim et al., 2019; Pertea et al., 2016). Sam files were generated which were converted to bam files and bam files were merged

across the 3 lanes of sequencing using samtools (Li et al., 2009). Files were sorted using samtools and bam indexed. Next, samtools idxstat, samtools flagstat and picard AlignmentSummaryMetrics were performed for quality control purposes. Lastly, reads were counted using featureCounts (Liao et al., 2014) and MultiQC (Ewels et al., 2016) was performed on all of the results.

2.8.1.4 Differential expression analysis

DESeq2 was used to find differentially expressed genes and specifically the apeglm method (Love et al, 2018) in R 3.5.1 for Bayesian shrinking estimation. For principal component analysis plots, the variance stabilizing transformation method was used. Finally, using biomaRt, gene symbols were obtained and plotted for differential expression as volcano plots using ggplot2.

2.8.1.5 Pathway analysis

For pathway analysis, fast gene set enrichment analysis (fgsea) (Korotkevich, 2019) was performed using Hallmark pathways from the MSigDb (Broad Institute). For gene ontology analyzer for RNA-seq (GO-seq) analysis (Young et al., 2010), the TxDb hg38 database was used to calculate gene lengths in order to fit the probability weight function prior to performing go-seq on significantly differentially expressed samples ($p<0.05$ and $log2FC>1$).

2.8.1.6 Weighted Gene Correlation Network Analysis

For Weighted Gene Correlation Network Analysis the 'WGCNA' R package was used (Langfelder and Horvath, 2008) with parameters being softpower=10, minmodsize=30, merge tree dissimilarity=0.25. The results were exported and used in Cytoscape (Shannon et al.,

2003) with the ClueGO plugin (Bindea et al., 2009) for pathway analysis and visualization. Specifically, the network analyzer function in Cytoscape was used to determine the top hub genes in the green2 module. The parameters used were a p value < 0.05 and terms were searched for in gene ontology's cellular component, molecular function and biological process databases as well as KEGG pathways with the ClueGO plugin. A network of the top 200 hub genes of the green2 module was visualized. Heatmaps were made for selected hub genes using heatmap.2.

2.8.2 Publicly available datasets

2.8.2.1 STRING analysis of IBD risk loci and Mendelian diseases

In order to investigate overlaps between monogenic IBD genes and IBD risk candidate genes, the STRING network database for protein-protein interactions (Szklarczyk et al., 2017) was used. For monogenic IBD, a comprehensive review of Mendelian diseases presenting with IBD was employed (Uhlig, 2013). For polygenic IBD comparisons, three GWAS reports were used and the candidate genes that had been identified by two or more candidate gene approaches were chosen (de Lange et al., 2017; Jostins et al., 2012; Liu et al., 2015). Lastly, HPS1, HPS4, Rab32 and Rab38 were added to these lists to reveal potential protein-protein interactions.

2.8.2.2 Transcriptomics of small intestinal myeloid subsets

In order to visualize RNA-seq data from macrophage subsets in the small intestine, the EGAS00001002093 dataset (Bujko et al., 2018) was analyzed in R 3.5.1. Genes with low expression in fragments per kilo base per million mapped reads were filtered out of the analysis (sum>=0.5 in 10 samples) and gene expression of genes of interest were plotted using the pheatmap package in R.

2.8.2.3 Single cell RNA-seq of monocyte-derived macrophages

The GSE111049 dataset (Schulthess et al., 2019) was used to analyze the expression of the *HPS1, HPS4, Rab32* and *Rab38* genes in monocyte-derived macrophage subsets. Specifically, the Seurat pipeline was employed to visualize the clusters of cells (Butler et al., 2018; Stuart et al., 2019). Cells that had more than 15 % mitochondrial counts were excluded along with those that had more than 2,500 unique counts or fewer than 200 unique counts. Data was then normalized and scaled prior to dimensionality reduction with UMAP. The expression of *HPS1, HPS4, Rab32* and *Rab38* was then interrogated. The analysis was performed in R 3.5.1 using Seurat 3.0.1.

2.8.2.4 Single cell RNA-seq of peripheral blood mononuclear cells

The Seurat pipeline PBMC tutorial dataset was used for analysis as described above. The data used is the '3k PBMCs from a Healthy Donor' dataset, available through 10X Genomics. In total, this assay detected 2,700 cells, which were sequenced on an Illumina NextSeq 500.

2.8.2.5 Human protein atlas

The Human protein atlas (Human Protein Atlas, 2021) provides a platform to interrogate expression in different cell types, including blood cells (Uhlen et al., 2019). The Consensus dataset available on the platform is based on three datasets denoted HPA, GTEx and FANTOM5, which have been integrated and batch-corrected to provide a normalized expression value for each blood cell type (Uhlen et al., 2019). The results for the indicated genes (*HPS1, HPS4, RAB32* and *RAB38*) using the Consensus dataset presented in this thesis were saved from the Human Protein Atlas website.

2.8.2.6 HPS1 knockout epithelial cell transcriptomics

HPS1 knockout lung organoid epithelial cell adhesion molecule $(EPCAM)^+$ epithelial cells were FACS sorted to perform RNA-seq and identify changes compared to control cells (Strikoudis et al., 2019). These cells are derived from gene-edited induced pluripotent stem cells and differentiated into lung organoids. The GSE121999 dataset (Strikoudis et al., 2019) was used for epithelial differential expression in DESeq2, which was performed as described for HPS-1 patient macrophages. Similarly, fgsea and GO-seq analysis was executed following the HPS-1 patient macrophage RNA-seq pipeline.

2.9 Statistical analyses and figure preparation

Data analyses apart from transcriptomic and proteomic analyses (described above) were performed using GraphPad software (GraphPad software, Inc., San Diego, CA). Statistical significance was calculated using different statistical tests depending on the experimental situation and are stated in the figure legends. The graphical elements used to prepare illustrations have been obtained from Servier Medical Art under a creative commons license (Les Laboratoires Servier, 2021).

Briefly, for flow cytometry experiments, a ratio paired t-test on mean fluorescence intensity was used. For gentamicin protection assays, replicates were averaged for each experiment and a ratio paired t-test on colony forming units was performed. When the data were not paired for the flow cytometry and gentamicin protection assays, data were log-transformed and an unpaired t-test was used. For the *HPS1* and *HPS4* qPCR, a Tukey multiple comparisons test was utilized on log-transformed data. For the Rab32 knockdown qPCR, a paired t-test was performed. In order to quantify the ratio of mTOR to LAMP2 using Western

blotting, a paired t-test was used on ratio data. Similarly, autophagy flux significance was determined using a paired t-test on the flux calculation. In order to quantify the bacterial infection stages in macrophages, an unpaired t-test was performed. The pS6-to-GAPDH Western blot densitometry was tested for significance using an unpaired t-test on the ratio data.

For mass cytometry, populations were compared with an unpaired t-test with Bonferroni-Dunn correction for multiple comparisons. On the other hand, for the $CD14^+$ monocyte quantification on manual gating, an unpaired t-test was used. For the Olink proteomics analysis, the Benjamini, Krieger and Yekutieli multiple nonparametric t-test was performed. Results with a $p < 0.05$ were considered significant (*$p < 0.05$, **$p < 0.01$, ***$p < 0.001$, ****$p < 0.0001$).

2.10 Data access

The bulk RNA-seq dataset of HPS-1 and control macrophages have been deposited under EGAD00001006978 at the European Genome-Phenome Archive. The proteomics data have been deposited to the ProteomeXchange Consortium via PRIDE with the identifier PXD024435 and 10.6019/PXD024435.

Chapter 3 - HPS-1-associated gene signatures and pathways

3.1 Introduction

IBD is a complex, multifactorial disorder that results in intestinal inflammation. Over the last few years, transcriptomics and single cell analyses have propelled our understanding of the mechanisms underlying IBD. Single cell analyses of gastrointestinal samples have handed us an innovative understanding of epithelial cells (Parikh et al., 2019), fibroblasts (Kinchen et al., 2018) and immune cells in Crohn's disease (Martin et al., 2019) and ulcerative colitis (Boland et al., 2020; Corridoni et al., 2020; Smillie et al., 2019). These investigations highlight the complex nature of disease and the need for integrative analyses to disentangle mechanisms.

Complementary to these analyses, Mendelian diseases that present with inflammation in the gastrointestinal tract can provide snapshots into pathways that are relevant for IBD. One such disorder is Hermansky-Pudlak Syndrome type 1. HPS-1 is a lysosome-related organelle disorder that can result in intestinal inflammation and lung fibrosis (Gahl et al., 1998). However, the immune pathology in HPS-1 is not clear and unbiased approaches are required to examine the dysregulation in cell types and pathways.

In the context of HPS-associated lung fibrosis, a lung organoid epithelial transcriptomic dataset revealed that IL-11 plays a major role in the fibrotic phenotype of HPS1 and HPS4 knockout organoids (Strikoudis et al., 2019). Importantly, a double knockout of HPS4 and IL11 could rescue the profibrotic signature in organoids. Therefore, transcriptomic experiments have provided valuable tools to chart mechanisms in HPS1-deficient lung epithelial cells. Nevertheless, identifying inflammation biomarkers and triggers can facilitate

the mechanistic understanding of HPS-1 pathology. More broadly, these findings, coupled with functional experiments, can provide puzzle pieces to understand common IBD.

The aims of this chapter are three-fold. Firstly, I aim to identify the immune cell types harboring the highest expression of the BLOC-3 pathway genes. Secondly, to investigate the gene expression differences between HPS-1 patients and controls in relevant cell types. Thirdly, to understand whether pathway dysregulations are shared among cell types as a validation by using publicly available RNA-seq datasets.

3.2 Results

3.2.1 IBD risk loci and monogenic diseases with IBD do not overlap with the BLOC-3 pathway

Current knowledge into IBD risk loci allows the generation of protein interaction networks on platforms including STRING (Szklarczyk et al., 2017). I investigated potential overlaps between Mendelian diseases with IBD and IBD risk loci in order to identify relevant pathways. Specifically, I used genes that had been identified as associated with polygenic IBD (de Lange et al., 2017; Jostins et al., 2012; Liu et al., 2015; Uhlig, 2013). I plotted genes implicated in IBD using the STRING network database and included HPS1 and HPS4, which form BLOC-3, along with the effectors of this complex, Rab32 and Rab38, to identify interactions with other IBD nodes **(Figure 3.1A)**. HPS1, HPS4, Rab32 and Rab38 separate from other IBD risk loci. Since HPS-1 and HPS-4 are monogenic diseases that can present with IBD, I used the STRING network database to also visualize relationships between monogenic IBD proteins **(Figure 3.1B)**. I found that HPS1, HPS4, Rab32 and Rab38 do not cluster with other monogenic diseases with IBD. These findings highlight the yet to be explored roles for these proteins in intestinal homeostasis.

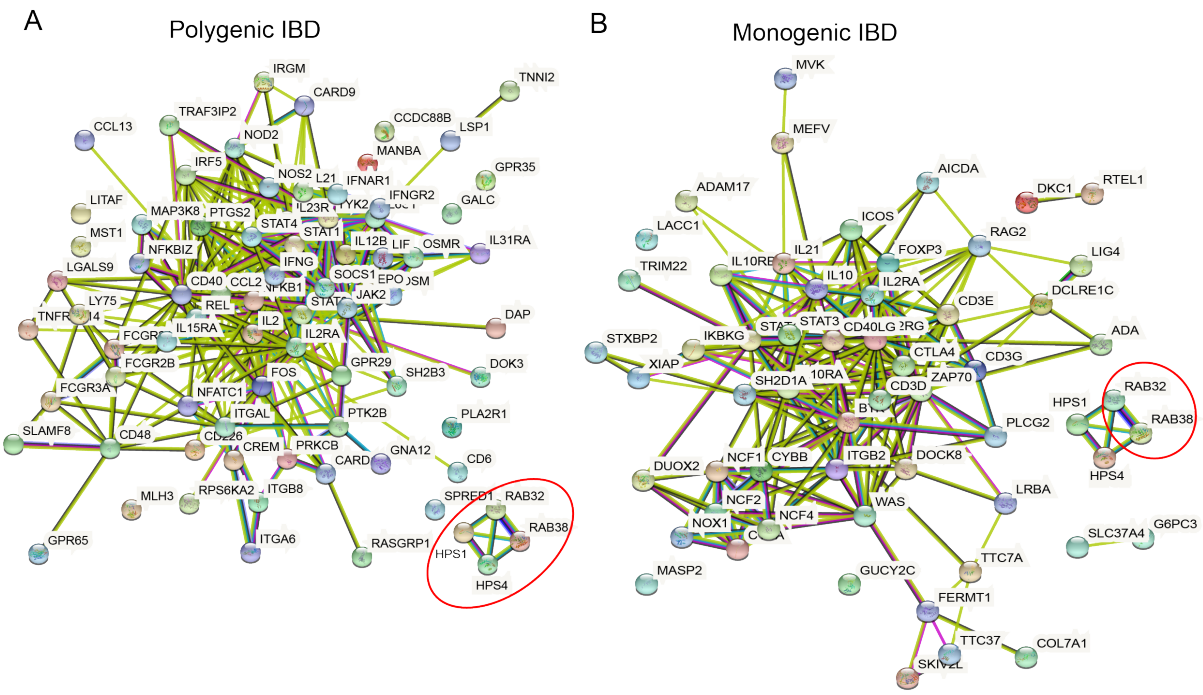


Figure 3.1. Polygenic IBD risk loci and monogenic diseases with IBD do not overlap with the BLOC-3 pathway. Indicated IBD risk genes and HPS genes from A) polygenic IBD and B) monogenic IBD. Using STRING, the interactions between IBD risk genes and HPS1, HPS4, Rab32 and Rab38 were visualized, with a probability of interaction = 0.4. Proteins in red circles have been added to the polygenic or monogenic lists for purposes of comparison. The different colors of the interaction lines indicate the source of information regarding the interaction. Known interactions are in pink for experimental evidence and in light blue for curated database information. Predicted interactions are denoted as green (within the gene neighborhood), red (gene fusions) or dark blue (gene co-occurrence). Interaction data from text mining is in lime, co-expression in black and protein homology in lilac.

3.2.2 BLOC-3 is strongly expressed in myeloid cells

3.2.2.1 BLOC-3 pathway expression in the blood

HPS-1 and HPS-4 patients presenting with intestinal inflammation can have granuloma formation and lipid-laden macrophages (O'Brien et al., 2021). Granulomata are characterized by an aggregation of macrophages, which can either fuse or become foam cells (Petersen and Smith, 2013; Ramakrishnan, 2012). I investigated the expression of *HPS1* and *HPS4* through

qPCR on healthy control immune cell types, including CD8⁺ T cells, naïve and memory CD4⁺ T cells, CD19⁺ B cells, CD1c⁺ DCs, CD56⁺ natural killer cells, CD14⁺ monocytes and monocyte-derived macrophages. I found that macrophages expressed the highest levels of *HPS1* and *HPS4* compared to other immune cells **(Figure 3.2)**. This result fits with the granuloma formation in patients, which may be driven by dysregulated macrophages.

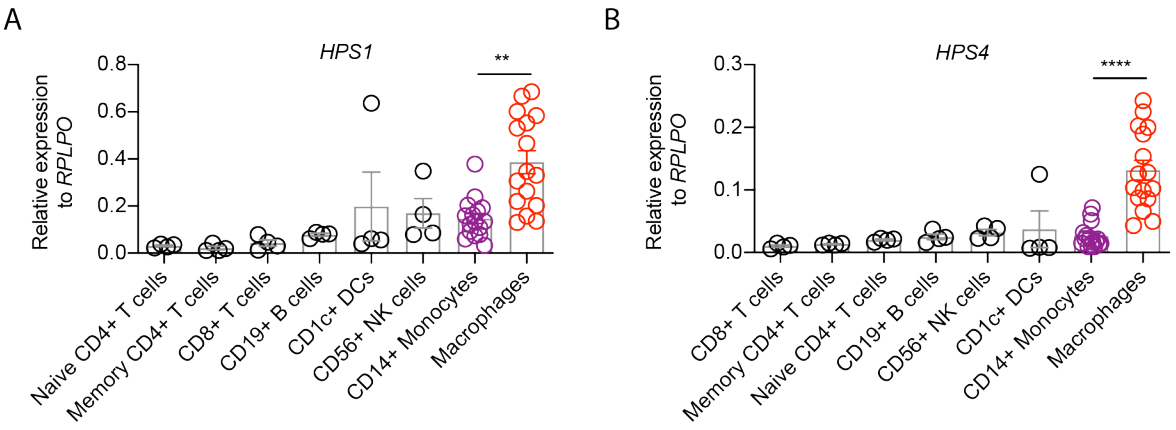


Figure 3.2. Macrophages express high levels of *HPS1* and *HPS4*. Immune cells from peripheral blood of healthy controls. Specifically, cells were sorted to obtain naïve CD4⁺ T cells, memory CD4⁺ T cells, CD8⁺ T cells, CD19⁺ B cells, CD1c⁺ dendritic cells, CD56⁺ NK cells and CD14⁺ monocytes. CD14⁺ monocytes were differentiated into macrophages. A) *HPS1* and B) *HPS4* expression were quantified in different immune cell types (n=4-16). **p<0.01, ****p<0.0001; statistical significance was determined using a Tukey multiple comparisons test on log-transformed data. NK: natural killer, DC: dendritic cell.

Since the above gene expression investigations include PBMCs and macrophages but not granulocytes, I used the Consensus dataset available on the Human Protein Atlas (Human Protein Atlas, 2021) to examine the expression of *HPS1, HPS4, RAB32* and *RAB38* in a broad range of hematopoietic cells **(Figure 3.3)**. Eosinophils expressed *HPS1* to a large extent, while basophils expressed the highest amount of *HPS4* and *RAB32*. On the other hand, *RAB38* expression was mostly absent in cell types other than natural killer cells. These expression

profiles suggest that *HPS1, HPS4* and *RAB32*, and particularly *HPS1* and *RAB32*, are expressed consistently in monocyte subtypes and myeloid dendritic cells. However, monocyte-derived macrophages were not part of this dataset.

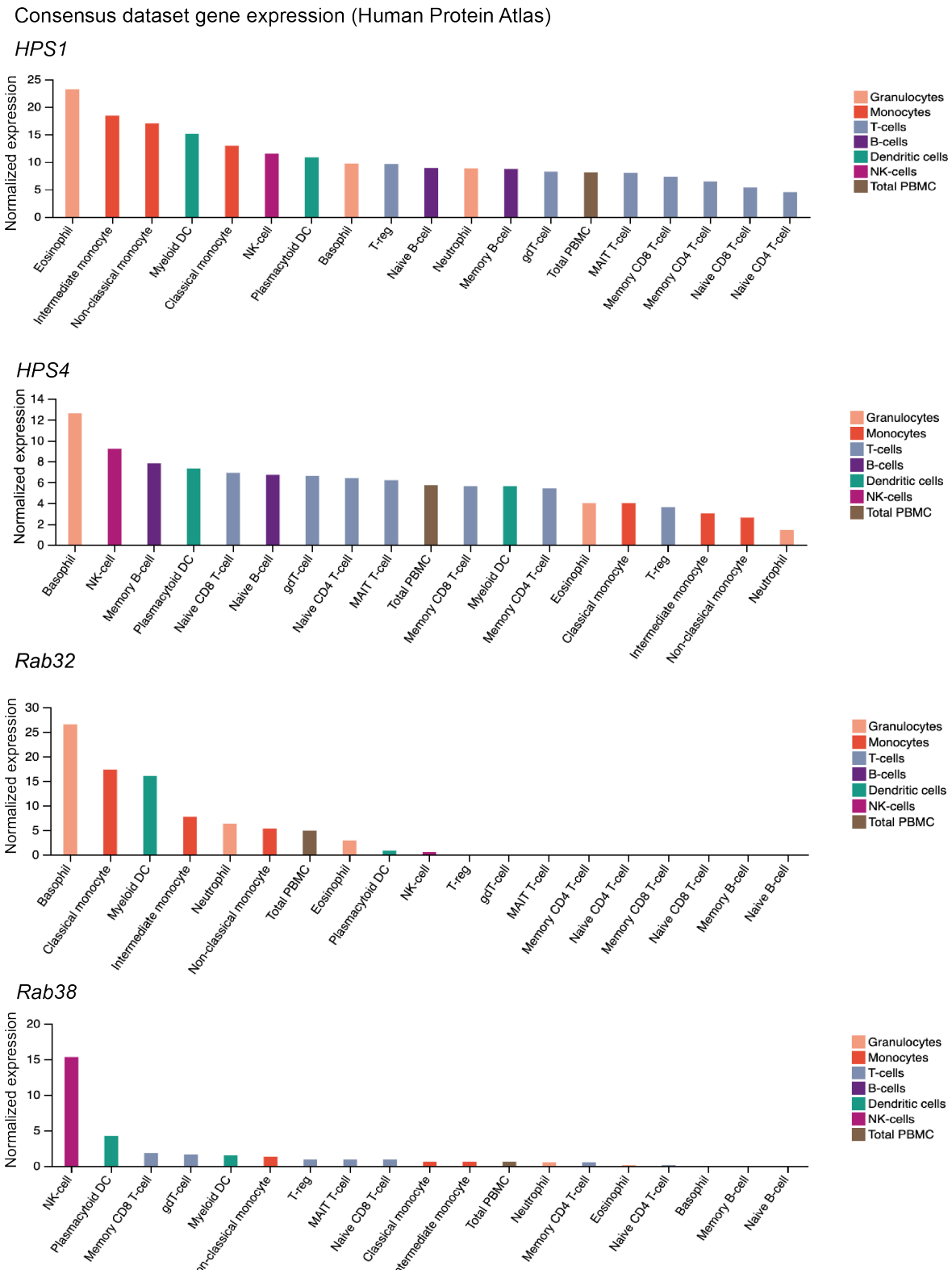


Figure 3.3. BLOC-3 pathway expression in blood cells reveals a myeloid and granulocyte signature. Using the Human Protein Atlas online tool, the normalized gene expression of *HPS1, HPS4, RAB32* and *RAB38* in different blood cell types was examined.

Single cell sequencing of peripheral blood cells allows the visualization of different cell subsets and their expression of specific genes. I used a peripheral blood dataset to examine the expression of *HPS1, HPS4, RAB32* and *RAB38*. Firstly, the standard deviation explained by each principal component is shown **(Figure 3.4A)**. Dimensionality reduction of peripheral blood cells identifies two monocyte clusters and a dendritic cell cluster **(Figure 3.4B)**. I found that *RAB32* in particular was highly expressed in monocytes **(Figure 3.4C)**. The expression pattern of *HPS1* and *HPS4* was dispersed and very low for *RAB38* in all immune cell subsets. It is possible that *RAB32* therefore defines and restricts the use of the BLOC-3 pathway to certain cell types, such as myeloid cells.

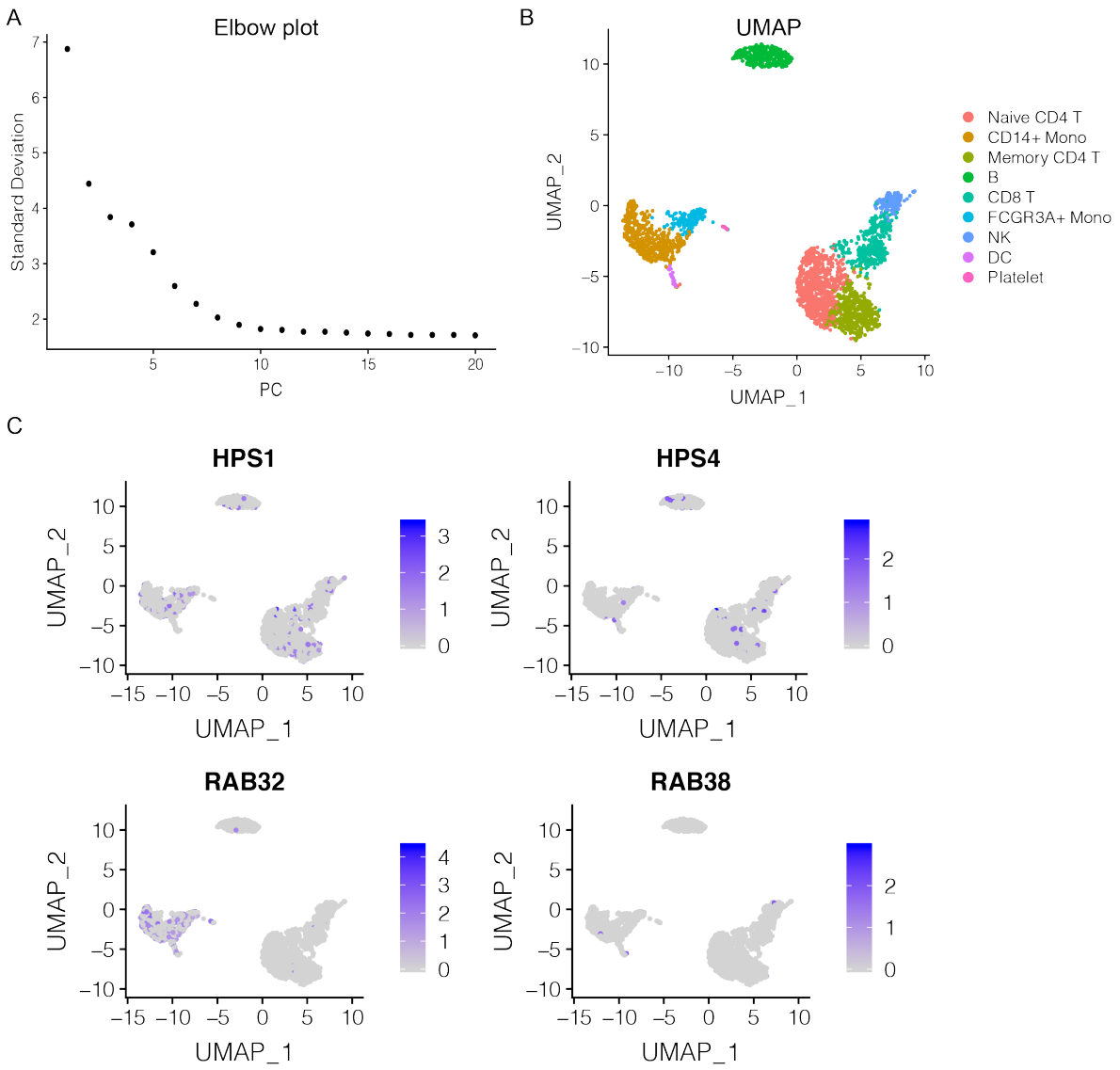


Figure 3.4. Single cell RNA-seq of peripheral blood reveals monocytes as highly expressing *RAB32*. Single cell RNA-seq analysis (PBMC 3k dataset from 10X Genomics) of peripheral blood mononuclear cells (PBMCs). A) Elbow plot showing the standard deviation in each principal component (PC) of PBMCs. B) Uniform Manifold Approximation and Projection (UMAP) was used for dimensionality reduction and cell subsets were annotated. C) Gene expression of *HPS1, HPS4, RAB32* and *RAB38*.

3.2.2.2 BLOC-3 myeloid expression is homogeneous in the small intestine

Since myeloid cells appeared to be the strongest *HPS1* and *RAB32* expressing cell types, I explored a small intestinal myeloid transcriptomic dataset in search of the gene

expression profile of the BLOC-2 (*HPS3, HPS5, HPS6*), BLOC-3 (*HPS1, HPS4, RAB32, RAB38*) pathways as well as *AP3B1* and *RAB9A,* which HPS4 interacts with. Across myeloid subsets, *HPS1* and *RAB32* had the most similar expression level and pattern and clustered together **(Figure 3.5)**. Overall, the expression of these pathways across the myeloid compartment was uniform, arguing against a subset-specific expression or utilization of these pathways.

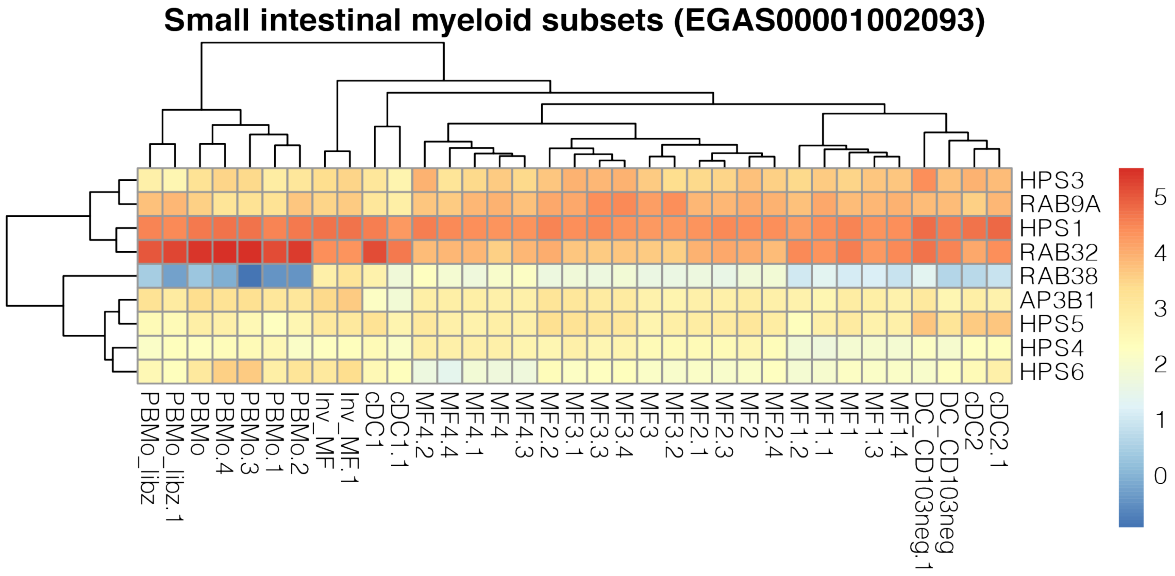


Figure 3.5. Small intestinal myeloid dataset reveals homogeneous HPS-related gene expression. Heatmap of HPS gene expression in fragments per kilo base per million mapped reads across myeloid subtypes from the EGAS00001002093 dataset.

I examined whether specific Rab GTPases had higher expression in the myeloid compartment of the small intestine. The Rab GTPase gene expression in all myeloid cell types was fairly uniform **(Figure 3.6)**. *RAB32* was one of the highest expressed Rab GTPases in myeloid cells. Based on these expression levels, the Rab GTPase network may act in a similar manner and regulation pattern across these cell types.

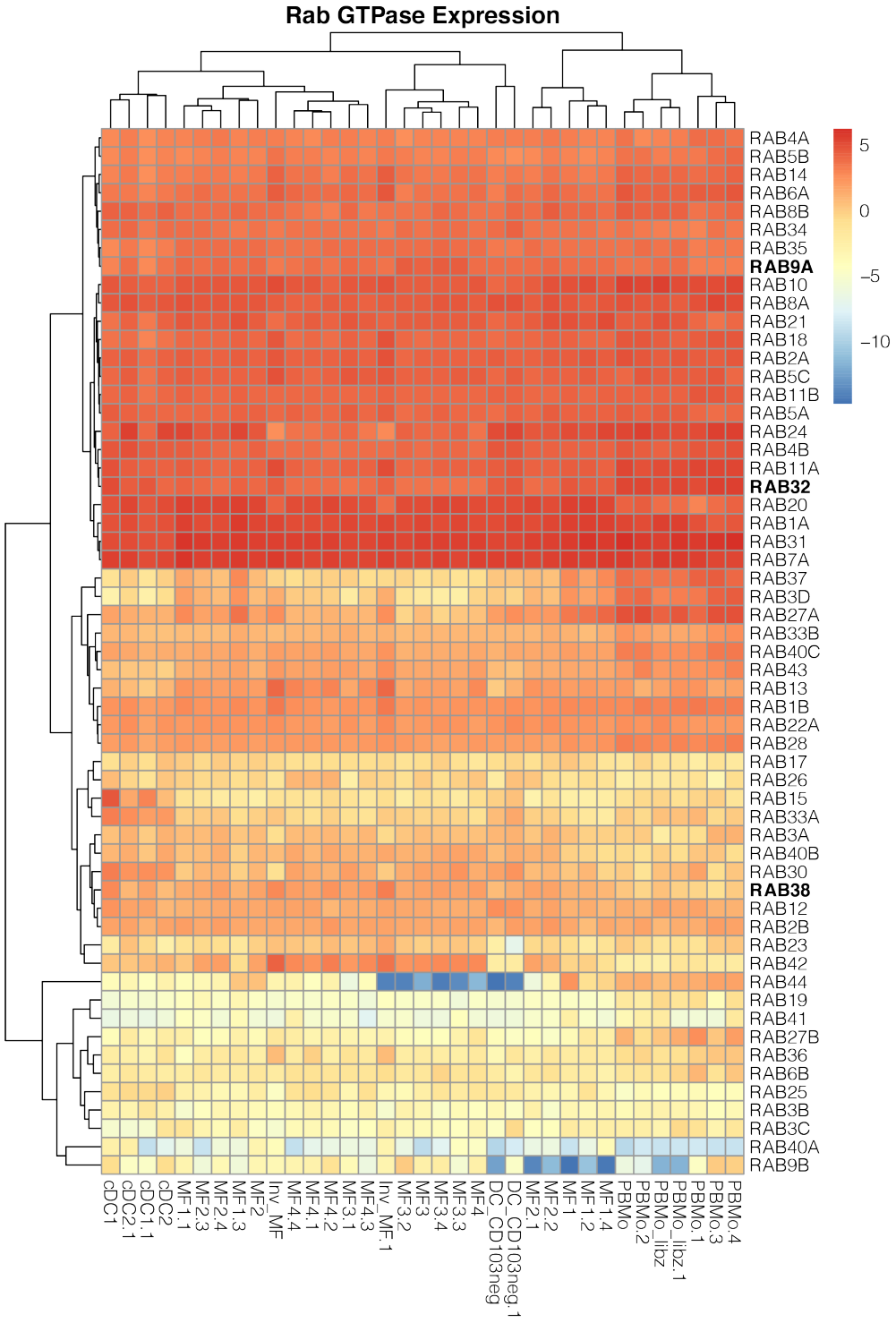


Figure 3.6. Rab GTPase gene expression in small intestinal myeloid cells is uniform. Heatmap of Rab GTPase gene expression in fragments per kilo base per million mapped reads across small intestinal myeloid subtypes from the EGAS00001002093 dataset.

3.2.2.3 Macrophage single cell RNA-seq shows uniform expression of BLOC-3 across subsets

While I did not find any appreciable differences between myeloid cell types in terms of *HPS1, HPS4, RAB32* and *RAB38* gene expression, I hypothesized that there may be expression changes within macrophage subsets. I used the publicly available GSE111049 dataset and visualized the deviation explained by the principal components in the dataset for one macrophage donor **(Figure 3.7A)**. I performed dimensionality reduction of the dataset and found six clusters of macrophages **(Figure 3.7B)**. Plotting the expression of the *HPS1, HPS4, RAB32* and *RAB38* genes shows that the expression was homogeneous across macrophage clusters **(Figure 3.7C)**. BLOC-3 pathway genes are expressed throughout macrophage subsets, with *RAB38* having very low levels of expression.

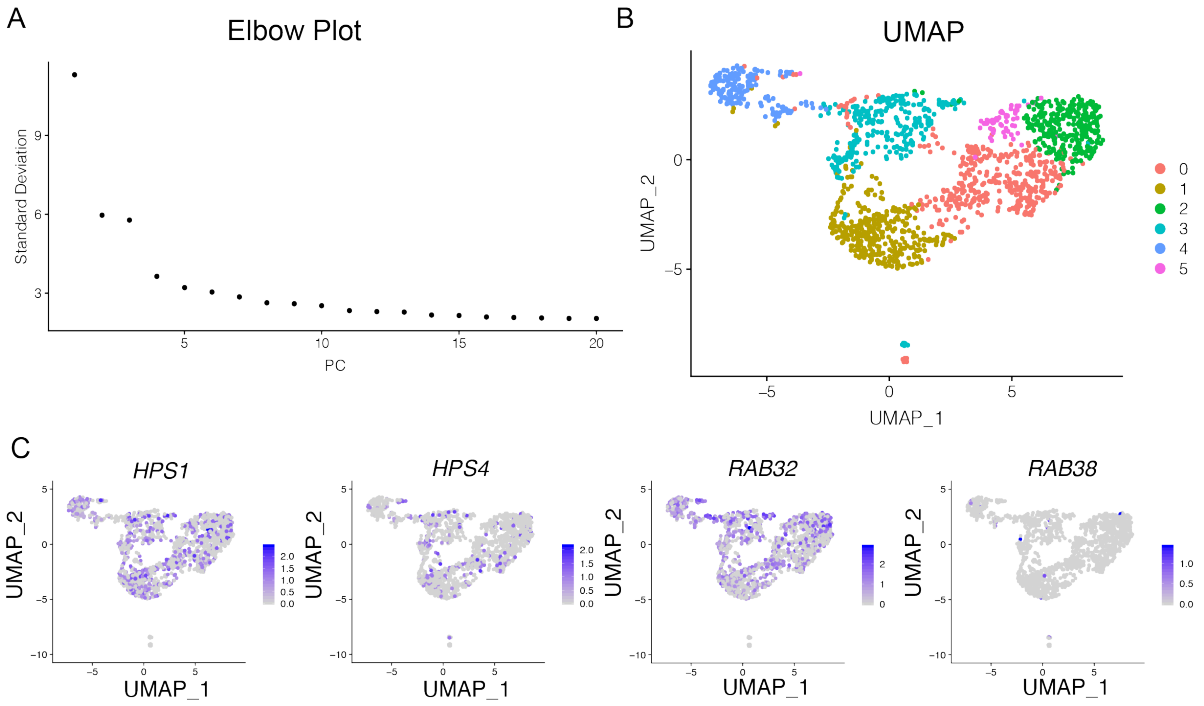


Figure 3.7. Macrophage single cell RNA-seq shows a homogeneous expression of the BLOC-3 pathway genes. Single cell RNA-seq analysis (GSE111049) of monocyte-derived macrophages differentiated in the presence of M-CSF for 5 days. A) Standard deviation in each principal component (PC) of macrophages. B) UMAP was used for dimensionality reduction of macrophage clusters. C) Gene expression of *HPS1, HPS4, RAB32* and *RAB38* across macrophage subsets.

In this section I explored the expression of the BLOC-3 pathway in different immune cell types to focus on relevant cell types for further investigation. BLOC-3 pathway genes are highly expressed in the myeloid compartment, with *RAB32* having the highest expression levels. The expression of the BLOC-3 pathway appeared uniform across macrophage subsets, suggesting that it does not have a subset-specific role.

3.2.3 HPS-1 patient macrophage transcriptomics

In order to understand the underlying transcriptional profile of macrophages in disease, we performed RNA-seq in HPS-1 patient macrophages at steady state and during infection with *Salmonella enterica* serovar Typhimurium (hereafter *Salmonella* Typhimurium). The patient samples were obtained through a collaboration with Dr. Louis Cohen at the Icahn School of Medicine, Mount Sinai, and the sequencing was performed at the Wellcome Trust Center for Human Genetics in Oxford.

We used 4 healthy donors and 4 HPS-1 patients for our RNA-seq analysis. Specifically, we infected macrophages with *Salmonella* Typhimurium for 3 hours or left the cells untreated **(Figure 3.8)**. Subsequently, we performed paired-end polyA-enrichment RNA-seq and I used differential expression analysis, pathway analysis and weighted gene correlation network analysis to reveal genes and pathways that are altered in the disease state.

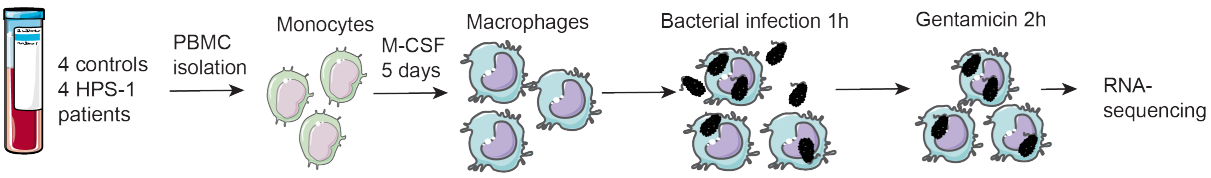


Figure 3.8. Experimental design for HPS-1 macrophage RNA-seq. Patient and healthy donor PBMCs were extracted and monocytes were differentiated into macrophages for 5 days in

the presence of M-CSF. Macrophages were infected with *Salmonella* Typhimurium and extracellular microbes were eliminated with gentamicin. RNA was extracted and RNA-sequencing was performed.

3.2.3.1 Principal Component Analysis

Firstly, I used principal component analysis to examine whether HPS-1 patient macrophages have a globally different transcriptional pattern compared to controls. At both baseline and during infection, HPS-1 patient macrophages cluster closer to each other **(Figure 3.9A and C)**. I also plotted the variance explained by each principal component and found that 5 principal components explain at least 10 % of the variance each, indicating that the samples are heterogeneous and/or that there may be additional transcriptional drivers **(Figure 3.9B and D)**.

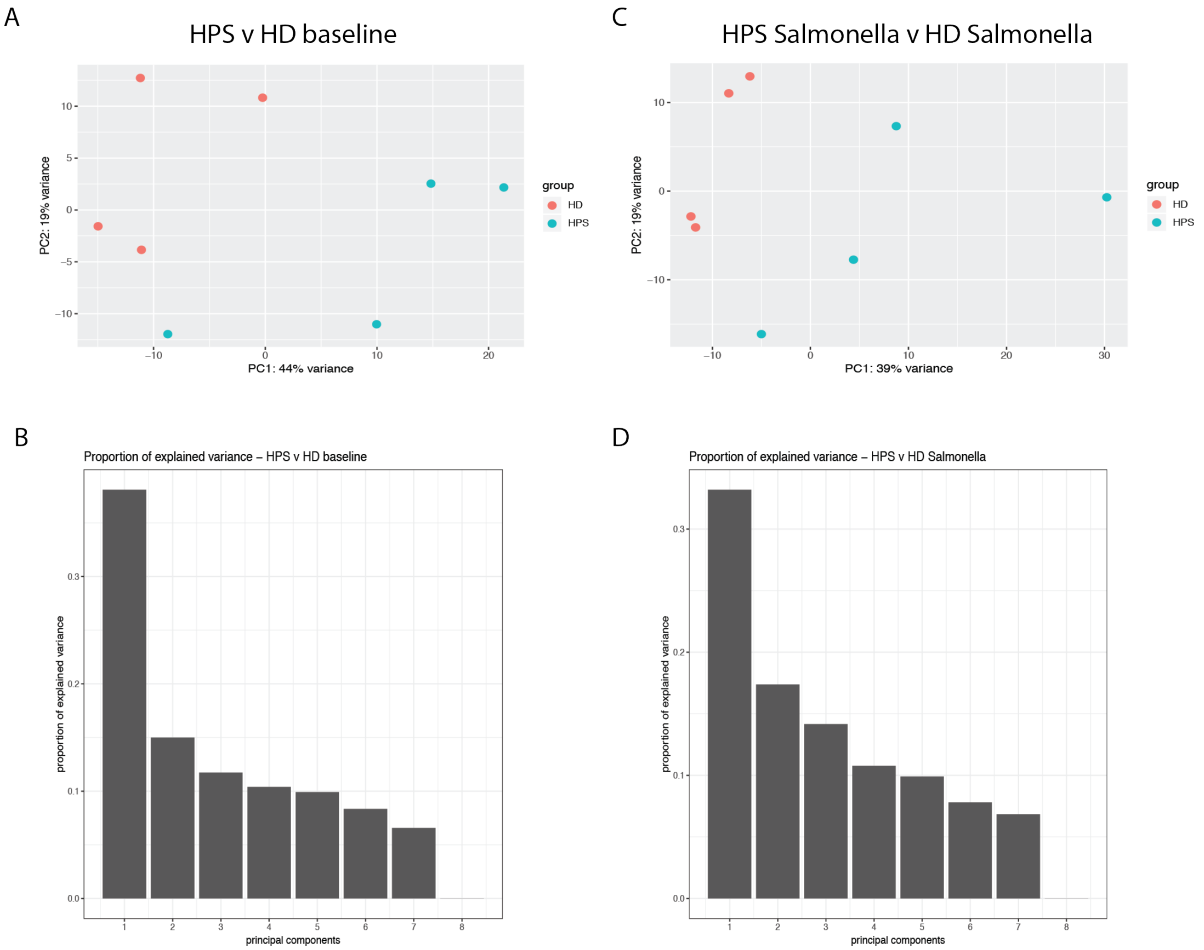


Figure 3.9. Principal component analysis of HPS-1 and control macrophages. Principal component analysis was performed on variance stabilization transformed data. A) Principal component analysis of HPS-1 versus HD. B) Principal component variance explained by different principal components for HPS-1 versus HD. C) Principal component analysis of HPS-1 *Salmonella* Typhimurium versus HD *Salmonella* Typhimurium. D) Principal component variance explained by different principal components for HPS-1 *Salmonella* Typhimurium versus HD *Salmonella* Typhimurium. HD: healthy donor.

3.2.3.2 Differential expression analysis uncovers an inflammatory gene signature in HPS-1

I set out to identify differentially expressed genes between HPS-1 macrophages and healthy donor macrophages at baseline **(Figure 3.10A)**. *HPS1* is upregulated in HPS-1 macrophages compared to controls, potentially as a feedback mechanism since the protein is

defective. HPS-1 macrophages have an upregulation of genes including the chemokine *CCL2* and *PTGS2,* which encodes the prostaglandin E2-producing enzyme prostaglandin-endoperoxide synthase 2 (Lin et al., 2018).

I also examined differential expression in macrophages during *Salmonella* Typhimurium infection **(Figure 3.10B)**. *TNF* and *OSM* are upregulated in patient HPS-1 macrophages compared to healthy controls, which is also observed in IBD (West et al., 2017). Furthermore, there is an increase in the gene expression of *NLRP3, NOD2, RGS1* and *CCR7*. Variants in *NOD2* (Inohara et al., 2003; Ogura et al., 2001) and *NLRP3* (Villani et al., 2009) predispose to Crohn's disease and act in the context of innate immunity to protect against pathogens. At the same time, C-C chemokine receptor type 7 (CCR7), whose mRNA levels are higher in HPS-1, is involved in homing to the mesenteric lymph node (Jang et al., 2006). The regulator of G-protein signaling-1 (RGS1) protein is increased in atherosclerosis, mediating the accumulation of macrophages in the disease (Patel et al., 2015). Thioredoxin interacting protein is a negative regulator of mTOR activation, measured through S6 phosphorylation (Jin et al., 2011), and *TXNIP* mRNA levels are dampened in HPS-1 macrophages during infection.

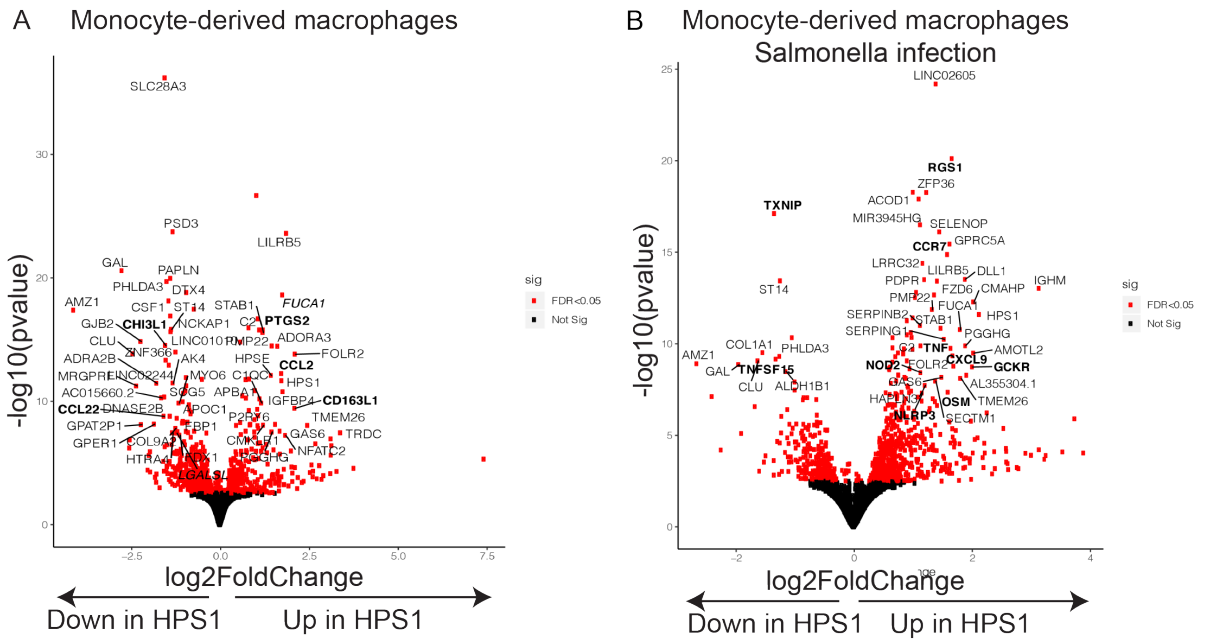


Figure 3.10. Differential gene expression between HPS-1 patient and control macrophages. A) Differential expression between HPS-1 and control macrophages. B) Differential expression between HPS-1 patient macrophages and control macrophages following *Salmonella* Typhimurium infection. FDR: false discovery rate; sig: significance.

3.2.3.3 Pathway analysis

After performing differential gene expression, I used these findings to delineate dysregulated pathways in HPS-1. I initially used fast gene set enrichment analysis (fgsea) to evaluate the pathways that may be affected based on differentially expressed genes. The top upregulated hallmark pathway at steady state was allograft rejection, which may point to macrophage activation, and the most downregulated pathway was oxidative phosphorylation **(Figure 3.11)**. Similarly, in the *Salmonella* Typhimurium-infected setting, IFN-γ response was highly amplified, whereas oxidative phosphorylation was the top downregulated pathway **(Figure 3.12)**. Both steady state and infected macrophages therefore have a high degree of similarity and point to an important decrease in oxidative phosphorylation, highlighting deregulated bioenergetics in HPS-1 macrophages.

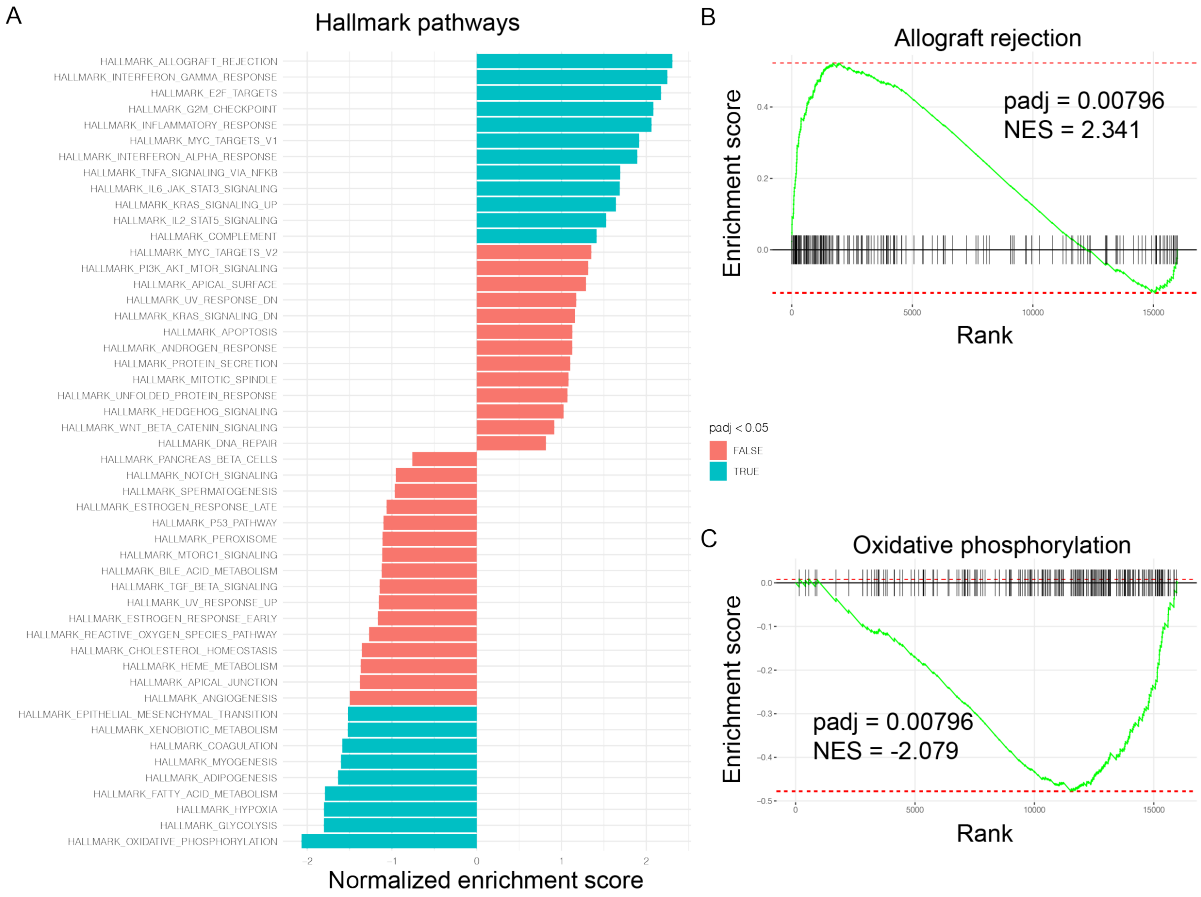


Figure 3.11. HPS-1 and control macrophage gene set enrichment analysis. A) Hallmark pathway gene set enrichment analysis identifies significantly increased or decreased pathways in HPS-1 macrophages. B) Top increased and C) decreased pathways shown with adjusted p value (padj) and normalized enrichment score (NES).

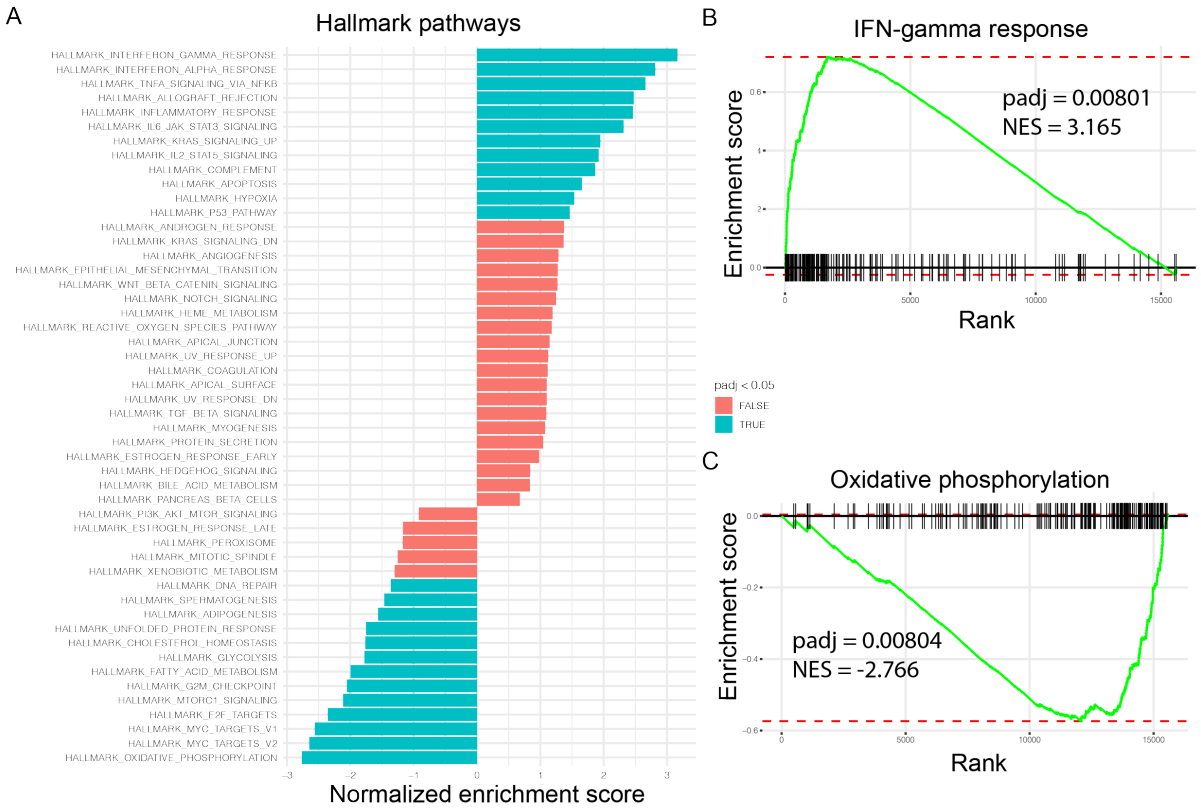


Figure 3.12. *Salmonella* Typhimurium-infected macrophage gene set enrichment analysis. A) Hallmark pathway gene set enrichment analysis identifies significantly increased or decreased pathways in HPS-1 infected macrophages. B) Top increased and C) decreased pathways shown with adjusted p value (padj) and normalized enrichment score (NES).

In addition, gene ontology analyzer for RNA-seq (GO-seq), which takes gene length into account to regress out the probability that a gene is differentially expressed based on its gene length (Young et al., 2010), was used. The molecular function terms that are overrepresented in the HPS-1 macrophages include G-protein coupled receptor signaling, MHC complexes, low-density lipoprotein and insulin-like growth factor binding **(Figure 3.13A)**. On the other hand, following *Salmonella* Typhimurium infection, MHC binding and cytokine terms predominate **(Figure 3.13B)**. Overall, these pathway analyses using fast gene set enrichment analysis hint at oxidative phosphorylation downregulation, while the GO-seq analyses accentuate a change in metabolism and cytokine activity.

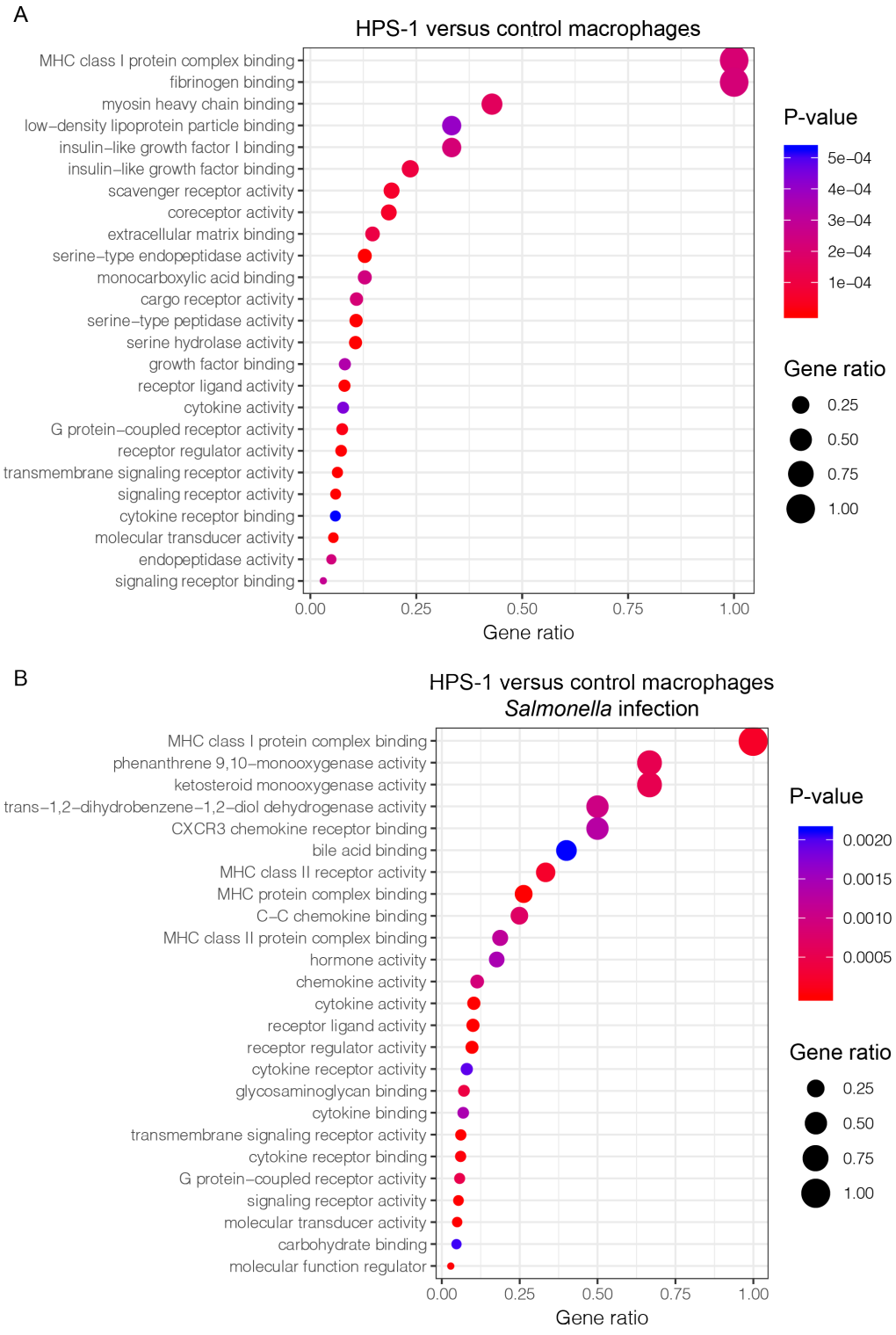


Figure 3.13. Gene ontology analysis of HPS-1 and control macrophages. A) Gene ontology molecular function terms were used to compare HPS-1 and control at baseline and B) after *Salmonella* Typhimurium infection. Gene ratio: proportion of differentially expressed genes in a given pathway to total genes in that pathway.

3.2.3.4 Correlation network analysis reveals an LDL metabolism module in HPS-1

I created a co-expression network to identify modules (sets of genes) that are associated with HPS-1. Weighted Gene Correlation Network Analysis is a correlative technique to pinpoint co-expression modules associated with disease and can help in identifying modules and module hub genes (Langfelder and Horvath, 2008). Module hub genes are centrally located genes within modules, and are likely key drivers of the co-expression module.

I visualized the modules and disease trait as a dendrogram in order to pinpoint the disease trait clustering with a set of genes **(Figure 3.14A)**. The disease trait for HPS-1 was most highly correlated with a module termed green2. There was a high correlation between the importance of the genes in green2 for HPS-1 and the membership of the genes in the green2 module **(Figure 3.14B)**.

The green2 module results were exported and Cytoscape (Shannon et al., 2003) was used to visualize this particular highly correlated disease-module network. The top terms in the green2 module hub genes are predominantly LDL-associated terms **(Figure 3.14C)**. Changes in the response to fatty acids also emerged in this module. The hub genes contributing to the LDL module were plotted as a heatmap, highlighting the differences in LDL-associated genes between HPS-1 and control macrophages **(Figure 3.14D)**. In summary, the correlation network analysis emphasizes an LDL signature, with implications for altered lipid metabolism in HPS-1 macrophages, which may contribute to the ceroid lipofuscin accumulation in the disease.

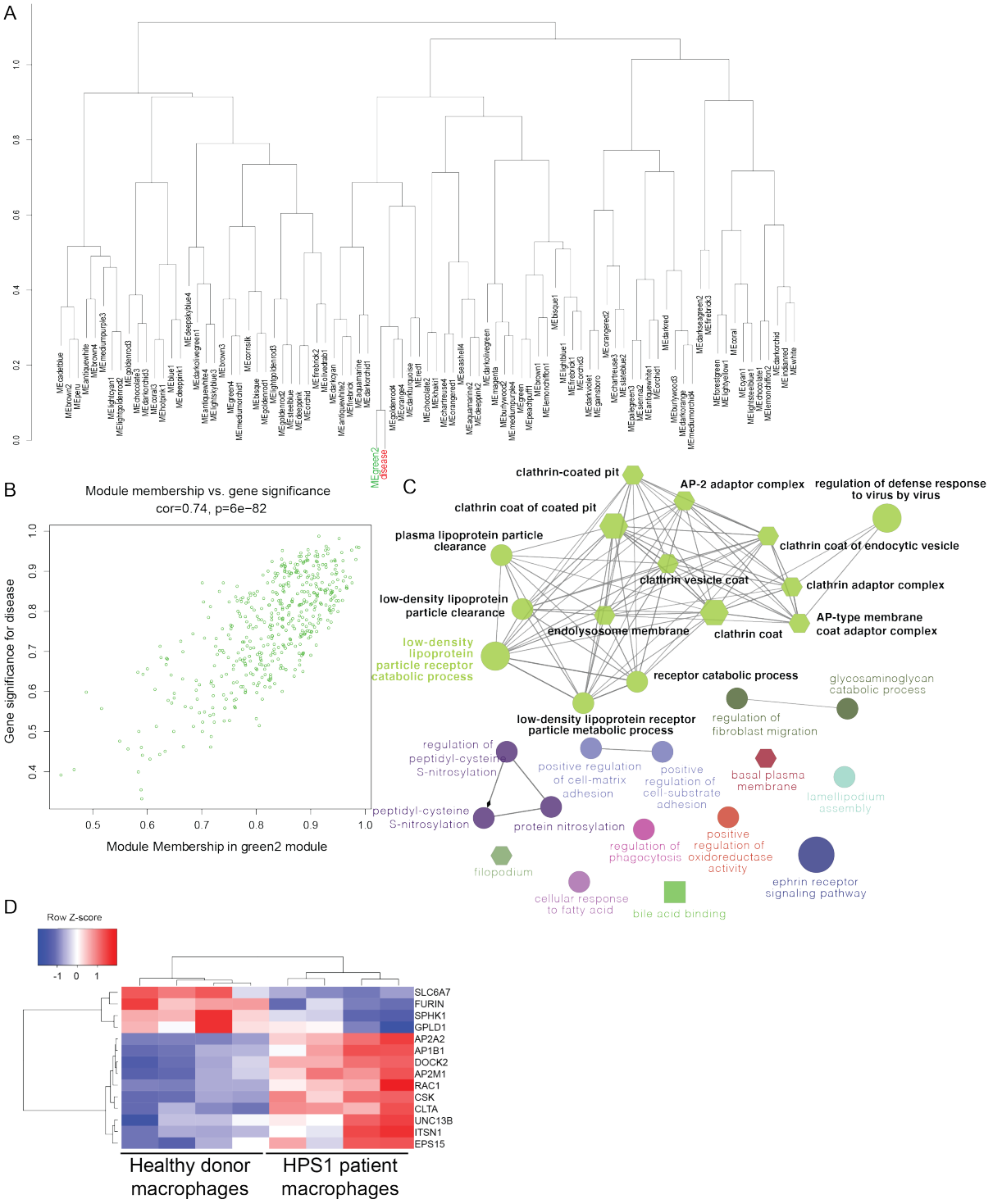


Figure 3.14. Correlation network analysis of HPS-1 macrophages reveals an LDL metabolism module. A) Dendrogram of modules and HPS-1 disease trait (green = green2 module; red = HPS-1 disease trait). B) Module membership of genes from the green2 module plotted against the significance of each gene for the disease trait. C) Network of top 200 hub genes of the green2 module. D) Heatmap of low-density-lipoprotein associated genes as counts per million and scaled per row.

3.2.4 HPS1 knockout lung organoid transcriptomics

Hermansky-Pudlak Syndrome patients, and especially those with mutations in *HPS1, AP3B1* and *HPS4*, develop lung fibrosis. A recent study used induced pluripotent stem cells differentiated into lung organoids to model HPS1 deficiency (Strikoudis et al., 2019). I used this RNA-seq dataset of $EPCAM^{+}$ sorted epithelial cells from lung organoids to understand whether the disease-associated pathways we identified in HPS-1 patient macrophages were conserved across epithelial cells.

First, I investigated differences between control and HPS1 knockout cells in a principal component analysis **(Figure 3.15A-B)**. The first principal component explained a large amount of the variance. Additionally, I performed differential expression analysis and found that insulin-like growth factor 2 (*IGF2*) was highly expressed in HPS1 knockout epithelial cells, showcasing a metabolic change **(Figure 3.15C)**.

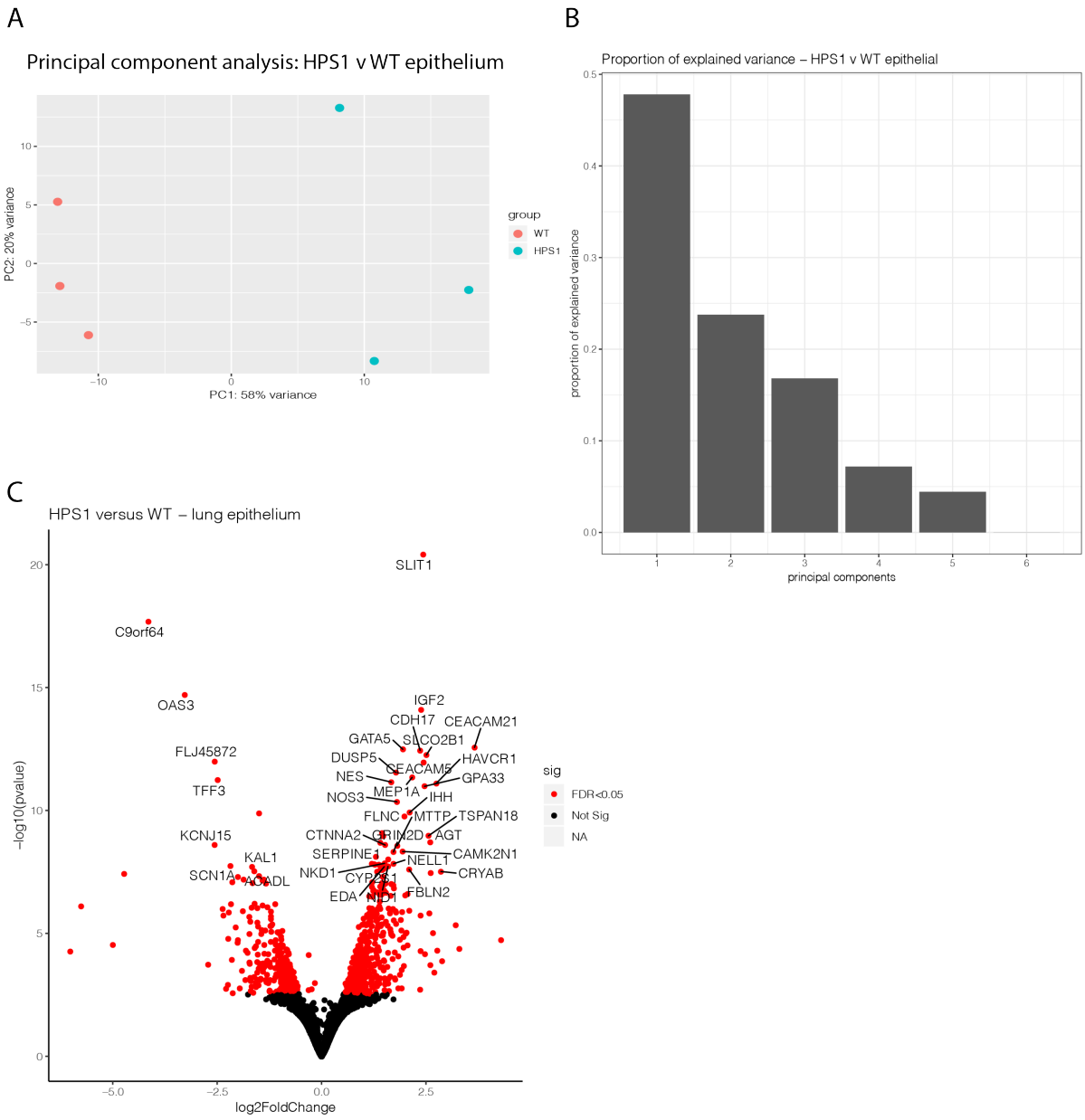


Figure 3.15. Principal component and differential expression analysis of HPS1 knockout epithelial cells. A) Principal component analysis of variance stabilizing transformed data. B) Proportion of variance between HPS1 knockout and control explained by each principal component. C) Differential gene expression of HPS1 knockout epithelial cells from lung organoids compared to control epithelial cells. FDR: false discovery rate; sig: significance; PC: principal component.

Furthermore, I aimed to delineate pathways that are affected in HPS1-deficient lung organoid epithelial cells. Using fast gene set enrichment analysis, I identified that the top

upregulated pathway in HPS1 knockout epithelial cells is epithelial to mesenchymal transition **(Figure 3.16A-B)**. Myc targets was the top downregulated pathway, while oxidative phosphorylation was the third most downregulated hallmark pathway, mirroring the HPS-1 patient macrophage data **(Figure 3.16C)**. This result highlights the diminished oxidative phosphorylation in HPS1 deficiency and thereby the altered metabolism of these cells on a transcriptional level.

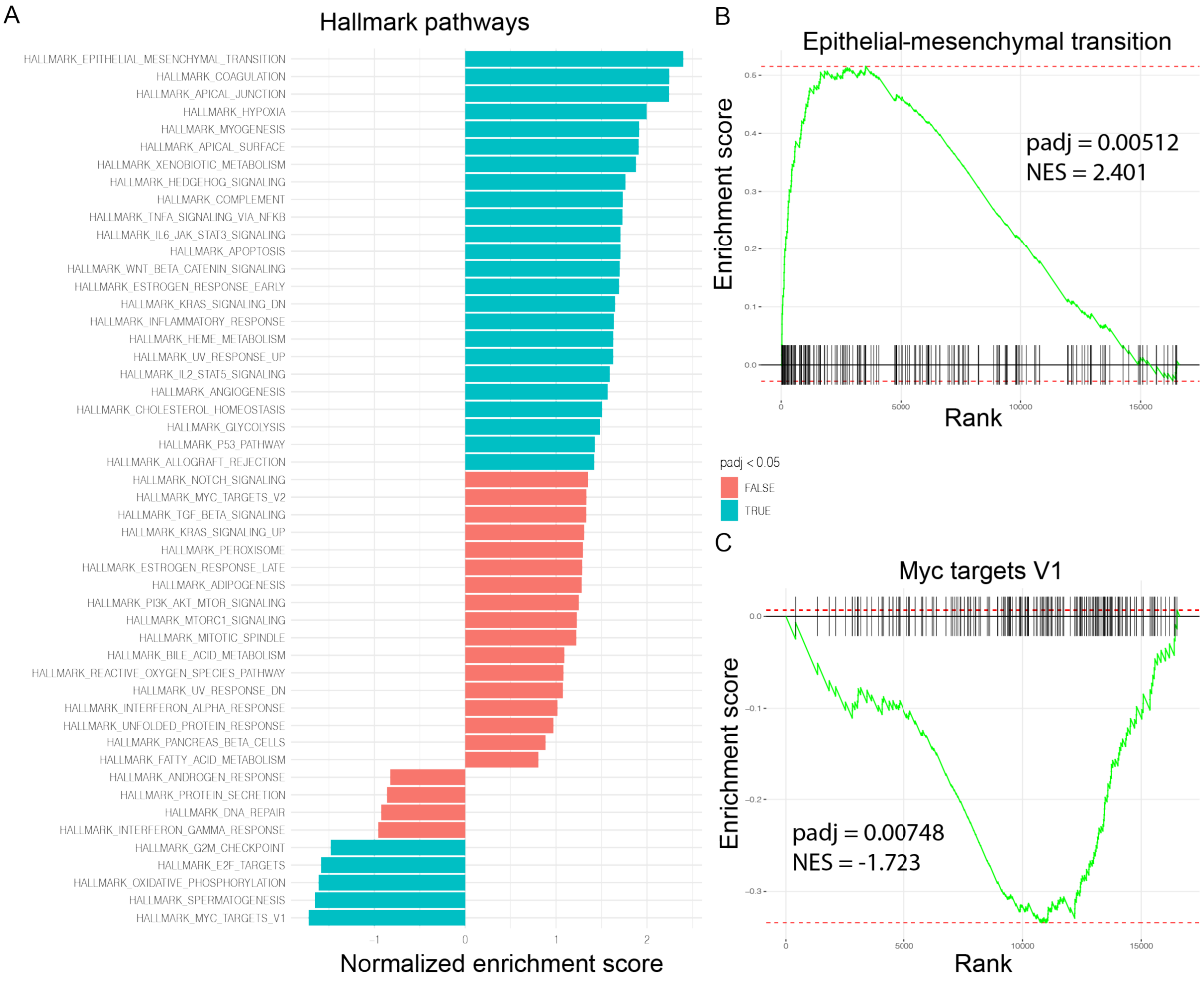


Figure 3.16. Lung organoid epithelial gene set enrichment analysis. A) Hallmark pathway gene set enrichment analysis identifies significantly increased or decreased pathways in HPS1 knockout epithelial cells. B) Top increased and decreased pathways shown with adjusted p value (padj) and normalized enrichment score (NES).

In addition, I explored the molecular function terms enhanced in epithelial HPS1 deficiency using gene ontology analyzer for RNA-seq. The top molecular function term was lipoprotein particle receptor binding **(Figure 3.17)**, which fits with our HPS-1 patient macrophage module results. This finding accentuates the conserved nature of the LDL signature in HPS1 deficiency in these cell types.

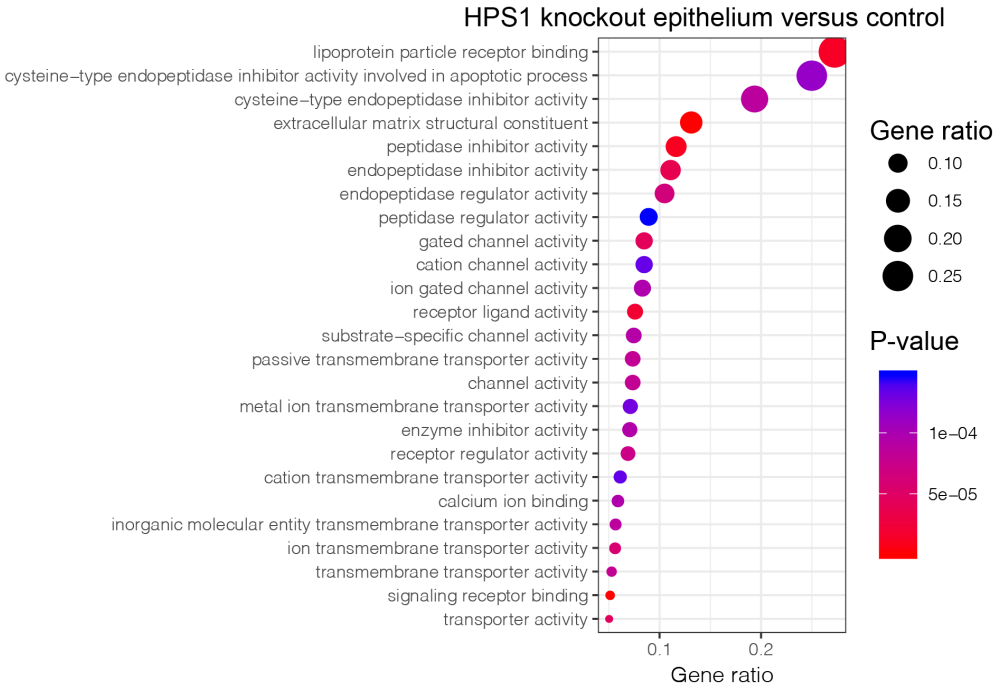


Figure 3.17. Gene ontology molecular function analysis of HPS1-deficient and control epithelial cells. Gene ontology molecular function terms were used to compare HPS1 knockout and control lung epithelial cells.

In conclusion, the HPS1-deficient lung organoid-derived epithelial RNA-seq dataset highlights a number of perturbed mechanisms that are shared with the HPS-1 patient macrophage data. Specifically, oxidative phosphorylation appears reduced in both settings, which likely has implications for cellular metabolism. Additionally, the lipoprotein receptor

binding term in HPS1-deficient epithelial cells is in agreement with the correlation network analysis of HPS-1 macrophages, pointing to altered LDL metabolism in the disease.

3.3 Discussion

In this chapter, I show that BLOC-3 pathway genes are expressed in myeloid cells. Furthermore, I identify metabolic changes in HPS-1 patient macrophages using transcriptomics. Specifically, there is an LDL metabolism signature in HPS-1 macrophages, which is conserved in epithelial cells, and a reduction in oxidative phosphorylation. These findings hint towards dysregulated metabolic signaling, which could contribute to the pathology of the disease.

HPS1 and HPS4, which form BLOC-3 (Nazarian et al., 2003), and its guanine nucleotide exchange factor targets Rab32 and Rab38 (Gerondopoulos et al., 2012), do not have known interactions with IBD risk loci. Since variants in several autophagy and endosome genes are risk factors for IBD (Lassen and Xavier, 2018), monogenic diseases such as HPS-1 can provide insight into dysregulated pathways. In order to study an appropriate cellular system and draw mechanistic understanding for HPS pathology, I investigated the expression of *HPS1, HPS4, RAB32* and *RAB38* across primary sorted immune cell types. Macrophages and myeloid cells in general highly expressed the BLOC-3 pathway compared to other immune cells such as T and B cells.

Using RNA-sequencing of HPS-1 patient monocyte-derived macrophages, we identified signatures that are associated with the disease. I discovered that the expression of the IBD risk locus *PTGS2* (Liu et al., 2015) is increased in HPS-1 macrophages, pointing to basal inflammation in these macrophages. Prostaglandin-endoperoxide synthase 2 (PTGS2) generates prostaglandin E2, and is involved in the inflammatory response in DSS colitis (Lin et

al., 2018). The macrophage chemoattractant *CCL2* is significantly expressed in HPS-1 macrophages. A previous study has underlined that alveolar epithelial cells in HPS produce high levels of CCL2 to attract macrophages (Young et al., 2016).

Anti-TNF therapies are extensively used in IBD and HPS-1 patients have been treated with infliximab and have responded relatively well in most cases (Erzin et al., 2006; Felipez et al., 2010; Girot et al., 2019; O'Brien et al., 2021; Rutgeerts et al., 2005; Sands et al., 2004; Yoshiyama et al., 2009). Recent single cell RNA-seq advances have pointed to a pivotal interplay between macrophages and fibroblasts in the gut, with OSM being a driving factor in predicting anti-TNF responsiveness (Smillie et al., 2019; West et al., 2017). Our RNA-seq results show that *TNF* and *OSM* gene expression is upregulated in HPS-1 macrophages after infection. Furthermore, a weighted gene correlation network analysis of the Risk Stratification and Identification of Immunogenetic and Microbial Markers of Rapid Disease Progression in Children with Crohn's Disease (RISK) cohort (Kugathasan et al., 2017) has shown that Crohn's disease is associated with an inflammatory module, containing genes such as *IL1B, IL6* and *OSM* (Aschenbrenner et al., 2020). These studies showcase modules correlated with IBD and treatment response, shedding light on new potential therapeutics.

Additionally, fibroblasts and macrophages have been shown to regulate cell numbers through growth factors, leading to an important cell circuit (Zhou et al., 2018a). Therefore, perturbations in the macrophage-fibroblast homeostatic circuit in the subset of HPS-1 that develop Crohn's-like inflammation could contribute to the fistulizing disease observed. Further analyses directly on gastrointestinal biopsies will be important to investigate these interactions in the future. For instance, spatial transcriptomic profiling of inflamed and uninflamed gut tissue in HPS-IBD could elucidate pathogenic cell-cell interactions and pinpoint relevant genes and pathways in a tissue setting. Additionally, *in vitro* co-culture

studies of patient fibroblasts and macrophages could yield insights into the interactions of these cells in disease.

The most significant term in the correlation network analysis associated with HPS-1 was LDL metabolism. Previous research has shown that lipid metabolism is impacted in Hps1$^{-/-}$ mice, with the accumulation of atherosclerotic lipids (Ma et al., 2019). In atherosclerosis, chronic inflammation, macrophage activation and lipid accumulation obstruct blood vessels (Moore et al., 2013). Interestingly, the accumulation of lipids that results in foam cell formation differs between diseases (Guerrini et al., 2018). In atherosclerosis, cholesterol accumulates in macrophages whereas in tuberculosis, triglycerides accumulate. Furthermore, patients have ceroid lipofuscin buildup (Gahl et al., 1998), which might exacerbate inflammation in the lung and gut. However, the functional implications of a deregulated lipid metabolic loop remain elusive. The LDL signature identified in HPS-1 macrophages was replicated in HPS1 knockout epithelial cells, pointing to a shared mechanism in HPS1 deficiency. These results highlight the intricate balance underlying metabolic signaling and its role in tissue homeostasis.

Macrophage metabolism and cytokine production are intimately linked to preserve gut homeostasis. IL-10 signaling defects result in an altered macrophage phenotype with a switch to glycolytic metabolism (Ip et al., 2017). A systems-level analysis accentuated that M1 macrophages rely on glycolysis, whereas M2 macrophages have a more potent oxidative phosphorylation profile (Jha et al., 2015). Increased glycolysis, succinate oxidation and reduced oxidative phosphorylation can drive pro-inflammatory cytokine production (Mills et al., 2016). Interestingly, Hps2$^{-/-}$ murine alveolar epithelial cells have a dampened oxygen consumption rate and enhanced mitochondrial ROS (Cuevas-Mora et al., 2021), which may contribute to the lung fibrosis in this HPS subtype. Our transcriptomic analysis of HPS-1

macrophages and HPS1 knockout epithelial cells pinpointed a significant downregulation in in oxidative phosphorylation. The suppression of oxidative phosphorylation in HPS-1 macrophages may share features with HPS-2 and have implications for metabolic signaling, cytokine production and inflammation. It is important to note that these results shed light on the transcriptional level, but metabolic changes are often post-transcriptional. Therefore, functional and mechanistic studies are required to validate these findings. Additionally, this signature was identified in macrophages and epithelial cells and may not play a large role in other cell types.

Rare diseases featuring intestinal inflammation and disease-causative mutations in a particular gene, such as HPS-1, can provide novel insights into IBD. Gastrointestinal inflammation is characterized by immunometabolic alterations, which have not been elucidated in detail. For instance, isolated intestinal macrophages from IBD patients feature reduced levels of oxidative phosphorylation and fatty acid degradation (Dharmasiri et al., 2021). Furthermore, prostaglandin E2 (synthesized by PTGS2) and TNF signaling result in high levels of lipid droplets in DSS-treated mice (Heller et al., 2016). These findings suggest a role for HPS1 in modulating immunometabolic pathways, which are not well defined in IBD.

In conclusion, I found that the BLOC-3 pathway is highly expressed in myeloid cells. HPS-1 patient macrophages highlighted a pro-inflammatory cytokine network and a novel LDL module at the transcriptomic level. Lastly, oxidative phosphorylation is diminished in HPS-1 patient macrophages and induced pluripotent stem cell-derived epithelial cells according to their transcriptional profile, suggesting metabolic changes in HPS1 deficiency. In the next chapters, I extend these findings using cell lines and patient cells to shed a more targeted light on the cellular underpinnings of HPS-1.

Chapter 4 - The role of lipid metabolism and mTORC1 signaling in HPS1 deficiency

4.1 Introduction

In the previous chapter, I identified a transcriptional metabolic signature as a driver in HPS-1. One of the clinical features of Hermansky-Pudlak Syndrome is the presence of ceroid lipofuscin in multiple organs (Gahl et al., 1998). Ceroid lipofuscin is regarded as an aging pigment, which is amassed with age (Thelen and Zoncu, 2017), but in some lysosome-related disorders, including HPS, it occurs earlier. Which perturbations lead to such a dysregulation in lipid metabolism in HPS is a major outstanding question in the field.

Lipid metabolism is not only regulated from within cells, but is also impacted by lipids, such as LDL, when taken up from the extracellular environment. LDL is composed of apolipoproteins, cholesterol and phospholipids on the exterior along with triglycerides and cholesteryl esters at the core (Ridker, 2014). LDL binds the LDL receptor and undergoes receptor-mediated endocytosis (Bartuzi et al., 2016). LDL can also be internalized through scavenger receptors on macrophages, such as CD36 and lectin-type oxidized LDL receptor 1 (LOX-1) (Chistiakov et al., 2017). Alternatively, LDL can be internalized through macropinocytosis (Kruth et al., 2005). Within the lysosome, lysosomal acid lipase breaks down triglycerides and cholesteryl esters into fatty acids and cholesterol (Meng et al., 2020). Lipid droplets are a lipid storage organelle that can supply triglycerides and cholesteryl esters for hydrolysis, providing a source of fatty acids and cholesterol (Ouimet et al., 2011; Rambold et al., 2015; Thelen and Zoncu, 2017).

Lipid metabolism is crucial for homeostasis and its dysregulation is associated with several diseases, ranging from atherosclerosis to *Mycobacterium tuberculosis* infection

(Guerrini et al., 2018) and lysosomal storage disorders (Thelen and Zoncu, 2017). In the context of HPS-1, lipidome profiling of plasma from $Hps1^{-/-}$ mice identified the accumulation of atherogenic lipids such as cholesterol, triacylglycerol and sphingomyelin (Ma et al., 2019).

Studies on lipid metabolism, autophagy as well as lysosomal storage disorders converge on the lysosome as a key checkpoint. The investigation of lysosomal composition has benefited from lysosomal purification techniques, which include ultracentrifugation and organelle extraction or commercially available kits. However, techniques that include ultracentrifugation can lead to contaminating compartments in the enriched sample and might not necessarily yield intact organelles (Fritsch et al., 2019). A novel method involving the immunomagnetic isolation of lysosomes generates high-quality, intact lysosomes, while excluding contaminating compartments (Abu-Remaileh et al., 2017).

In this chapter, I use an HPS1 knockout system to investigate the metabolic changes emerging from the correlation network analysis. I interrogate the lysosomal proteome of HPS1-deficient cells through a recently described immunomagnetic lysosomal isolation method. Subsequently, I delineate functional consequences of the lysosomal proteome findings on processes such as autophagy and bacterial clearance. Lastly, I leverage information from the molecular mechanism to identify a new therapeutic target and ameliorate anti-microbial activity.

4.2 Results

4.2.1 Generation of an HPS1 deficiency model system in HAP1 cells

In order to identify a suitable model system to study HPS-1, I investigated the expression of *HPS1* across different cell types using online databases. I found that HAP1 cells expressed *HPS1* (25.69 transcripts per million) (Horizon Discovery, 2021). HAP1 cells are a

haploid cell line derived from the pro-myelocytic leukemia KBM7 cells (Carette et al., 2011), which allows for easier gene editing. I used the gene editing tool CRISPR/Cas9 to create an HPS1 knockout in HAP1 cells. I obtained a clone with a 7 base pair (bp) deletion in exon 5 of the *HPS1* gene **(Figure 4.1)**, causing a frameshift. On the protein level, HPS1 is 701 amino acids long and this deletion results in changes to the amino acid sequence at position 130, leading to an early stop codon at amino acid position 172. This HPS1 knockout clone was used for all subsequent experiments in this chapter.

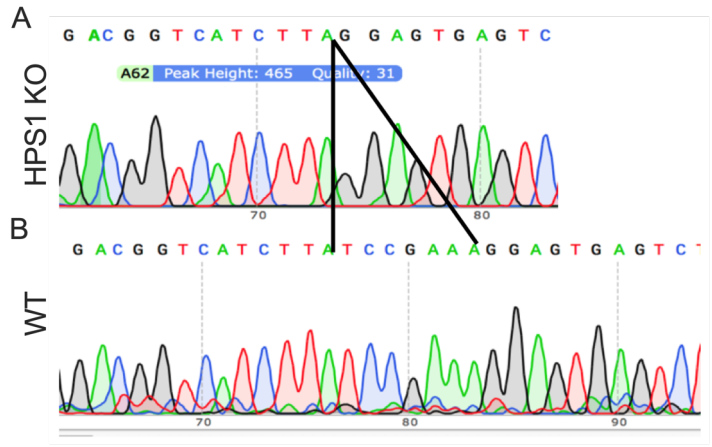


Figure 4.1. HPS1 knockout generation in HAP1 cells. Sanger sequencing identifies a CRISPR/Cas9-mediated 7 bp deletion in the *HPS1* gene in HAP1 cells. A) Sanger sequencing trace of HPS1 knockout. B) Sanger sequencing trace of wild type HAP1 cell line.

4.2.2 LDL uptake and cholesterol metabolism are perturbed in HPS1-deficient HAP1 cells

The macrophage HPS-1 patient RNA-seq in the previous chapter revealed the emergence of an LDL metabolism module in HPS-1. I sought to evaluate this finding in the HPS1 knockout HAP1 cells at a functional level. Specifically, I treated HAP1 cells with LDL-BODIPY, where BODIPY serves as a fluorescent label for LDL, for indicated periods of time and

tracked the uptake of LDL **(Figure 4.2A-C)**. Across different time points, there was a marked increase in LDL uptake in HPS1 knockout cells, confirming the gene expression data.

Since HPS1-deficient cells have increased LDL uptake, I interrogated whether this effect could be saturated. I treated cells with unlabeled LDL for 1 hour and subsequently stimulated cells with LDL-BODIPY for 3 hours to quantify the amount taken up. There was a decrease in LDL taken up by both the control and HPS1 knockout cells **(Figure 4.2D)**, revealing that the augmented LDL uptake in HPS1 knockout cells can be saturated.

I wondered whether these findings of enhanced uptake could be extended to free cholesterol. To this end, HAP1 cells were stained with free BODIPY, which has been used to probe the amount of lipids within cells (Riffelmacher et al., 2017). There was an increased amount of lipids within the HPS1 knockout cells at baseline **(Figure 4.2E)**. At the same time, cholesterol treatment greatly amplified the lipid content of HPS1 knockout cells in particular. These results suggest that HPS1 deficiency may result in boosted uptake of cholesterol or could be concentrated within cells due to a defect in cholesterol degradation.

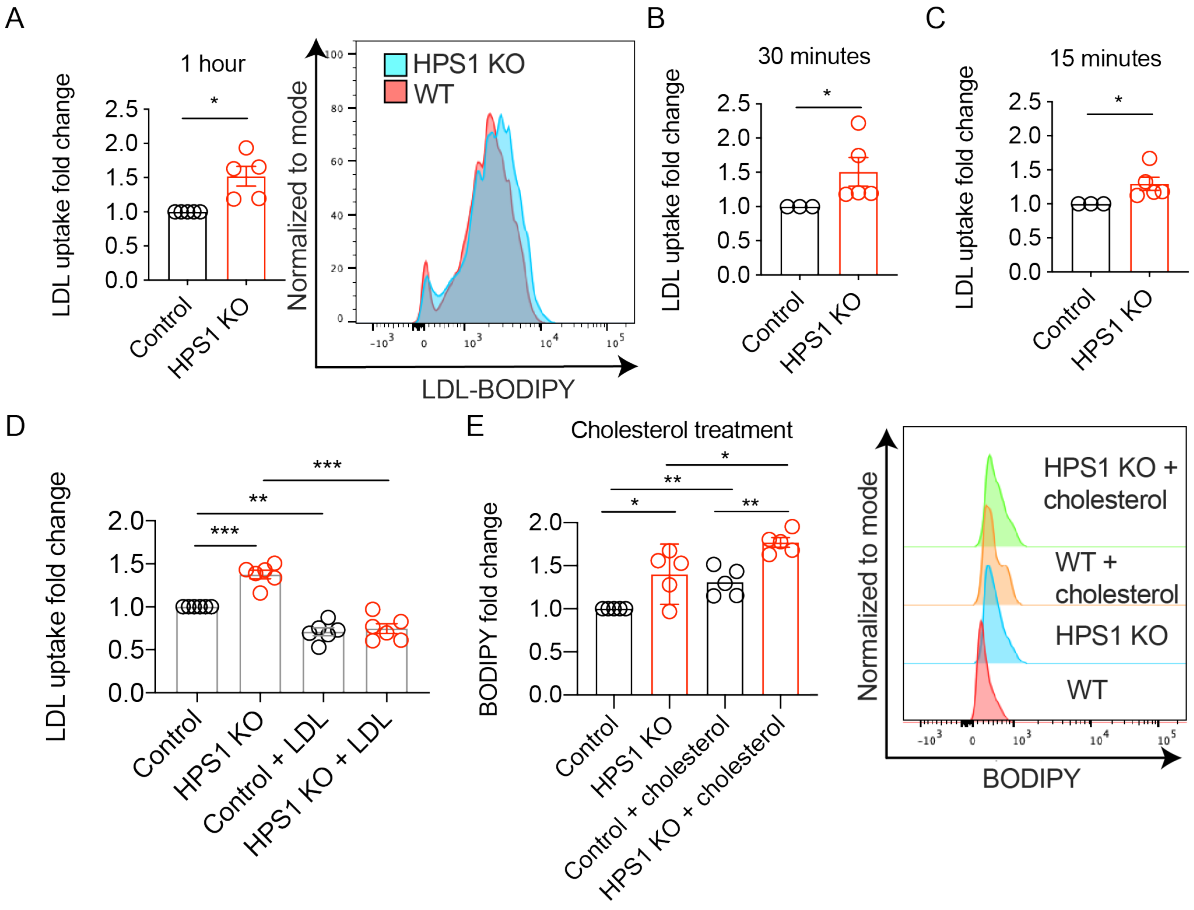


Figure 4.2. LDL uptake and cholesterol metabolism are dysregulated in HPS1 deficiency. A) HAP1 cells were treated with 10 µg/mL LDL-BODIPY for 1 hour (n=5). B) Control and HPS1 KO cells were treated with 10 µg/mL LDL-BODIPY for 30 minutes (n=5). C) HAP1 cells were treated with 10 µg/mL LDL-BODIPY for 15 minutes (n=5). D) Control and HPS1 KO cells were treated with 2.5 µg/mL unlabeled LDL for 1 hour and then stimulated with LDL-BODIPY for 3 hours (n=6). E) Control and HPS1 KO cells were treated with 1 X cholesterol lipid concentrate for 2 hours and stained for BODIPY (n=5). Ratio paired t-test on mean fluorescence intensity; *p<0.05, **p<0.01, ***p<0.001.

4.2.3 Lysosomal proteolytic activity in HPS1 deficiency is intact

Since HPS-1 is a lysosome-related organelle disorder, I wondered whether lysosomal function itself is affected. DQ-Ovalbumin was used to assess the proteolytic activity, or degradative capacity, of lysosomes, in serum-starved and serum-fed conditions. DQ-Ovalbumin emits a fluorescent signal when proteases cleave the molecule. While HPS1

knockout cells had intact proteolytic activity **(Figure 4.3A)**, LDL reduced the ability of lysosomes to function in the starved setting for both the control and HPS1 knockout cells. I used serum starvation prior to LDL treatment in order to avoid the interference of other lipids that could be taken up from the fetal bovine serum. Under serum-fed conditions, the proteolytic activity of the lysosomes in HPS1 knockout cells was similar to control cells **(Figure 4.3B)**. In summary, the proteolytic activity of lysosomes does not appear to be impacted in HPS1 deficiency. At the same time, it is possible that the increased LDL uptake in HPS1-deficient cells could lead to diminished lysosomal function in a chronic setting.

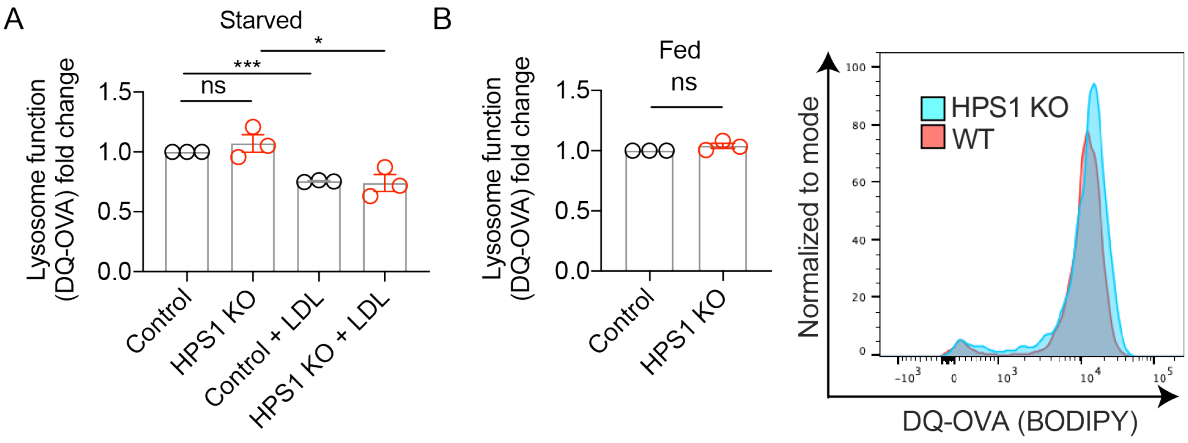


Figure 4.3. Lysosomal function is intact in HPS1 deficiency. A) HAP1 cells were stimulated with 25 µg/mL LDL for 1 hour and treated with 10 µg/mL DQ-Ovalbumin for 2 hours during serum starvation (n=3). B) HAP1 cells were treated with 10 µg/mL DQ-Ovalbumin for 2 hours during fed conditions (n=3). Ratio paired t-test on mean fluorescence intensity; *p<0.05, ***p<0.001. DQ-OVA: DQ-Ovalbumin.

4.2.4 HPS1-deficient cells have higher levels of lysosomal mTOR

In order to investigate whether lysosomal composition is altered in HPS1 knockout cells, I used a lysosomal immunoprecipitation (LysoIP) technique that relies upon immunomagnetic purification (Abu-Remaileh et al., 2017). This method uses the lysosomal

transmembrane protein 192 (TMEM192) with a triple HA tag for the isolation of lysosomes. Specifically, cells are homogenized and incubated with anti-HA magnetic beads, and isolated lysosomes are washed under mild buffer conditions to not disrupt the lysosomes **(Figure 4.4A)**.

Since this technique was established in human embryonic kidney 293 T-antigen cells, I first adapted the protocol for use in the HAP1 cell system. I used flow cytometry to quantify the tagging of HAP1 cells **(Figure 4.4B)**. In addition, I stained cells for the HA-tag and LysoTracker to assess lysosomal co-localization of the tag using confocal microscopy, finding that the HA tag co-localized with lysosomes **(Figure 4.4C)**.

Using Western blotting, I investigated the amounts of LAMP2, a lysosomal integral membrane protein, β-actin, which primarily localizes to the cytosol, and cathepsin C, which resides in the lysosomal lumen. The whole cell fraction contained all of these proteins, but the lysosomes lacked β-actin **(Figure 4.4D)**, arguing for a robust exclusion of the cytosolic fraction. I used a standard curve of different cell numbers and probed for LAMP2, in order to quantify the amount of lysosomes extracted, as previously described for mitochondrial isolation (Chen et al., 2017). I could recover an average of 6 % of lysosomes from cells **(Figure 4.4E-F)**.

Furthermore, I developed a flow cytometric approach to evaluate lysosomal integrity. Using a low number of magnetic beads allowed an increased number of lysosomes to attach per bead. Therefore, I visualized the increased size of the beads when lysosomes were attached, compared to non-HA expressing HAP1 cells, which served as a negative control **(Figure 4.4G)**. In addition, LysoTracker staining confirmed the integrity of lysosomes, since the dye accumulates in intact acidic compartments. In conclusion, the lysosome isolation technique in HAP1 cells led to the purification of intact lysosomes.

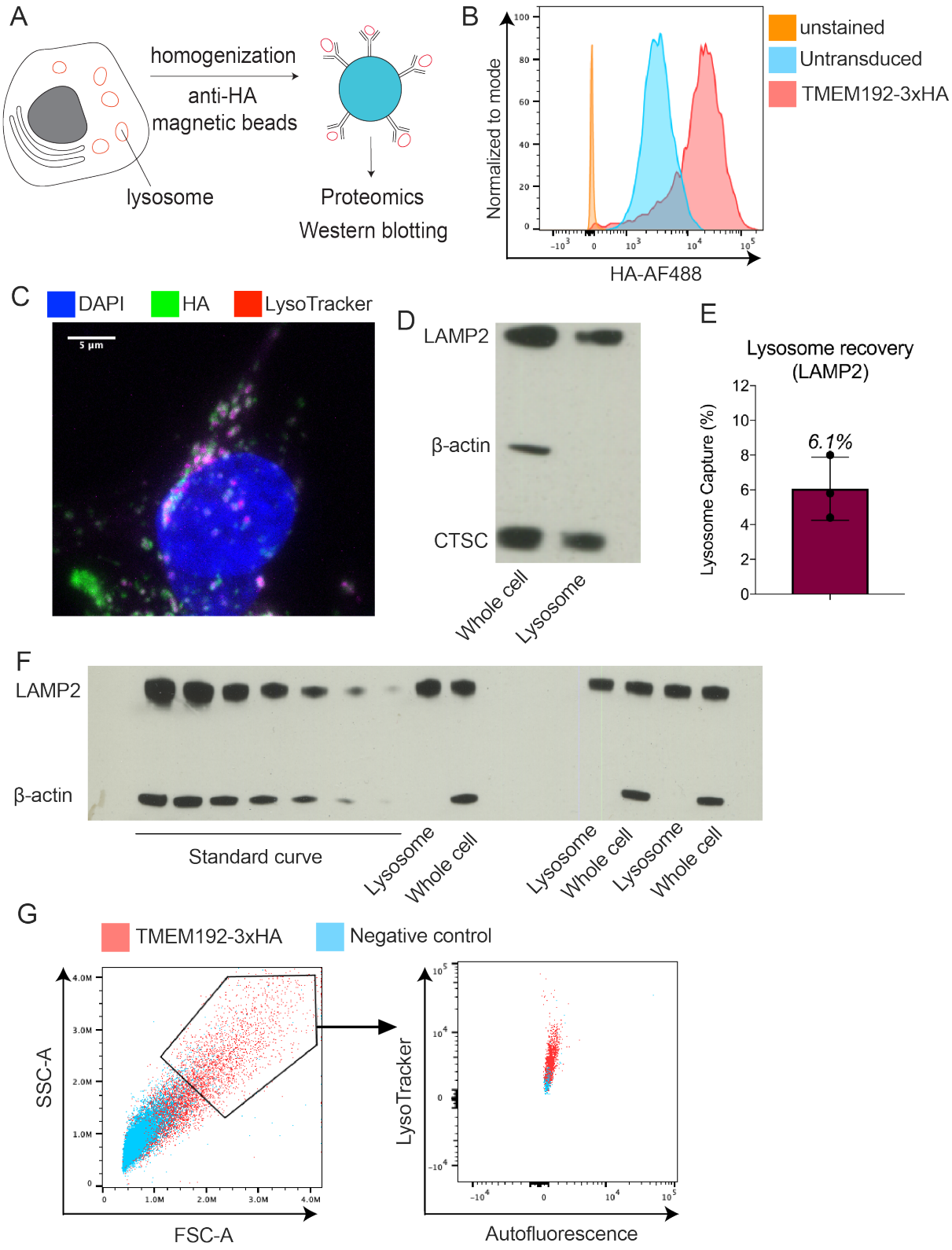


Figure 4.4. Lysosomal tagging and enrichment. A) Schematic of TMEM192-3xHA LysoIP and downstream analysis. B) Flow cytometry for HA in intact HAP1 cells. C) Confocal microscopy of TMEM192-3xHA transduced HAP1 cells using LysoTracker Deep Red, an anti-HA-AF488

antibody and DAPI. D) Following lysosome purification, a Western blot was performed to determine lysosomal capture. E) Lysosome capture quantification based on the standard curve (n=3). F) LAMP2 standard curve. G) Flow cytometry plots for lysosomal-bead LysoTracker staining.

Next, I employed proteomics on LysoIP samples to identify changes in the lysosomal proteome of HPS1-deficient cells, in collaboration with the Kessler group at the Target Discovery Institute, University of Oxford. In this analysis, the largest fraction of the most abundantly expressed proteins belonged to the lysosomal compartment **(Figure 4.5A)**. A KEGG analysis found that the strongest term was the lysosome, followed by endoplasmic reticulum (ER) protein processing **(Figure 4.5B)**. This analysis also revealed that degradation processes were upregulated in the enriched samples, potentially owing to the function of the lysosome in degradation.

At the same time, proteins of other compartments appeared to be highly expressed in the enriched lysosome samples, such as the mitochondrion, ER, cytosol as well as ribonucleoproteins **(Figure 4.5A and C)**. Both mitochondria (Wong et al., 2018) and the ER (Lim et al., 2019) form close contact sites with the lysosome, important for mitochondrial fission and cholesterol transfer, respectively. While I detected lysosomal proteins having the highest abundance, I also found multiple ribonucleoproteins, which are likely contaminants (Mellacheruvu et al., 2013). These data highlight the close contacts formed with other organelles, such as mitochondria and the ER **(Figure 4.5D)**.

When I investigated the abundance of soluble lysosomal proteins in HPS1 knockout cells compared to control cells, I did not find any large differences **(Figure 4.5E)**. The LysoIP strategy therefore highlights that trafficking to the lysosome remains intact in HPS1 knockout cells for known soluble lysosomal proteins.

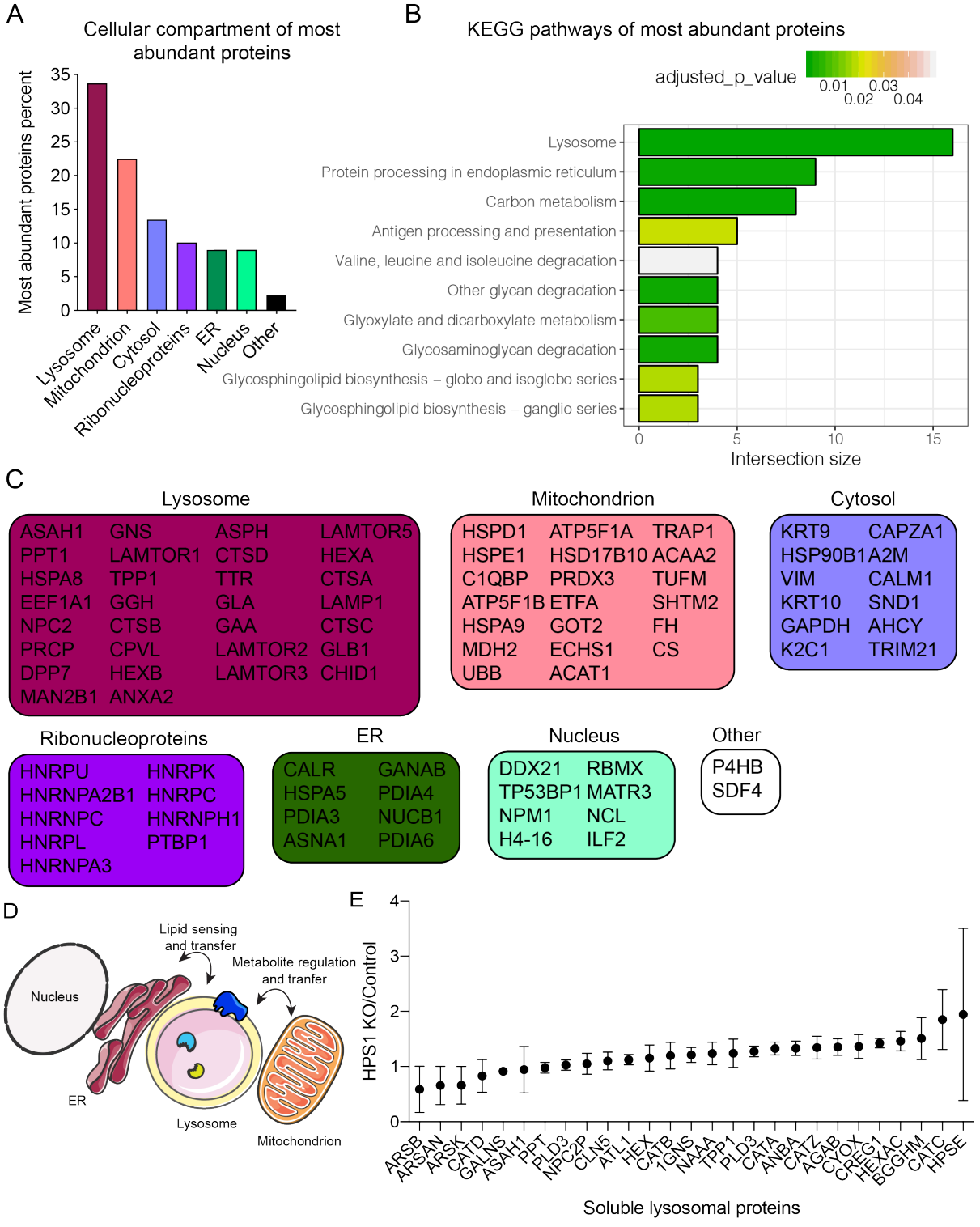


Figure 4.5. Lysosomal proteins and proteins of known lysosomal contact sites are the highest abundance proteins following LysoIP. A) The compartments where the most highly abundant proteins are found. B) KEGG pathway analysis using gProfiler for highest abundance proteins identified from proteomics. C) The highest abundance proteins were found in the

lysosome, mitochondrion and cytosol. Additionally, ribonucleoproteins, ER proteins, nuclear proteins and others were pinpointed. The 89 most highly abundant proteins were identified by averaging the control and HPS1 knockout samples. D) The lysosome forms close contact sites with the mitochondrion and the ER to mediate transfer of lipids or metabolites. E) Ratio of soluble lysosomal proteins in HPS1 knockout versus control samples.

Interestingly, the lysosomal proteomics results reveal an increased trend of mTOR present on HPS1 knockout cell lysosomes **(Figure 4.6A)**. Additionally, late endosomal/lysosomal adaptor, MAPK and mTOR activator (LTOR) 1, LTOR2 and LTOR4, which are part of the mTORC1 signaling cascade, also had increased trends in the HPS1 knockout lysosomes. Sequestosome 1 (SQSTM1), a marker of autophagy flux also known as p62, had an enhanced trend in HPS1-deficient lysosomes, suggesting a blockade in autophagy flux. I validated these results using Western blotting, where I probed for mTOR, LAMP2 and the tagged TMEM192 used for isolation **(Figure 4.6B)**. I quantified the ratio of mTOR to LAMP2 to ensure that mTOR abundance on lysosomes is amplified in HPS1 deficiency, instead of this finding being a product of an increased number of lysosomes being isolated. These results demonstrate that HPS1 deficiency results in higher levels of lysosomal mTOR.

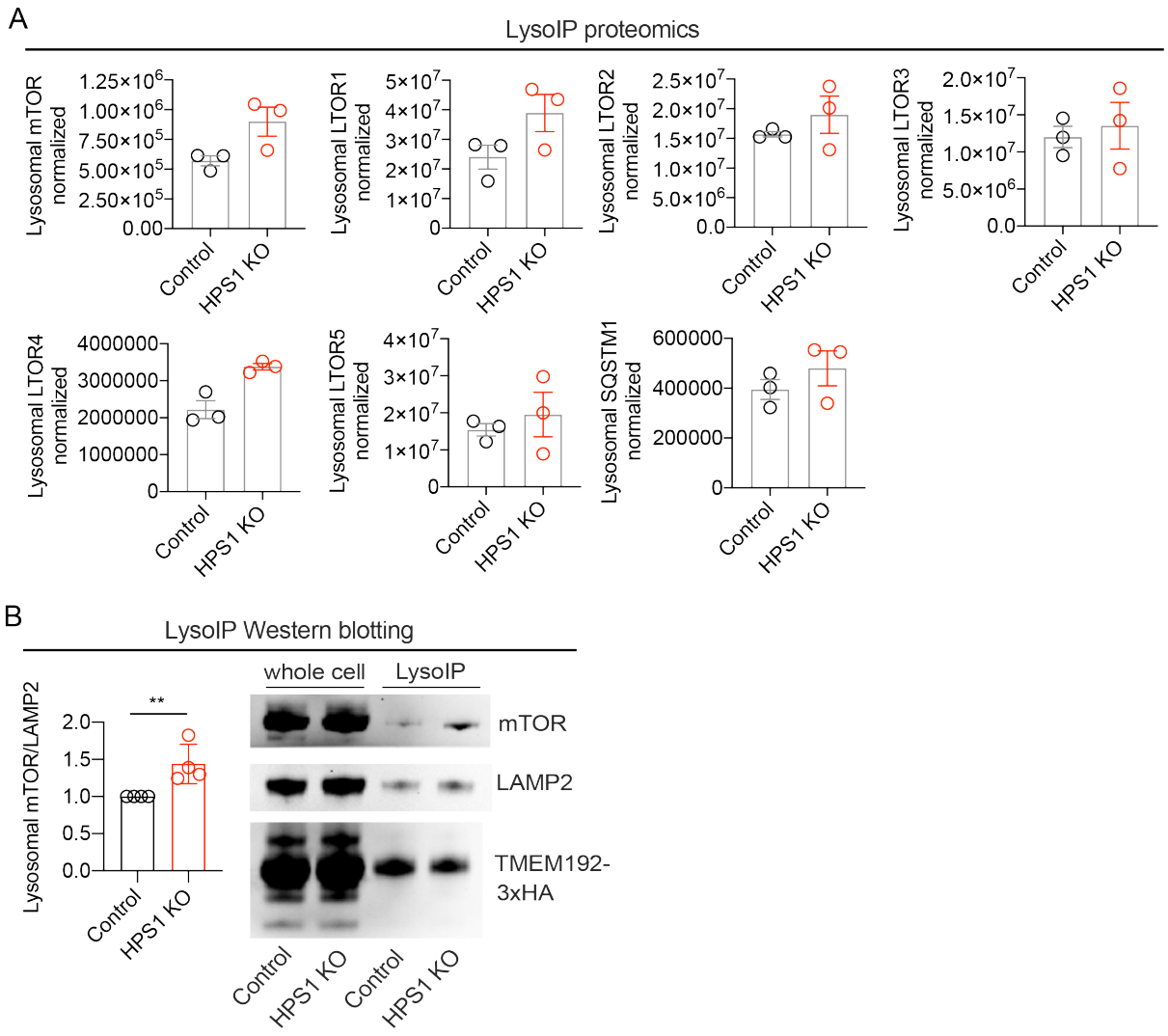


Figure 4.6. Lysosomal proteomics identifies enhanced mTOR on HPS1 knockout lysosomes. A) Lysosomal immunoprecipitation proteomics (n=3). B) Western blotting of lysosomal immunoprecipitation samples for mTOR, LAMP2 and TMEM192-3xHA tag (n=4). Relative quantification of band intensity. Paired t-test on ratio data; **p<0.01.

4.2.5 mTORC1 signaling is amplified in HPS1 deficiency and is mediated by Rab32

Since I found heightened levels of mTOR on HPS1 knockout lysosomes, which is the site of mTORC1 activation (Sancak et al., 2010), I investigated whether this had any impact on mTORC1 signaling. Specifically, I used the phosphorylation of S6 (pS6) as a readout for the activation of mTORC1. mTORC1 phosphorylates S6K1, which in turn phosphorylates S6 (Liu and Sabatini, 2020). HPS1 knockout cells had a higher level of pS6, which could be reduced

with the mTORC1 inhibitor rapamycin **(Figure 4.7A)**. Studies have shown that one of the functions of mTORC1 is to regulate cell size (Dowling et al., 2010; Pollizzi et al., 2015). I used the area of the forward sideward scatter (FSC-A) to approximate cell size, finding that HPS1 knockout HAP1 cells had a larger cellular size compared to the control **(Figure 4.7B)**.

Since HPS1 knockout cells internalized more LDL and oxidized LDL has previously been shown to stimulate mTORC1 (Zhou et al., 2016), I sought to confirm this in HPS1-deficient cells. LDL treatment increased S6 phosphorylation in control cells, and even more so in HPS1 knockout cells **(Figure 4.7C)**. These data suggest that mTORC1 is hyperactive in HPS1 knockout cells and that LDL further exacerbates mTORC1 signaling. I speculated that mTORC1 might be controlling the uptake of LDL. Strikingly, I found that the internalization of LDL was greatly reduced following rapamycin treatment **(Figure 4.7D)**. These results suggest that HPS1 knockout cells have an amplified loop of LDL uptake and mTORC1 signaling.

mTORC1 suppresses the efflux of cholesterol from the lysosomes to the ER, where low cholesterol levels lead to the nuclear translocation of sterol regulatory element-binding protein (SREBP), a transcription factor regulating lipid biogenesis and uptake (Eid et al., 2017). I treated HAP1 cells with LDL for 24 hours and performed a qPCR for the *LDLR*, *FASN* and *HMGCR* genes, since their expression is controlled by SREBP. I found that *LDLR* and *FASN* expression levels were significantly higher in HPS1 knockout cells compared to controls **(Figure 4.7E)**. At the same time, *HMGCR* levels had an increased trend in HPS1 deficiency. However, these differences are marginal and might not account for all of the change in lipid uptake observed. In summary, enhanced transcription of SREBP target genes may explain some of the lipid metabolism alterations found between controls and HPS-1.

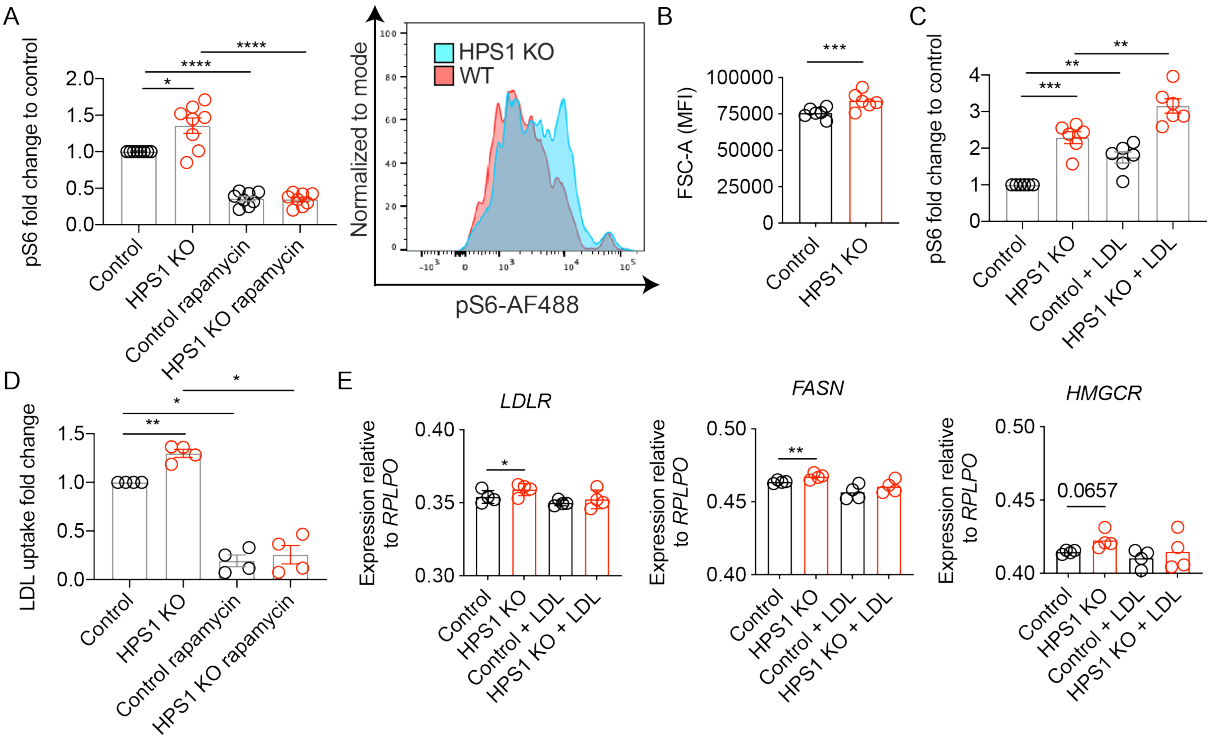


Figure 4.7. HPS1 knockout cells have heightened mTORC1 signaling. A) HAP1 cells were treated 50 µM rapamycin for 3 hours and stained for pS6-AF488 (n=4). Representative flow cytometry plots of HPS1 knockout cells or control cells for pS6-AF488 at baseline. B) Cell size was determined using the FSC-A mean fluorescence intensity of HAP1 cells (n=6). C) Control and HPS1 knockout cells were treated with 25 µg/mL LDL for 1 hour and then stained for pS6-AF647 (n=3). D) LDL uptake in HAP1 cells using LDL-BODIPY for 1 hour at 25 µg/mL were pre-treated with 50 µM rapamycin for 3 hours (n=4). E) Control and HPS1 knockout HAP1 cells were treated with 2.5 µg/mL LDL for 24 hours (n=4). RNA extraction, reverse transcription and qPCR were performed for *LDLR*, *FASN* and *HMGCR*. Expression is shown relative to the housekeeping gene *RPLPO* and each dot is the mean of two technical replicates. Ratio paired t-test on mean fluorescence intensity; paired t-test on qPCR data; *p<0.05, **p<0.01, ***p<0.001, ****p<0.0001.

Recently, Rab32 has been shown to anchor mTORC1 to the lysosomal surface (Drizyte-Miller et al., 2020). Additionally, BLOC-3 is the guanine nucleotide exchange factor of Rab32 and controls its localization (Gerondopoulos et al., 2012). I hypothesize that in the absence of HPS1, Rab32 could preferentially mediate mTORC1 signaling from the lysosome. Rab32 was

knocked down, using siRNA, to investigate the effect on mTORC1 signaling. Strikingly, Rab32 depletion in HPS1-deficient cells reverted the heightened mTORC1 signaling **(Figure 4.8A-B)**. This result suggests that the upregulated mTORC1 activity in HPS1 knockout cells is mediated through Rab32.

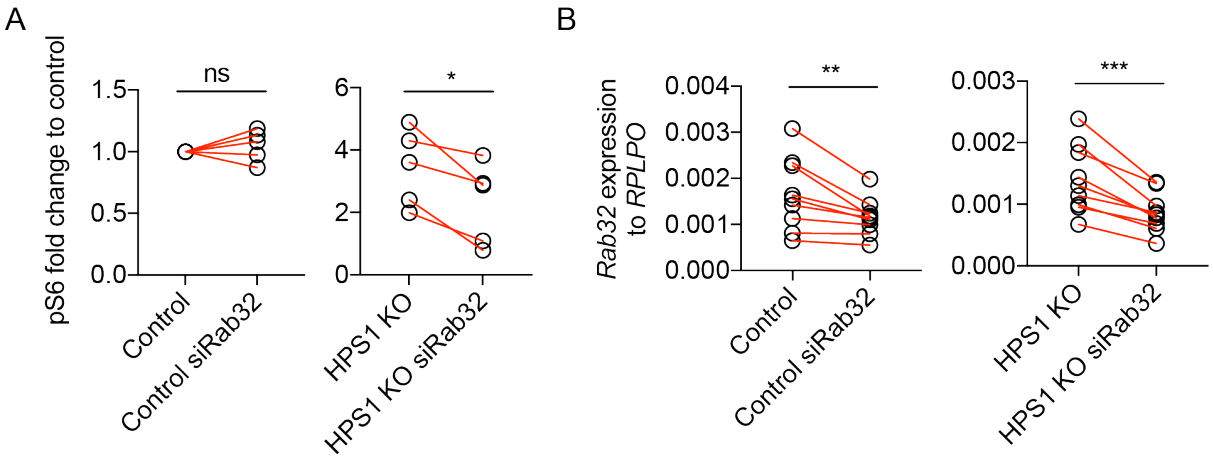


Figure 4.8. Rab32 knockdown reverts the increased mTORC1 signaling in HPS1 deficiency. A) HAP1 cells were transfected with siRNA against Rab32 and probed for S6 phosphorylation conjugated to AF647 (n=5). Cells were gated on singlets and live cells. B) Gene expression of Rab32 following knockdown in control and HPS1 knockout cells (n=9). Flow cytometry: ratio paired t-test on mean fluorescence intensity; qPCR: paired t-test. *p<0.05, **p<0.01, ***p<0.001.

4.2.6 Oxidative phosphorylation is reduced in HPS1 deficiency

Since I observed an augmented mTORC1 signature in HPS1 knockout cells and found dampened oxidative phosphorylation transcriptionally, oxidative phosphorylation was investigated on a functional level. We performed a mito stress test using a Seahorse assay to reveal differences in oxidative phosphorylation. We found that the HPS1 knockout cells had a decreased oxygen consumption rate **(Figure 4.9A)**. Therefore, oxidative phosphorylation is

diminished in HPS1-deficient HAP1 cells, consistent with the transcriptional reduction observed in HPS-1 patient macrophages in Chapter 3.

Furthermore, I evaluated the generation of mitochondrial ROS (mtROS) in HPS1 knockout HAP1 cells. HPS1 deficiency resulted in heightened mtROS production, as measured by the superoxide indicator MitoSOX **(Figure 4.9B)**. It has previously been shown in the mouse lung epithelial cell line MLE15 that AP3B1 deficiency (HPS-2) leads to reduced oxidative phosphorylation and increased mtROS (Cuevas-Mora et al., 2021). It is plausible that deregulated bioenergetics facilitate HPS-pulmonary fibrosis (PF), since HPS-1, HPS-2 and HPS-4 patients develop PF (Yokoyama and Gochuico, 2021).

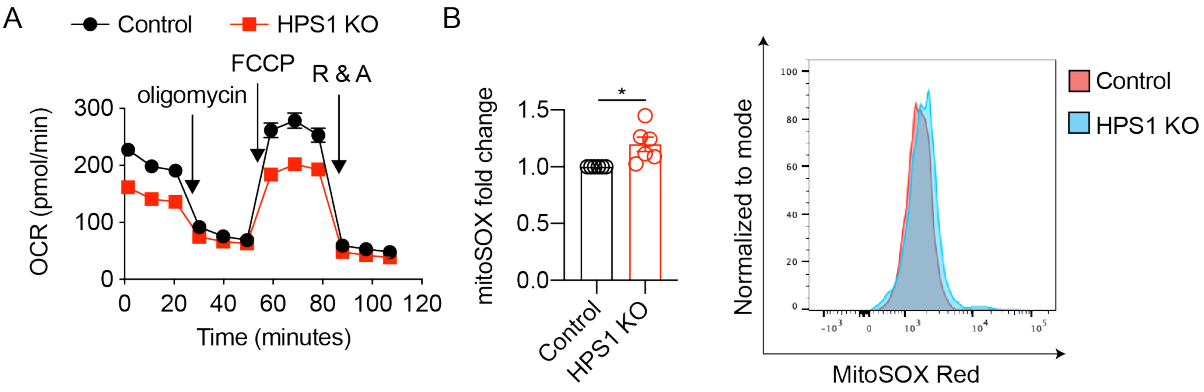


Figure 4.9. Decreased oxidative phosphorylation and enhanced mitochondrial ROS in HPS1 deficiency. A) Oxygen consumption rate of control and HPS1 knockout cells (representative of two independent experiments, 12 replicates per experiment). B) MitoSOX staining on control and HPS1 knockout cells, gated on singlets (n=6). A representative histogram of MitoSOX flow cytometry is shown. Ratio paired t-test on mean fluorescence intensity; *p<0.05. Error bars in SEM. R & A: rotenone and antimycin A.

4.2.7 HPS1 deficiency causes hampered bacterial clearance

mTORC1 signaling has demonstrated roles in reducing autophagy, which is crucial for host defense (Nazio et al., 2013). In order to investigate whether autophagy was dampened

in line with the increased p62 (SQSTM1) levels in HPS1-deficient lysosomes, I used the FlowCellect autophagy kit. Bafilomycin A1 blocks the degradation of LC3-II following its conversion from LC3-I and therefore allows for the calculation of the amount of autophagy blocked in cells (Klionsky et al., 2021). I found that autophagy flux was stifled in HPS1-deficient cells compared to controls **(Figure 4.10)**.

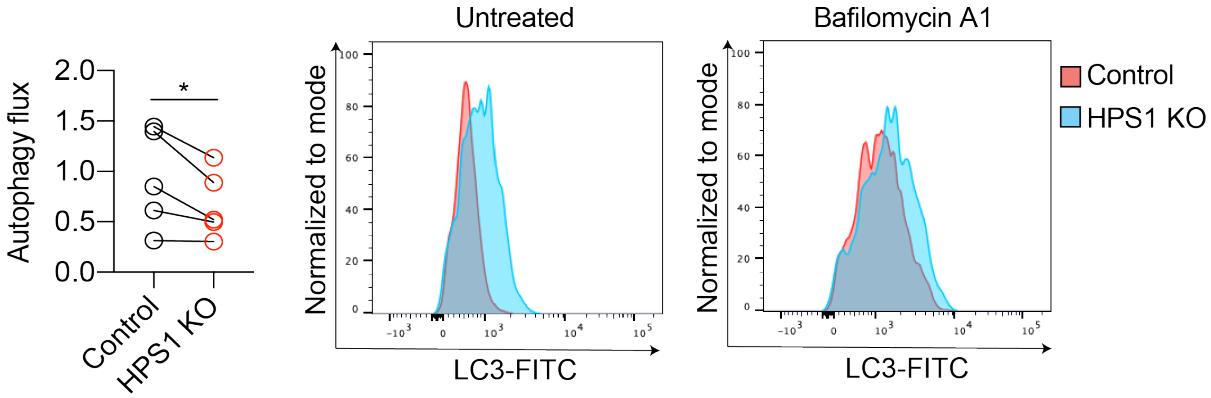


Figure 4.10. Autophagy flux is attenuated in HPS1 deficiency. HAP1 cells were treated with 10 nM bafilomycin A1 for 2 hours. Autophagy flux was calculated as (bafilomycin - untreated)/untreated for control and HPS1 knockout cells (n=5). Representative flow cytometry plots for LC3-FITC staining are provided. Significance was determined using a paired t-test on the autophagy flux values; *p<0.05.

Since autophagy is crucial for microbial elimination, I investigated whether HPS1 knockout cells were able to handle bacteria using a gentamicin protection assay **(Figure 4.11A)**. Briefly, this assay measures the number of bacterial colonies formed after lysing infected cells, demonstrating the ability of cells to efficiently clear microbes. I found that HPS1 deficiency resulted in a bacterial elimination defect against *Salmonella* Typhimurium, Adherent Invasive *Escherichia coli* (AIEC) and *Staphylococcus aureus* **(Figure 4.11B)**. *Salmonella* Typhimurium is an intracellular gram-negative bacterium that infects the

gastrointestinal tract (Keestra-Gounder et al., 2015). AIEC, which is also gram-negative, is found in Crohn's disease ileal lesions and healthy mucosa (Conte et al., 2014; Darfeuille-Michaud et al., 2004; Mukhopadhya et al., 2012). Lastly, *Staphylococcus aureus* is a gram positive bacterium, infecting the skin and respiratory tract rather than the gastrointestinal tract (Lowy, 1998).

In order to exclude that this was the result of a phagocytosis defect, I examined bacterial uptake using pHrodo Red *Escherichia coli (E. coli)* particles. I found that bacterial uptake was unaltered in HPS1 knockout cells at different time points, indicating that the bacterial handling defect was not related to a change in bacterial uptake **(Figure 4.11C)**. Microbes can be taken up when opsonized by IgG, which can bind to Fcγ receptors (Freeman and Grinstein, 2014). However, I did not opsonize microbes and test bacterial uptake because HAP1 cells do not express Fcγ receptors, rendering this type of phagocytosis in HAP1 cells highly unlikely **(Figure 4.11D)**. Together, these data suggest that there is an anti-microbial activity defect in HPS1 deficiency and this is not a product of increased bacterial uptake.

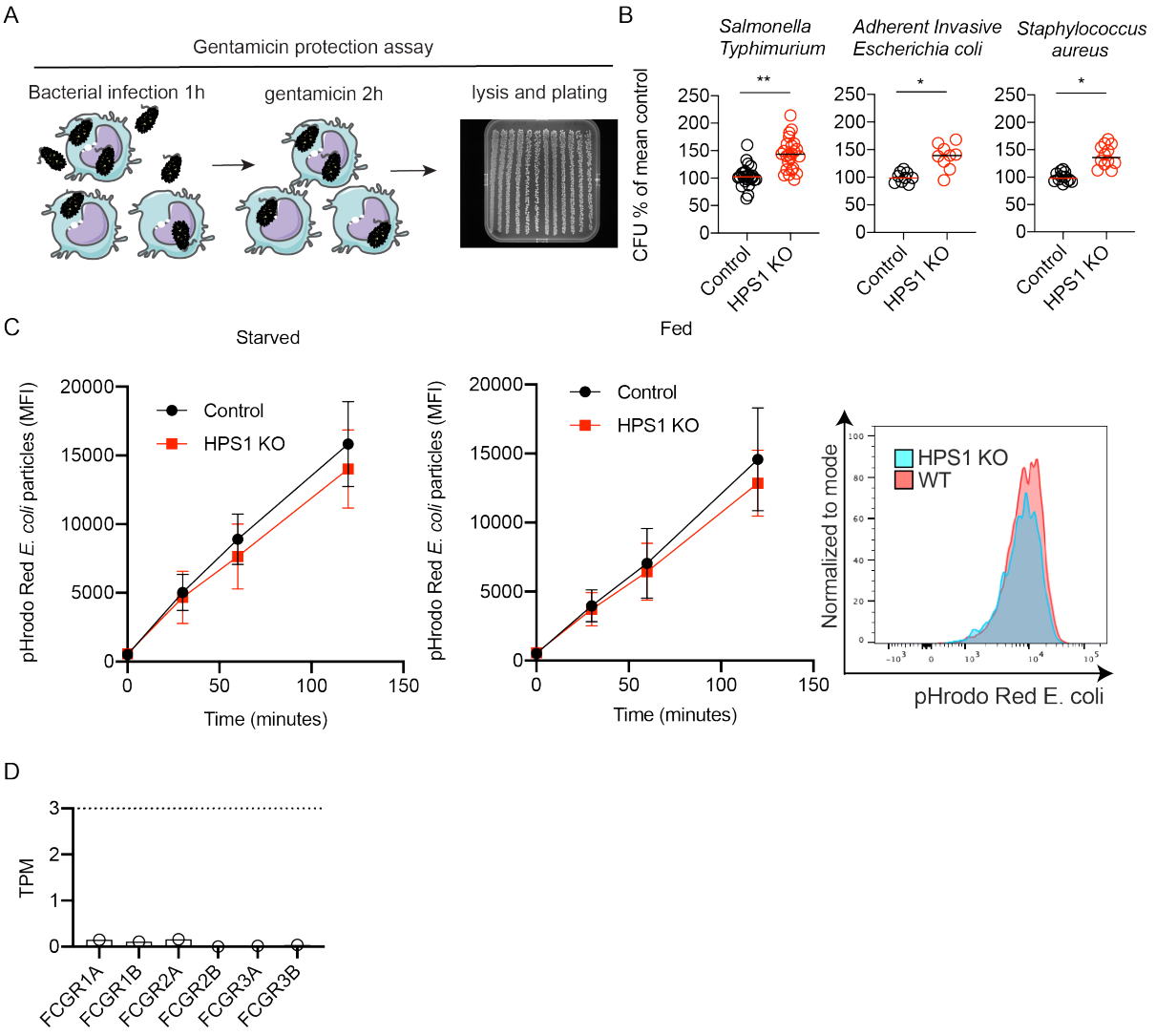


Figure 4.11. Impaired anti-microbial activity in HPS1-deficient HAP1 cells. A) Gentamicin protection assay experimental protocol. B) The gentamicin protection assay was performed in HAP1 cells at MOI 1:100 using GFP-*Salmonella* Typhimurium (n=8), Adherent Invasive *E. coli* (n=3) or *Staphylococcus aureus* (n=4). C) Bacterial uptake was measured using *E. coli* particles for indicated time points in HAP1 cells during serum-starvation and under fed conditions (n=3). D) Expression of Fcγ receptors in HAP1 cells (Horizon Discovery, 2021). A value of 3.0 transcripts per million or less is considered as not expressed. Ratio paired t-test on average colony forming unit counts; *p<0.05, **p<0.01. TPM: transcripts per million; CFU: colony forming units.

Rab32 is a lipid droplet resident protein (Bosch et al., 2020) and has been implicated in lipid metabolism (Li et al., 2016a; Wang et al., 2012). I hypothesized that free fatty acids

(FFA) are not readily available in HPS1 deficiency, and are instead sequestered in lipid droplets. To test this hypothesis, I stimulated HAP1 cells with fatty acids and found that a mixture of FFA could ameliorate the bacterial clearance defect in HPS1 knockout cells **(Figure 4.12A)**. Interestingly, FFA supplementation dampened mTORC1 signaling in HPS1 knockout cells, which could explain the rescue of the bacterial clearance defect **(Figure 4.12B)**. On the other hand, cholesterol increased the number of colonies in both control and HPS1 knockout cells, suggesting that cholesterol accumulation dampens bacterial clearance **(Figure 4.12C)**. Fatty acids undergo fatty acid oxidation, which can eventually feed into oxidative phosphorylation (Wang et al., 2010). Using the fatty acid oxidation inhibitor etomoxir, I discovered that eliminating fatty acid oxidation inhibited the degradation of microbes in control cells, but left HPS1 knockout cells unaffected **(Figure 4.12D)**. Etomoxir may not affect HPS1-deficient cells since fatty acid oxidation levels might already be diminished, owing to the unavailability of fatty acids to be oxidized.

Since the increased mTORC1 signaling could be attributed to the actions of Rab32 in HPS1 deficiency, I wondered whether its knockdown would affect bacterial clearance. As reported in previous studies (Baldassarre et al., 2021; Hu et al., 2019; Spano and Galan, 2012) and confirmed here, Rab32 depletion dampens bacterial handling in control cells **(Figure 4.12E)**. However, knockdown of Rab32 did not affect HPS1 knockout cells, potentially because the BLOC-3/Rab32 anti-microbial pathway is already defective.

mTORC1 signaling has emerged as a hallmark in HPS1 deficiency according to the findings described in this chapter. Strikingly, I found that rapamycin treatment reverts the impaired bacterial clearance in HPS1 knockout cells **(Figure 4.12F)**. In summary, I found that FFA supplementation and mTORC1 inhibition ameliorate the bacterial clearance defect in HPS1 deficiency, while cholesterol exacerbates it.

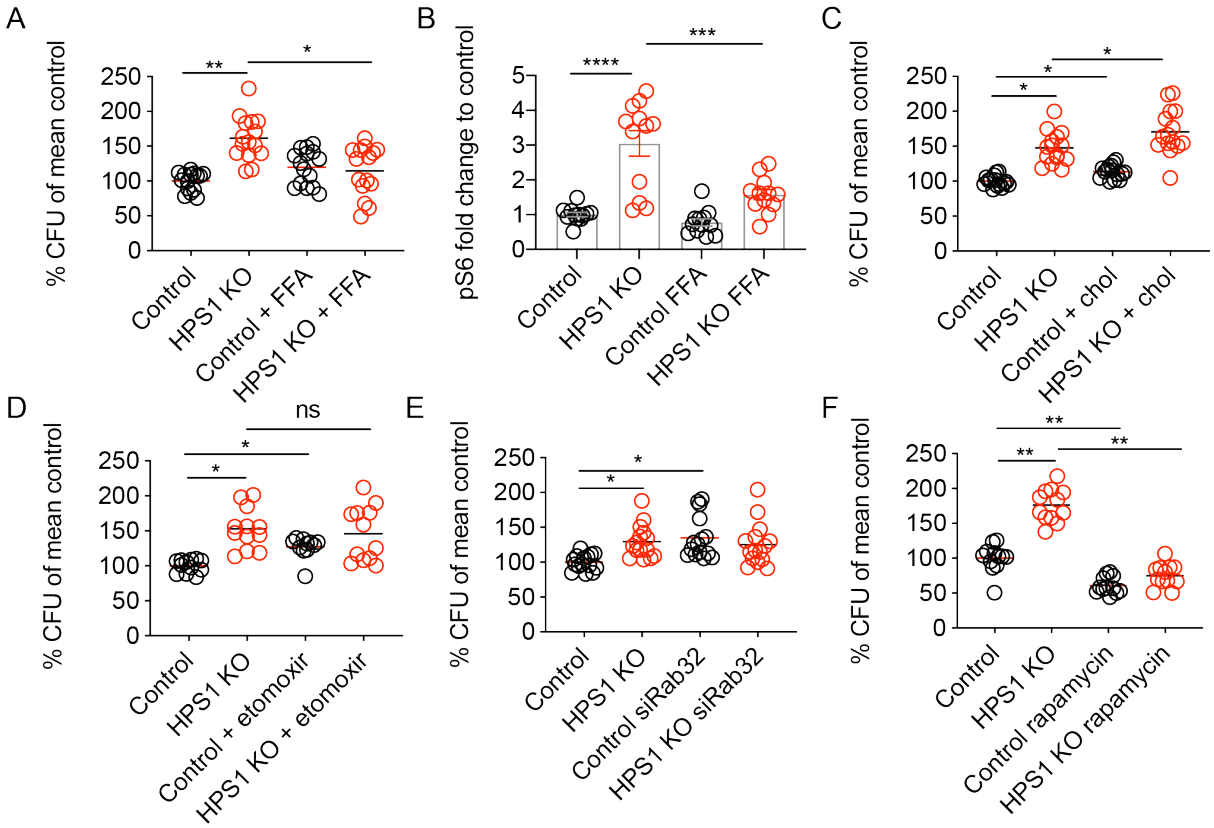


Figure 4.12. Dysregulated lipid metabolism in HPS1 deficiency dampens bacterial clearance. A) HAP1 cells were treated with free fatty acids (FFA) for 2 hours prior to a gentamicin protection assay (n=5). B) HAP1 cells were treated with FFA for 2 hours and stained for S6 phosphorylation conjugated to AF647 (n=6). C) HAP1 cells were stimulated with 50 µM cholesterol for 2 hours prior to the gentamicin protection assay (n=5). D) Gentamicin protection assay following 50 µM etomoxir treatment for 16 hours (n=4). E) HAP1 cells were transfected with siRNA against Rab32 or a control pool 72 hours before the gentamicin protection assay (n=5). F) HAP1 cells were treated with 50 µM rapamycin for 3 hours followed by the gentamicin protection assay (n=4). All gentamicin protection assays in this figure were performed using *Salmonella* Typhimurium. Ratio paired t-test; *p<0.05, **p<0.01, ***p<0.001, ****p<0.0001. FFA: free fatty acids; chol: cholesterol; CFU: colony forming units.

4.3 Discussion

The results in this chapter indicate that HPS1 deficiency leads to hampered bacterial clearance, triggered by perturbed metabolism and increased mTORC1 signaling. Interestingly,

the amplified mTORC1 signaling in HPS1 knockout cells was mediated by Rab32 **(Figure 4.13).** mTORC1 inhibition emerges as a metabolic checkpoint in HPS1 deficiency that can rescue the bacterial elimination defect, suggesting that rapamycin could be considered as a potential treatment for HPS-1 patients.

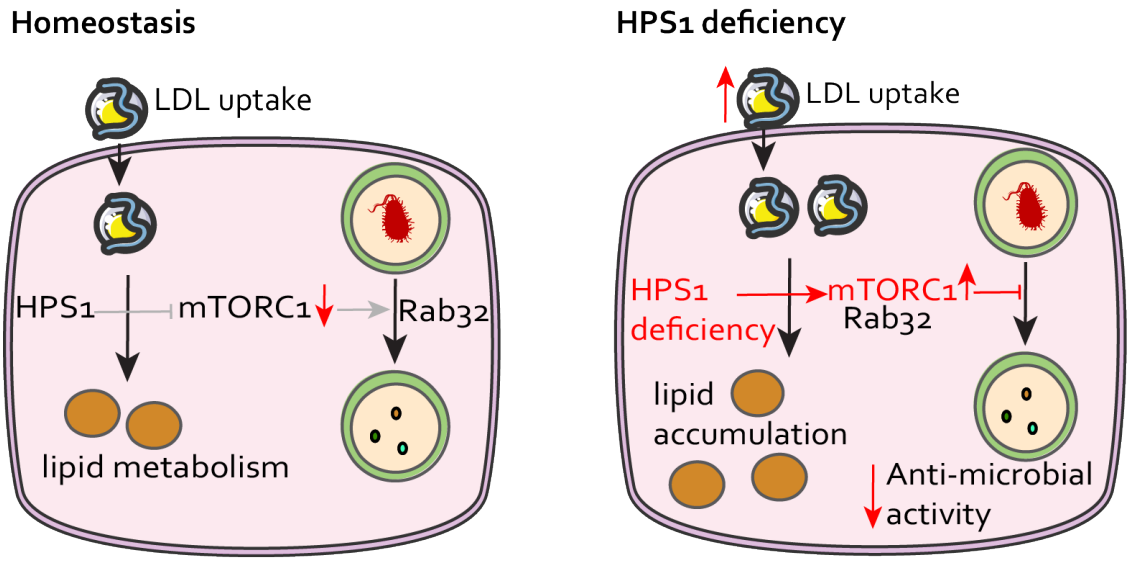


Figure 4.13. Summary of the molecular mechanism underlying HPS1 deficiency. HPS1 sufficiency leads to appropriate lipid metabolism levels, homeostatic mTORC1 signaling and Rab32 can contribute to bacterial elimination. In the HPS1-deficient setting, mTORC1 signaling is heightened through the actions of Rab32, lipids accumulate and bacterial elimination is hampered.

I have shown that HPS1 knockout HAP1 cells internalize a higher amount of LDL compared to control cells. LDL further exacerbated mTORC1 activation and mTORC1 was the trigger for increased LDL uptake in HPS1 deficiency. Additionally, HPS1 knockout cells had enhanced expression of SREBP target genes, which could in part contribute to the metabolic changes observed. While this is the first report of HPS1 deficiency having enhanced LDL uptake, which can be normalized by rapamycin, rapamycin treatment has previously been shown to dampen oxidized LDL uptake in endothelial cells (Zhou et al., 2016). These results

highlight that mTORC1 and LDL uptake form a positive, potentially pathogenic feedback loop in HPS1 deficiency.

Interestingly, heightened mTORC1 signaling in HPS1 deficiency was caused by Rab32, a target of BLOC-3 (Gerondopoulos et al., 2012). Recently, Rab32 was described to localize to the lysosome and mediate the anchoring of mTORC1 and its activation by amino acid signals (Drizyte-Miller et al., 2020). Moreover, Rab32 associates with multiple other organelles including phagosomes (Li et al., 2016b), lipid droplets (Bosch et al., 2020), mitochondria (Alto et al., 2002) and the ER (Bui et al., 2010; Hirota and Tanaka, 2009), carrying out diverse functions. The balancing act of regulating the localization of Rab32 to these compartments may be controlled by BLOC-3. It has previously been shown that BLOC-3 anchored to mitochondria can direct Rab32 to this compartment (Gerondopoulos et al., 2012). In addition, BLOC-3 overexpression enhances the localization of Rab32 to phagosomes, further lending credence to this hypothesis (Balci et al., 2020). Interrogating the localization of Rab32 in HPS1 deficiency could help delineate this hypothesis.

HPS1 knockout cells could not efficiently degrade *Salmonella* Typhimurium, Adherent Invasive *E. coli* and *Staphylococcus aureus,* suggesting that impaired bacterial handling in HPS1 deficiency is not pathogen-specific. This finding is further supported by studies in mice and human cell lines. For instance, Rab32 deficiency in murine macrophages and a dendritic cell line results in aberrant bacterial handling of *Salmonella typhi* (Spano and Galan, 2012) and *Listeria monocytogenes* (Li et al., 2016b), respectively. Similarly, Rab32 has been shown to be essential for the clearance of *Burkholderia pseudomallei* in the murine macrophage RAW264.7 cell line (Hu et al., 2019). Specifically, Rab32 was associated with phagosomes and Rab32 depletion led to decreased phagosome-lysosome fusion. In a small hairpin RNA screen, HPS1 knockdown in murine bone marrow-derived macrophages hampered *Salmonella typhi*

elimination (Solano-Collado et al., 2021). Additionally, HPS4-deficient induced pluripotent stem cell-derived macrophages have impaired elimination of *Staphylococcus aureus* and *Candida albicans* (Baldassarre et al., 2021).

In this chapter, I showed that HPS1-deficient HAP1 cells are not able to handle *Salmonella* Typhimurium effectively. Other studies found that *Salmonella* Typhimurium has effectors (SopD2, GtgE) that antagonize the BLOC-3 pathway (Baldassarre et al., 2021; Spano et al., 2016). Still, Rab32$^{-/-}$ or Hps4$^{-/-}$ mice have a bacterial clearance defect following *Salmonella* Typhimurium infection in earlier studies. While I have used GFP-*Salmonella* Typhimurium strain NCTC 12023 in my experiments, the previous studies were conducted with the SL1344 strain. Interestingly, the NCTC 12023 strain I used has reduced pathogenicity and decreased expression of key virulence and evasion genes (Clark et al., 2011). Therefore, there may be differences in the ability of the strain I used to antagonize host defense pathways.

Furthermore, I show that there is a hampered autophagy flux in HPS1 knockout HAP1 cells. Since mTORC1 has been shown to negatively regulate autophagy (Kim et al., 2011; Settembre et al., 2012), it is possible that the bacterial handling defect is due to enhanced mTORC1 signaling in HPS1 deficiency. HPS1 knockdown in the lung epithelial A549 cell line resulted in the accumulation of p62 and LC3-II (Ahuja et al., 2016), highlighting a blockade in autophagy flux. Furthermore, I show that the suppression of mTORC1 signaling results in the reversion of the bacterial elimination defect in HPS1 deficiency. Since rapamycin stimulates autophagy, the enhanced bacterial clearance may be caused by increased autophagy and not necessarily mTORC1 inhibition. Nevertheless, these findings showcase the potential for rapalogs to act as therapeutic agents in HPS-1 patients who have intestinal inflammation.

Alternatively, alterations in metabolism may explain the impaired bacterial handling in HPS1 knockout cells. In support of this hypothesis, I treated HPS1-deficient cells with free fatty acids, which led to a normalization in bacterial clearance capacity. This result suggests that free fatty acids may not be readily available in HPS1 knockout cells due to dysregulated metabolism. It would be interesting to pulse-chase fatty acids within cells and determine the degree of co-localization of fatty acids with lipid droplets and mitochondria. These experiments could shed light on where fatty acids end up in HPS1 deficiency compared to controls. The experiments in this chapter have been performed on HAP1 cells, and patient-derived cells would be useful to validate these mechanisms.

Interestingly, *LACC1* variants, which predispose to Crohn's disease and juvenile idiopathic arthritis, impair autophagy flux, bacterial clearance and mitochondrial respiration through lipid droplet defects (Cader et al., 2016; Omarjee et al., 2021). We identified attenuated oxidative phosphorylation and amplified mtROS in HPS1-deficient HAP1 cells, underlining the derailed metabolic program in the disease. It would be prudent to examine whether fatty acid treatment could revert this metabolic dysregulation in HPS1 deficiency, as is the case for Laccase domain containing 1 (LACC1) deficiency. Furthermore, Niemann-Pick Type C1 (NPC1) causes lipid accumulation (Vanier, 2010) and anti-microbial activity defects and features Crohn's-like inflammation (Schwerd et al., 2016). NPC1 negatively regulates the activation of mTORC1 signaling (Castellano et al., 2017). My findings stressing the role of HPS1 and Rab32 in mTOR signaling and cholesterol accumulation add to a spectrum of genetic deficiencies with metabolic signaling dysregulation which can cause hampered bacterial elimination.

In summary, LDL uptake was increased in HPS1 knockout cells, consistent with the LDL signature from the transcriptomics data in HPS-1 patient macrophages. Additionally, mTORC1

signaling was enhanced in HPS1 deficiency in a Rab32-dependent manner. Interestingly, HPS1 knockout HAP1 cells have impaired bacterial clearance, which can be rescued with the supplementation of free fatty acids or through mTORC1 inhibition using rapamycin. These results accentuate plausible mechanisms underlying HPS-1-associated IBD and the potential for rapalogs to treat this disease.

Chapter 5 - Defective anti-microbial activity and inflammation in HPS-1 patients

5.1 Introduction

Some HPS subtypes are associated with the development of lung fibrosis and intestinal inflammation. Specifically, HPS-1 and HPS-4 patients develop Crohn's-like intestinal inflammation (Hussain et al., 2006; O'Brien et al., 2021). The HPS1 and HPS4 proteins are the two components of BLOC-3 (Gerondopoulos et al., 2012). Histologically, these patients have granulomata, lymphoid follicles, pigmented macrophages and abscesses and present with several gastrointestinal symptoms including diarrhea, hematochezia and pain (O'Brien et al., 2021). BLOC-2 is a heterotrimeric complex composed of the HPS3, HPS5 and HPS6 proteins (Di Pietro et al., 2004). Most recently, some HPS-3 patients and one HPS-6 patient have been reported to exhibit IBD, although it appears to be less severe than BLOC-3-associated IBD (O'Brien et al., 2021). The reason for the discrepancy in the severity of clinical manifestations between BLOC-3 and BLOC-2-associated IBD is unclear.

HPS1 deficiency in HAP1 cells seems to impair bacterial clearance through deregulated lipid metabolism and mTORC1 signaling. Interestingly, CD11c-specific Rab32$^{-/-}$ mice treated with DSS to promote intestinal inflammation highlighted an enhanced expression of *Il1a, Il1b* and *Il6*, along with increased bacterial translocation (Xie et al., 2018). Furthermore, another study has shown that HPS-1 patients with pulmonary fibrosis have a distinct inflammatory signature featuring IFN-γ, TNF and IL-8 (El-Chemaly et al., 2018). However, a comprehensive phenotype of immune cells in HPS-1 has not been performed previously.

Several aspects of HPS-1 point to similarities with the lysosomal storage disorder NPC1. NPC1 patients have neurodegeneration and can develop intestinal inflammation with

granuloma formation (Schwerd et al., 2016). Interestingly, NPC1 binds to SLC38A9, which can sense intra-lysosomal cholesterol and arginine, and negatively regulates mTORC1 signaling (Castellano et al., 2017). NPC1 is involved in mediating the egress of cholesterol from the lysosome to the ER through contact sites, and artificial tethering of the ER to the lysosome can reverse lysosomal cholesterol accumulation (Hoglinger et al., 2019). On the other hand, in NPC1 deficiency, OSBP-mediated transfer of cholesterol from the ER to the lysosome enhances mTORC1 signaling (Lim et al., 2019). Therefore, NPC1 emerges as a critical regulator of lysosomal contact sites, which are crucial for nutrient sensing and mTORC1 signaling.

In this chapter, we interrogate the defects in lipid metabolism and bacterial handling in HPS-1, HPS-3 and NPC1 patients. Importantly, we investigate whether mTORC1 inhibition can rescue the bacterial elimination defect, which has implications for therapeutic strategies in HPS patients with IBD. Lastly, we inspect the immunological phenotype of HPS-1 patients using mass cytometry and serum proteomics to unravel mechanisms of inflammation.

5.2 Results

5.2.1 Cholesterol metabolism is deregulated in macrophages from HPS-1 patients

Since ceroid lipofuscin accumulation is characteristic of HPS, I tested the ability of HPS-1 patient monocyte-derived macrophages to degrade an external source of cholesterol. Following 2 hours of cholesterol treatment, I evaluated the amount of neutral lipids present in cells using a BODIPY dye. While at baseline HPS-1 patients had a similar level of neutral lipids compared to controls **(Figure 5.1)**, the exogenous cholesterol resulted in a higher amount of lipids in HPS-1 patient cells. This indicates that HPS-1 patient macrophages are not able to degrade cholesterol efficiently or that the cells are internalizing a higher amount of cholesterol.

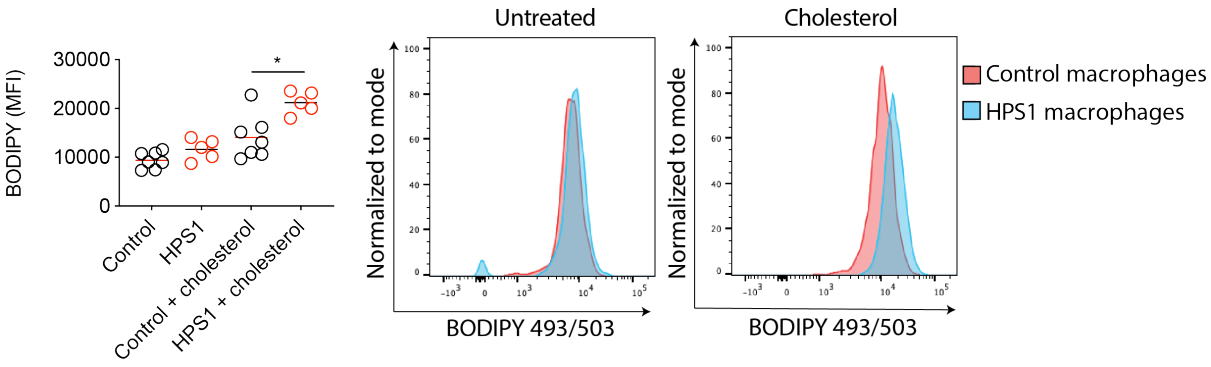


Figure 5.1. HPS-1 patient macrophages have altered cholesterol metabolism. Cholesterol stimulation (5 X) was performed for 2 hours prior to staining with 1 µg/mL BODIPY 493/503 in patient monocyte-derived macrophages (5 HPS-1 patients, 7 healthy controls). Representative flow cytometry plots for BODIPY staining is provided. Unpaired t-test on log-transformed mean fluorescence intensity; *p<0.05.

5.2.2 HPS-1 patient macrophages have impaired bacterial handling

Since I found a defect in anti-microbial activity in HPS1-deficient HAP1 cells, the bacterial handling capacity of HPS-1 patient monocyte-derived macrophages was interrogated through a gentamicin protection assay. We found that patient macrophages were less able to eliminate bacteria, resulting in a higher number of colonies compared to controls **(Figure 5.2A)**. In order to validate and visualize the high bacterial load, we used confocal microscopy with a GFP-expressing *Salmonella* Typhimurium strain and DAPI to stain cell nuclei and bacterial DNA. We found a significantly higher number of *Salmonella* Typhimurium in HPS-1 patient macrophages **(Figure 5.2B-C)**. In addition, more live (GFP^+DAPI^+) bacteria were present in HPS-1 patient macrophages, but the number of bacteria in the process of being degraded ($GFP^{dim}DAPI^+$) or that were already degraded (GFP^-DAPI^+) were unchanged. These results suggest that the bacterial elimination defect is present in HPS-1 patient macrophages. It is possible that bacteria replicate more easily in HPS1 deficiency.

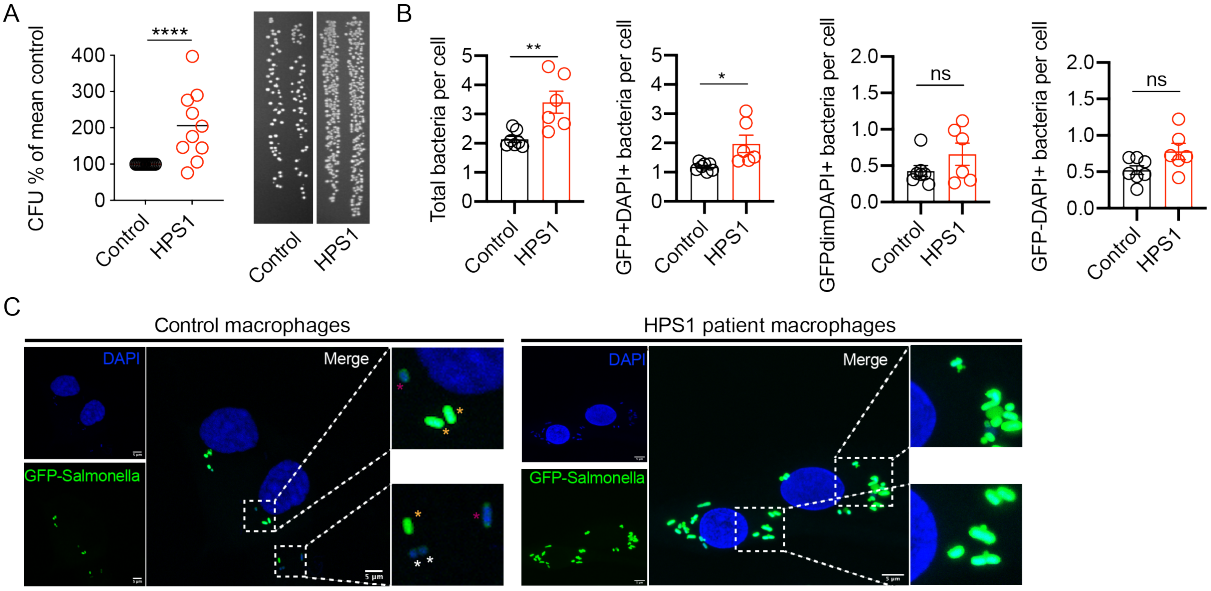


Figure 5.2. HPS-1 patient macrophages show impaired anti-bacterial activity. A) Gentamicin protection assay of healthy donor and HPS-1 patient derived macrophages (n=10). Macrophages were infected with *Salmonella* Typhimurium (MOI of 1 cell : 10 bacteria), followed by 100 µg/mL gentamicin. Each dot shows the average for each donor from two technical replicates. Representative agar plate of gentamicin protection assay. B) Quantification of number of bacteria in each cell using confocal microscopy in control and HPS-1 macrophages (n=6; average per donor shown). C) Representative confocal microscopy images. For the gentamicin protection assay, an unpaired t-test was performed on log-transformed colony forming units; for microscopy data an unpaired t-test was performed; *p<0.05, **p<0.01, ****p<0.0001. Yellow asterisk: $GFP^{+}DAPI^{+}$, magenta asterisk: $GFP^{dim}DAPI^{+}$, white asterisk: $GFP^{-}DAPI^{+}$ bacteria. CFU: colony forming units.

5.2.3 HPS-1 and NPC1 bacterial handling defects rescued by rapamycin

In Chapter 4, I identified a pathogenic loop of mTORC1 signaling in HPS1 knockout HAP1 cells, which could be responsible for the bacterial elimination defect, since mTORC1 negatively regulates autophagy (Kim et al., 2011; Settembre et al., 2012). We used a gentamicin protection assay to investigate the effect of rapamycin on *Salmonella*

Typhimurium elimination in patient macrophages **(Figure 5.3A)**. We found that rapamycin was able to greatly reduce the bacterial load in HPS-1 patient macrophages, rescuing the bacterial handling defect. Rapamycin was also able to induce bacterial elimination in control cells, likely through autophagy induction.

NPC1 is also a lysosomal storage disorder with deregulated lipid metabolism and anti-microbial activity (Schwerd et al., 2016), similar to HPS-1. The NPC1 protein has been shown to curtail mTORC1 activation (Castellano et al., 2017). Using NPC1 monocyte-derived macrophages from one patient, I was able to replicate the bacterial handling defect and rescue it using rapamycin **(Figure 5.3B)**. These findings highlight that rapamycin or rapalogs more generally can provide a novel therapeutic avenue for both HPS-1 and NPC1.

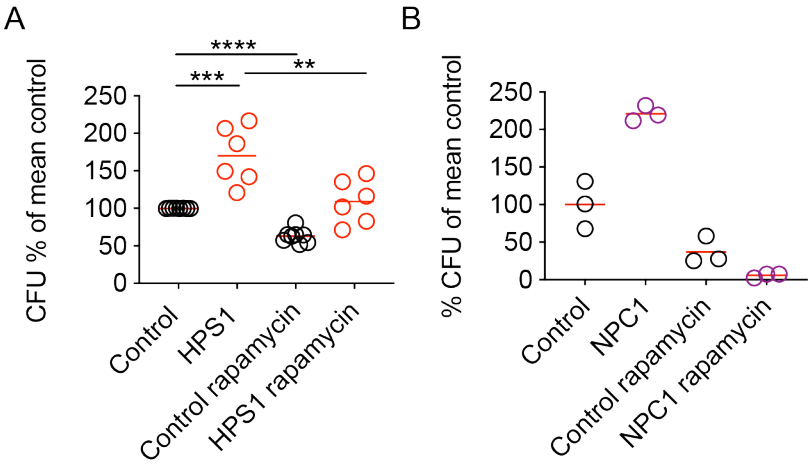


Figure 5.3. Defective bacterial handling in HPS-1 and NPC1 can be rescued by mTORC1 inhibition. A) Macrophages were treated with 50 µM rapamycin for 2 hours prior to *Salmonella* Typhimurium infection (MOI 1:10) and the gentamicin protection assay (6 HPS-1, 10 controls; average per donor shown). B) Macrophages from one NPC1 patient were used and treated with 50 µM rapamycin prior to the gentamicin protection assay (3 technical replicates shown). Unpaired t-test on log-transformed data of colony forming units; **p<0.01, ***p<0.001, ****p<0.0001.

5.2.4 HPS3 deficiency causes impaired bacterial clearance but does not affect mTORC1 signaling

BLOC-2 is composed of the HPS3, HPS5 and HPS6 proteins (Di Pietro et al., 2004). HPS-3 and HPS-6 cause a mild form of IBD compared to defects in BLOC-3, composed of HPS1 and HPS4 (O'Brien et al., 2021). Specifically, HPS-3 patients with IBD do not have fistulizing disease and have less severe symptoms compared to HPS-1. However, the level of penetrance of IBD in HPS-3 patients (17 %) is similar to HPS-1 (15 %).

In order to interrogate the cellular and molecular mechanisms that may underlie these disparities, we examined cholesterol metabolism and bacterial elimination in HPS-3 patients. We found that HPS-3 patient macrophages have a higher lipid accumulation at baseline compared to controls **(Figure 5.4A)**. Cholesterol stimulation results in a non-significant increase of lipid abundance for HPS-3 macrophages. Since we identified a bacterial elimination defect in HPS-1, we sought to evaluate the effects of HPS3 deficiency on macrophage anti-microbial activity. HPS-3 patient macrophages were less able to degrade bacteria in comparison to controls **(Figure 5.4B)**. In summary, HPS-3 triggers lipid accumulation and defective bacterial elimination, similar to HPS-1.

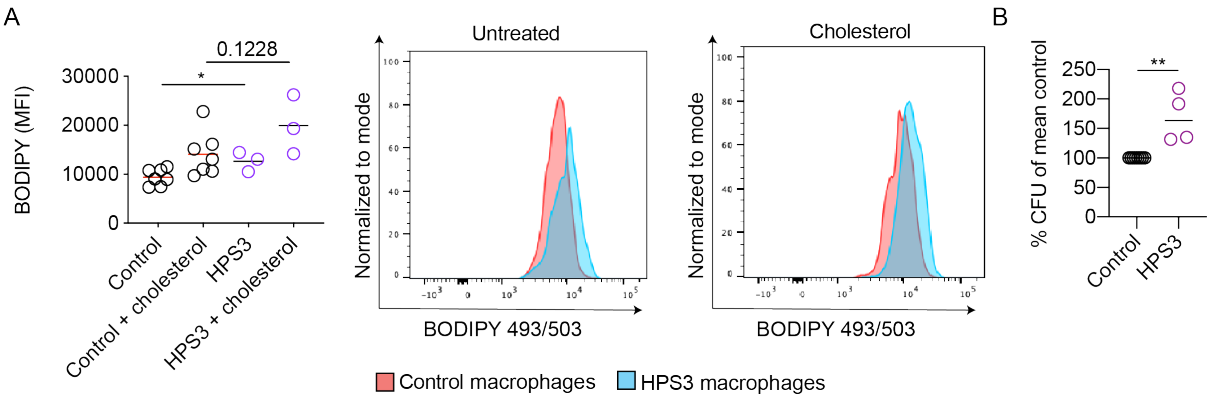


Figure 5.4. HPS-3 patient macrophages show signs of altered lipid metabolism and exhibit attenuated bacterial clearance. A) Cholesterol stimulation (5 X) was performed for 2 hours

prior to staining with 1 µg/mL BODIPY 493/503 in patient monocyte-derived macrophages (3 HPS-3 patients, 7 healthy controls). Representative flow cytometry plots for BODIPY staining is provided. B) Macrophages were infected with *Salmonella* Typhimurium (MOI 1:10) and the gentamicin protection assay was performed (4 HPS-3, 8 healthy controls; average per donor shown). The controls used in this figure are the same samples and experiment as used for HPS-1 in Figures 5.1 and 5.2. Unpaired t-test on log-transformed mean fluorescence intensity; unpaired t-test on log-transformed data of colony forming units; *p<0.05, **p<0.01.

BLOC-2 immunoprecipitates with Rab32-GTP, but not Rab32-GDP (Bultema et al., 2012). Given that BLOC-3 determines GDP release for Rab32 (Gerondopoulos et al., 2012), we reasoned that BLOC-2 deficiency does not affect the GDP/GTP status of Rab32. Therefore, BLOC-2 could interact with Rab32-GTP to mediate bacterial clearance, but would not affect mTORC1 signaling, which can be mediated by Rab32-GDP (Drizyte-Miller et al., 2020). On the other hand, BLOC-3 deficiency would lead to the accumulation of Rab32-GDP, which cannot be converted to Rab32-GTP, resulting in dampened bacterial elimination and heightened mTORC1 signaling, as described in Chapter 4. In line with this hypothesis, we found that HPS-1 increased S6 phosphorylation, a surrogate marker for mTORC1 signaling, but HPS-3 did not **(Figure 5.5A-B)**. Therefore, HPS3 deficiency can deregulate anti-microbial activity but has no impact on mTORC1 signaling.

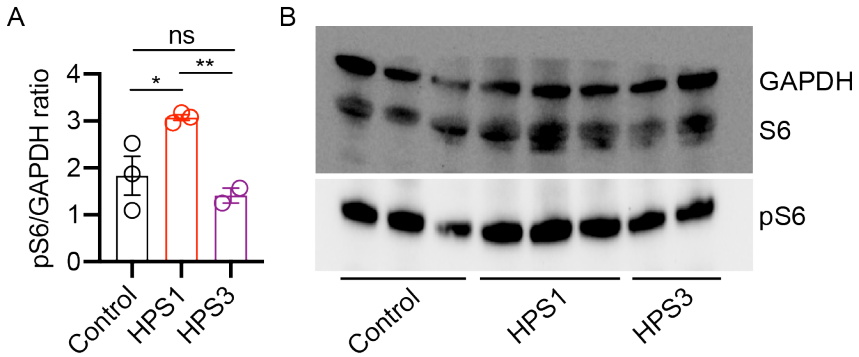


Figure 5.5. HPS-1 causes deregulated mTORC1 signaling but HPS-3 does not alter mTORC1 activity. A) Quantification of Western blot of control, HPS-1 and HPS-3 patient macrophage samples for pS6 and GAPDH (n=3 for healthy controls and HPS-1 patients; n=2 for HPS-3 patients). Quantification was performed using ImageJ. B) Western blot image used for quantification. An unpaired t-test on ratio data was performed; *p<0.05, **p<0.01, ns=0.4984.

5.2.5 HPS-1 patient peripheral blood mass cytometry identifies inflammatory monocytes

In collaboration with Dr. Louis Cohen at the Icahn School of Medicine at Mount Sinai, we sought to profile the immune cells in HPS-1 patient peripheral blood. Specifically, we recruited 8 HPS-1 patients and 12 healthy controls and performed mass cytometry using antibodies against immune cell surface markers **(Figure 5.6A)**. Using the unsupervised clustering method flow self-organizing map (FlowSOM), we obtained 13 metaclusters **(Figure 5.6B)**. These 13 metaclusters represent 13 different cell types, and contain 100 distinct clusters. We used a heatmap to identify the cell types that corresponded to each metacluster **(Figure 5.6C)**.

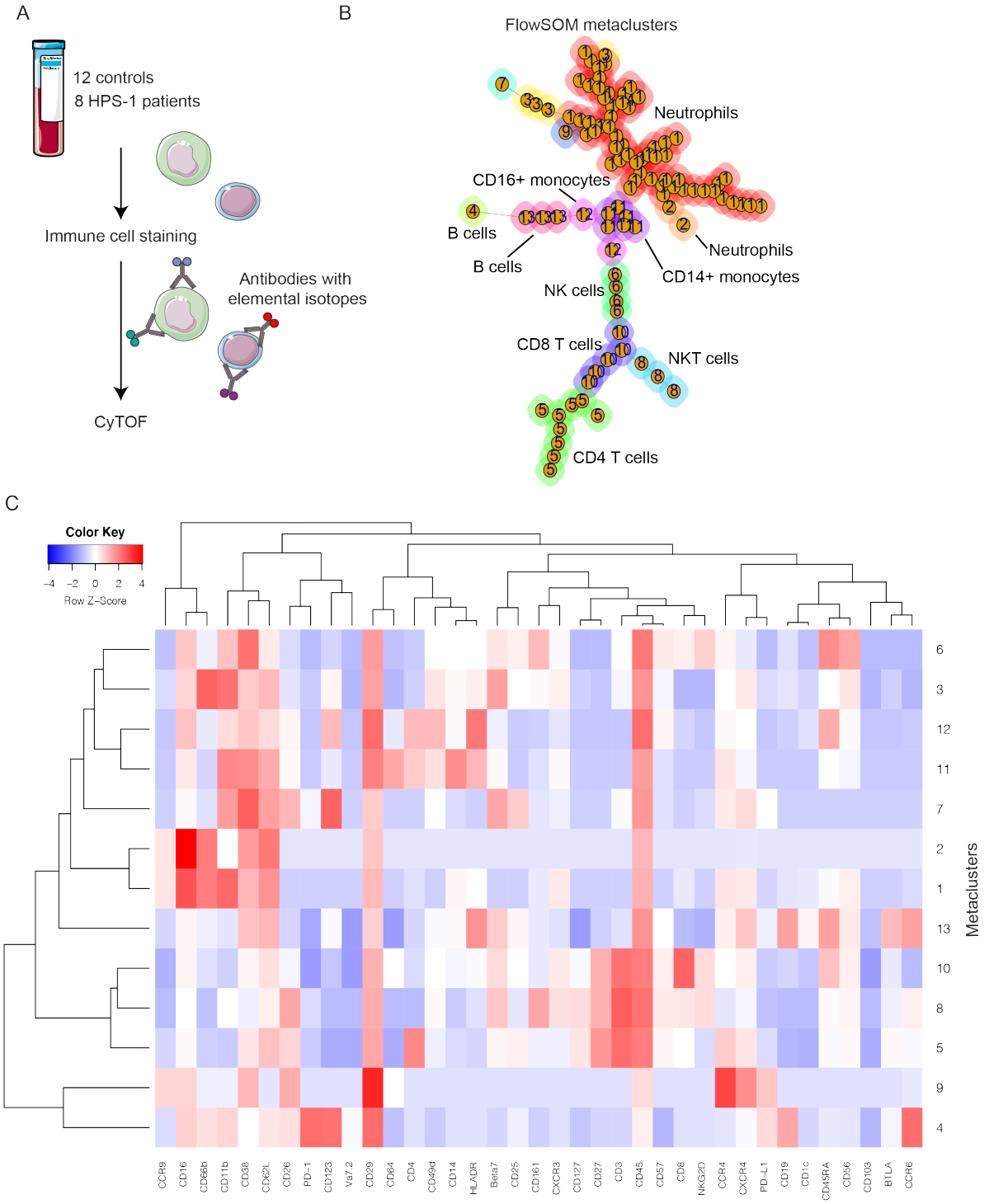


Figure 5.6. Mass cytometry of peripheral blood in HPS-1 patients and controls. A) Experimental scheme for mass cytometry analysis of 12 controls and 8 HPS-1 patients. B) FlowSOM analysis of CyTOF data defines 100 cell clusters (individual nodes) organized into 13 metaclusters (node number and color). Clusters were assigned cell types based on the expression of specific surface markers. C) Heatmap of metaclusters against protein expression.

We identified that metaclusters 5 and 11 have different relative proportions between HPS-1 patients and controls **(Figure 5.7A)**. Within metacluster 5, the cluster that was significantly different in HPS-1 was $CD4^{+}CD25^{+}CD127^{low}$, indicative of a T regulatory cell type **(Figure 5.7B)**. Metacluster 11 expressed monocytic markers such as CD14 and contained 3 significantly different clusters between controls and HPS-1 patients **(Figure 5.7C)**. Cluster 11.1 had high levels of CD64 and CD62L, which are associated with inflammation (Luo et al., 2018) and migration to the periphery (Ivetic et al., 2019), respectively. Cluster 11.2 exhibited heightened integrin β_7, CD64 and CD62L expression. On the other hand, cluster 11.3 was demarcated by CD16, a non-conventional monocyte marker. In summary, we discovered a decrease in T regulatory cells and an increase in inflammatory monocytes in HPS-1.

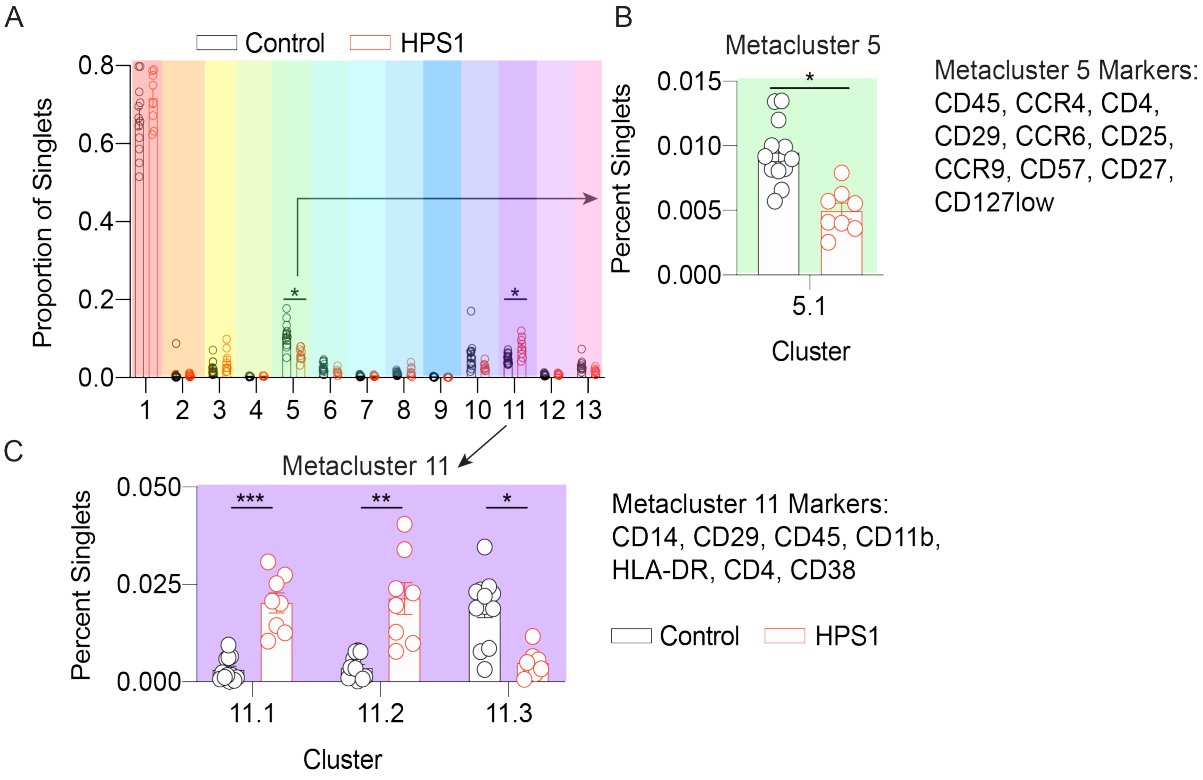


Figure 5.7. Mass cytometry identifies changes in monocytes and T regulatory cells in HPS-1. A) Metaclusters 5 and 11 were significantly associated with HPS-1 patients. B) Cluster 5.1 had

a profile of $CD4^{+}CD25^{+}CD127^{low}$ expression. C) Cluster 11.1 was defined by CXCR3, $CD64^{hi}$, $CD62L^{hi}$, cluster 11.2 by β_7^{hi}, $CD64^{hi}$, $CD62L^{hi}$ and 11.3 by CD16. Populations were compared with an unpaired t-test with Bonferroni-Dunn correction for multiple comparisons. Data are mean +/- SEM. *p<0.05, **p<0.01, ***p<0.001. All p values are adjusted.

A principal component analysis demonstrates that HPS-1 patient peripheral blood separates in terms of immune cell surface markers from controls **(Figure 5.8A)**. Following the identification of a potentially inflammatory monocyte compartment, we focused on these changes. Specifically, we used t-distributed stochastic neighbor embedding (tSNE) plots to visualize the enhanced expression of CD64 and CD62L, which were altered in clusters 11.1 and 11.2 **(Figure 5.8B)**. Histograms of surface marker expression in monocytes further underlines this difference **(Figure 5.8C)**. Additionally, we took a manual gating approach of $CD14^{+}$ monocytes to validate our findings from the unsupervised clustering algorithm. We found a significant increase of classical $CD14^{+}$ monocytes in HPS-1 **(Figure 5.8D-E)**. These analyses highlight an activated monocyte compartment in HPS-1 patient peripheral blood.

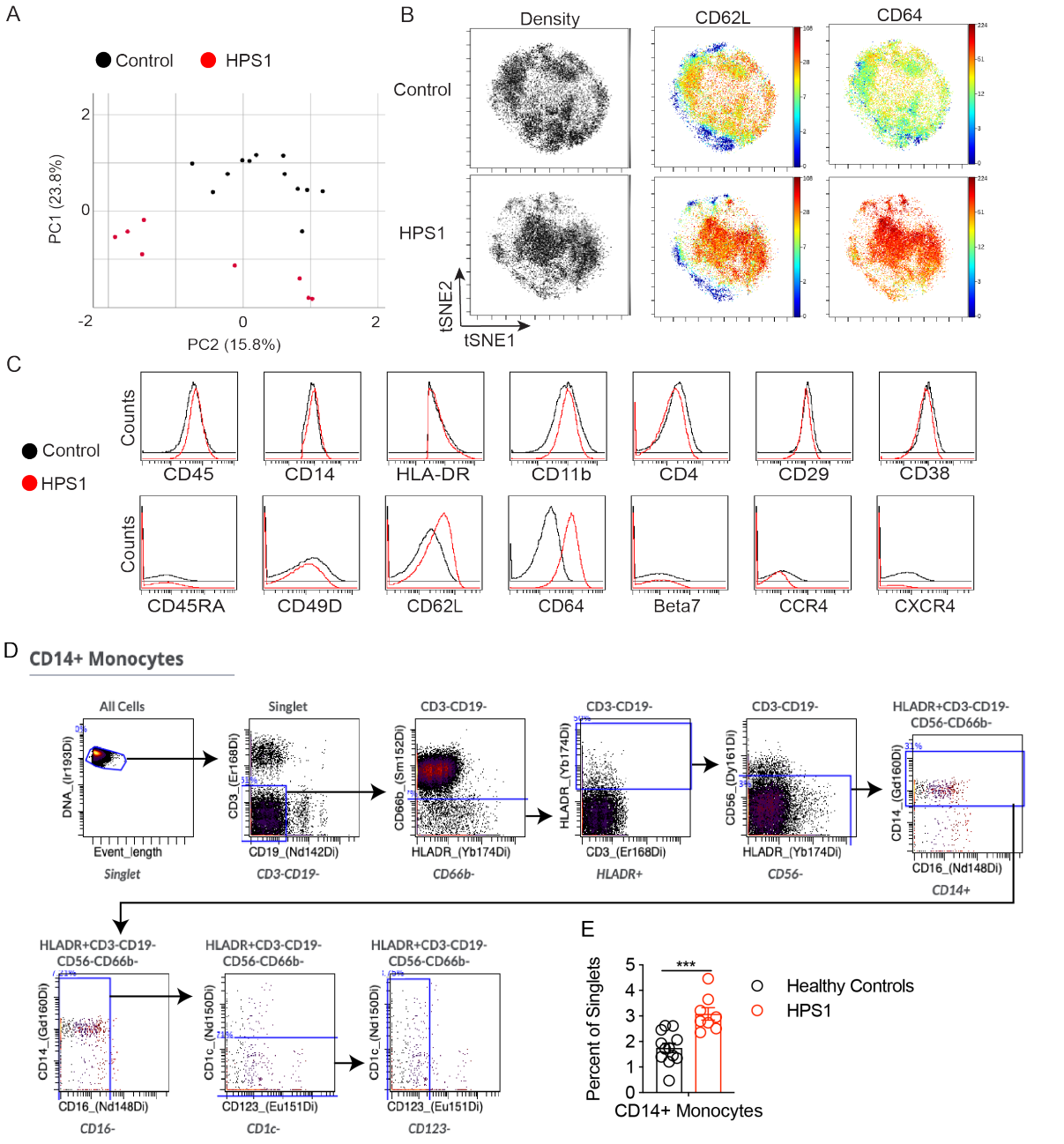


Figure 5.8. Mass cytometry pinpoints an inflammatory monocyte compartment in HPS-1. A) Principal component analysis of FlowSOM clusters separates HPS-1 patients and healthy controls. B) SNE analysis of CD14^{+} monocytes defines distinct populations of monocytes in patients with HPS-1 highly expressing CD62L and CD64. C) Histogram of marker expression in monocytes of patients with HPS-1 or controls. D) Gating hierarchy for CD14^{+} monocytes. E) Comparison of CD14^{+} monocyte abundance in patients with HPS-1 or controls. Populations are compared with an unpaired t-test. Data are mean +/- SEM, *** p<0.001.

5.2.6 HPS-1 patient serum proteomics reveals a TNF/IL-1α signature

Our mass cytometry analysis utilized surface marker expression to reveal changes in immune cell composition. In order to further our understanding of disease mechanisms, we used Olink proteomics, in collaboration with Dr. Louis Cohen, to discover alterations in proteins and signaling cascades. Specifically, we employed a panel targeting 92 proteins using the inflammation panel. The experiment was performed on the serum of 50 controls, 5 HPS-1 patients, 4 HPS-1 patients with IBD and 2 HPS-1 patients with pulmonary fibrosis (PF) **(Figure 5.9A)**. A principal component analysis illustrates that HPS-1 patients segregate from controls regardless of phenotype, suggesting that the inflammatory protein changes are caused by the genotype **(Figure 5.9B)**.

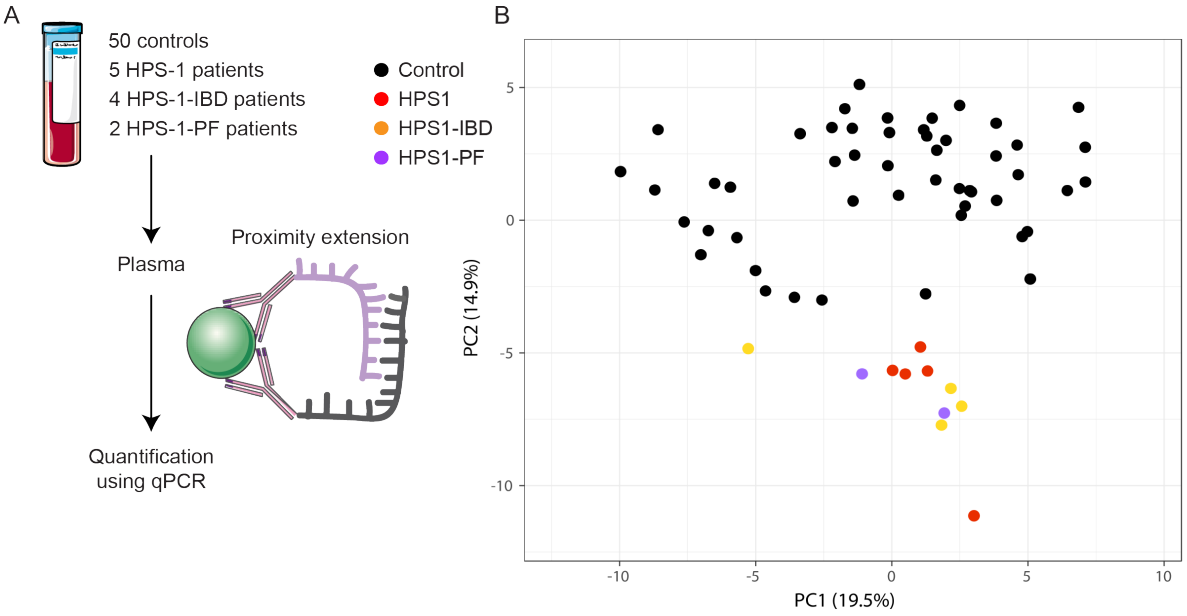


Figure 5.9. Serum Olink proteomics reveals differences between HPS-1 patients and controls. A) Experimental scheme used for the detection of proteins using the Olink inflammation panel, a proximity extension assay, on 50 controls, 5 HPS-1, 2 HPS-1 PF and 4 HPS-1 IBD patients. B) Principal component analysis of the Olink inflammation panel results.

In a hierarchical clustering heatmap, all HPS-1 patients clustered together regardless of phenotype and had an increase in several inflammatory proteins **(Figure 5.10A)**. For instance, HPS-1 patient serum included the significantly increased TNF, IL-1α, IL-2 and TGF-α **(Figure 5.10B-C)** as well as heightened trends for IL-6 and IFN-γ. In summary, HPS-1 patient serum proteomics identifies an inflammatory signature that includes TNF and IL-1α.

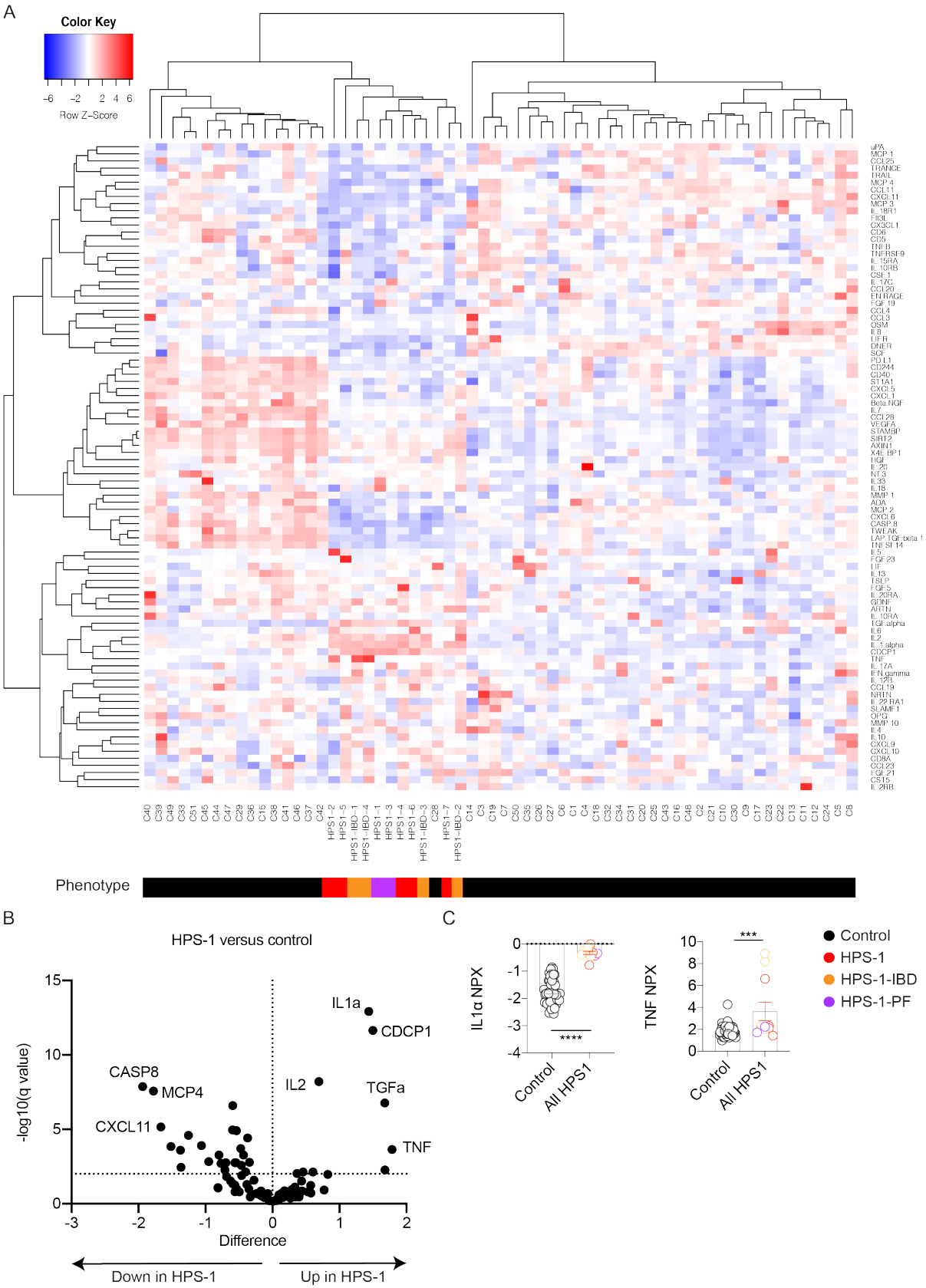


Figure 5.10. Serum Olink proteomics reveals a TNF/IL-1α signature in HPS-1. A) Heatmap of normalized protein expression with hierarchical clustering of inflammatory proteins using the Olink inflammation panel. B) Volcano plot of all HPS-1 samples compared to controls. C) Dot

plots of IL-1α and TNF protein expression. The Benjamini, Krieger and Yekutieli multiple nonparametric t-test was performed, *** adjusted p<0.001, **** adjusted p<0.0001. NPX: normalized protein expression.

5.2.7 NOD2 and TLR4 signaling are intact in HPS-1

Given the bacterial elimination defect, we investigated whether bacterial recognition was intact. In order to test this, we investigated NF-κB signaling downstream of the PRRs TLR4 and NOD2, using the ligands LPS and L-18 MDP, respectively (Schwerd et al., 2016). The readout of NF-κB activation was TNF production in monocytes, and we did not find any significant differences following stimulation **(Figure 5.11)**. These data suggest that sensing through TLR4 and NOD2, and the downstream signaling cascade, remains unchanged.

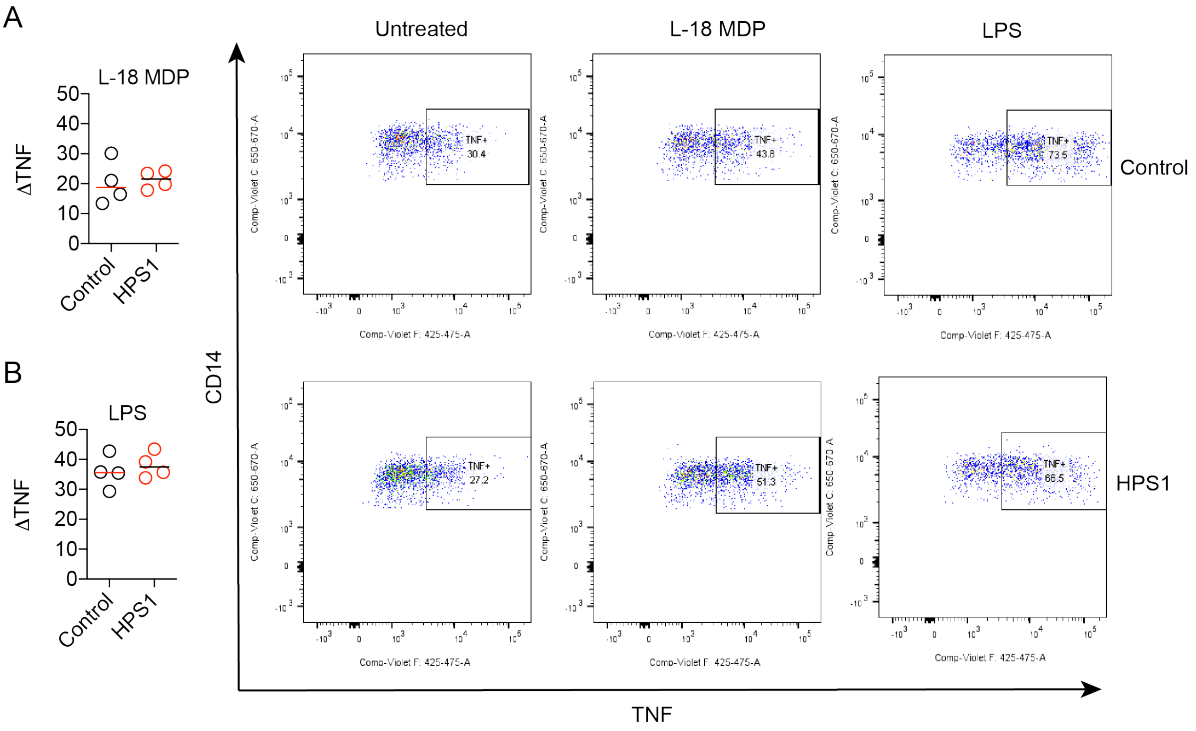


Figure 5.11. HPS-1 patient monocytes display normal TNF responses to MDP and LPS. A) Change in TNF production in response to 200 ng/mL L-18 MDP and B) 100 ng/mL LPS compared to the untreated condition in healthy donors and HPS-1 patients measured by flow

cytometry and gated on live, $CD14^+$ and $HLA\text{-}DR^+$ cells. C) Representative flow cytometry plots of untreated, MDP and LPS stimulated conditions in a healthy donor and HPS-1 patient.

5.3 Discussion

Hermansky-Pudlak Syndrome types 1 and 4 can present with severe Crohn's-like colitis (O'Brien et al., 2021). We have shown that HPS-1 patient macrophages have impaired bacterial clearance and cholesterol metabolism. At the same time, we found that HPS-3 patients, who can develop a milder form of IBD (O'Brien et al., 2021), have a bacterial clearance defect. Intriguingly, a potential explanation for the less severe intestinal inflammation may lie with the absence of amplified mTORC1 signaling in HPS-3. Furthermore, HPS-1 peripheral blood has an expanded and inflammatory monocyte compartment in addition to a TNF/IL-1α signature in serum. These dysregulations may contribute to the intestinal inflammation observed in HPS-1 patients.

One crucial aspect of intestinal homeostasis are host-microbe interactions (Uhlig and Powrie, 2018). In IBD, host-microbial interactions can be disrupted, resulting in aberrant sensing or degradation of microbes. For instance, *NOD2* and *ATG16L1* are risk loci for IBD, and their encoded proteins participate in sensing MDP and triggering the autophagy pathway to mediate microbial degradation (Cooney et al., 2010; Homer et al., 2010; Travassos et al., 2010). In the monogenic disease realm, NPC1 can present with intestinal inflammation, which has been attributed to an inability to handle bacteria (Cavounidis and Uhlig, 2018; Cougnoux, 2018; Schwerd et al., 2016). These emerging studies, combined with our finding that HPS1 deficiency leads to a microbial elimination defect, highlight the important role of bacterial degradation in intestinal homeostasis.

In this chapter, we have shown that the bacterial elimination defect in HPS-1 and NPC1 patient macrophages can be rescued by rapamycin. Moreover, since NPC1 modulates mTORC1 activation (Castellano et al., 2017), NPC1 deficiency potentiates aberrant growth and metabolic signaling, negatively impacting lysosomal degradation. Aberrant mTORC1 signaling is also central to the lysosomal storage disorder mucopolysaccharidoses, highlighting its role in lysosomal function in the skeletal system (Bartolomeo et al., 2017). At the same time, studies have accentuated that the overexpression of TFEB, which positively regulates lysosomal function, can rescue degradation defects in Batten's disease (Palmieri et al., 2017) and atherosclerosis (Emanuel et al., 2014). Rapamycin treatment of LPS-stimulated monocyte-derived macrophages from patients with IL-10R defects diminishes IL-1β secretion (Ip et al., 2017), likely dampening inflammation. Furthermore, rapamycin-eluting stents used in the treatment of atherosclerosis reduce inflammation (Liu et al., 2018). Therefore, the data presented in this chapter add to mTORC1-driven disorders which can be reverted with mTORC1 modulators. Use of mTORC1 inhibition clinically in HPS-1 patients with IBD would provide proof-of-concept that modulation of this axis can act as a novel therapy. It is tempting to speculate that mTORC1 inhibitors might be beneficial in other diseases with defective metabolic signaling and lipid accumulation.

Small clinical trials and case reports have examined the potential therapeutic benefit of mTORC1 inhibition in IBD. A patient with Crohn's disease, who was losing response to infliximab, was successfully treated with rapamycin and infliximab and went into remission (Massey et al., 2008). In addition, a retrospective analysis in children with UC or Crohn's disease treated with rapamycin showed some clinical response (Mutalib et al., 2014). Of 11 UC patients, 7 responded to therapy, and of 3 Crohn's patients, all responded. However, this study is limited since it is a retrospective, observational analysis and several patients were

excluded without explanation. Another study on adult Crohn's disease patients emphasized that rapamycin ameliorated symptoms in 5 of 6 patients with strictures in the upper gastrointestinal tract, but not patients with lower gastrointestinal tract strictures (Zhong et al., 2020). Clinical response was calculated as a combined score including abdominal pain, distention and dietary tolerance as well as need for surgical intervention. This investigation features a small cohort of patients and was not randomized or placebo-controlled. Overall, large, randomized and placebo-controlled clinical trials are required to assess the clinical efficacy of mTORC1 inhibition in IBD. It is tempting to speculate that especially patients harboring bacterial clearance defects may respond to mTORC1 inhibition. However, newer classes of rapalogs may hold greater promise than rapamycin, which can have adverse events (Lamming et al., 2013).

Previous studies have suggested that Rab32-GTP co-immunoprecipitates with AP-3 and BLOC-2 (Bultema et al., 2012). We found that the distinction between HPS-1 and HPS-3 lies with mTORC1 activity; HPS-1 results in augmented mTORC1 signaling, whereas HPS-3 does not, even though both feature abrogated microbial elimination. One potential explanation is that BLOC-2 might have a role downstream of BLOC-3 stimulating Rab32-GTP binding. Specifically, BLOC-2 may aid Rab32 in facilitating bacterial clearance. Since both AP-3 and BLOC-2 co-immunoprecipitate with Rab32-GTP, it is possible that both BLOC-2 and AP-3 are required for this function (Bultema et al., 2012). In support of this, AP-3 deficient mice are unable to degrade bacteria efficiently following *Salmonella* Typhimurium infection (Mantegazza et al., 2017). A larger number of patients with AP-3 defects may help dissect this hypothesis, since our data would suggest that patients with defined AP-3 defects may develop IBD. However, out of 3 patients so far examined for intestinal manifestations, none had IBD (O'Brien et al., 2021). In summary, the differential phenotypes in patients with deficiencies in

the BLOC-2, BLOC-3 and AP-3 complexes may be a consequence of Rab32 being in the GDP or GTP status and its interactions with these complexes.

HPS-1 patients have an enhanced monocyte compartment with inflammatory markers. In a previous study on HPS-1 patients with pulmonary fibrosis, these patients had an increased percentage of monocytes compared to familial pulmonary fibrosis (El-Chemaly et al., 2018). Additionally, a cluster of HPS-1 monocytes had high expression of the β_7 integrin, which is associated with homing to the gastrointestinal tract (Schippers et al., 2016). Specifically, β_7 deficiency partially protects mice from DSS colitis, as $\alpha_4\beta_7$ on immune cells binds MAdCAM-1 in the endothelium, allowing them to migrate to the intestine.

In parallel, a study found that HPS-1 pulmonary fibrosis patients have enhanced expression of TNF and IFN-γ levels in serum (El-Chemaly et al., 2018), consistent with our findings of a TNF/IL-1α signature in HPS-1. IL-1 is emerging as an important inflammatory cytokine in IBD, and blocking this signaling cascade may provide a novel target for patients who are unresponsive to conventional therapies (Aschenbrenner et al., 2020; Friedrich et al., 2021). Targeting TNF or IL-1 in patients with HPS-1 who have IBD, in addition to ameliorating impaired bacterial clearance, may be an attractive combination therapy.

However, inflammatory cytokine production and hampered anti-microbial immunity may not be the only factors contributing to HPS-IBD. A study in Hps1-deficient mice has suggested that Paneth cells cannot secrete the anti-microbial factor lysozyme and that microbial composition in the gut is affected (Yu et al., 2020b). Specifically, HPS-1 patients and $Hps1^{-/-}$ mice have an increase in the *Prevotellaceae* bacterial family compared to controls (Yu et al., 2020b), which are associated with intestinal inflammation (Iljazovic et al., 2021). These studies highlight that there may be several layers that contribute to intestinal inflammation in HPS-1.

In this chapter, we show that TNF production is maintained following MDP or LPS stimulation in HPS-1 patient monocytes. AP-3-deficient cells have blunted responses to particulate LPS stimulation, but not soluble LPS, suggesting that trafficking to the phagosome and priming TLR4 intracellularly may be defective (Mantegazza et al., 2012). Therefore, it would be interesting to investigate whether particulate LPS is able to signal through TLR4 efficiently in HPS1 deficiency.

We indicate that mTORC1 inhibition can be beneficial in ameliorating the bacterial handling defect in HPS-1, and potentially, NPC1. Combining anti-TNF or anti-IL-1 therapies with rapalogs could improve the gastrointestinal manifestations in HPS-IBD and curb inflammation. In addition, mTORC1 modulation may benefit a wide array of immune-mediated diseases that are characterized by metabolic dysregulation.

Chapter 6 - Discussion

While inflammatory bowel disease remains a complex disease, research is focused on understanding relevant processes that can help stratify patients and improve therapeutic options. Monogenic diseases that present with intestinal inflammation have provided invaluable clues into pertinent mechanisms underlying inflammation. These include a diverse range of defects, such as FOXP3 deficiency leading to T regulatory cell dysfunction and defects in the NADPH oxidase complex, which is crucial for reactive oxygen species generation (Charbit-Henrion et al., 2021). The lysosomal storage disorder NPC1 has neurological and gastrointestinal manifestations and on a cellular level features lipid accumulation (Lloyd-Evans et al., 2008), abrogated bacterial clearance (Schwerd et al., 2016) and deregulated mTORC1 signaling (Castellano et al., 2017). Similarly, HPS-1 is a lysosome-related organelle disorder that results in ceroid lipofuscin deposition, pulmonary fibrosis (Gahl et al., 1998) and intestinal inflammation (O'Brien et al., 2021).

In this thesis, I demonstrate that the BLOC-3 pathway is expressed in myeloid cells and that HPS-1 patient macrophages have aberrant metabolic signaling on the transcriptional level. In addition, I discovered that HPS1 deficiency results in heightened mTORC1 signaling, mediated by Rab32, and hampered microbial elimination. mTORC1 inhibition or fatty acid supplementation could revert this bacterial clearance defect. Lastly, we emphasize that HPS-1 patients have an expanded inflammatory monocyte compartment in peripheral blood and dysregulated pro-inflammatory cytokine production in serum.

In this discussion, I focus on the potential causes of tissue inflammation in HPS-1, informed by the findings presented here. Furthermore, I highlight the role of lipids in microbial clearance, the functions of BLOC-2 and BLOC-3, and the potential mTORC1

inhibitors hold for the treatment of metabolic and immune-mediated diseases. Finally, I discuss whether or not HPS-1 can be considered an immunodeficiency and propose future directions for this project.

6.1 Inflammation in HPS-1

In this thesis, I have investigated the molecular mechanisms underlying Hermansky-Pudlak Syndrome type 1. Patients with mutations in the *HPS1* and *HPS4* genes can develop lung fibrosis and intestinal inflammation. The encoded proteins, HPS1 and HPS4, form the BLOC-3 complex (Nazarian et al., 2003). BLOC-3 acts as a guanine nucleotide exchange factor for Rab32 and Rab38 (Gerondopoulos et al., 2012).

We used mass cytometry to identify key cellular populations that are dysregulated in HPS-1. Specifically, we pinpointed an expanded and inflammatory monocyte compartment in HPS-1 patient peripheral blood that highly expressed the Fc receptor CD64. A cluster of monocytes in HPS-1 was $\beta7^{hi}$. The $\alpha_4\beta_7$ integrin helps direct immune cells to the intestine (Schippers et al., 2016), which might result in increased numbers of leukocytes in the gut that drive or exacerbate inflammation in HPS-1.

Transcriptomics on HPS-1 patient macrophages revealed aberrant lipid metabolism. Following infection with *Salmonella* Typhimurium, HPS-1 patient macrophages exhibited enhanced expression of *TNF* and *OSM*. Moreover, we identify elevated serum levels of IL-1α and TNF in HPS-1 patients. TNF and OSM are two key inflammatory cytokines implicated in the pathogenesis of inflammatory bowel disease. OSM is produced by myeloid cells and influences the stromal compartment, which expresses its receptor OSMR (West et al., 2017). Additional inflammatory circuits between different cell types in the gut are being unraveled. For instance, fibroblasts communicate with neutrophils in IBD in an IL-1-dependent manner

and this interaction is associated with deep intestinal ulcers (Friedrich et al., 2021). Our transcriptomic results have started laying out the blueprint for potential pathogenic cell-to-cell interactions in HPS-1. Novel technologies such as spatial transcriptomics could further steer our understanding of HPS-1 pathology to the tissue level.

In this thesis, I showcase a novel mechanism involving HPS1-Rab32-dependent mTOR signaling and lipid metabolism alterations in HPS-1. The deregulation of this mechanism results in hampered bacterial clearance, which can be rescued with mTORC1 inhibition or fatty acid supplementation. BLOC-3-mediated anti-microbial activity is likely one of several pathways that contribute to microbial clearance. There are no reports of HPS-1 patients suffering from chronic infections, which may be explained by other pathways compensating for the deficiency. However, it may take more time to efficiently clear microbes, which could act as a trigger for inflammation **(Figure 6.1)**. In addition to the hampered bacterial clearance in HPS-1 macrophages, Paneth cells, which play a role in maintaining barrier integrity, are defective in lysozyme secretion (Yu et al., 2020b). The abrogated secretion of this antimicrobial factor may add to the severity of intestinal inflammation observed in HPS-1 and HPS-4 patients.

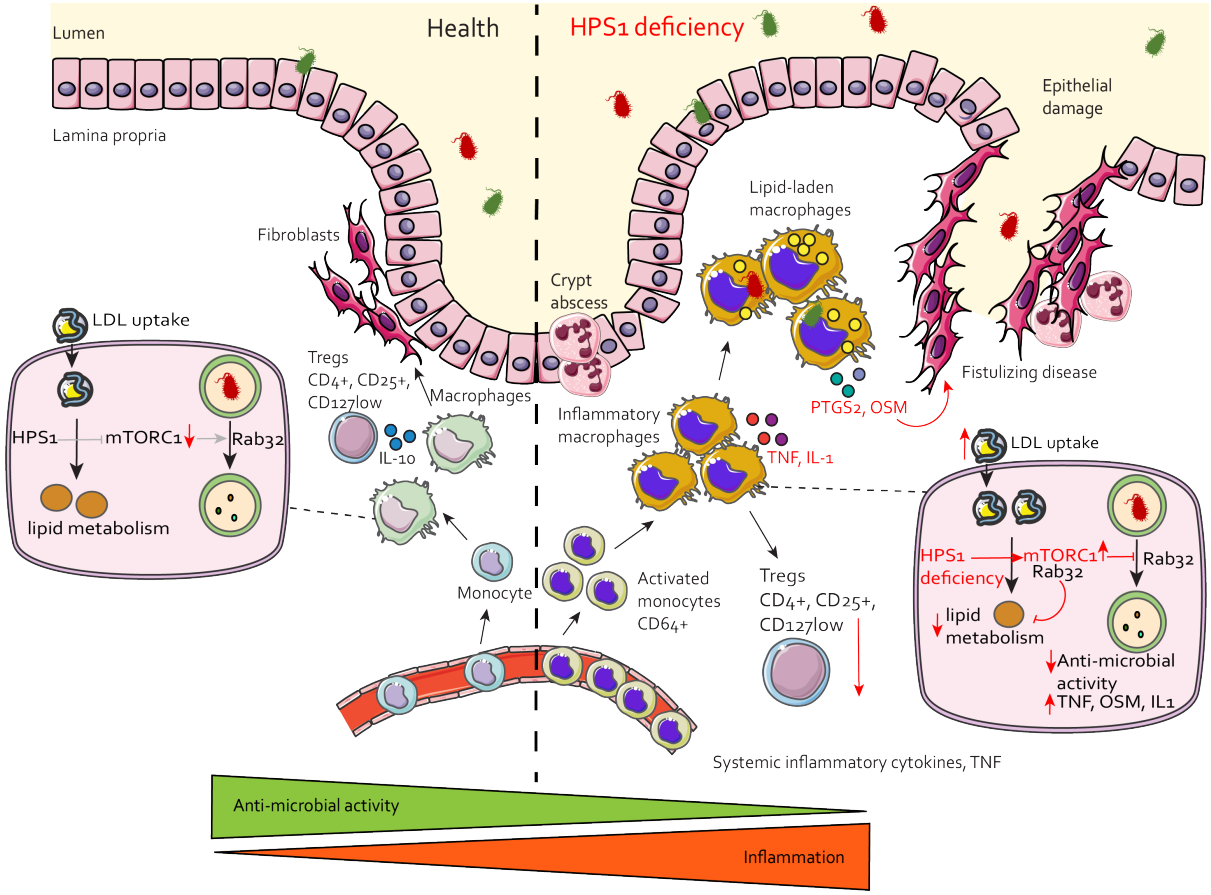


Figure 6.1. Summary of intestinal inflammation and molecular mechanisms in HPS1 deficiency. In health, monocytes from the blood differentiate into macrophages, which interact with regulatory T cells and fibroblasts, promoting homeostasis. On a molecular level, lipid droplet metabolism and lower mTORC1 levels facilitate the degradation of microbes, where Rab32 plays a key role in phagosome maturation. In HPS1 deficiency, activated monocytes are recruited from the blood, differentiating into macrophages that express inflammatory mediators such as TNF, IL-1, OSM and PTGS2. On an intracellular level, high levels of mTORC1 activity mediated through Rab32 and deregulated lipid metabolism dampen anti-microbial activity. The suppressed degradation of bacteria and increased cytokine production in HPS-1 patients can lead to tissue inflammation involving crypt abscesses, epithelial barrier damage and fistulizing disease.

The lung and the gut, two organs affected in HPS-1 and HPS-4, are constantly exposed to microbes and must strike a balance between tolerance and inflammation. HPS pulmonary fibrosis (HPS-PF) shares features with IPF but is additionally characterized by lipofuscin

deposits (Yokoyama and Gochuico, 2021). IPF involves epithelial injury and fibrosis on a tissue level and mitochondrial dysregulation on a cellular level (Lederer and Martinez, 2018). For instance, the release of surfactants, primarily composed of lipids, by alveolar type II epithelial cells, maintains homeostasis in the lung and depends on mitochondrial function (Chung et al., 2019). We show that compared to controls, HPS-1 patients have an expanded monocyte compartment in the peripheral blood and high levels of TNF and IL-1α in the serum. Previous investigations have highlighted that HPS-PF patients have higher levels of TNF and IFN-γ in serum and increased monocyte proportions in blood compared to patients with familial PF (El-Chemaly et al., 2018). These results, while restricted to HPS-PF patients, are in agreement with our mass cytometry and serum proteomic data.

Furthermore, lung-resident microbiota play a role in the development of lung fibrosis in the bleomycin-induced mouse model of disease (Yang et al., 2019). Interestingly, the authors found that *Prevotella melaninogenica* exacerbated lung fibrosis. The Prevotellaceae family has been associated with HPS-1 in stool samples in humans and mice (Yu et al., 2020b). These findings suggest overlapping pathways in the lung and gut microbiome that predispose to lung fibrosis and IBD and might be relevant for HPS-1, warranting further examination.

HPS-1 and HPS-4 patients can develop severe IBD and lung fibrosis. HPS-2 patients can also have lung fibrosis (Vicary et al., 2016), while mild IBD has been reported in HPS-3 and HPS-6 patients (O'Brien et al., 2021; Yokoyama and Gochuico, 2021). Specifically, 100 % and 15 % of HPS-1 patients develop lung fibrosis and IBD, respectively, while HPS-4-associated IBD and lung fibrosis have also been reported. The severity of disease in HPS-1 and HPS-4 and the findings presented in this thesis for HPS-1 showing defective metabolic wiring and anti-microbial responses underline shared mechanisms between the gut and lung. Additionally, the microbiota in both the lung and gut may be crucial in sculpting tolerance, which might

become awry in HPS-1 and HPS-4, causing disease at these mucosal sites. At the same time, tissue-specific mechanisms of disease might explain the differences in penetrance.

HPS1-deficient lung organoids have been shown to have high levels of IL-11 compared to controls (Strikoudis et al., 2019). In parallel, we have found that HPS-1 patient macrophages have increased *OSM* gene expression following microbial infection. In our Olink proteomics, we identified a trend towards enhanced IL-6 levels in HPS-1 patients. These three cytokines, IL-11, OSM and IL-6, all signal through the glycoprotein 130 (gp130) co-receptor (Bravo and Heath, 2000). Gp130 acts as a co-receptor for leukemia inhibitory factor, ciliary neurotrophic factor, cardiotrophin-1, IL-6, IL-11 and OSM (Bravo and Heath, 2000). Recently, in a DSS-induced colitis zebrafish model, blockade of gp130 through bazedoxifene treatment reduced inflammation (Nayar et al., 2021). Therefore, gp130 inhibition could be another potential therapeutic target to address the IBD and pulmonary fibrosis seen in HPS-1 and HPS-4 patients. Bazedoxifene is a clinically approved drug for osteoporosis and pre-clinical cancer models in mice have shown potential for colon cancer treatment (Thilakasiri et al., 2019). It is important to keep in mind that HPS-IBD patients do not develop intestinal strictures as observed in IBD associated with *NOD2* variants. Specifically, a pathogenic myeloid-fibroblast circuit is thought to play a role, with PDGFRA and CD14 being at increased levels in strictures (Nayar et al., 2021). Therefore, there may be underlying differences in the crosstalk between cells, which may be relevant for therapeutic interventions.

To conclude, inflammatory cytokine production has emerged as a key node in HPS-1 and HPS-4 gut and lung pathology. Unraveling the intricacies of myeloid-fibroblast interactions in these patients may provide a new therapeutic avenue for both pulmonary fibrosis and intestinal inflammation.

6.2 The distinct functions of BLOC-2 and BLOC-3

Defects in the BLOC-3 components HPS1 and HPS4 cause severe inflammatory bowel disease (O'Brien et al., 2021). On the other hand, BLOC-2 defects such as HPS-3 result in a less severe manifestation of gastrointestinal inflammation (O'Brien et al., 2021). I hypothesize that these differential clinical findings are a product of the GDP/GTP status of Rab32.

BLOC-3 triggers the exchange of GDP for GTP on Rab32 (Gerondopoulos et al., 2012), clearing the way for the interaction between Rab32-GTP and BLOC-2/AP-3 (Bultema et al., 2012). In parallel, Rab32-GDP is sufficient to mediate the attachment of mTOR to the lysosome, facilitating mTORC1 signaling (Drizyte-Miller et al., 2020). I speculate that the interaction between Rab32-GTP and BLOC-2/AP-3 may be fundamental for its attachment to the phagosome. At the phagosome, Rab32 can deliver itaconate (Chen et al., 2020), an anti-microbial metabolite. Therefore, patients with BLOC-2 defects would feature hampered bacterial clearance but intact mTORC1 signaling, as we found in HPS-3 patient macrophages. On the other hand, BLOC-3 defects, which may be further upstream of BLOC-2 in anti-microbial defense, result in impaired anti-microbial activity and amplified mTORC1 signaling, perhaps because Rab32 remains in the GDP-bound form **(Figure 6.2)**. Overexpression of constitutively GTP- and GDP-bound forms of Rab32 could aid the investigation of this hypothesis.

In summary, BLOC-2 and BLOC-3 both contribute to bacterial handling. However, these two complexes appear to act at distinct steps of this mechanism, since BLOC-3 deficiency leads to aberrant mTORC1 signaling, while BLOC-2 deficiency does not. The precise role of Rab32 and its GDP/GTP status in this process warrants further study.

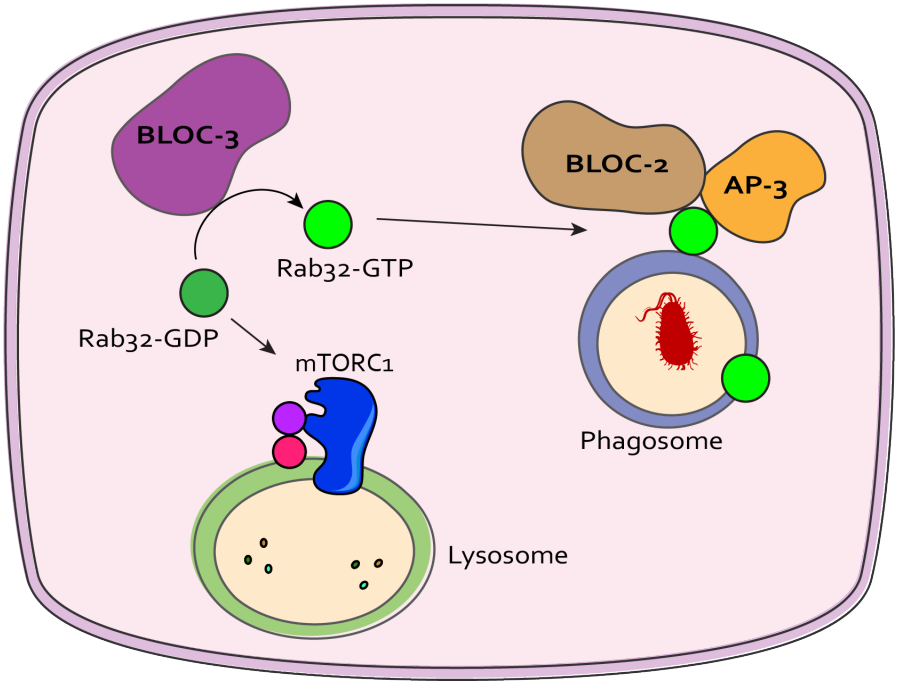


Figure 6.2. Potential mechanism of BLOC-2, BLOC-3, AP-3 and Rab32 involvement in bacterial elimination and mTORC1 signaling. BLOC-3 facilitates the exchange of GDP for GTP on Rab32, possibly shifting the balance between mTOR signaling and bacterial clearance. BLOC-2 and AP-3 may have secondary roles in facilitating the localization and/or attachment of Rab32 to bacteria-containing phagosomes, thereby resulting in microbial clearance.

6.3 The intersection of lipid metabolism and bacterial clearance in intestinal inflammation

Bacterial elimination and lipid metabolism are intertwined and can define the shift from homeostasis to disease. Lipid droplets have been regarded as an energy source to be exploited by pathogens, but recent evidence suggests that lipid droplets can also deliver antimicrobial factors. Several diseases showcase this balance between lipid metabolism or accumulation and microbial elimination.

Lipid droplets localize to phagosomes containing mycobacteria, where they are thought to provide energy sources (Roingeard and Melo, 2017). On the other hand, lipid droplets can deliver anti-microbial factors that facilitate bacterial degradation (Bosch et al., 2020). Specifically, perilipin 5 tethers lipid droplets to mitochondria for fatty acid oxidation

but shift to perilipin 2-containing lipid droplets upon infection, which can clear microbes. Furthermore, IFN-γ stimulation in combination with *Mycobacterium tuberculosis* infection triggers lipid droplet formation in macrophages (Knight et al., 2018). This process elicits eicosanoid production to facilitate microbial clearance. It is tempting to speculate that adaptive immune responses such as the release of IFN-γ can shape the role of lipid droplets in macrophages, with implications for granuloma formation. These disparate and conflicting mechanisms can be pathogen-specific but the role of lipid droplets in host defense is only beginning to be elucidated.

Short chain fatty acids derived from bacteria can play an important role in gastrointestinal homeostasis. For instance, while antibiotics deplete the gut flora and can cause T cell dysregulation in mice, the administration of butyrate reprograms macrophages and keeps T cells in check (Scott et al., 2018). In parallel, butyrate drives anti-microbial activity in macrophages through histone deacetylase inhibition, suppressing mTOR signaling and boosting autophagy (Schulthess et al., 2019). Lastly, butyrate abrogates bacterial translocation in mice, attributed to its effects on intestinal epithelial cells (Fachi et al., 2019). In conclusion, microbe-derived fatty acids can contribute to host defense indirectly by exerting their effects on immune and epithelial cells.

Multiple lines of evidence link bacterial handling and lipid metabolism in IBD. A *GPR65* variant, which predisposes to IBD, results in diminished macrophage bacterial clearance and dysfunctional lipid droplet formation (Lassen et al., 2016). In this thesis, I show that HPS1 deficiency results in attenuated anti-microbial activity and deregulated metabolic signaling. At the same time, the monogenic disorder NPC1 causes lipid accumulation and defective bacterial elimination in macrophages (Schwerd et al., 2016). Variants in *LACC1* can cause Crohn's disease and juvenile idiopathic arthritis and can connect metabolism and bacterial

elimination. Specifically, one study has shown that LACC1 deficiency impairs autophagy flux, the accumulation of lipid droplets and oxidative phosphorylation (Omarjee et al., 2021). A different study highlights that LACC1 deficiency causes a reduction in fatty acid oxidation and diminished clearance of *Mycobacterium bovis* bacillus Calmette-Guérin and *Salmonella* Typhimurium (Cader et al., 2016). On the other hand, defects in lysosomal acid lipase (LAL), which is responsible for the hydrolysis of cholesteryl esters into cholesterol (Ouimet et al., 2011), does not result in intestinal inflammation. While LAL deficiency is characterized by lipid accumulation, I hypothesize that it does not trigger Crohn's disease since mTOR is activated by cholesterol instead of cholesteryl esters. Therefore, the link between Crohn's disease and lipid metabolism might require a concomitant dysregulation in autophagy or mTOR signaling. In line with this hypothesis, LAL inhibition in NPC1-deficient fibroblasts reduces cholesterol accumulation (Rosenbaum et al., 2009) **(Figure 6.3)**.

Lipid droplets act as a double edged sword in host-microbe interactions, with microbes using lipid droplets for fuel and the host for anti-microbial responses. Several diseases featuring lipid metabolic dysregulation present with IBD. Delineating the triggers for lipid accumulation can facilitate targeting this axis for treatment in subsets of patients.

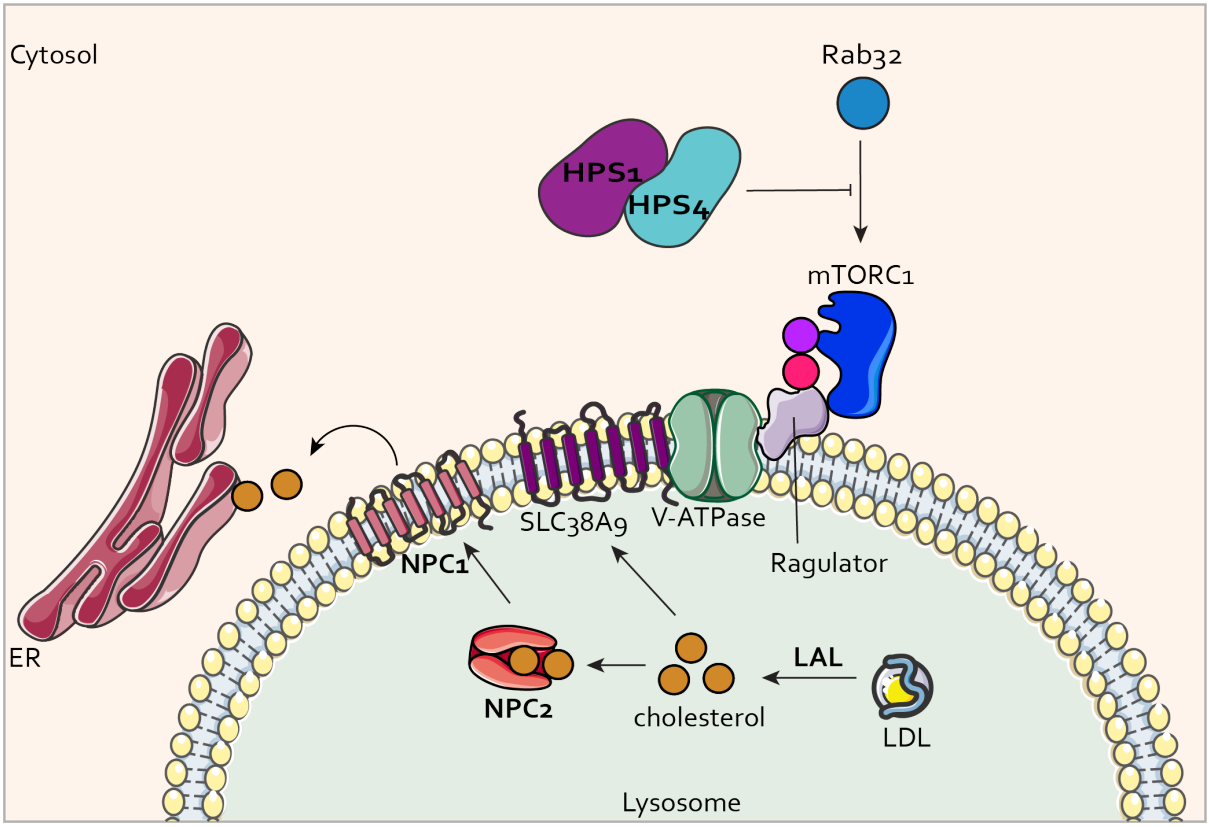


Figure 6.3. Proposed mechanism of LAL-NPC-BLOC-3 cholesterol homeostasis and mTOR signaling. Cholesteryl esters from LDL can be hydrolyzed into free cholesterol through LAL. Cholesterol is shuttled by NPC2 in the lysosomal lumen to NPC1 and onto extra-lysosomal organelles such as the endoplasmic reticulum. Cholesterol stimulates mTORC1 signaling. On the other hand, BLOC-3 controls Rab32-mediated mTORC1 activation. While defects in NPC1 and HPS-1/HPS-4 can lead to intestinal inflammation, LAL deficiency does not, which might be reflected by normal levels of mTOR signaling.

6.4 mTORC1 inhibition as a metabolic checkpoint

Mycobacterium tuberculosis infection, atherosclerosis and sarcoidosis involve foam cell formation (Moore et al., 2013; Russell et al., 2009), which are lipid-laden macrophages. Macrophage activation underlies all three diseases, which share features with HPS-1. A recent study illustrated the accumulation of atherogenic lipids in the plasma of $Hps1^{-/-}$ mice (Ma et al., 2019). In addition, in this thesis, I show that HPS1 deficiency results in enhanced LDL uptake and deregulated cholesterol metabolism. mTORC1 inhibition could lead to

metabolic reprogramming and the degradation of accumulated lipids, acting as a therapeutic target for these diseases.

Mycobacterium tuberculosis infection causes granuloma formation, characterized by an aggregation of macrophages (Russell et al., 2009). Macrophages become foamy through the internalization of lipids such as LDL, resulting in bacterial persistence. In tuberculous lesions, triglyceride accumulation leads to mTORC1 signaling in lipid-laden macrophages (Guerrini et al., 2018). Therefore, there is evidence of a tight connection between mTOR activation and foam cell formation in tuberculosis, where granulomata form in tissues.

Atherosclerosis results in the narrowing of blood vessels (Moore et al., 2013). On a cellular level, atherosclerosis is characterized by foam cell formation with deranged lipid metabolism in macrophages. mTORC1 inhibition has been considered and implemented in atherosclerosis as a therapeutic option (Liu et al., 2018). Specifically, rapamycin-releasing stents have been trialed, which stifle inflammation.

Sarcoidosis is a disease involving the development of granulomata in several organs including the lung and skin (Petersen and Smith, 2013). Deletion of *Tsc2*, a negative regulator of mTORC1, in myeloid cells, leads to granuloma formation in mice, which can be resolved by mTORC1 inhibition (Linke et al., 2017). Notably, a patient with sarcoidosis was treated successfully with rapamycin following liver transplantation (Manzia et al., 2011).

HPS-1 shares important features with these diseases. Atherosclerosis involves foamy macrophages that are activated, while tuberculosis and sarcoidosis have granuloma formation, as observed in HPS-1 Crohn's-like inflammation. It is tempting to speculate that dampening mTORC1 signaling could serve as a relevant therapeutic target for these disorders that feature deregulated metabolism.

6.5 Is HPS-1 an immunodeficiency?

Several lines of evidence point to an innate immune defect in BLOC-3 deficiency. Potentially the most critical innate immune aspects of HPS-1 are hampered bacterial clearance and dysregulated pro-inflammatory cytokine production. In this section, I discuss the bacterial handling defect in HPS-1 and whether it should be regarded as a primary immunodeficiency.

Whereas primary immunodeficiencies tend to predispose to recurrent infections, there is little evidence for infection susceptibility in HPS-1. In light of the observed defective anti-microbial activity in monocyte-derived macrophages this is surprising and suggests that other mechanisms compensate for this defect. Firstly, in this project, I have focused on monocyte-derived macrophages, while another cell type with potent anti-microbial activity is neutrophils. Therefore, it would be important to document whether the anti-microbial activity defect in HPS-1 macrophages extends to this cell type. On the other hand, neutrophils may clear microbes efficiently where HPS-1 macrophages might not be able to. Secondly, it is likely that the defective anti-microbial activity causes a delay in microbial elimination but additional macrophage pathways may instigate bacterial clearance independent of BLOC-3 as a compensatory mechanism. The results in this thesis suggest that lysosomal degradation is intact in HPS1 deficiency, which can act as an endpoint of other anti-microbial pathways. These compensatory pathways could include IFN-γ-mediated autophagy (Fabri et al., 2011), LC3-associated phagocytosis (Martinez et al., 2015) or conventional autophagy (Chauhan et al., 2015). It is possible that these overlapping anti-microbial pathways may have evolved to override such defects, which can be genetic or pathogen-induced. For example,

Mycobacterium tuberculosis possesses mycolic lipids which can trigger a phenotype similar to NPC1 (Fineran et al., 2016).

Primary immune deficiencies are categorized into different classes, such as immune dysregulation, innate immune deficiencies and phagocyte number or function defects (Picard et al., 2018). HPS-2 and HPS-10 fall into the immune dysregulation immunodeficiency category, since patients are neutropenic (Ammann et al., 2016; de Boer et al., 2017), have recurrent infections (Jones et al., 2013; Wenham et al., 2010) and their cytotoxic T cells and natural killer cells cannot secrete granules (Ammann et al., 2016; Clark et al., 2003; Wenham et al., 2010). However, BLOC-3 defects, caused by mutations in *HPS1* and *HPS4*, do not impair cytotoxic lymphocyte function (Bossi et al., 2005) and there are no reports of neutropenia in these patients. In addition, another type of immunodeficiency characterized by immune dysregulation includes IPEX, which leads to autoimmunity (Schmidt et al., 2017). Once again, there are no reports showing that HPS-1 can cause autoimmune disease.

Furthermore, defects in innate immunity can involve abrogated TLR signaling or attenuated IFN-γ signaling, causing bacterial infections (Picard et al., 2018). Similarly, defects in phagocyte number or function, including chronic granulomatous disease (Yu et al., 2020a), result in persistent bacterial and fungal infections accompanied by autoinflammation (Picard et al., 2018). Once again, increased infection susceptibility has not been reported for HPS-1, ruling out its classification as an innate immunity or phagocyte function defect. In addition, HPS-1 patients do not have a type I interferon signature or lupus-like symptoms, which are characteristic of interferonopathies, a type of autoinflammatory disorder (Picard et al., 2018). Furthermore, cellular and humoral immunity-related immunodeficiencies, a category that includes severe combined immunodeficiency (Schmidt et al., 2017), cause low immune cell counts or recurrent infections (Picard et al., 2018). However, HPS-1 does not fall into this

group since HPS-1 patients do not have different blood count parameters compared to controls (El-Chemaly et al., 2018).

In conclusion, while HPS-1 involves an anti-microbial activity defect, other pathways are likely to compensate for the impaired bacterial clearance. Therefore, HPS-1 could be regarded as an inborn error of immunity of the phagocyte compartment but cannot be considered a primary immunodeficiency since there is no infection susceptibility.

6.6 Future directions

Several questions emerge from this thesis that can be addressed experimentally. These include understanding the immune cell composition in the gut and the associated cellular interactions, which can be examined through transcriptional profiling of inflamed regions. Additionally, an interrogation of the translocating microbes into the lamina propria can help decipher the role specific microbes might play in triggering inflammation. Furthermore, induced pluripotent stem cells and patient cells can be used to validate and extend the mechanistic findings presented here. Lastly, I propose a mechanism whereby LAL, NPC1, NPC2 and BLOC-3 have distinct functions that lead to disparate clinical findings, which could be tested *in vitro*.

Spatial transcriptomics has taken off by uncovering pathogenic mechanisms in tissue, such as in COVID-19, using NanoString technologies (Rendeiro et al., 2021). This technique allows the visualization of gene expression in specific areas of interest and the identification of specific cell types using antibodies. We have established a collaboration with Dr. Fadi Issa in the Nuffield Department of Surgical Sciences at Oxford to perform spatial transcriptomics. Moreover, we have already obtained 5 HPS-1-IBD paraffin-embedded gut biopsies from Dr. Esther Torres in Puerto Rico to perform this experiment. In other words, we can map the gene

expression profiles and associated pathways directly in the gastrointestinal tract of patients. Furthermore, single cell RNA sequencing or mass cytometry on gastrointestinal tissue from HPS-IBD patients could help discern the similarities and differences to Crohn's disease. However, fresh gut samples might be difficult to obtain since the disorder causes a bleeding diathesis and therefore non-essential surgeries and biopsies are avoided.

We are in the process of obtaining induced pluripotent stem cells derived from HPS-1 and HPS-4 patients from Dr. Darrell Kotton at Boston University. Using these lines, we could perform more mechanistic experiments in differentiated macrophages, which resemble primary macrophages more so than HAP1 cells. Additionally, gut and lung organoids could be generated to study the cytokine response and gene expression changes on the epithelium following bacterial infection. The induced pluripotent stem cells could be differentiated into various cell types and used for co-culture studies once novel cellular interactions are established using spatial transcriptomics. Therefore, we could answer questions relating to pathogenic cellular interactions and the role of the epithelium in HPS-IBD.

It would be interesting to identify particular microbes that translocate in HPS-IBD, which might be relevant for the induction of inflammation. These studies could be performed using gut sample biopsies from Puerto Rico and laser capture microdissection at the Wellcome Trust Center for Human Genetics in Oxford. By targeting mucosal regions and using 16S rRNA-sequencing, as has been done previously (Chassaing and Gewirtz, 2019), this method could uncover specific bacteria that translocate and trigger inflammation.

In this thesis, I have postulated that while HPS-1, NPC1 and LAL deficiencies result in lipid accumulation, LAL defects might not cause Crohn's disease because mTOR signaling is not hyperactive. In order to interrogate this, HAP1 cell knockouts of the *LIPA* (LAL), *NPC1, NPC2* and *HPS4* genes could kickstart our understanding of this cascade. Specifically, I would

expect that NPC1, NPC2 and HPS4 deficiencies lead to aberrant mTOR signaling and impaired microbial clearance (as in HPS-1), but that LAL deficiency would not. On the other hand, I hypothesize that lipid accumulation would characterize all of these deficiencies. Additionally, lipid profiling of lysosomes and lipid droplets in these deficiencies would broaden our view on how lipid metabolism phenotypes cause distinct clinical manifestations.

The experiments proposed here stem directly from my work, but several other questions still remain in the field. For instance, a better understanding of the proteins that are mistrafficked to melanosomes in HPS is lacking. Additionally, the roles of BLOC-2 (HPS3, HPS5, HPS6) and AP-3 in microbial elimination await further interrogation. Furthermore, how the BLOC-3 complex has evolved and which domains are important for interactions with Rab GTPases among others remain to be elucidated. The HPS1 and HPS4 proteins are present in the amoeba *Dictyostelium discoideum* (Cheli and Dell'Angelica, 2010), and structural studies can shed light on the different domains and interactions. These are three of myriads of questions relating to Hermansky-Pudlak Syndrome, and more research is certainly needed to shed a brighter and broader light on this disorder.

6.7 Conclusion

This thesis focuses on HPS-1, which causes impaired bacterial elimination through deregulated mTOR signaling and aberrant metabolism. mTORC1 emerges as a potential therapeutic target for this disease, with broader implications for lipid accumulation disorders and IBD. Even disorders that result from a specific genetic deficiency such as HPS-1 can require different types of treatments for the multiple organs affected. That allows one to speculate about the difficulty of using a one-size-fits-all approach. Three exciting options can help address this challenge. Firstly, patient stratification can bring about process- and

pathway-driven therapeutic intervention. Secondly, combination therapies might have greater effect than single therapies. Thirdly, understanding the timing of disease development can help physicians administer the appropriate medication at the right time. Armed with ever-evolving technology and machine learning approaches, it is thrilling to contemplate the advances that await the field in the coming years.

Chapter 7 - References

Abu-Remaileh, M., G.A. Wyant, C. Kim, N.N. Laqtom, M. Abbasi, S.H. Chan, E. Freinkman, and D.M. Sabatini. 2017. Lysosomal metabolomics reveals V-ATPase- and mTOR-dependent regulation of amino acid efflux from lysosomes. *Science*. 358:807-813.

Adams, J., M. Feuerborn, J.A. Molina, A.R. Wilden, B. Adhikari, T. Budden, and S.Y. Lee. 2019. Autophagy-lysosome pathway alterations and alpha-synuclein up-regulation in the subtype of neuronal ceroid lipofuscinosis, CLN5 disease. *Sci Rep*. 9:151.

Aguilar, C., C. Lenoir, N. Lambert, B. Begue, N. Brousse, D. Canioni, D. Berrebi, M. Roy, S. Gerart, H. Chapel, T. Schwerd, L. Siproudhis, M. Schappi, A. Al-Ahmari, M. Mori, A. Yamaide, L. Galicier, B. Neven, J. Routes, H.H. Uhlig, S. Koletzko, S. Patel, H. Kanegane, C. Picard, A. Fischer, N.C. Bensussan, F. Ruemmele, J.P. Hugot, and S. Latour. 2014. Characterization of Crohn disease in X-linked inhibitor of apoptosis-deficient male patients and female symptomatic carriers. *J Allergy Clin Immunol*. 134:1131-1141 e1139.

Ahern, P.P., A. Izcue, K.J. Maloy, and F. Powrie. 2008. The interleukin-23 axis in intestinal inflammation. *Immunol Rev*. 226:147-159.

Ahern, P.P., C. Schiering, S. Buonocore, M.J. McGeachy, D.J. Cua, K.J. Maloy, and F. Powrie. 2010. Interleukin-23 drives intestinal inflammation through direct activity on T cells. *Immunity*. 33:279-288.

Ahuja, S., L. Knudsen, S. Chillappagari, I. Henneke, C. Ruppert, M. Korfei, B.R. Gochuico, S. Bellusci, W. Seeger, M. Ochs, A. Guenther, and P. Mahavadi. 2016. MAP1LC3B overexpression protects against Hermansky-Pudlak syndrome type-1-induced defective autophagy in vitro. *Am J Physiol Lung Cell Mol Physiol*. 310:L519-531.

Alsaleh, G., I. Panse, L. Swadling, H. Zhang, F.C. Richter, A. Meyer, J. Lord, E. Barnes, P. Klenerman, C. Green, and A.K. Simon. 2020. Autophagy in T cells from aged donors is maintained by spermidine and correlates with function and vaccine responses. *Elife*. 9.

Alto, N.M., J. Soderling, and J.D. Scott. 2002. Rab32 is an A-kinase anchoring protein and participates in mitochondrial dynamics. *J Cell Biol*. 158:659-668.

Ammann, S., A. Schulz, I. Krageloh-Mann, N.M. Dieckmann, K. Niethammer, S. Fuchs, K.M. Eckl, R. Plank, R. Werner, J. Altmuller, H. Thiele, P. Nurnberg, J. Bank, A. Strauss, H. von Bernuth, U. Zur Stadt, S. Grieve, G.M. Griffiths, K. Lehmberg, H.C. Hennies, and S. Ehl. 2016. Mutations in AP3D1 associated with immunodeficiency and seizures define a new type of Hermansky-Pudlak syndrome. *Blood*. 127:997-1006.

Anderson, P.D., M. Huizing, D.A. Claassen, J. White, and W.A. Gahl. 2003. Hermansky-Pudlak syndrome type 4 (HPS-4): clinical and molecular characteristics. *Hum Genet*. 113:10-17.

Anikster, Y., M. Huizing, J. White, Y.O. Shevchenko, D.L. Fitzpatrick, J.W. Touchman, J.G. Compton, S.J. Bale, R.T. Swank, W.A. Gahl, and J.R. Toro. 2001. Mutation of a new gene causes a unique form of Hermansky-Pudlak syndrome in a genetic isolate of central Puerto Rico. *Nat Genet*. 28:376-380.

Armaka, M., M. Apostolaki, P. Jacques, D.L. Kontoyiannis, D. Elewaut, and G. Kollias. 2008. Mesenchymal cell targeting by TNF as a common pathogenic principle in chronic inflammatory joint and intestinal diseases. *J Exp Med*. 205:331-337.

Arnold, D.E., and J.R. Heimall. 2017. A Review of Chronic Granulomatous Disease. *Adv Ther*. 34:2543-2557.

Arnold, I.C., S. Mathisen, J. Schulthess, C. Danne, A.N. Hegazy, and F. Powrie. 2016. CD11c(+) monocyte/macrophages promote chronic Helicobacter hepaticus-induced intestinal inflammation through the production of IL-23. *Mucosal Immunol*. 9:352-363.

Aschenbrenner, D., M. Quaranta, S. Banerjee, N. Ilott, J. Jansen, B. Steere, Y.H. Chen, S. Ho, K. Cox, C.V. Arancibia-Carcamo, M. Coles, E. Gaffney, S.P. Travis, L. Denson, S. Kugathasan, J. Schmitz, F. Powrie, S.N. Sansom, and H.H. Uhlig. 2020. Deconvolution of monocyte responses in inflammatory bowel disease reveals an IL-1 cytokine network that regulates IL-23 in genetic and acquired IL-10 resistance. *Gut*.

Atarashi, K., T. Tanoue, T. Shima, A. Imaoka, T. Kuwahara, Y. Momose, G. Cheng, S. Yamasaki, T. Saito, Y. Ohba, T. Taniguchi, K. Takeda, S. Hori, Ivanov, II, Y. Umesaki, K. Itoh, and K. Honda. 2011. Induction of colonic regulatory T cells by indigenous Clostridium species. *Science*. 331:337-341.

Bager, P., J. Simonsen, N.M. Nielsen, and M. Frisch. 2012. Cesarean section and offspring's risk of inflammatory bowel disease: a national cohort study. *Inflamm Bowel Dis*. 18:857-862.

Bain, C.C., A. Bravo-Blas, C.L. Scott, E. Gomez Perdiguero, F. Geissmann, S. Henri, B. Malissen, L.C. Osborne, D. Artis, and A.M. Mowat. 2014. Constant replenishment from circulating monocytes maintains the macrophage pool in the intestine of adult mice. *Nat Immunol*. 15:929-937.

Balci, A., V. Solano-Collado, M. Baldassarre, and S. Spano. 2020. VARP and Rab9 Are Dispensable for the Rab32/BLOC-3 Dependent Salmonella Killing. *Front Cell Infect Microbiol*. 10:581024.

Baldassarre, M., V. Solano-Collado, A. Balci, R.A. Colamarino, I.M. Dambuza, D.M. Reid, H.M. Wilson, G.D. Brown, S. Mukhopadhyay, G. Dougan, and S. Spano. 2021. The Rab32/BLOC-3-dependent pathway mediates host defense against different pathogens in human macrophages. *Sci Adv*. 7.

Bantel, H., C. Berg, M. Vieth, M. Stolte, W. Kruis, and K. Schulze-Osthoff. 2000. Mesalazine inhibits activation of transcription factor NF-kappaB in inflamed mucosa of patients with ulcerative colitis. *Am J Gastroenterol*. 95:3452-3457.

Bar-Peled, L., L.D. Schweitzer, R. Zoncu, and D.M. Sabatini. 2012. Ragulator is a GEF for the rag GTPases that signal amino acid levels to mTORC1. *Cell*. 150:1196-1208.

Barker, N., J.H. van Es, J. Kuipers, P. Kujala, M. van den Born, M. Cozijnsen, A. Haegebarth, J. Korving, H. Begthel, P.J. Peters, and H. Clevers. 2007. Identification of stem cells in small intestine and colon by marker gene Lgr5. *Nature*. 449:1003-1007.

Bartolomeo, R., L. Cinque, C. De Leonibus, A. Forrester, A.C. Salzano, J. Monfregola, E. De Gennaro, E. Nusco, I. Azario, C. Lanzara, M. Serafini, B. Levine, A. Ballabio, and C. Settembre. 2017. mTORC1 hyperactivation arrests bone growth in lysosomal storage disorders by suppressing autophagy. *J Clin Invest*. 127:3717-3729.

Bartuzi, P., D.D. Billadeau, R. Favier, S. Rong, D. Dekker, A. Fedoseienko, H. Fieten, M. Wijers, J.H. Levels, N. Huijkman, N. Kloosterhuis, H. van der Molen, G. Brufau, A.K. Groen, A.M. Elliott, J.A. Kuivenhoven, B. Plecko, G. Grangl, J. McGaughran, J.D. Horton, E. Burstein, M.H. Hofker, and B. van de Sluis. 2016. CCC- and WASH-mediated endosomal sorting of LDLR is required for normal clearance of circulating LDL. *Nat Commun*. 7:10961.

Baumgart, M., B. Dogan, M. Rishniw, G. Weitzman, B. Bosworth, R. Yantiss, R.H. Orsi, M. Wiedmann, P. McDonough, S.G. Kim, D. Berg, Y. Schukken, E. Scherl, and K.W. Simpson. 2007. Culture independent analysis of ileal mucosa reveals a selective increase in invasive Escherichia coli of novel phylogeny relative to depletion of Clostridiales in Crohn's disease involving the ileum. *ISME J*. 1:403-418.

Bennett, C.L., J. Christie, F. Ramsdell, M.E. Brunkow, P.J. Ferguson, L. Whitesell, T.E. Kelly, F.T. Saulsbury, P.F. Chance, and H.D. Ochs. 2001. The immune dysregulation, polyendocrinopathy, enteropathy, X-linked syndrome (IPEX) is caused by mutations of FOXP3. *Nat Genet*. 27:20-21.

Bevins, C.L., and N.H. Salzman. 2011. Paneth cells, antimicrobial peptides and maintenance of intestinal homeostasis. *Nat Rev Microbiol*. 9:356-368.

Bindea, G., B. Mlecnik, H. Hackl, P. Charoentong, M. Tosolini, A. Kirilovsky, W.H. Fridman, F. Pages, Z. Trajanoski, and J. Galon. 2009. ClueGO: a Cytoscape plug-in to decipher functionally grouped gene ontology and pathway annotation networks. *Bioinformatics*. 25:1091-1093.

Blasius, A.L., C.N. Arnold, P. Georgel, S. Rutschmann, Y. Xia, P. Lin, C. Ross, X. Li, N.G. Smart, and B. Beutler. 2010. Slc15a4, AP-3, and Hermansky-Pudlak syndrome proteins are required for Toll-like receptor signaling in plasmacytoid dendritic cells. *Proc Natl Acad Sci U S A*. 107:19973-19978.

Boland, B.S., Z. He, M.S. Tsai, J.G. Olvera, K.D. Omilusik, H.G. Duong, E.S. Kim, A.E. Limary, W. Jin, J.J. Milner, B. Yu, S.A. Patel, T.L. Louis, T. Tysl, N.S. Kurd, A. Bortnick, L.K. Quezada, J.N. Kanbar, A. Miralles, D. Huylebroeck, M.A. Valasek, P.S. Dulai, S. Singh, L.F. Lu, J.D. Bui, C. Murre, W.J. Sandborn, A.W. Goldrath, G.W. Yeo, and J.T. Chang. 2020. Heterogeneity and clonal relationships of adaptive immune cells in ulcerative colitis revealed by single-cell analyses. *Sci Immunol*. 5.

Bosch, M., M. Sanchez-Alvarez, A. Fajardo, R. Kapetanovic, B. Steiner, F. Dutra, L. Moreira, J.A. Lopez, R. Campo, M. Mari, F. Morales-Paytuvi, O. Tort, A. Gubern, R.M. Templin, J.E.B. Curson, N. Martel, C. Catala, F. Lozano, F. Tebar, C. Enrich, J. Vazquez, M.A. Del Pozo, M.J. Sweet, P.T. Bozza, S.P. Gross, R.G. Parton, and A. Pol. 2020. Mammalian lipid droplets are innate immune hubs integrating cell metabolism and host defense. *Science*. 370.

Bossi, G., S. Booth, R. Clark, E.G. Davis, R. Liesner, K. Richards, M. Starcevic, J. Stinchcombe, C. Trambas, E.C. Dell'Angelica, and G.M. Griffiths. 2005. Normal lytic granule secretion by cytotoxic T lymphocytes deficient in BLOC-1, -2 and -3 and myosins Va, VIIa and XV. *Traffic*. 6:243-251.

Bowman, S.L., J. Bi-Karchin, L. Le, and M.S. Marks. 2019. The road to lysosome-related organelles: Insights from Hermansky-Pudlak syndrome and other rare diseases. *Traffic*. 20:404-435.

Bravo, J., and J.K. Heath. 2000. Receptor recognition by gp130 cytokines. *EMBO J*. 19:2399-2411.

Bui, M., S.Y. Gilady, R.E. Fitzsimmons, M.D. Benson, E.M. Lynes, K. Gesson, N.M. Alto, S. Strack, J.D. Scott, and T. Simmen. 2010. Rab32 modulates apoptosis onset and mitochondria-associated membrane (MAM) properties. *J Biol Chem*. 285:31590-31602.

Bujko, A., N. Atlasy, O.J.B. Landsverk, L. Richter, S. Yaqub, R. Horneland, O. Oyen, E.M. Aandahl, L. Aabakken, H.G. Stunnenberg, E.S. Baekkevold, and F.L. Jahnsen. 2018.

Transcriptional and functional profiling defines human small intestinal macrophage subsets. *J Exp Med*. 215:441-458.

Bultema, J.J., A.L. Ambrosio, C.L. Burek, and S.M. Di Pietro. 2012. BLOC-2, AP-3, and AP-1 proteins function in concert with Rab38 and Rab32 proteins to mediate protein trafficking to lysosome-related organelles. *J Biol Chem*. 287:19550-19563.

Bultema, J.J., J.A. Boyle, P.B. Malenke, F.E. Martin, E.C. Dell'Angelica, R.E. Cheney, and S.M. Di Pietro. 2014. Myosin vc interacts with Rab32 and Rab38 proteins and works in the biogenesis and secretion of melanosomes. *J Biol Chem*. 289:33513-33528.

Buonocore, S., P.P. Ahern, H.H. Uhlig, Ivanov, II, D.R. Littman, K.J. Maloy, and F. Powrie. 2010. Innate lymphoid cells drive interleukin-23-dependent innate intestinal pathology. *Nature*. 464:1371-1375.

Burton, B.K., M. Balwani, F. Feillet, I. Baric, T.A. Burrow, C. Camarena Grande, M. Coker, A. Consuelo-Sanchez, P. Deegan, M. Di Rocco, G.M. Enns, R. Erbe, F. Ezgu, C. Ficicioglu, K.N. Furuya, J. Kane, C. Laukaitis, E. Mengel, E.G. Neilan, S. Nightingale, H. Peters, M. Scarpa, K.O. Schwab, V. Smolka, V. Valayannopoulos, M. Wood, Z. Goodman, Y. Yang, S. Eckert, S. Rojas-Caro, and A.G. Quinn. 2015. A Phase 3 Trial of Sebelipase Alfa in Lysosomal Acid Lipase Deficiency. *N Engl J Med*. 373:1010-1020.

Butler, A., P. Hoffman, P. Smibert, E. Papalexi, and R. Satija. 2018. Integrating single-cell transcriptomic data across different conditions, technologies, and species. *Nat Biotechnol*. 36:411-420.

Byles, V., A.J. Covarrubias, I. Ben-Sahra, D.W. Lamming, D.M. Sabatini, B.D. Manning, and T. Horng. 2013. The TSC-mTOR pathway regulates macrophage polarization. *Nat Commun*. 4:2834.

Cader, M.Z., K. Boroviak, Q. Zhang, G. Assadi, S.L. Kempster, G.W. Sewell, S. Saveljeva, J.W. Ashcroft, S. Clare, S. Mukhopadhyay, K.P. Brown, M. Tschurtschenthaler, T. Raine, B. Doe, E.R. Chilvers, J.L. Griffin, N.C. Kaneider, R.A. Floto, M. D'Amato, A. Bradley, M.J. Wakelam, G. Dougan, and A. Kaser. 2016. C13orf31 (FAMIN) is a central regulator of immunometabolic function. *Nat Immunol*. 17:1046-1056.

Cao, Y., J.A. Espinola, E. Fossale, A.C. Massey, A.M. Cuervo, M.E. MacDonald, and S.L. Cotman. 2006. Autophagy is disrupted in a knock-in mouse model of juvenile neuronal ceroid lipofuscinosis. *J Biol Chem*. 281:20483-20493.

Carette, J.E., M. Raaben, A.C. Wong, A.S. Herbert, G. Obernosterer, N. Mulherkar, A.I. Kuehne, P.J. Kranzusch, A.M. Griffin, G. Ruthel, P. Dal Cin, J.M. Dye, S.P. Whelan, K. Chandran, and T.R. Brummelkamp. 2011. Ebola virus entry requires the cholesterol transporter Niemann-Pick C1. *Nature*. 477:340-343.

Carmona-Rivera, C., D.R. Simeonov, N.D. Cardillo, W.A. Gahl, and C.L. Cadilla. 2013. A divalent interaction between HPS1 and HPS4 is required for the formation of the biogenesis of lysosome-related organelle complex-3 (BLOC-3). *Biochim Biophys Acta*. 1833:468-478.

Carroll, B., D. Maetzel, O.D. Maddocks, G. Otten, M. Ratcliff, G.R. Smith, E.A. Dunlop, J.F. Passos, O.R. Davies, R. Jaenisch, A.R. Tee, S. Sarkar, and V.I. Korolchuk. 2016. Control of TSC2-Rheb signaling axis by arginine regulates mTORC1 activity. *Elife*. 5.

Castellano, B.M., A.M. Thelen, O. Moldavski, M. Feltes, R.E. van der Welle, L. Mydock-McGrane, X. Jiang, R.J. van Eijkeren, O.B. Davis, S.M. Louie, R.M. Perera, D.F. Covey, D.K. Nomura, D.S. Ory, and R. Zoncu. 2017. Lysosomal cholesterol activates mTORC1 via an SLC38A9-Niemann-Pick C1 signaling complex. *Science*. 355:1306-1311.

Cavounidis, A., and H.H. Uhlig. 2018. Crohn's Disease in Niemann-Pick Disease Type C1: Caught in the Cross-Fire of Host-Microbial Interactions. *Dig Dis Sci*.

CGAT developers. 2019. CGAT core.

Chantranupong, L., S.M. Scaria, R.A. Saxton, M.P. Gygi, K. Shen, G.A. Wyant, T. Wang, J.W. Harper, S.P. Gygi, and D.M. Sabatini. 2016. The CASTOR Proteins Are Arginine Sensors for the mTORC1 Pathway. *Cell*. 165:153-164.

Charbit-Henrion, F., M. Parlato, G. Malamut, F. Ruemmele, and N. Cerf-Bensussan. 2021. Intestinal immunoregulation: lessons from human mendelian diseases. *Mucosal Immunol*.

Chassaing, B., and A.T. Gewirtz. 2019. Identification of Inner Mucus-Associated Bacteria by Laser Capture Microdissection. *Cell Mol Gastroenterol Hepatol*. 7:157-160.

Chauhan, S., M.A. Mandell, and V. Deretic. 2015. IRGM governs the core autophagy machinery to conduct antimicrobial defense. *Mol Cell*. 58:507-521.

Cheli, V.T., and E.C. Dell'Angelica. 2010. Early origin of genes encoding subunits of biogenesis of lysosome-related organelles complex-1, -2 and -3. *Traffic*. 11:579-586.

Chellapandian, D., J. Krueger, T. Schechter, A. Gassas, S. Weitzman, A. Naqvi, and M. Ali. 2016. Successful Allogeneic Hematopoietic Stem Cell Transplantation in XIAP Deficiency Using Reduced-Intensity Conditioning. *Pediatr Blood Cancer*. 63:355-357.

Chen, M., H. Sun, M. Boot, L. Shao, S.J. Chang, W. Wang, T.T. Lam, M. Lara-Tejero, E.H. Rego, and J.E. Galan. 2020. Itaconate is an effector of a Rab GTPase cell-autonomous host defense pathway against Salmonella. *Science*. 369:450-455.

Chen, T.J., and N. Kotecha. 2014. Cytobank: providing an analytics platform for community cytometry data analysis and collaboration. *Curr Top Microbiol Immunol*. 377:127-157.

Chen, W.W., E. Freinkman, and D.M. Sabatini. 2017. Rapid immunopurification of mitochondria for metabolite profiling and absolute quantification of matrix metabolites. *Nat Protoc*. 12:2215-2231.

Chiang, S.C.C., S.M. Wood, B. Tesi, H.H. Akar, W. Al-Herz, S. Ammann, F.B. Belen, U. Caliskan, Z. Kaya, K. Lehmberg, T. Patiroglu, H. Tokgoz, A. Unuvar, W.J. Introne, J.I. Henter, M. Nordenskjold, H.G. Ljunggren, M. Meeths, S. Ehl, K. Krzewski, and Y.T. Bryceson. 2017. Differences in Granule Morphology yet Equally Impaired Exocytosis among Cytotoxic T Cells and NK Cells from Chediak-Higashi Syndrome Patients. *Front Immunol*. 8:426.

Chistiakov, D.A., A.A. Melnichenko, V.A. Myasoedova, A.V. Grechko, and A.N. Orekhov. 2017. Mechanisms of foam cell formation in atherosclerosis. *J Mol Med (Berl)*. 95:1153-1165.

Chu, H., A. Khosravi, I.P. Kusumawardhani, A.H. Kwon, A.C. Vasconcelos, L.D. Cunha, A.E. Mayer, Y. Shen, W.L. Wu, A. Kambal, S.R. Targan, R.J. Xavier, P.B. Ernst, D.R. Green, D.P. McGovern, H.W. Virgin, and S.K. Mazmanian. 2016. Gene-microbiota interactions contribute to the pathogenesis of inflammatory bowel disease. *Science*. 352:1116-1120.

Chung, K.P., C.L. Hsu, L.C. Fan, Z. Huang, D. Bhatia, Y.J. Chen, S. Hisata, S.J. Cho, K. Nakahira, M. Imamura, M.E. Choi, C.J. Yu, S.M. Cloonan, and A.M.K. Choi. 2019. Mitofusins regulate lipid metabolism to mediate the development of lung fibrosis. *Nat Commun*. 10:3390.

Clark, L., C.A. Perrett, L. Malt, C. Harward, S. Humphrey, K.A. Jepson, I. Martinez-Argudo, L.J. Carney, R.M. La Ragione, T.J. Humphrey, and M.A. Jepson. 2011. Differences in

Salmonella enterica serovar Typhimurium strain invasiveness are associated with heterogeneity in SPI-1 gene expression. *Microbiology (Reading)*. 157:2072-2083.
Clark, R.H., J.C. Stinchcombe, A. Day, E. Blott, S. Booth, G. Bossi, T. Hamblin, E.G. Davies, and G.M. Griffiths. 2003. Adaptor protein 3-dependent microtubule-mediated movement of lytic granules to the immunological synapse. *Nat Immunol*. 4:1111-1120.
Conte, M.P., C. Longhi, M. Marazzato, A.L. Conte, M. Aleandri, M.S. Lepanto, C. Zagaglia, M. Nicoletti, M. Aloi, V. Totino, A.T. Palamara, and S. Schippa. 2014. Adherent-invasive Escherichia coli (AIEC) in pediatric Crohn's disease patients: phenotypic and genetic pathogenic features. *BMC Res Notes*. 7:748.
Cooney, R., J. Baker, O. Brain, B. Danis, T. Pichulik, P. Allan, D.J. Ferguson, B.J. Campbell, D. Jewell, and A. Simmons. 2010. NOD2 stimulation induces autophagy in dendritic cells influencing bacterial handling and antigen presentation. *Nat Med*. 16:90-97.
Corridoni, D., A. Antanaviciute, T. Gupta, D. Fawkner-Corbett, A. Aulicino, M. Jagielowicz, K. Parikh, E. Repapi, S. Taylor, D. Ishikawa, R. Hatano, T. Yamada, W. Xin, H. Slawinski, R. Bowden, G. Napolitani, O. Brain, C. Morimoto, H. Koohy, and A. Simmons. 2020. Single-cell atlas of colonic CD8(+) T cells in ulcerative colitis. *Nat Med*. 26:1480-1490.
Cougnoux, A., et al. 2018. Gastrointestinal track pathology in a Balb/c Niemann-Pick disease type C1 null mouse model. *Digestive Diseases and Sciences*.
Cuevas-Mora, K., W. Roque, H. Shaghaghi, B.R. Gochuico, I.O. Rosas, R. Summer, and F. Romero. 2021. Hermansky-Pudlak syndrome-2 alters mitochondrial homeostasis in the alveolar epithelium of the lung. *Respir Res*. 22:49.
D'Haens, G., K. Geboes, E. Ponette, F. Penninckx, and P. Rutgeerts. 1997. Healing of severe recurrent ileitis with azathioprine therapy in patients with Crohn's disease. *Gastroenterology*. 112:1475-1481.
Damgaard, R.B., U. Nachbur, M. Yabal, W.W. Wong, B.K. Fiil, M. Kastirr, E. Rieser, J.A. Rickard, A. Bankovacki, C. Peschel, J. Ruland, S. Bekker-Jensen, N. Mailand, T. Kaufmann, A. Strasser, H. Walczak, J. Silke, P.J. Jost, and M. Gyrd-Hansen. 2012. The ubiquitin ligase XIAP recruits LUBAC for NOD2 signaling in inflammation and innate immunity. *Mol Cell*. 46:746-758.
Darfeuille-Michaud, A., J. Boudeau, P. Bulois, C. Neut, A.L. Glasser, N. Barnich, M.A. Bringer, A. Swidsinski, L. Beaugerie, and J.F. Colombel. 2004. High prevalence of adherent-invasive Escherichia coli associated with ileal mucosa in Crohn's disease. *Gastroenterology*. 127:412-421.
de Boer, M., K. van Leeuwen, J. Geissler, F. van Alphen, E. de Vries, M. van der Kuip, S.W.J. Terheggen, H. Janssen, T.K. van den Berg, A.B. Meijer, D. Roos, and T.W. Kuijpers. 2017. Hermansky-Pudlak syndrome type 2: Aberrant pre-mRNA splicing and mislocalization of granule proteins in neutrophils. *Hum Mutat*. 38:1402-1411.
de Lange, K.M., L. Moutsianas, J.C. Lee, C.A. Lamb, Y. Luo, N.A. Kennedy, L. Jostins, D.L. Rice, J. Gutierrez-Achury, S.G. Ji, G. Heap, E.R. Nimmo, C. Edwards, P. Henderson, C. Mowat, J. Sanderson, J. Satsangi, A. Simmons, D.C. Wilson, M. Tremelling, A. Hart, C.G. Mathew, W.G. Newman, M. Parkes, C.W. Lees, H. Uhlig, C. Hawkey, N.J. Prescott, T. Ahmad, J.C. Mansfield, C.A. Anderson, and J.C. Barrett. 2017. Genome-wide association study implicates immune activation of multiple integrin genes in inflammatory bowel disease. *Nat Genet*. 49:256-261.
Delevoye, C., X. Heiligenstein, L. Ripoll, F. Gilles-Marsens, M.K. Dennis, R.A. Linares, L. Derman, A. Gokhale, E. Morel, V. Faundez, M.S. Marks, and G. Raposo. 2016. BLOC-1

Brings Together the Actin and Microtubule Cytoskeletons to Generate Recycling Endosomes. *Curr Biol*. 26:1-13.

Dell'Angelica, E.C., V. Shotelersuk, R.C. Aguilar, W.A. Gahl, and J.S. Bonifacino. 1999. Altered trafficking of lysosomal proteins in Hermansky-Pudlak syndrome due to mutations in the beta 3A subunit of the AP-3 adaptor. *Mol Cell*. 3:11-21.

Dennis, M.K., C. Delevoye, A. Acosta-Ruiz, I. Hurbain, M. Romao, G.G. Hesketh, P.S. Goff, E.V. Sviderskaya, D.C. Bennett, J.P. Luzio, T. Galli, D.J. Owen, G. Raposo, and M.S. Marks. 2016. BLOC-1 and BLOC-3 regulate VAMP7 cycling to and from melanosomes via distinct tubular transport carriers. *J Cell Biol*. 214:293-308.

Dennis, M.K., A.R. Mantegazza, O.L. Snir, D. Tenza, A. Acosta-Ruiz, C. Delevoye, R. Zorger, A. Sitaram, W. de Jesus-Rojas, K. Ravichandran, J. Rux, E.V. Sviderskaya, D.C. Bennett, G. Raposo, M.S. Marks, and S.R. Setty. 2015. BLOC-2 targets recycling endosomal tubules to melanosomes for cargo delivery. *J Cell Biol*. 209:563-577.

Dharmasiri, S., E.M. Garrido-Martin, R.J. Harris, A.C. Bateman, J.E. Collins, J.R.F. Cummings, and T. Sanchez-Elsner. 2021. Human Intestinal Macrophages Are Involved in the Pathology of Both Ulcerative Colitis and Crohn Disease. *Inflamm Bowel Dis*.

Di Pietro, S.M., J.M. Falcon-Perez, and E.C. Dell'Angelica. 2004. Characterization of BLOC-2, a complex containing the Hermansky-Pudlak syndrome proteins HPS3, HPS5 and HPS6. *Traffic*. 5:276-283.

Di Pietro, S.M., J.M. Falcon-Perez, D. Tenza, S.R. Setty, M.S. Marks, G. Raposo, and E.C. Dell'Angelica. 2006. BLOC-1 interacts with BLOC-2 and the AP-3 complex to facilitate protein trafficking on endosomes. *Mol Biol Cell*. 17:4027-4038.

Dikic, I., and Z. Elazar. 2018. Mechanism and medical implications of mammalian autophagy. *Nat Rev Mol Cell Biol*. 19:349-364.

Doench, J.G., N. Fusi, M. Sullender, M. Hegde, E.W. Vaimberg, K.F. Donovan, I. Smith, Z. Tothova, C. Wilen, R. Orchard, H.W. Virgin, J. Listgarten, and D.E. Root. 2016. Optimized sgRNA design to maximize activity and minimize off-target effects of CRISPR-Cas9. *Nat Biotechnol*. 34:184-191.

Dooley, H.C., M. Razi, H.E. Polson, S.E. Girardin, M.I. Wilson, and S.A. Tooze. 2014. WIPI2 links LC3 conjugation with PI3P, autophagosome formation, and pathogen clearance by recruiting Atg12-5-16L1. *Mol Cell*. 55:238-252.

Dowling, R.J., I. Topisirovic, T. Alain, M. Bidinosti, B.D. Fonseca, E. Petroulakis, X. Wang, O. Larsson, A. Selvaraj, Y. Liu, S.C. Kozma, G. Thomas, and N. Sonenberg. 2010. mTORC1-mediated cell proliferation, but not cell growth, controlled by the 4E-BPs. *Science*. 328:1172-1176.

Drizyte-Miller, K., J. Chen, H. Cao, M.B. Schott, and M.A. McNiven. 2020. The small GTPase Rab32 resides on lysosomes to regulate mTORC1 signaling. *J Cell Sci*.

Du, X., J. Kumar, C. Ferguson, T.A. Schulz, Y.S. Ong, W. Hong, W.A. Prinz, R.G. Parton, A.J. Brown, and H. Yang. 2011. A role for oxysterol-binding protein-related protein 5 in endosomal cholesterol trafficking. *J Cell Biol*. 192:121-135.

Duvel, K., J.L. Yecies, S. Menon, P. Raman, A.I. Lipovsky, A.L. Souza, E. Triantafellow, Q. Ma, R. Gorski, S. Cleaver, M.G. Vander Heiden, J.P. MacKeigan, P.M. Finan, C.B. Clish, L.O. Murphy, and B.D. Manning. 2010. Activation of a metabolic gene regulatory network downstream of mTOR complex 1. *Mol Cell*. 39:171-183.

Eid, W., K. Dauner, K.C. Courtney, A. Gagnon, R.J. Parks, A. Sorisky, and X. Zha. 2017. mTORC1 activates SREBP-2 by suppressing cholesterol trafficking to lysosomes in mammalian cells. *Proc Natl Acad Sci U S A*. 114:7999-8004.

El-Chemaly, S., F. Cheung, Y. Kotliarov, K.J. O'Brien, W.A. Gahl, J. Chen, S.Y. Perl, A. Biancotto, and B.R. Gochuico. 2018. The Immunome in Two Inherited Forms of Pulmonary Fibrosis. *Front Immunol*. 9:76.

El-Chemaly, S., and L.R. Young. 2016. Hermansky-Pudlak Syndrome. *Clin Chest Med*. 37:505-511.

Emanuel, R., I. Sergin, S. Bhattacharya, J. Turner, S. Epelman, C. Settembre, A. Diwan, A. Ballabio, and B. Razani. 2014. Induction of lysosomal biogenesis in atherosclerotic macrophages can rescue lipid-induced lysosomal dysfunction and downstream sequelae. *Arterioscler Thromb Vasc Biol*. 34:1942-1952.

Emmanuel, N., S. Ragunathan, Q. Shan, F. Wang, A. Giannakou, N. Huser, G. Jin, J. Myers, R.T. Abraham, and K. Unsal-Kacmaz. 2017. Purine Nucleotide Availability Regulates mTORC1 Activity through the Rheb GTPase. *Cell Rep*. 19:2665-2680.

Engelhardt, K.R., N. Shah, I. Faizura-Yeop, D.F. Kocacik Uygun, N. Frede, A.M. Muise, E. Shteyer, S. Filiz, R. Chee, M. Elawad, B. Hartmann, P.D. Arkwright, C. Dvorak, C. Klein, J.M. Puck, B. Grimbacher, and E.O. Glocker. 2013. Clinical outcome in IL-10- and IL-10 receptor-deficient patients with or without hematopoietic stem cell transplantation. *J Allergy Clin Immunol*. 131:825-830.

Erzin, Y., S. Cosgun, A. Dobrucali, M. Tasyurekli, S. Erdamar, and M. Tuncer. 2006. Complicated granulomatous colitis in a patient with Hermansky-Pudlak syndrome, successfully treated with infliximab. *Acta Gastroenterol Belg*. 69:213-216.

Ewels, P., M. Magnusson, S. Lundin, and M. Kaller. 2016. MultiQC: summarize analysis results for multiple tools and samples in a single report. *Bioinformatics*. 32:3047-3048.

Fabri, M., S. Stenger, D.M. Shin, J.M. Yuk, P.T. Liu, S. Realegeno, H.M. Lee, S.R. Krutzik, M. Schenk, P.A. Sieling, R. Teles, D. Montoya, S.S. Iyer, H. Bruns, D.M. Lewinsohn, B.W. Hollis, M. Hewison, J.S. Adams, A. Steinmeyer, U. Zugel, G. Cheng, E.K. Jo, B.R. Bloom, and R.L. Modlin. 2011. Vitamin D is required for IFN-gamma-mediated antimicrobial activity of human macrophages. *Sci Transl Med*. 3:104ra102.

Fachi, J.L., J.S. Felipe, L.P. Pral, B.K. da Silva, R.O. Correa, M.C.P. de Andrade, D.M. da Fonseca, P.J. Basso, N.O.S. Camara, E.S.E.L. de Sales, F. Dos Santos Martins, S.E.S. Guima, A.M. Thomas, J.C. Setubal, Y.T. Magalhaes, F.L. Forti, T. Candreva, H.G. Rodrigues, M.B. de Jesus, S.R. Consonni, A.D.S. Farias, P. Varga-Weisz, and M.A.R. Vinolo. 2019. Butyrate Protects Mice from Clostridium difficile-Induced Colitis through an HIF-1-Dependent Mechanism. *Cell Rep*. 27:750-761 e757.

Fairfax, B.P., P. Humburg, S. Makino, V. Naranbhai, D. Wong, E. Lau, L. Jostins, K. Plant, R. Andrews, C. McGee, and J.C. Knight. 2014. Innate immune activity conditions the effect of regulatory variants upon monocyte gene expression. *Science*. 343:1246949.

Falcon-Perez, J.M., R. Nazarian, C. Sabatti, and E.C. Dell'Angelica. 2005. Distribution and dynamics of Lamp1-containing endocytic organelles in fibroblasts deficient in BLOC-3. *J Cell Sci*. 118:5243-5255.

Favier, L.A., and G.S. Schulert. 2016. Mevalonate kinase deficiency: current perspectives. *Appl Clin Genet*. 9:101-110.

Feagan, B.G., R.N. Fedorak, E.J. Irvine, G. Wild, L. Sutherland, A.H. Steinhart, G.R. Greenberg, J. Koval, C.J. Wong, M. Hopkins, S.B. Hanauer, and J.W. McDonald. 2000. A comparison of methotrexate with placebo for the maintenance of remission in Crohn's disease. North American Crohn's Study Group Investigators. *N Engl J Med*. 342:1627-1632.

Feagan, B.G., W.J. Sandborn, G. D'Haens, J. Panes, A. Kaser, M. Ferrante, E. Louis, D. Franchimont, O. Dewit, U. Seidler, K.J. Kim, M.F. Neurath, S. Schreiber, P. Scholl, C. Pamulapati, B. Lalovic, S. Visvanathan, S.J. Padula, I. Herichova, A. Soaita, D.B. Hall, and W.O. Bocher. 2017. Induction therapy with the selective interleukin-23 inhibitor risankizumab in patients with moderate-to-severe Crohn's disease: a randomised, double-blind, placebo-controlled phase 2 study. *Lancet*. 389:1699-1709.

Feagan, B.G., W.J. Sandborn, C. Gasink, D. Jacobstein, Y. Lang, J.R. Friedman, M.A. Blank, J. Johanns, L.L. Gao, Y. Miao, O.J. Adedokun, B.E. Sands, S.B. Hanauer, S. Vermeire, S. Targan, S. Ghosh, W.J. de Villiers, J.F. Colombel, Z. Tulassay, U. Seidler, B.A. Salzberg, P. Desreumaux, S.D. Lee, E.V. Loftus, Jr., L.A. Dieleman, S. Katz, P. Rutgeerts, and U.-I.-U.S. Group. 2016. Ustekinumab as Induction and Maintenance Therapy for Crohn's Disease. *N Engl J Med*. 375:1946-1960.

Felipez, L.M., R. Gokhale, and S. Guandalini. 2010. Hermansky-Pudlak syndrome: severe colitis and good response to infliximab. *J Pediatr Gastroenterol Nutr*. 51:665-667.

Fineran, P., E. Lloyd-Evans, N.A. Lack, N. Platt, L.C. Davis, A.J. Morgan, D. Hoglinger, R.V.V. Tatituri, S. Clark, I.M. Williams, P. Tynan, N. Al Eisa, E. Nazarova, A. Williams, A. Galione, D.S. Ory, G.S. Besra, D.G. Russell, M.B. Brenner, E. Sim, and F.M. Platt. 2016. Pathogenic mycobacteria achieve cellular persistence by inhibiting the Niemann-Pick Type C disease cellular pathway. *Wellcome Open Res*. 1:18.

Freeman, S.A., and S. Grinstein. 2014. Phagocytosis: receptors, signal integration, and the cytoskeleton. *Immunol Rev*. 262:193-215.

Friedrich, M., Matthew A. Jackson, Ilya Korsunsky, Samuel, K.R.-A. Bullers, Zoe Christoforidou, Dharshan Sathananthan, Rahul, R.S.P. Ravindran, Hannah Sharpe, Kevin Wei, Gerald F. M. Watts,, A.G. Elizabeth H. Mann, Tom Thomas, Moustafa Attar, Oxford IBD, R.F.N.C. Cohort Investigators, Sarah McCuaig, Lloyd, E.C. Thomas, Holm H. Uhlig, Stephen Sansom, Alistair Easton, Soumya, and S.P.T. Raychaudhuri, Fiona M. Powrie. 2021. IL-1-driven stromal-neutrophil interaction in deep ulcers defines a pathotype of therapy non-responsive inflammatory bowel disease. *bioRxiv*.

Fritsch, J., V. Tchikov, L. Hennig, R. Lucius, and S. Schutze. 2019. A toolbox for the immunomagnetic purification of signaling organelles. *Traffic*. 20:246-258.

Fuss, I.J., C. Becker, Z. Yang, C. Groden, R.L. Hornung, F. Heller, M.F. Neurath, W. Strober, and P.J. Mannon. 2006. Both IL-12p70 and IL-23 are synthesized during active Crohn's disease and are down-regulated by treatment with anti-IL-12 p40 monoclonal antibody. *Inflamm Bowel Dis*. 12:9-15.

Gahl, W.A., M. Brantly, M.I. Kaiser-Kupfer, F. Iwata, S. Hazelwood, V. Shotelersuk, L.F. Duffy, E.M. Kuehl, J. Troendle, and I. Bernardini. 1998. Genetic defects and clinical characteristics of patients with a form of oculocutaneous albinism (Hermansky-Pudlak syndrome). *N Engl J Med*. 338:1258-1264.

Galeotti, C., U. Meinzer, P. Quartier, L. Rossi-Semerano, B. Bader-Meunier, P. Pillet, and I. Kone-Paut. 2012. Efficacy of interleukin-1-targeting drugs in mevalonate kinase deficiency. *Rheumatology (Oxford)*. 51:1855-1859.

Garay, S.M., J.E. Gardella, E.P. Fazzini, and R.M. Goldring. 1979. Hermansky-Pudlak syndrome. Pulmonary manifestations of a ceroid storage disorder. *Am J Med*. 66:737-747.

Gathungu, G., M.O. Kim, J.P. Ferguson, Y. Sharma, W. Zhang, S.M. Ng, E. Bonkowski, K. Ning, L.A. Simms, A.R. Croft, J.M. Stempak, N. Walker, N. Huang, Y. Xiao, M.S. Silverberg, B. Trapnell, J.H. Cho, G.L. Radford-Smith, and L.A. Denson. 2013. Granulocyte-

macrophage colony-stimulating factor autoantibodies: a marker of aggressive Crohn's disease. *Inflamm Bowel Dis*. 19:1671-1680.
Gatica, D., V. Lahiri, and D.J. Klionsky. 2018. Cargo recognition and degradation by selective autophagy. *Nat Cell Biol*. 20:233-242.
Gerondopoulos, A., L. Langemeyer, J.R. Liang, A. Linford, and F.A. Barr. 2012. BLOC-3 mutated in Hermansky-Pudlak syndrome is a Rab32/38 guanine nucleotide exchange factor. *Curr Biol*. 22:2135-2139.
Gevers, D., S. Kugathasan, L.A. Denson, Y. Vazquez-Baeza, W. Van Treuren, B. Ren, E. Schwager, D. Knights, S.J. Song, M. Yassour, X.C. Morgan, A.D. Kostic, C. Luo, A. Gonzalez, D. McDonald, Y. Haberman, T. Walters, S. Baker, J. Rosh, M. Stephens, M. Heyman, J. Markowitz, R. Baldassano, A. Griffiths, F. Sylvester, D. Mack, S. Kim, W. Crandall, J. Hyams, C. Huttenhower, R. Knight, and R.J. Xavier. 2014. The treatment-naive microbiome in new-onset Crohn's disease. *Cell Host Microbe*. 15:382-392.
Ghoreschi, K., A. Laurence, X.P. Yang, C.M. Tato, M.J. McGeachy, J.E. Konkel, H.L. Ramos, L. Wei, T.S. Davidson, N. Bouladoux, J.R. Grainger, Q. Chen, Y. Kanno, W.T. Watford, H.W. Sun, G. Eberl, E.M. Shevach, Y. Belkaid, D.J. Cua, W. Chen, and J.J. O'Shea. 2010. Generation of pathogenic T(H)17 cells in the absence of TGF-beta signalling. *Nature*. 467:967-971.
Girot, P., C. Le Berre, A. De Maissin, M. Freyssinet, C. Trang-Poisson, and A. Bourreille. 2019. Crohn's-like acute severe colitis associated with Hermansky-Pudlak syndrome: A case report. *World J Gastroenterol*. 25:1031-1036.
Glassberg, J., A.H. Rahman, M. Zafar, C. Cromwell, A. Punzalan, J.J. Badimon, and L. Aledort. 2018. Application of phospho-CyTOF to characterize immune activation in patients with sickle cell disease in an ex vivo model of thrombosis. *J Immunol Methods*. 453:11-19.
Graham, D.B., and R.J. Xavier. 2020. Pathway paradigms revealed from the genetics of inflammatory bowel disease. *Nature*. 578:527-539.
Griseri, T., I.C. Arnold, C. Pearson, T. Krausgruber, C. Schiering, F. Franchini, J. Schulthess, B.S. McKenzie, P.R. Crocker, and F. Powrie. 2015. Granulocyte Macrophage Colony-Stimulating Factor-Activated Eosinophils Promote Interleukin-23 Driven Chronic Colitis. *Immunity*. 43:187-199.
Griseri, T., B.S. McKenzie, C. Schiering, and F. Powrie. 2012. Dysregulated hematopoietic stem and progenitor cell activity promotes interleukin-23-driven chronic intestinal inflammation. *Immunity*. 37:1116-1129.
Grucela, A.L., P. Patel, E. Goldstein, R. Palmon, D.B. Sachar, and R.M. Steinhagen. 2006. Granulomatous enterocolitis associated with Hermansky-Pudlak syndrome. *Am J Gastroenterol*. 101:2090-2095.
Gu, X., J.M. Orozco, R.A. Saxton, K.J. Condon, G.Y. Liu, P.A. Krawczyk, S.M. Scaria, J.W. Harper, S.P. Gygi, and D.M. Sabatini. 2017. SAMTOR is an S-adenosylmethionine sensor for the mTORC1 pathway. *Science*. 358:813-818.
Guerrini, V., B. Prideaux, L. Blanc, N. Bruiners, R. Arrigucci, S. Singh, H.P. Ho-Liang, H. Salamon, P.Y. Chen, K. Lakehal, S. Subbian, P. O'Brien, L.E. Via, C.E. Barry, 3rd, V. Dartois, and M.L. Gennaro. 2018. Storage lipid studies in tuberculosis reveal that foam cell biogenesis is disease-specific. *PLoS Pathog*. 14:e1007223.
Haile, Y., X. Deng, C. Ortiz-Sandoval, N. Tahbaz, A. Janowicz, J.Q. Lu, B.J. Kerr, N.J. Gutowski, J.E. Holley, P. Eggleton, F. Giuliani, and T. Simmen. 2017. Rab32 connects ER stress to mitochondrial defects in multiple sclerosis. *J Neuroinflammation*. 14:19.

Halfvarson, J., C.J. Brislawn, R. Lamendella, Y. Vazquez-Baeza, W.A. Walters, L.M. Bramer, M. D'Amato, F. Bonfiglio, D. McDonald, A. Gonzalez, E.E. McClure, M.F. Dunklebarger, R. Knight, and J.K. Jansson. 2017. Dynamics of the human gut microbiome in inflammatory bowel disease. *Nat Microbiol*. 2:17004.

Hampe, J., A. Franke, P. Rosenstiel, A. Till, M. Teuber, K. Huse, M. Albrecht, G. Mayr, F.M. De La Vega, J. Briggs, S. Gunther, N.J. Prescott, C.M. Onnie, R. Hasler, B. Sipos, U.R. Folsch, T. Lengauer, M. Platzer, C.G. Mathew, M. Krawczak, and S. Schreiber. 2007. A genome-wide association scan of nonsynonymous SNPs identifies a susceptibility variant for Crohn disease in ATG16L1. *Nat Genet*. 39:207-211.

Hartlova, A., S. Herbst, J. Peltier, A. Rodgers, O. Bilkei-Gorzo, A. Fearns, B.D. Dill, H. Lee, R. Flynn, S.A. Cowley, P. Davies, P.A. Lewis, I.G. Ganley, J. Martinez, D.R. Alessi, A.D. Reith, M. Trost, and M.G. Gutierrez. 2018. LRRK2 is a negative regulator of Mycobacterium tuberculosis phagosome maturation in macrophages. *EMBO J*. 37.

Hasegawa, M., Y. Fujimoto, P.C. Lucas, H. Nakano, K. Fukase, G. Nunez, and N. Inohara. 2008. A critical role of RICK/RIP2 polyubiquitination in Nod-induced NF-kappaB activation. *EMBO J*. 27:373-383.

Hazzan, D., S. Seward, H. Stock, S. Zisman, K. Gabriel, N. Harpaz, and J.J. Bauer. 2006. Crohn's-like colitis, enterocolitis and perianal disease in Hermansky-Pudlak syndrome. *Colorectal Dis*. 8:539-543.

Heller, S., C. Cable, H. Penrose, R. Makboul, D. Biswas, M. Cabe, S.E. Crawford, and S.D. Savkovic. 2016. Intestinal inflammation requires FOXO3 and prostaglandin E2-dependent lipogenesis and elevated lipid droplets. *Am J Physiol Gastrointest Liver Physiol*. 310:G844-854.

Hermansky, F., and P. Pudlak. 1959. Albinism associated with hemorrhagic diathesis and unusual pigmented reticular cells in the bone marrow: report of two cases with histochemical studies. *Blood*. 14:162-169.

Hirota, Y., and Y. Tanaka. 2009. A small GTPase, human Rab32, is required for the formation of autophagic vacuoles under basal conditions. *Cell Mol Life Sci*. 66:2913-2932.

Hoglinger, D., T. Burgoyne, E. Sanchez-Heras, P. Hartwig, A. Colaco, J. Newton, C.E. Futter, S. Spiegel, F.M. Platt, and E.R. Eden. 2019. NPC1 regulates ER contacts with endocytic organelles to mediate cholesterol egress. *Nat Commun*. 10:4276.

Holland, P., M.L. Torgersen, K. Sandvig, and A. Simonsen. 2014. LYST affects lysosome size and quantity, but not trafficking or degradation through autophagy or endocytosis. *Traffic*. 15:1390-1405.

Homer, C.R., A.L. Richmond, N.A. Rebert, J.P. Achkar, and C. McDonald. 2010. ATG16L1 and NOD2 interact in an autophagy-dependent antibacterial pathway implicated in Crohn's disease pathogenesis. *Gastroenterology*. 139:1630-1641, 1641 e1631-1632.

Horizon Discovery. 2021. HAP1 knockout cell lines. https://horizondiscovery.com/en/engineered-cell-lines/products/human-hap1-knockout-cell-lines

Hu, Z.Q., C.L. Rao, M.L. Tang, Y. Zhang, X.X. Lu, J.G. Chen, C. Mao, L. Deng, Q. Li, and X.H. Mao. 2019. Rab32 GTPase, as a direct target of miR-30b/c, controls the intracellular survival of Burkholderia pseudomallei by regulating phagosome maturation. *PLoS Pathog*. 15:e1007879.

Huang, J., V. Canadien, G.Y. Lam, B.E. Steinberg, M.C. Dinauer, M.A. Magalhaes, M. Glogauer, S. Grinstein, and J.H. Brumell. 2009. Activation of antibacterial autophagy by NADPH oxidases. *Proc Natl Acad Sci U S A*. 106:6226-6231.

Hugot, J.P., M. Chamaillard, H. Zouali, S. Lesage, J.P. Cezard, J. Belaiche, S. Almer, C. Tysk, C.A. O'Morain, M. Gassull, V. Binder, Y. Finkel, A. Cortot, R. Modigliani, P. Laurent-Puig, C. Gower-Rousseau, J. Macry, J.F. Colombel, M. Sahbatou, and G. Thomas. 2001. Association of NOD2 leucine-rich repeat variants with susceptibility to Crohn's disease. *Nature*. 411:599-603.

Hui, K.Y., H. Fernandez-Hernandez, J. Hu, A. Schaffner, N. Pankratz, N.Y. Hsu, L.S. Chuang, S. Carmi, N. Villaverde, X. Li, M. Rivas, A.P. Levine, X. Bao, P.R. Labrias, T. Haritunians, D. Ruane, K. Gettler, E. Chen, D. Li, E.R. Schiff, N. Pontikos, N. Barzilai, S.R. Brant, S. Bressman, A.S. Cheifetz, L.N. Clark, M.J. Daly, R.J. Desnick, R.H. Duerr, S. Katz, T. Lencz, R.H. Myers, H. Ostrer, L. Ozelius, H. Payami, Y. Peter, J.D. Rioux, A.W. Segal, W.K. Scott, M.S. Silverberg, J.M. Vance, I. Ubarretxena-Belandia, T. Foroud, G. Atzmon, I. Pe'er, Y. Ioannou, D.P.B. McGovern, Z. Yue, E.E. Schadt, J.H. Cho, and I. Peter. 2018. Functional variants in the LRRK2 gene confer shared effects on risk for Crohn's disease and Parkinson's disease. *Sci Transl Med*. 10.

Huizing, M., Y. Anikster, and W.A. Gahl. 2000. Hermansky-Pudlak syndrome and related disorders of organelle formation. *Traffic*. 1:823-835.

Huizing, M., A. Helip-Wooley, W. Westbroek, M. Gunay-Aygun, and W.A. Gahl. 2008. Disorders of lysosome-related organelle biogenesis: clinical and molecular genetics. *Annu Rev Genomics Hum Genet*. 9:359-386.

Huizing, M., M.C.V. Malicdan, J.A. Wang, H. Pri-Chen, R.A. Hess, R. Fischer, K.J. O'Brien, M.A. Merideth, W.A. Gahl, and B.R. Gochuico. 2020. Hermansky-Pudlak syndrome: Mutation update. *Hum Mutat*. 41:543-580.

Human Protein Atlas. 2021. Blood Atlas.

Hume, A.N., L.M. Collinson, C.R. Hopkins, M. Strom, D.C. Barral, G. Bossi, G.M. Griffiths, and M.C. Seabra. 2002. The leaden gene product is required with Rab27a to recruit myosin Va to melanosomes in melanocytes. *Traffic*. 3:193-202.

Hussain, N., M. Quezado, M. Huizing, D. Geho, J.G. White, W. Gahl, and P. Mannon. 2006. Intestinal disease in Hermansky-Pudlak syndrome: occurrence of colitis and relation to genotype. *Clin Gastroenterol Hepatol*. 4:73-80.

Iljazovic, A., U. Roy, E.J.C. Galvez, T.R. Lesker, B. Zhao, A. Gronow, L. Amend, S.E. Will, J.D. Hofmann, M.C. Pils, K. Schmidt-Hohagen, M. Neumann-Schaal, and T. Strowig. 2021. Perturbation of the gut microbiome by Prevotella spp. enhances host susceptibility to mucosal inflammation. *Mucosal Immunol*. 14:113-124.

Inohara, N., Y. Ogura, A. Fontalba, O. Gutierrez, F. Pons, J. Crespo, K. Fukase, S. Inamura, S. Kusumoto, M. Hashimoto, S.J. Foster, A.P. Moran, J.L. Fernandez-Luna, and G. Nunez. 2003. Host recognition of bacterial muramyl dipeptide mediated through NOD2. Implications for Crohn's disease. *J Biol Chem*. 278:5509-5512.

Ip, W.K.E., N. Hoshi, D.S. Shouval, S. Snapper, and R. Medzhitov. 2017. Anti-inflammatory effect of IL-10 mediated by metabolic reprogramming of macrophages. *Science*. 356:513-519.

Ishihara, J., T. Mizuochi, T. Uchida, Y. Takaki, K.I. Konishi, M. Joo, Y. Takahashi, S. Yoshioka, H. Kusano, Y. Sasahara, and Y. Yamashita. 2019. Infantile-onset inflammatory bowel disease in a patient with Hermansky-Pudlak syndrome: a case report. *BMC Gastroenterol*. 19:9.

Itakura, E., C. Kishi-Itakura, and N. Mizushima. 2012. The hairpin-type tail-anchored SNARE syntaxin 17 targets to autophagosomes for fusion with endosomes/lysosomes. *Cell*. 151:1256-1269.

Ito, S., T. Suzuki, K. Inagaki, N. Suzuki, K. Takamori, T. Yamada, M. Nakazawa, M. Hatano, H. Takiwaki, Y. Kakuta, R.A. Spritz, and Y. Tomita. 2005. High frequency of Hermansky-Pudlak syndrome type 1 (HPS1) among Japanese albinism patients and functional analysis of HPS1 mutant protein. *J Invest Dermatol*. 125:715-720.

Ivetic, A., H.L. Hoskins Green, and S.J. Hart. 2019. L-selectin: A Major Regulator of Leukocyte Adhesion, Migration and Signaling. *Front Immunol*. 10:1068.

Iyer, S., S. Suresh, D. Guo, K. Daman, J.C.J. Chen, P. Liu, M. Zieger, K. Luk, B.P. Roscoe, C. Mueller, O.D. King, C.P. Emerson, Jr., and S.A. Wolfe. 2019. Precise therapeutic gene correction by a simple nuclease-induced double-stranded break. *Nature*. 568:561-565.

Jang, M.H., N. Sougawa, T. Tanaka, T. Hirata, T. Hiroi, K. Tohya, Z. Guo, E. Umemoto, Y. Ebisuno, B.G. Yang, J.Y. Seoh, M. Lipp, H. Kiyono, and M. Miyasaka. 2006. CCR7 is critically important for migration of dendritic cells in intestinal lamina propria to mesenteric lymph nodes. *J Immunol*. 176:803-810.

Jha, A.K., S.C. Huang, A. Sergushichev, V. Lampropoulou, Y. Ivanova, E. Loginicheva, K. Chmielewski, K.M. Stewart, J. Ashall, B. Everts, E.J. Pearce, E.M. Driggers, and M.N. Artyomov. 2015. Network integration of parallel metabolic and transcriptional data reveals metabolic modules that regulate macrophage polarization. *Immunity*. 42:419-430.

Jin, H.O., S.K. Seo, Y.S. Kim, S.H. Woo, K.H. Lee, J.Y. Yi, S.J. Lee, T.B. Choe, J.H. Lee, S. An, S.I. Hong, and I.C. Park. 2011. TXNIP potentiates Redd1-induced mTOR suppression through stabilization of Redd1. *Oncogene*. 30:3792-3801.

Johansson, M.E., and G.C. Hansson. 2016. Immunological aspects of intestinal mucus and mucins. *Nat Rev Immunol*. 16:639-649.

Jones, M.L., S.L. Murden, C. Brooks, V. Maloney, R.A. Manning, K.C. Gilmour, V. Bharadwaj, J. de la Fuente, S. Chakravorty, and A.D. Mumford. 2013. Disruption of AP3B1 by a chromosome 5 inversion: a new disease mechanism in Hermansky-Pudlak syndrome type 2. *BMC Med Genet*. 14:42.

Jostins, L., S. Ripke, R.K. Weersma, R.H. Duerr, D.P. McGovern, K.Y. Hui, J.C. Lee, L.P. Schumm, Y. Sharma, C.A. Anderson, J. Essers, M. Mitrovic, K. Ning, I. Cleynen, E. Theatre, S.L. Spain, S. Raychaudhuri, P. Goyette, Z. Wei, C. Abraham, J.P. Achkar, T. Ahmad, L. Amininejad, A.N. Ananthakrishnan, V. Andersen, J.M. Andrews, L. Baidoo, T. Balschun, P.A. Bampton, A. Bitton, G. Boucher, S. Brand, C. Buning, A. Cohain, S. Cichon, M. D'Amato, D. De Jong, K.L. Devaney, M. Dubinsky, C. Edwards, D. Ellinghaus, L.R. Ferguson, D. Franchimont, K. Fransen, R. Gearry, M. Georges, C. Gieger, J. Glas, T. Haritunians, A. Hart, C. Hawkey, M. Hedl, X. Hu, T.H. Karlsen, L. Kupcinskas, S. Kugathasan, A. Latiano, D. Laukens, I.C. Lawrance, C.W. Lees, E. Louis, G. Mahy, J. Mansfield, A.R. Morgan, C. Mowat, W. Newman, O. Palmieri, C.Y. Ponsioen, U. Potocnik, N.J. Prescott, M. Regueiro, J.I. Rotter, R.K. Russell, J.D. Sanderson, M. Sans, J. Satsangi, S. Schreiber, L.A. Simms, J. Sventoraityte, S.R. Targan, K.D. Taylor, M. Tremelling, H.W. Verspaget, M. De Vos, C. Wijmenga, D.C. Wilson, J. Winkelmann, R.J. Xavier, S. Zeissig, B. Zhang, C.K. Zhang, H. Zhao, I.B.D.G.C. International, M.S. Silverberg, V. Annese, H. Hakonarson, S.R. Brant, G. Radford-Smith, C.G. Mathew, J.D. Rioux, et al. 2012. Host-microbe interactions have shaped the genetic architecture of inflammatory bowel disease. *Nature*. 491:119-124.

Jung, J., G. Bohn, A. Allroth, K. Boztug, G. Brandes, I. Sandrock, A.A. Schaffer, C. Rathinam, I. Kollner, C. Beger, R. Schilke, K. Welte, B. Grimbacher, and C. Klein. 2006.

Identification of a homozygous deletion in the AP3B1 gene causing Hermansky-Pudlak syndrome, type 2. *Blood*. 108:362-369.
Kane, P.M. 1995. Disassembly and reassembly of the yeast vacuolar H(+)-ATPase in vivo. *J Biol Chem*. 270:17025-17032.
Kanehisa, M., and S. Goto. 2000. KEGG: kyoto encyclopedia of genes and genomes. *Nucleic Acids Res*. 28:27-30.
Karanasios, E., E. Stapleton, M. Manifava, T. Kaizuka, N. Mizushima, S.A. Walker, and N.T. Ktistakis. 2013. Dynamic association of the ULK1 complex with omegasomes during autophagy induction. *J Cell Sci*. 126:5224-5238.
Keestra-Gounder, A.M., R.M. Tsolis, and A.J. Baumler. 2015. Now you see me, now you don't: the interaction of Salmonella with innate immune receptors. *Nat Rev Microbiol*. 13:206-216.
Kim, D., J.M. Paggi, C. Park, C. Bennett, and S.L. Salzberg. 2019. Graph-based genome alignment and genotyping with HISAT2 and HISAT-genotype. *Nat Biotechnol*. 37:907-915.
Kim, J., M. Kundu, B. Viollet, and K.L. Guan. 2011. AMPK and mTOR regulate autophagy through direct phosphorylation of Ulk1. *Nat Cell Biol*. 13:132-141.
Kinchen, J., H.H. Chen, K. Parikh, A. Antanaviciute, M. Jagielowicz, D. Fawkner-Corbett, N. Ashley, L. Cubitt, E. Mellado-Gomez, M. Attar, E. Sharma, Q. Wills, R. Bowden, F.C. Richter, D. Ahern, K.D. Puri, J. Henault, F. Gervais, H. Koohy, and A. Simmons. 2018. Structural Remodeling of the Human Colonic Mesenchyme in Inflammatory Bowel Disease. *Cell*. 175:372-386 e317.
Kinghorn, K.J., A.M. Asghari, and J.I. Castillo-Quan. 2017. The emerging role of autophagic-lysosomal dysfunction in Gaucher disease and Parkinson's disease. *Neural Regen Res*. 12:380-384.
Kinghorn, K.J., S. Gronke, J.I. Castillo-Quan, N.S. Woodling, L. Li, E. Sirka, M. Gegg, K. Mills, J. Hardy, I. Bjedov, and L. Partridge. 2016. A Drosophila Model of Neuronopathic Gaucher Disease Demonstrates Lysosomal-Autophagic Defects and Altered mTOR Signalling and Is Functionally Rescued by Rapamycin. *J Neurosci*. 36:11654-11670.
Klionsky, D.J., A.K. Abdel-Aziz, S. Abdelfatah, M. Abdellatif, A. Abdoli, S. Abel, H. Abeliovich, M.H. Abildgaard, Y.P. Abudu, A. Acevedo-Arozena, I.E. Adamopoulos, K. Adeli, T.E. Adolph, A. Adornetto, E. Aflaki, G. Agam, A. Agarwal, B.B. Aggarwal, M. Agnello, P. Agostinis, J.N. Agrewala, A. Agrotis, P.V. Aguilar, S.T. Ahmad, Z.M. Ahmed, U. Ahumada-Castro, S. Aits, S. Aizawa, Y. Akkoc, T. Akoumianaki, H.A. Akpinar, A.M. Al-Abd, L. Al-Akra, A. Al-Gharaibeh, M.A. Alaoui-Jamali, S. Alberti, E. Alcocer-Gomez, C. Alessandri, M. Ali, M.A. Alim Al-Bari, S. Aliwaini, J. Alizadeh, E. Almacellas, A. Almasan, A. Alonso, G.D. Alonso, N. Altan-Bonnet, D.C. Altieri, E.M.C. Alvarez, S. Alves, C. Alves da Costa, M.M. Alzaharna, M. Amadio, C. Amantini, C. Amaral, S. Ambrosio, A.O. Amer, V. Ammanathan, Z. An, S.U. Andersen, S.A. Andrabi, M. Andrade-Silva, A.M. Andres, S. Angelini, D. Ann, U.C. Anozie, M.Y. Ansari, P. Antas, A. Antebi, Z. Anton, T. Anwar, L. Apetoh, N. Apostolova, T. Araki, Y. Araki, K. Arasaki, W.L. Araujo, J. Araya, C. Arden, M.A. Arevalo, S. Arguelles, E. Arias, J. Arikkath, H. Arimoto, A.R. Ariosa, D. Armstrong-James, L. Arnaune-Pelloquin, A. Aroca, D.S. Arroyo, I. Arsov, R. Artero, D.M.L. Asaro, M. Aschner, M. Ashrafizadeh, O. Ashur-Fabian, A.G. Atanasov, A.K. Au, P. Auberger, H.W. Auner, L. Aurelian, et al. 2021. Guidelines for the use and interpretation of assays for monitoring autophagy (4th edition)(1). *Autophagy*. 17:1-382.

Kloer, D.P., R. Rojas, V. Ivan, K. Moriyama, T. van Vlijmen, N. Murthy, R. Ghirlando, P. van der Sluijs, J.H. Hurley, and J.S. Bonifacino. 2010. Assembly of the biogenesis of lysosome-related organelles complex-3 (BLOC-3) and its interaction with Rab9. *J Biol Chem*. 285:7794-7804.

Knight, M., J. Braverman, K. Asfaha, K. Gronert, and S. Stanley. 2018. Lipid droplet formation in Mycobacterium tuberculosis infected macrophages requires IFN-gamma/HIF-1alpha signaling and supports host defense. *PLoS Pathog*. 14:e1006874.

Korotkevich, S., Sergushichev. 2019. Fast gene set enrichment analysis. *bioRxiv*.

Kotlarz, D., R. Beier, D. Murugan, J. Diestelhorst, O. Jensen, K. Boztug, D. Pfeifer, H. Kreipe, E.D. Pfister, U. Baumann, J. Puchalka, J. Bohne, O. Egritas, B. Dalgic, K.L. Kolho, A. Sauerbrey, S. Buderus, T. Gungor, A. Enninger, Y.K. Koda, G. Guariso, B. Weiss, S. Corbacioglu, P. Socha, N. Uslu, A. Metin, G.T. Wahbeh, K. Husain, D. Ramadan, W. Al-Herz, B. Grimbacher, M. Sauer, K.W. Sykora, S. Koletzko, and C. Klein. 2012. Loss of interleukin-10 signaling and infantile inflammatory bowel disease: implications for diagnosis and therapy. *Gastroenterology*. 143:347-355.

Kouklakis, G., E.I. Efremidou, M.S. Papageorgiou, E. Pavlidou, K.J. Manolas, and N. Liratzopoulos. 2007. Complicated Crohn's-like colitis, associated with Hermansky-Pudlak syndrome, treated with Infliximab: a case report and brief review of the literature. *J Med Case Rep*. 1:176.

Kruth, H.S., N.L. Jones, W. Huang, B. Zhao, I. Ishii, J. Chang, C.A. Combs, D. Malide, and W.Y. Zhang. 2005. Macropinocytosis is the endocytic pathway that mediates macrophage foam cell formation with native low density lipoprotein. *J Biol Chem*. 280:2352-2360.

Kugathasan, S., L.A. Denson, T.D. Walters, M.O. Kim, U.M. Marigorta, M. Schirmer, K. Mondal, C. Liu, A. Griffiths, J.D. Noe, W.V. Crandall, S. Snapper, S. Rabizadeh, J.R. Rosh, J.M. Shapiro, S. Guthery, D.R. Mack, R. Kellermayer, M.D. Kappelman, S. Steiner, D.E. Moulton, D. Keljo, S. Cohen, M. Oliva-Hemker, M.B. Heyman, A.R. Otley, S.S. Baker, J.S. Evans, B.S. Kirschner, A.S. Patel, D. Ziring, B.C. Trapnell, F.A. Sylvester, M.C. Stephens, R.N. Baldassano, J.F. Markowitz, J. Cho, R.J. Xavier, C. Huttenhower, B.J. Aronow, G. Gibson, J.S. Hyams, and M.C. Dubinsky. 2017. Prediction of complicated disease course for children newly diagnosed with Crohn's disease: a multicentre inception cohort study. *Lancet*. 389:1710-1718.

Kvedaraite, E., M. Lourda, M. Idestrom, P. Chen, S. Olsson-Akefeldt, M. Forkel, D. Gavhed, U. Lindforss, J. Mjosberg, J.I. Henter, and M. Svensson. 2016. Tissue-infiltrating neutrophils represent the main source of IL-23 in the colon of patients with IBD. *Gut*. 65:1632-1641.

Kwon, H.J., L. Abi-Mosleh, M.L. Wang, J. Deisenhofer, J.L. Goldstein, M.S. Brown, and R.E. Infante. 2009. Structure of N-terminal domain of NPC1 reveals distinct subdomains for binding and transfer of cholesterol. *Cell*. 137:1213-1224.

Lamble, S., E. Batty, M. Attar, D. Buck, R. Bowden, G. Lunter, D. Crook, B. El-Fahmawi, and P. Piazza. 2013. Improved workflows for high throughput library preparation using the transposome-based Nextera system. *BMC Biotechnol*. 13:104.

Lamming, D.W., L. Ye, D.M. Sabatini, and J.A. Baur. 2013. Rapalogs and mTOR inhibitors as anti-aging therapeutics. *J Clin Invest*. 123:980-989.

Langfelder, P., and S. Horvath. 2008. WGCNA: an R package for weighted correlation network analysis. *BMC Bioinformatics*. 9:559.

Lassen, K.G., C.I. McKenzie, M. Mari, T. Murano, J. Begun, L.A. Baxt, G. Goel, E.J. Villablanca, S.Y. Kuo, H. Huang, L. Macia, A.K. Bhan, M. Batten, M.J. Daly, F. Reggiori, C.R.

Mackay, and R.J. Xavier. 2016. Genetic Coding Variant in GPR65 Alters Lysosomal pH and Links Lysosomal Dysfunction with Colitis Risk. *Immunity*. 44:1392-1405.
Lassen, K.G., and R.J. Xavier. 2018. Mechanisms and function of autophagy in intestinal disease. *Autophagy*. 14:216-220.
Lawrence, R.E., and R. Zoncu. 2019. The lysosome as a cellular centre for signalling, metabolism and quality control. *Nat Cell Biol*. 21:133-142.
Lederer, D.J., and F.J. Martinez. 2018. Idiopathic Pulmonary Fibrosis. *N Engl J Med*. 379:797-798.
Les Laboratoires Servier. 2021. Servier Medical Art. https://smart.servier.com
Levy, M., A. Arion, D. Berrebi, L. Cuisset, C. Jeanne-Pasquier, B. Bader-Meunier, and C. Jung. 2013. Severe early-onset colitis revealing mevalonate kinase deficiency. *Pediatrics*. 132:e779-783.
Lewis, J.D., E.Z. Chen, R.N. Baldassano, A.R. Otley, A.M. Griffiths, D. Lee, K. Bittinger, A. Bailey, E.S. Friedman, C. Hoffmann, L. Albenberg, R. Sinha, C. Compher, E. Gilroy, L. Nessel, A. Grant, C. Chehoud, H. Li, G.D. Wu, and F.D. Bushman. 2015. Inflammation, Antibiotics, and Diet as Environmental Stressors of the Gut Microbiome in Pediatric Crohn's Disease. *Cell Host Microbe*. 18:489-500.
Li, H., B. Handsaker, A. Wysoker, T. Fennell, J. Ruan, N. Homer, G. Marth, G. Abecasis, R. Durbin, and S. Genome Project Data Processing. 2009. The Sequence Alignment/Map format and SAMtools. *Bioinformatics*. 25:2078-2079.
Li, Q., J. Wang, Y. Wan, and D. Chen. 2016a. Depletion of Rab32 decreases intracellular lipid accumulation and induces lipolysis through enhancing ATGL expression in hepatocytes. *Biochem Biophys Res Commun*. 471:492-496.
Li, Y., Y. Wang, L. Zou, X. Tang, Y. Yang, L. Ma, Q. Jia, Q. Ni, S. Liu, L. Tang, R. Lin, E. Wong, W. Sun, L. Wang, Q. Wei, H. Ran, L. Zhang, H. Lian, W. Huang, Y. Wu, Q.J. Li, and Y. Wan. 2016b. Analysis of the Rab GTPase Interactome in Dendritic Cells Reveals Anti-microbial Functions of the Rab32 Complex in Bacterial Containment. *Immunity*. 44:422-437.
Liao, Y., G.K. Smyth, and W. Shi. 2014. featureCounts: an efficient general purpose program for assigning sequence reads to genomic features. *Bioinformatics*. 30:923-930.
Lim, C.Y., O.B. Davis, H.R. Shin, J. Zhang, C.A. Berdan, X. Jiang, J.L. Counihan, D.S. Ory, D.K. Nomura, and R. Zoncu. 2019. ER-lysosome contacts enable cholesterol sensing by mTORC1 and drive aberrant growth signalling in Niemann-Pick type C. *Nat Cell Biol*. 21:1206-1218.
Lin, X., Q. Sun, L. Zhou, M. He, X. Dong, M. Lai, M. Liu, Y. Su, C. Jia, Z. Han, S. Liu, H. Zheng, Y. Jiang, H. Ling, M. Li, J. Chen, Z. Zou, and X. Bai. 2018. Colonic epithelial mTORC1 promotes ulcerative colitis through COX-2-mediated Th17 responses. *Mucosal Immunol*. 11:1663-1673.
Linke, M., H.T. Pham, K. Katholnig, T. Schnoller, A. Miller, F. Demel, B. Schutz, M. Rosner, B. Kovacic, N. Sukhbaatar, B. Niederreiter, S. Bluml, P. Kuess, V. Sexl, M. Muller, M. Mikula, W. Weckwerth, A. Haschemi, M. Susani, M. Hengstschlager, M.J. Gambello, and T. Weichhart. 2017. Chronic signaling via the metabolic checkpoint kinase mTORC1 induces macrophage granuloma formation and marks sarcoidosis progression. *Nat Immunol*. 18:293-302.
Liu, G.Y., and D.M. Sabatini. 2020. mTOR at the nexus of nutrition, growth, ageing and disease. *Nat Rev Mol Cell Biol*. 21:183-203.

Liu, J.Z., S. van Sommeren, H. Huang, S.C. Ng, R. Alberts, A. Takahashi, S. Ripke, J.C. Lee, L. Jostins, T. Shah, S. Abedian, J.H. Cheon, J. Cho, N.E. Daryani, L. Franke, Y. Fuyuno, A. Hart, R.C. Juyal, G. Juyal, W.H. Kim, A.P. Morris, H. Poustchi, W.G. Newman, V. Midha, T.R. Orchard, H. Vahedi, A. Sood, J.J. Sung, R. Malekzadeh, H.J. Westra, K. Yamazaki, S.K. Yang, C. International Multiple Sclerosis Genetics, I.B.D.G.C. International, J.C. Barrett, A. Franke, B.Z. Alizadeh, M. Parkes, K.T. B, M.J. Daly, M. Kubo, C.A. Anderson, and R.K. Weersma. 2015. Association analyses identify 38 susceptibility loci for inflammatory bowel disease and highlight shared genetic risk across populations. *Nat Genet*. 47:979-986.

Liu, Y., F. Yang, S. Zou, and L. Qu. 2018. Rapamycin: A Bacteria-Derived Immunosuppressant That Has Anti-atherosclerotic Effects and Its Clinical Application. *Front Pharmacol*. 9:1520.

Livak, K.J., and T.D. Schmittgen. 2001. Analysis of relative gene expression data using real-time quantitative PCR and the 2(-Delta Delta C(T)) Method. *Methods*. 25:402-408.

Lloyd-Evans, E., A.J. Morgan, X. He, D.A. Smith, E. Elliot-Smith, D.J. Sillence, G.C. Churchill, E.H. Schuchman, A. Galione, and F.M. Platt. 2008. Niemann-Pick disease type C1 is a sphingosine storage disease that causes deregulation of lysosomal calcium. *Nat Med*. 14:1247-1255.

Lodes, M.J., Y. Cong, C.O. Elson, R. Mohamath, C.J. Landers, S.R. Targan, M. Fort, and R.M. Hershberg. 2004. Bacterial flagellin is a dominant antigen in Crohn disease. *J Clin Invest*. 113:1296-1306.

Long, X., Y. Lin, S. Ortiz-Vega, K. Yonezawa, and J. Avruch. 2005. Rheb binds and regulates the mTOR kinase. *Curr Biol*. 15:702-713.

Lowy, F.D. 1998. Staphylococcus aureus infections. *N Engl J Med*. 339:520-532.

Lubke, T., P. Lobel, and D.E. Sleat. 2009. Proteomics of the lysosome. *Biochim Biophys Acta*. 1793:625-635.

Luo, Q., P. Xiao, X. Li, Z. Deng, C. Qing, R. Su, J. Xu, Y. Guo, Z. Huang, and J. Li. 2018. Overexpression of CD64 on CD14(++)CD16(-) and CD14(++)CD16(+) monocytes of rheumatoid arthritis patients correlates with disease activity. *Exp Ther Med*. 16:2703-2711.

Luzio, J.P., Y. Hackmann, N.M. Dieckmann, and G.M. Griffiths. 2014. The biogenesis of lysosomes and lysosome-related organelles. *Cold Spring Harb Perspect Biol*. 6:a016840.

Ma, J., R. Wang, S.M. Lam, C. Zhang, G. Shui, and W. Li. 2019. Plasma lipidomic profiling in murine mutants of Hermansky-Pudlak syndrome reveals differential changes in pro- and anti-atherosclerotic lipids. *Biosci Rep*. 39.

Mahadeo, R., J. Markowitz, S. Fisher, and F. Daum. 1991. Hermansky-Pudlak syndrome with granulomatous colitis in children. *J Pediatr*. 118:904-906.

Mahavadi, P., M. Korfei, I. Henneke, G. Liebisch, G. Schmitz, B.R. Gochuico, P. Markart, S. Bellusci, W. Seeger, C. Ruppert, and A. Guenther. 2010. Epithelial stress and apoptosis underlie Hermansky-Pudlak syndrome-associated interstitial pneumonia. *Am J Respir Crit Care Med*. 182:207-219.

Manifava, M., M. Smith, S. Rotondo, S. Walker, I. Niewczas, R. Zoncu, J. Clark, and N.T. Ktistakis. 2016. Dynamics of mTORC1 activation in response to amino acids. *Elife*. 5.

Mantegazza, A.R., S.H. Guttentag, J. El-Benna, M. Sasai, A. Iwasaki, H. Shen, T.M. Laufer, and M.S. Marks. 2012. Adaptor protein-3 in dendritic cells facilitates phagosomal toll-like receptor signaling and antigen presentation to CD4(+) T cells. *Immunity*. 36:782-794.

Mantegazza, A.R., M.A. Wynosky-Dolfi, C.N. Casson, A.J. Lefkovith, S. Shin, I.E. Brodsky, and M.S. Marks. 2017. Increased autophagic sequestration in adaptor protein-3 deficient dendritic cells limits inflammasome activity and impairs antibacterial immunity. *PLoS Pathog*. 13:e1006785.

Manzia, T.M., M.I. Bellini, L. Corona, L. Toti, S. Fratoni, A. Cillis, G. Orlando, and G. Tisone. 2011. Successful treatment of systemic de novo sarcoidosis with cyclosporine discontinuation and provision of rapamune after liver transplantation. *Transpl Int*. 24:e69-70.

Marks, M.S., H.F. Heijnen, and G. Raposo. 2013. Lysosome-related organelles: unusual compartments become mainstream. *Curr Opin Cell Biol*. 25:495-505.

Martin, J.C., C. Chang, G. Boschetti, R. Ungaro, M. Giri, J.A. Grout, K. Gettler, L.S. Chuang, S. Nayar, A.J. Greenstein, M. Dubinsky, L. Walker, A. Leader, J.S. Fine, C.E. Whitehurst, M.L. Mbow, S. Kugathasan, L.A. Denson, J.S. Hyams, J.R. Friedman, P.T. Desai, H.M. Ko, I. Laface, G. Akturk, E.E. Schadt, H. Salmon, S. Gnjatic, A.H. Rahman, M. Merad, J.H. Cho, and E. Kenigsberg. 2019. Single-Cell Analysis of Crohn's Disease Lesions Identifies a Pathogenic Cellular Module Associated with Resistance to Anti-TNF Therapy. *Cell*. 178:1493-1508 e1420.

Martinez, F.O., and S. Gordon. 2014. The M1 and M2 paradigm of macrophage activation: time for reassessment. *F1000Prime Rep*. 6:13.

Martinez, J., R.K. Malireddi, Q. Lu, L.D. Cunha, S. Pelletier, S. Gingras, R. Orchard, J.L. Guan, H. Tan, J. Peng, T.D. Kanneganti, H.W. Virgin, and D.R. Green. 2015. Molecular characterization of LC3-associated phagocytosis reveals distinct roles for Rubicon, NOX2 and autophagy proteins. *Nat Cell Biol*. 17:893-906.

Marubashi, S., H. Shimada, M. Fukuda, and N. Ohbayashi. 2016. RUTBC1 Functions as a GTPase-activating Protein for Rab32/38 and Regulates Melanogenic Enzyme Trafficking in Melanocytes. *J Biol Chem*. 291:1427-1440.

Massey, D.C., F. Bredin, and M. Parkes. 2008. Use of sirolimus (rapamycin) to treat refractory Crohn's disease. *Gut*. 57:1294-1296.

Mazzulli, J.R., Y.H. Xu, Y. Sun, A.L. Knight, P.J. McLean, G.A. Caldwell, E. Sidransky, G.A. Grabowski, and D. Krainc. 2011. Gaucher disease glucocerebrosidase and alpha-synuclein form a bidirectional pathogenic loop in synucleinopathies. *Cell*. 146:37-52.

McCauliff, L.A., A. Langan, R. Li, O. Ilnytska, D. Bose, M. Waghalter, K. Lai, P.C. Kahn, and J. Storch. 2019. Intracellular cholesterol trafficking is dependent upon NPC2 interaction with lysobisphosphatidic acid. *Elife*. 8.

McCole, D.F. 2014. IBD candidate genes and intestinal barrier regulation. *Inflamm Bowel Dis*. 20:1829-1849.

McGrath, E., D. Waschbusch, B.M. Baker, and A.R. Khan. 2019. LRRK2 binds to the Rab32 subfamily in a GTP-dependent manner via its armadillo domain. *Small GTPases*:1-14.

Medzhitov, R. 2007. Recognition of microorganisms and activation of the immune response. *Nature*. 449:819-826.

Mellacheruvu, D., Z. Wright, A.L. Couzens, J.P. Lambert, N.A. St-Denis, T. Li, Y.V. Miteva, S. Hauri, M.E. Sardiu, T.Y. Low, V.A. Halim, R.D. Bagshaw, N.C. Hubner, A. Al-Hakim, A. Bouchard, D. Faubert, D. Fermin, W.H. Dunham, M. Goudreault, Z.Y. Lin, B.G. Badillo, T. Pawson, D. Durocher, B. Coulombe, R. Aebersold, G. Superti-Furga, J. Colinge, A.J. Heck, H. Choi, M. Gstaiger, S. Mohammed, I.M. Cristea, K.L. Bennett, M.P. Washburn, B. Raught, R.M. Ewing, A.C. Gingras, and A.I. Nesvizhskii. 2013. The CRAPome: a

contaminant repository for affinity purification-mass spectrometry data. *Nat Methods*. 10:730-736.
Menasche, G., C.H. Ho, O. Sanal, J. Feldmann, I. Tezcan, F. Ersoy, A. Houdusse, A. Fischer, and G. de Saint Basile. 2003. Griscelli syndrome restricted to hypopigmentation results from a melanophilin defect (GS3) or a MYO5A F-exon deletion (GS1). *J Clin Invest*. 112:450-456.
Menasche, G., E. Pastural, J. Feldmann, S. Certain, F. Ersoy, S. Dupuis, N. Wulffraat, D. Bianchi, A. Fischer, F. Le Deist, and G. de Saint Basile. 2000. Mutations in RAB27A cause Griscelli syndrome associated with haemophagocytic syndrome. *Nat Genet*. 25:173-176.
Meng, Y., S. Heybrock, D. Neculai, and P. Saftig. 2020. Cholesterol Handling in Lysosomes and Beyond. *Trends Cell Biol*. 30:452-466.
Menon, S., C.C. Dibble, G. Talbott, G. Hoxhaj, A.J. Valvezan, H. Takahashi, L.C. Cantley, and B.D. Manning. 2014. Spatial control of the TSC complex integrates insulin and nutrient regulation of mTORC1 at the lysosome. *Cell*. 156:771-785.
Metsalu, T., and J. Vilo. 2015. ClustVis: a web tool for visualizing clustering of multivariate data using Principal Component Analysis and heatmap. *Nucleic Acids Res*. 43:W566-570.
Mills, E.L., B. Kelly, A. Logan, A.S.H. Costa, M. Varma, C.E. Bryant, P. Tourlomousis, J.H.M. Dabritz, E. Gottlieb, I. Latorre, S.C. Corr, G. McManus, D. Ryan, H.T. Jacobs, M. Szibor, R.J. Xavier, T. Braun, C. Frezza, M.P. Murphy, and L.A. O'Neill. 2016. Succinate Dehydrogenase Supports Metabolic Repurposing of Mitochondria to Drive Inflammatory Macrophages. *Cell*. 167:457-470 e413.
Moayyedi, P., M.G. Surette, P.T. Kim, J. Libertucci, M. Wolfe, C. Onischi, D. Armstrong, J.K. Marshall, Z. Kassam, W. Reinisch, and C.H. Lee. 2015. Fecal Microbiota Transplantation Induces Remission in Patients With Active Ulcerative Colitis in a Randomized Controlled Trial. *Gastroenterology*. 149:102-109 e106.
Mole, S.E., and S.L. Cotman. 2015. Genetics of the neuronal ceroid lipofuscinoses (Batten disease). *Biochim Biophys Acta*. 1852:2237-2241.
Montano, A.M., N. Lock-Hock, R.D. Steiner, B.H. Graham, M. Szlago, R. Greenstein, M. Pineda, A. Gonzalez-Meneses, M. Coker, D. Bartholomew, M.S. Sands, R. Wang, R. Giugliani, A. Macaya, G. Pastores, A.K. Ketko, F. Ezgu, A. Tanaka, L. Arash, M. Beck, R.E. Falk, K. Bhattacharya, J. Franco, K.K. White, G.A. Mitchell, L. Cimbalistiene, M. Holtz, and W.S. Sly. 2016. Clinical course of sly syndrome (mucopolysaccharidosis type VII). *J Med Genet*. 53:403-418.
Moore, K.J., F.J. Sheedy, and E.A. Fisher. 2013. Macrophages in atherosclerosis: a dynamic balance. *Nat Rev Immunol*. 13:709-721.
Mottet, C., H.H. Uhlig, and F. Powrie. 2003. Cutting edge: cure of colitis by CD4+CD25+ regulatory T cells. *J Immunol*. 170:3939-3943.
Mow, W.S., E.A. Vasiliauskas, Y.C. Lin, P.R. Fleshner, K.A. Papadakis, K.D. Taylor, C.J. Landers, M.T. Abreu-Martin, J.I. Rotter, H. Yang, and S.R. Targan. 2004. Association of antibody responses to microbial antigens and complications of small bowel Crohn's disease. *Gastroenterology*. 126:414-424.
Mukhopadhya, I., R. Hansen, E.M. El-Omar, and G.L. Hold. 2012. IBD-what role do Proteobacteria play? *Nat Rev Gastroenterol Hepatol*. 9:219-230.

Murthy, A., Y. Li, I. Peng, M. Reichelt, A.K. Katakam, R. Noubade, M. Roose-Girma, J. DeVoss, L. Diehl, R.R. Graham, and M. van Lookeren Campagne. 2014. A Crohn's disease variant in Atg16l1 enhances its degradation by caspase 3. *Nature*. 506:456-462.

Mutalib, M., O. Borrelli, S. Blackstock, F. Kiparissi, M. Elawad, N. Shah, and K. Lindley. 2014. The use of sirolimus (rapamycin) in the management of refractory inflammatory bowel disease in children. *J Crohns Colitis*. 8:1730-1734.

Nagle, D.L., M.A. Karim, E.A. Woolf, L. Holmgren, P. Bork, D.J. Misumi, S.H. McGrail, B.J. Dussault, Jr., C.M. Perou, R.E. Boissy, G.M. Duyk, R.A. Spritz, and K.J. Moore. 1996. Identification and mutation analysis of the complete gene for Chediak-Higashi syndrome. *Nat Genet*. 14:307-311.

Nakamura, N., J.R. Lill, Q. Phung, Z. Jiang, C. Bakalarski, A. de Maziere, J. Klumperman, M. Schlatter, L. Delamarre, and I. Mellman. 2014. Endosomes are specialized platforms for bacterial sensing and NOD2 signalling. *Nature*. 509:240-244.

Nayar, S., J.K. Morrison, M. Giri, K. Gettler, L.S. Chuang, L.A. Walker, H.M. Ko, E. Kenigsberg, S. Kugathasan, M. Merad, J. Chu, and J.H. Cho. 2021. A myeloid-stromal niche and gp130 rescue in NOD2-driven Crohn's disease. *Nature*.

Nazarian, R., J.M. Falcon-Perez, and E.C. Dell'Angelica. 2003. Biogenesis of lysosome-related organelles complex 3 (BLOC-3): a complex containing the Hermansky-Pudlak syndrome (HPS) proteins HPS1 and HPS4. *Proc Natl Acad Sci U S A*. 100:8770-8775.

Nazio, F., F. Strappazzon, M. Antonioli, P. Bielli, V. Cianfanelli, M. Bordi, C. Gretzmeier, J. Dengjel, M. Piacentini, G.M. Fimia, and F. Cecconi. 2013. mTOR inhibits autophagy by controlling ULK1 ubiquitylation, self-association and function through AMBRA1 and TRAF6. *Nat Cell Biol*. 15:406-416.

Neurath, M.F. 2017. Current and emerging therapeutic targets for IBD. *Nat Rev Gastroenterol Hepatol*. 14:269-278.

Newton, R., B. Priyadharshini, and L.A. Turka. 2016. Immunometabolism of regulatory T cells. *Nat Immunol*. 17:618-625.

Ng, S.C., H.Y. Shi, N. Hamidi, F.E. Underwood, W. Tang, E.I. Benchimol, R. Panaccione, S. Ghosh, J.C.Y. Wu, F.K.L. Chan, J.J.Y. Sung, and G.G. Kaplan. 2018. Worldwide incidence and prevalence of inflammatory bowel disease in the 21st century: a systematic review of population-based studies. *Lancet*. 390:2769-2778.

Ni, J., G.D. Wu, L. Albenberg, and V.T. Tomov. 2017. Gut microbiota and IBD: causation or correlation? *Nat Rev Gastroenterol Hepatol*. 14:573-584.

Nishida, Y., S. Arakawa, K. Fujitani, H. Yamaguchi, T. Mizuta, T. Kanaseki, M. Komatsu, K. Otsu, Y. Tsujimoto, and S. Shimizu. 2009. Discovery of Atg5/Atg7-independent alternative macroautophagy. *Nature*. 461:654-658.

Norman, J.M., S.A. Handley, M.T. Baldridge, L. Droit, C.Y. Liu, B.C. Keller, A. Kambal, C.L. Monaco, G. Zhao, P. Fleshner, T.S. Stappenbeck, D.P. McGovern, A. Keshavarzian, E.A. Mutlu, J. Sauk, D. Gevers, R.J. Xavier, D. Wang, M. Parkes, and H.W. Virgin. 2015. Disease-specific alterations in the enteric virome in inflammatory bowel disease. *Cell*. 160:447-460.

O'Brien, K., J. Troendle, B.R. Gochuico, T.C. Markello, J. Salas, H. Cardona, J. Yao, I. Bernardini, R. Hess, and W.A. Gahl. 2011. Pirfenidone for the treatment of Hermansky-Pudlak syndrome pulmonary fibrosis. *Mol Genet Metab*. 103:128-134.

O'Brien, K.J., W.J. Introne, O. Akal, T. Akal, A. Barbu, M.P. McGowan, M.A. Merideth, S.L. Seward, Jr., W.A. Gahl, and B.R. Gochuico. 2018. Prolonged treatment with open-

label pirfenidone in Hermansky-Pudlak syndrome pulmonary fibrosis. *Mol Genet Metab*. 125:168-173.
O'Brien, K.J., X. Parisi, N.R. Shelman, M.A. Merideth, W.J. Introne, T. Heller, W.A. Gahl, M.C.V. Malicdan, and B.R. Gochuico. 2021. Inflammatory bowel disease in Hermansky-Pudlak syndrome: a retrospective single-centre cohort study. *J Intern Med*.
O'Neill, L.A., and E.J. Pearce. 2016. Immunometabolism governs dendritic cell and macrophage function. *J Exp Med*. 213:15-23.
Ogura, Y., D.K. Bonen, N. Inohara, D.L. Nicolae, F.F. Chen, R. Ramos, H. Britton, T. Moran, R. Karaliuskas, R.H. Duerr, J.P. Achkar, S.R. Brant, T.M. Bayless, B.S. Kirschner, S.B. Hanauer, G. Nunez, and J.H. Cho. 2001. A frameshift mutation in NOD2 associated with susceptibility to Crohn's disease. *Nature*. 411:603-606.
Oh, J., T. Bailin, K. Fukai, G.H. Feng, L. Ho, J.I. Mao, E. Frenk, N. Tamura, and R.A. Spritz. 1996. Positional cloning of a gene for Hermansky-Pudlak syndrome, a disorder of cytoplasmic organelles. *Nat Genet*. 14:300-306.
Ohishi, Y., R. Kinoshita, S. Marubashi, M. Ishida, and M. Fukuda. 2019. The BLOC-3 subunit HPS4 is required for activation of Rab32/38 GTPases in melanogenesis, but its Rab9 activity is dispensable for melanogenesis. *J Biol Chem*. 294:6912-6922.
Olink. 2019. Olink Target 96 Inflammation.
Omarjee, O., A.L. Mathieu, G. Quiniou, M. Moreews, M. Ainouze, C. Frachette, I. Melki, C. Dumaine, M. Gerfaud-Valentin, A. Duquesne, T. Kallinich, E. Tahir Turanli, C. Malcus, S. Viel, R. Pescarmona, S. Georgin-Lavialle, Y. Jamilloux, J.P. Larbre, G. Sarrabay, F. Magnotti, G.I. Rice, F. Bleicher, J. Reboulet, S. Merabet, T. Henry, Y.J. Crow, M. Faure, T. Walzer, and A. Belot. 2021. LACC1 deficiency links juvenile arthritis with autophagy and metabolism in macrophages. *J Exp Med*. 218.
Ouimet, M., V. Franklin, E. Mak, X. Liao, I. Tabas, and Y.L. Marcel. 2011. Autophagy regulates cholesterol efflux from macrophage foam cells via lysosomal acid lipase. *Cell Metab*. 13:655-667.
Palm, N.W., M.R. de Zoete, T.W. Cullen, N.A. Barry, J. Stefanowski, L. Hao, P.H. Degnan, J. Hu, I. Peter, W. Zhang, E. Ruggiero, J.H. Cho, A.L. Goodman, and R.A. Flavell. 2014. Immunoglobulin A coating identifies colitogenic bacteria in inflammatory bowel disease. *Cell*. 158:1000-1010.
Palmieri, M., R. Pal, H.R. Nelvagal, P. Lotfi, G.R. Stinnett, M.L. Seymour, A. Chaudhury, L. Bajaj, V.V. Bondar, L. Bremner, U. Saleem, D.Y. Tse, D. Sanagasetti, S.M. Wu, J.R. Neilson, F.A. Pereira, R.G. Pautler, G.G. Rodney, J.D. Cooper, and M. Sardiello. 2017. mTORC1-independent TFEB activation via Akt inhibition promotes cellular clearance in neurodegenerative storage diseases. *Nat Commun*. 8:14338.
Parikh, K., A. Antanaviciute, D. Fawkner-Corbett, M. Jagielowicz, A. Aulicino, C. Lagerholm, S. Davis, J. Kinchen, H.H. Chen, N.K. Alham, N. Ashley, E. Johnson, P. Hublitz, L. Bao, J. Lukomska, R.S. Andev, E. Bjorklund, B.M. Kessler, R. Fischer, R. Goldin, H. Koohy, and A. Simmons. 2019. Colonic epithelial cell diversity in health and inflammatory bowel disease. *Nature*. 567:49-55.
Parkes, M., J.C. Barrett, N.J. Prescott, M. Tremelling, C.A. Anderson, S.A. Fisher, R.G. Roberts, E.R. Nimmo, F.R. Cummings, D. Soars, H. Drummond, C.W. Lees, S.A. Khawaja, R. Bagnall, D.A. Burke, C.E. Todhunter, T. Ahmad, C.M. Onnie, W. McArdle, D. Strachan, G. Bethel, C. Bryan, C.M. Lewis, P. Deloukas, A. Forbes, J. Sanderson, D.P. Jewell, J. Satsangi, J.C. Mansfield, C. Wellcome Trust Case Control, L. Cardon,

and C.G. Mathew. 2007. Sequence variants in the autophagy gene IRGM and multiple other replicating loci contribute to Crohn's disease susceptibility. *Nat Genet*. 39:830-832.

Patel, A.S., L. Lin, A. Geyer, J.A. Haspel, C.H. An, J. Cao, I.O. Rosas, and D. Morse. 2012. Autophagy in idiopathic pulmonary fibrosis. *PLoS One*. 7:e41394.

Patel, J., E. McNeill, G. Douglas, A.B. Hale, J. de Bono, R. Lee, A.J. Iqbal, D. Regan-Komito, E. Stylianou, D.R. Greaves, and K.M. Channon. 2015. RGS1 regulates myeloid cell accumulation in atherosclerosis and aortic aneurysm rupture through altered chemokine signalling. *Nat Commun*. 6:6614.

Pei, Y., L. Yue, W. Zhang, Y. Wang, B. Wen, L. Zhong, J. Xiang, J. Li, S. Zhang, H. Wang, H. Mu, Q. Wei, and J. Han. 2015. Improvement in Mouse iPSC Induction by Rab32 Reveals the Importance of Lipid Metabolism during Reprogramming. *Sci Rep*. 5:16539.

Pennamen, P., L. Le, A. Tingaud-Sequeira, M. Fiore, A. Bauters, N. Van Duong Beatrice, V. Coste, J.C. Bordet, C. Plaisant, M. Diallo, V. Michaud, A. Trimouille, D. Lacombe, E. Lasseaux, C. Delevoye, F.M. Picard, B. Delobel, M.S. Marks, and B. Arveiler. 2020. BLOC1S5 pathogenic variants cause a new type of Hermansky-Pudlak syndrome. *Genet Med*. 22:1613-1622.

Perera, R.M., and R. Zoncu. 2016. The Lysosome as a Regulatory Hub. *Annu Rev Cell Dev Biol*. 32:223-253.

Pertea, M., D. Kim, G.M. Pertea, J.T. Leek, and S.L. Salzberg. 2016. Transcript-level expression analysis of RNA-seq experiments with HISAT, StringTie and Ballgown. *Nat Protoc*. 11:1650-1667.

Petersen, H.J., and A.M. Smith. 2013. The role of the innate immune system in granulomatous disorders. *Front Immunol*. 4:120.

Picard, C., H. Bobby Gaspar, W. Al-Herz, A. Bousfiha, J.L. Casanova, T. Chatila, Y.J. Crow, C. Cunningham-Rundles, A. Etzioni, J.L. Franco, S.M. Holland, C. Klein, T. Morio, H.D. Ochs, E. Oksenhendler, J. Puck, M.L.K. Tang, S.G. Tangye, T.R. Torgerson, and K.E. Sullivan. 2018. International Union of Immunological Societies: 2017 Primary Immunodeficiency Diseases Committee Report on Inborn Errors of Immunity. *J Clin Immunol*. 38:96-128.

Pollizzi, K.N., A.T. Waickman, C.H. Patel, I.H. Sun, and J.D. Powell. 2015. Cellular size as a means of tracking mTOR activity and cell fate of CD4+ T cells upon antigen recognition. *PLoS One*. 10:e0121710.

Pryor, P.R., B.M. Mullock, N.A. Bright, M.R. Lindsay, S.R. Gray, S.C. Richardson, A. Stewart, D.E. James, R.C. Piper, and J.P. Luzio. 2004. Combinatorial SNARE complexes with VAMP7 or VAMP8 define different late endocytic fusion events. *EMBO Rep*. 5:590-595.

Pu, J., C. Schindler, R. Jia, M. Jarnik, P. Backlund, and J.S. Bonifacino. 2015. BORC, a multisubunit complex that regulates lysosome positioning. *Dev Cell*. 33:176-188.

Ramakrishnan, L. 2012. Revisiting the role of the granuloma in tuberculosis. *Nat Rev Immunol*. 12:352-366.

Rambold, A.S., S. Cohen, and J. Lippincott-Schwartz. 2015. Fatty acid trafficking in starved cells: regulation by lipid droplet lipolysis, autophagy, and mitochondrial fusion dynamics. *Dev Cell*. 32:678-692.

Raposo, G., M.S. Marks, and D.F. Cutler. 2007. Lysosome-related organelles: driving post-Golgi compartments into specialisation. *Curr Opin Cell Biol*. 19:394-401.

Raudvere, U., L. Kolberg, I. Kuzmin, T. Arak, P. Adler, H. Peterson, and J. Vilo. 2019. g:Profiler: a web server for functional enrichment analysis and conversions of gene lists (2019 update). *Nucleic Acids Res*. 47:W191-W198.

Ray, G.J., E.A. Boydston, E. Shortt, G.A. Wyant, S. Lourido, W.W. Chen, and D.M. Sabatini. 2020. A PEROXO-Tag Enables Rapid Isolation of Peroxisomes from Human Cells. *iScience*. 23:101109.

Reczek, D., M. Schwake, J. Schroder, H. Hughes, J. Blanz, X. Jin, W. Brondyk, S. Van Patten, T. Edmunds, and P. Saftig. 2007. LIMP-2 is a receptor for lysosomal mannose-6-phosphate-independent targeting of beta-glucocerebrosidase. *Cell*. 131:770-783.

Rendeiro, A.F., H. Ravichandran, Y. Bram, V. Chandar, J. Kim, C. Meydan, J. Park, J. Foox, T. Hether, S. Warren, Y. Kim, J. Reeves, S. Salvatore, C.E. Mason, E.C. Swanson, A.C. Borczuk, O. Elemento, and R.E. Schwartz. 2021. The spatial landscape of lung pathology during COVID-19 progression. *Nature*.

Ridker, P.M. 2014. LDL cholesterol: controversies and future therapeutic directions. *Lancet*. 384:607-617.

Riffelmacher, T., A. Clarke, F.C. Richter, A. Stranks, S. Pandey, S. Danielli, P. Hublitz, Z. Yu, E. Johnson, T. Schwerd, J. McCullagh, H. Uhlig, S.E.W. Jacobsen, and A.K. Simon. 2017. Autophagy-Dependent Generation of Free Fatty Acids Is Critical for Normal Neutrophil Differentiation. *Immunity*. 47:466-480 e465.

Rigaud, S., M.C. Fondaneche, N. Lambert, B. Pasquier, V. Mateo, P. Soulas, L. Galicier, F. Le Deist, F. Rieux-Laucat, P. Revy, A. Fischer, G. de Saint Basile, and S. Latour. 2006. XIAP deficiency in humans causes an X-linked lymphoproliferative syndrome. *Nature*. 444:110-114.

Roingeard, P., and R.C. Melo. 2017. Lipid droplet hijacking by intracellular pathogens. *Cell Microbiol*. 19.

Rosenbaum, A.I., M. Rujoi, A.Y. Huang, H. Du, G.A. Grabowski, and F.R. Maxfield. 2009. Chemical screen to reduce sterol accumulation in Niemann-Pick C disease cells identifies novel lysosomal acid lipase inhibitors. *Biochim Biophys Acta*. 1791:1155-1165.

Rossen, N.G., S. Fuentes, M.J. van der Spek, J.G. Tijssen, J.H. Hartman, A. Duflou, M. Lowenberg, G.R. van den Brink, E.M. Mathus-Vliegen, W.M. de Vos, E.G. Zoetendal, G.R. D'Haens, and C.Y. Ponsioen. 2015. Findings From a Randomized Controlled Trial of Fecal Transplantation for Patients With Ulcerative Colitis. *Gastroenterology*. 149:110-118 e114.

Rouhani, F.N., M.L. Brantly, T.C. Markello, A. Helip-Wooley, K. O'Brien, R. Hess, M. Huizing, W.A. Gahl, and B.R. Gochuico. 2009. Alveolar macrophage dysregulation in Hermansky-Pudlak syndrome type 1. *Am J Respir Crit Care Med*. 180:1114-1121.

Roy, D., D.R. Liston, V.J. Idone, A. Di, D.J. Nelson, C. Pujol, J.B. Bliska, S. Chakrabarti, and N.W. Andrews. 2004. A process for controlling intracellular bacterial infections induced by membrane injury. *Science*. 304:1515-1518.

Russell, D.G., P.J. Cardona, M.J. Kim, S. Allain, and F. Altare. 2009. Foamy macrophages and the progression of the human tuberculosis granuloma. *Nat Immunol*. 10:943-948.

Russo, R.C., C.C. Garcia, M.M. Teixeira, and F.A. Amaral. 2014. The CXCL8/IL-8 chemokine family and its receptors in inflammatory diseases. *Expert Rev Clin Immunol*. 10:593-619.

Rutgeerts, P., W.J. Sandborn, B.G. Feagan, W. Reinisch, A. Olson, J. Johanns, S. Travers, D. Rachmilewitz, S.B. Hanauer, G.R. Lichtenstein, W.J. de Villiers, D. Present, B.E. Sands,

and J.F. Colombel. 2005. Infliximab for induction and maintenance therapy for ulcerative colitis. *N Engl J Med*. 353:2462-2476.
Saftig, P., and J. Klumperman. 2009. Lysosome biogenesis and lysosomal membrane proteins: trafficking meets function. *Nat Rev Mol Cell Biol*. 10:623-635.
Sancak, Y., L. Bar-Peled, R. Zoncu, A.L. Markhard, S. Nada, and D.M. Sabatini. 2010. Ragulator-Rag complex targets mTORC1 to the lysosomal surface and is necessary for its activation by amino acids. *Cell*. 141:290-303.
Sands, B.E., F.H. Anderson, C.N. Bernstein, W.Y. Chey, B.G. Feagan, R.N. Fedorak, M.A. Kamm, J.R. Korzenik, B.A. Lashner, J.E. Onken, D. Rachmilewitz, P. Rutgeerts, G. Wild, D.C. Wolf, P.A. Marsters, S.B. Travers, M.A. Blank, and S.J. van Deventer. 2004. Infliximab maintenance therapy for fistulizing Crohn's disease. *N Engl J Med*. 350:876-885.
Sands, B.E., J. Chen, B.G. Feagan, M. Penney, W.A. Rees, S. Danese, P.D.R. Higgins, P. Newbold, R. Faggioni, K. Patra, J. Li, P. Klekotka, C. Morehouse, E. Pulkstenis, J. Drappa, R. van der Merwe, and R.A. Gasser, Jr. 2017. Efficacy and Safety of MEDI2070, an Antibody Against Interleukin 23, in Patients With Moderate to Severe Crohn's Disease: A Phase 2a Study. *Gastroenterology*. 153:77-86 e76.
Sands, B.E., L. Peyrin-Biroulet, E.V. Loftus, Jr., S. Danese, J.F. Colombel, M. Toruner, L. Jonaitis, B. Abhyankar, J. Chen, R. Rogers, R.A. Lirio, J.D. Bornstein, S. Schreiber, and V.S. Group. 2019a. Vedolizumab versus Adalimumab for Moderate-to-Severe Ulcerative Colitis. *N Engl J Med*. 381:1215-1226.
Sands, B.E., W.J. Sandborn, R. Panaccione, C.D. O'Brien, H. Zhang, J. Johanns, O.J. Adedokun, K. Li, L. Peyrin-Biroulet, G. Van Assche, S. Danese, S. Targan, M.T. Abreu, T. Hisamatsu, P. Szapary, C. Marano, and U.S. Group. 2019b. Ustekinumab as Induction and Maintenance Therapy for Ulcerative Colitis. *N Engl J Med*. 381:1201-1214.
Santiago Borrero, P.J., Y. Rodriguez-Perez, J.Y. Renta, N.J. Izquierdo, L. Del Fierro, D. Munoz, N.L. Molina, S. Ramirez, G. Pagan-Mercado, I. Ortiz, E. Rivera-Caragol, R.A. Spritz, and C.L. Cadilla. 2006. Genetic testing for oculocutaneous albinism type 1 and 2 and Hermansky-Pudlak syndrome type 1 and 3 mutations in Puerto Rico. *J Invest Dermatol*. 126:85-90.
Sarkar, S., B. Carroll, Y. Buganim, D. Maetzel, A.H. Ng, J.P. Cassady, M.A. Cohen, S. Chakraborty, H. Wang, E. Spooner, H. Ploegh, J. Gsponer, V.I. Korolchuk, and R. Jaenisch. 2013. Impaired autophagy in the lipid-storage disorder Niemann-Pick type C1 disease. *Cell Rep*. 5:1302-1315.
Saxton, R.A., L. Chantranupong, K.E. Knockenhauer, T.U. Schwartz, and D.M. Sabatini. 2016a. Mechanism of arginine sensing by CASTOR1 upstream of mTORC1. *Nature*. 536:229-233.
Saxton, R.A., K.E. Knockenhauer, R.L. Wolfson, L. Chantranupong, M.E. Pacold, T. Wang, T.U. Schwartz, and D.M. Sabatini. 2016b. Structural basis for leucine sensing by the Sestrin2-mTORC1 pathway. *Science*. 351:53-58.
Schafer, I.B., G.G. Hesketh, N.A. Bright, S.R. Gray, P.R. Pryor, P.R. Evans, J.P. Luzio, and D.J. Owen. 2012. The binding of Varp to VAMP7 traps VAMP7 in a closed, fusogenically inactive conformation. *Nat Struct Mol Biol*. 19:1300-1309.
Schippers, A., M. Muschaweck, T. Clahsen, S. Tautorat, L. Grieb, K. Tenbrock, N. Gassler, and N. Wagner. 2016. beta7-Integrin exacerbates experimental DSS-induced colitis in mice by directing inflammatory monocytes into the colon. *Mucosal Immunol*. 9:527-538.

Schmidt, R.E., B. Grimbacher, and T. Witte. 2017. Autoimmunity and primary immunodeficiency: two sides of the same coin? *Nat Rev Rheumatol*. 14:7-18.

Schulthess, J., S. Pandey, M. Capitani, K.C. Rue-Albrecht, I. Arnold, F. Franchini, A. Chomka, N.E. Ilott, D.G.W. Johnston, E. Pires, J. McCullagh, S.N. Sansom, C.V. Arancibia-Carcamo, H.H. Uhlig, and F. Powrie. 2019. The Short Chain Fatty Acid Butyrate Imprints an Antimicrobial Program in Macrophages. *Immunity*. 50:432-445 e437.

Schwerd, T., S. Pandey, H.T. Yang, K. Bagola, E. Jameson, J. Jung, R.H. Lachmann, N. Shah, S.Y. Patel, C. Booth, H. Runz, G. Duker, R. Bettels, M. Rohrbach, S. Kugathasan, H. Chapel, S. Keshav, A. Elkadri, N. Platt, A.M. Muise, S. Koletzko, R.J. Xavier, T. Marquardt, F. Powrie, J.E. Wraith, M. Gyrd-Hansen, F.M. Platt, and H.H. Uhlig. 2016. Impaired antibacterial autophagy links granulomatous intestinal inflammation in Niemann-Pick disease type C1 and XIAP deficiency with NOD2 variants in Crohn's disease. *Gut*.

Scott, N.A., A. Andrusaite, P. Andersen, M. Lawson, C. Alcon-Giner, C. Leclaire, S. Caim, G. Le Gall, T. Shaw, J.P.R. Connolly, A.J. Roe, H. Wessel, A. Bravo-Blas, C.A. Thomson, V. Kastele, P. Wang, D.A. Peterson, A. Bancroft, X. Li, R. Grencis, A.M. Mowat, L.J. Hall, M.A. Travis, S.W.F. Milling, and E.R. Mann. 2018. Antibiotics induce sustained dysregulation of intestinal T cell immunity by perturbing macrophage homeostasis. *Sci Transl Med*. 10.

Seranova, E., K.J. Connolly, M. Zatyka, T.R. Rosenstock, T. Barrett, R.I. Tuxworth, and S. Sarkar. 2017. Dysregulation of autophagy as a common mechanism in lysosomal storage diseases. *Essays Biochem*. 61:733-749.

Settembre, C., C. Di Malta, V.A. Polito, M. Garcia Arencibia, F. Vetrini, S. Erdin, S.U. Erdin, T. Huynh, D. Medina, P. Colella, M. Sardiello, D.C. Rubinsztein, and A. Ballabio. 2011. TFEB links autophagy to lysosomal biogenesis. *Science*. 332:1429-1433.

Settembre, C., R. Zoncu, D.L. Medina, F. Vetrini, S. Erdin, S. Erdin, T. Huynh, M. Ferron, G. Karsenty, M.C. Vellard, V. Facchinetti, D.M. Sabatini, and A. Ballabio. 2012. A lysosome-to-nucleus signalling mechanism senses and regulates the lysosome via mTOR and TFEB. *EMBO J*. 31:1095-1108.

Setty, S.R., D. Tenza, S.T. Truschel, E. Chou, E.V. Sviderskaya, A.C. Theos, M.L. Lamoreux, S.M. Di Pietro, M. Starcevic, D.C. Bennett, E.C. Dell'Angelica, G. Raposo, and M.S. Marks. 2007. BLOC-1 is required for cargo-specific sorting from vacuolar early endosomes toward lysosome-related organelles. *Mol Biol Cell*. 18:768-780.

Shakya, S., P. Sharma, A.M. Bhatt, R.A. Jani, C. Delevoye, and S.R. Setty. 2018. Rab22A recruits BLOC-1 and BLOC-2 to promote the biogenesis of recycling endosomes. *EMBO Rep*. 19.

Shannon, P., A. Markiel, O. Ozier, N.S. Baliga, J.T. Wang, D. Ramage, N. Amin, B. Schwikowski, and T. Ideker. 2003. Cytoscape: a software environment for integrated models of biomolecular interaction networks. *Genome Res*. 13:2498-2504.

Shouval, D.S., A. Biswas, J.A. Goettel, K. McCann, E. Conaway, N.S. Redhu, I.D. Mascanfroni, Z. Al Adham, S. Lavoie, M. Ibourk, D.D. Nguyen, J.N. Samsom, J.C. Escher, R. Somech, B. Weiss, R. Beier, L.S. Conklin, C.L. Ebens, F.G. Santos, A.R. Ferreira, M. Sherlock, A.K. Bhan, W. Muller, J.R. Mora, F.J. Quintana, C. Klein, A.M. Muise, B.H. Horwitz, and S.B. Snapper. 2014. Interleukin-10 receptor signaling in innate immune cells regulates mucosal immune tolerance and anti-inflammatory macrophage function. *Immunity*. 40:706-719.

Smillie, C.S., M. Biton, J. Ordovas-Montanes, K.M. Sullivan, G. Burgin, D.B. Graham, R.H. Herbst, N. Rogel, M. Slyper, J. Waldman, M. Sud, E. Andrews, G. Velonias, A.L. Haber, K. Jagadeesh, S. Vickovic, J. Yao, C. Stevens, D. Dionne, L.T. Nguyen, A.C. Villani, M. Hofree, E.A. Creasey, H. Huang, O. Rozenblatt-Rosen, J.J. Garber, H. Khalili, A.N. Desch, M.J. Daly, A.N. Ananthakrishnan, A.K. Shalek, R.J. Xavier, and A. Regev. 2019. Intra- and Inter-cellular Rewiring of the Human Colon during Ulcerative Colitis. *Cell*. 178:714-730 e722.

Smith, P.M., M.R. Howitt, N. Panikov, M. Michaud, C.A. Gallini, Y.M. Bohlooly, J.N. Glickman, and W.S. Garrett. 2013. The microbial metabolites, short-chain fatty acids, regulate colonic Treg cell homeostasis. *Science*. 341:569-573.

Snippert, H.J., L.G. van der Flier, T. Sato, J.H. van Es, M. van den Born, C. Kroon-Veenboer, N. Barker, A.M. Klein, J. van Rheenen, B.D. Simons, and H. Clevers. 2010. Intestinal crypt homeostasis results from neutral competition between symmetrically dividing Lgr5 stem cells. *Cell*. 143:134-144.

Sofia, M.A., A. Sakuraba, and D.T. Rubin. 2017. Two Complex Cases of Hermansky-Pudlak Syndrome Highlight a Potential Biologic Explanation for an Associated Crohn's Disease Phenotype. *ACG Case Rep J*. 4:e14.

Sokol, H., V. Leducq, H. Aschard, H.P. Pham, S. Jegou, C. Landman, D. Cohen, G. Liguori, A. Bourrier, I. Nion-Larmurier, J. Cosnes, P. Seksik, P. Langella, D. Skurnik, M.L. Richard, and L. Beaugerie. 2016. Fungal microbiota dysbiosis in IBD. *Gut*.

Sokol, H., B. Pigneur, L. Watterlot, O. Lakhdari, L.G. Bermudez-Humaran, J.J. Gratadoux, S. Blugeon, C. Bridonneau, J.P. Furet, G. Corthier, C. Grangette, N. Vasquez, P. Pochart, G. Trugnan, G. Thomas, H.M. Blottiere, J. Dore, P. Marteau, P. Seksik, and P. Langella. 2008. Faecalibacterium prausnitzii is an anti-inflammatory commensal bacterium identified by gut microbiota analysis of Crohn disease patients. *Proc Natl Acad Sci U S A*. 105:16731-16736.

Solano-Collado, V., R.A. Colamarino, D.A. Calderwood, M. Baldassarre, and S. Spano. 2021. A Small-Scale shRNA Screen in Primary Mouse Macrophages Identifies a Role for the Rab GTPase Rab1b in Controlling Salmonella Typhi Growth. *Front Cell Infect Microbiol*. 11:660689.

Spano, S., and J.E. Galan. 2012. A Rab32-dependent pathway contributes to Salmonella typhi host restriction. *Science*. 338:960-963.

Spano, S., X. Gao, S. Hannemann, M. Lara-Tejero, and J.E. Galan. 2016. A Bacterial Pathogen Targets a Host Rab-Family GTPase Defense Pathway with a GAP. *Cell Host Microbe*. 19:216-226.

Steger, M., F. Tonelli, G. Ito, P. Davies, M. Trost, M. Vetter, S. Wachter, E. Lorentzen, G. Duddy, S. Wilson, M.A. Baptista, B.K. Fiske, M.J. Fell, J.A. Morrow, A.D. Reith, D.R. Alessi, and M. Mann. 2016. Phosphoproteomics reveals that Parkinson's disease kinase LRRK2 regulates a subset of Rab GTPases. *Elife*. 5.

Stinchcombe, J.C., D.C. Barral, E.H. Mules, S. Booth, A.N. Hume, L.M. Machesky, M.C. Seabra, and G.M. Griffiths. 2001. Rab27a is required for regulated secretion in cytotoxic T lymphocytes. *J Cell Biol*. 152:825-834.

Stockinger, B., and S. Omenetti. 2017. The dichotomous nature of T helper 17 cells. *Nat Rev Immunol*. 17:535-544.

Strikoudis, A., A. Cieslak, L. Loffredo, Y.W. Chen, N. Patel, A. Saqi, D.J. Lederer, and H.W. Snoeck. 2019. Modeling of Fibrotic Lung Disease Using 3D Organoids Derived from Human Pluripotent Stem Cells. *Cell Rep*. 27:3709-3723 e3705.

Stuart, T., A. Butler, P. Hoffman, C. Hafemeister, E. Papalexi, W.M. Mauck, 3rd, Y. Hao, M. Stoeckius, P. Smibert, and R. Satija. 2019. Comprehensive Integration of Single-Cell Data. *Cell*. 177:1888-1902 e1821.

Szklarczyk, D., J.H. Morris, H. Cook, M. Kuhn, S. Wyder, M. Simonovic, A. Santos, N.T. Doncheva, A. Roth, P. Bork, L.J. Jensen, and C. von Mering. 2017. The STRING database in 2017: quality-controlled protein-protein association networks, made broadly accessible. *Nucleic Acids Res*. 45:D362-D368.

Thelen, A.M., and R. Zoncu. 2017. Emerging Roles for the Lysosome in Lipid Metabolism. *Trends Cell Biol*. 27:833-850.

Thelen, M., M. Damme, M. Schweizer, C. Hagel, A.M. Wong, J.D. Cooper, T. Braulke, and G. Galliciotti. 2012. Disruption of the autophagy-lysosome pathway is involved in neuropathology of the nclf mouse model of neuronal ceroid lipofuscinosis. *PLoS One*. 7:e35493.

Thilakasiri, P., J. Huynh, A.R. Poh, C.W. Tan, T.L. Nero, K. Tran, A.C. Parslow, S. Afshar-Sterle, D. Baloyan, N.J. Hannan, M. Buchert, A.M. Scott, M.D. Griffin, F. Hollande, M.W. Parker, T.L. Putoczki, M. Ernst, and A.L. Chand. 2019. Repurposing the selective estrogen receptor modulator bazedoxifene to suppress gastrointestinal cancer growth. *EMBO Mol Med*. 11.

Torres, J., S. Mehandru, J.F. Colombel, and L. Peyrin-Biroulet. 2017. Crohn's disease. *Lancet*. 389:1741-1755.

Travassos, L.H., L.A. Carneiro, M. Ramjeet, S. Hussey, Y.G. Kim, J.G. Magalhaes, L. Yuan, F. Soares, E. Chea, L. Le Bourhis, I.G. Boneca, A. Allaoui, N.L. Jones, G. Nunez, S.E. Girardin, and D.J. Philpott. 2010. Nod1 and Nod2 direct autophagy by recruiting ATG16L1 to the plasma membrane at the site of bacterial entry. *Nat Immunol*. 11:55-62.

Tsuma, Y., T. Imamura, E. Ichise, K. Sakamoto, K. Ouchi, S. Osone, H. Ishida, T. Wada, and H. Hosoi. 2015. Successful treatment of idiopathic colitis related to XIAP deficiency with allo-HSCT using reduced-intensity conditioning. *Pediatr Transplant*. 19:E25-28.

Tyanova, S., T. Temu, P. Sinitcyn, A. Carlson, M.Y. Hein, T. Geiger, M. Mann, and J. Cox. 2016. The Perseus computational platform for comprehensive analysis of (prote)omics data. *Nat Methods*. 13:731-740.

Uhlen, M., M.J. Karlsson, W. Zhong, A. Tebani, C. Pou, J. Mikes, T. Lakshmikanth, B. Forsstrom, F. Edfors, J. Odeberg, A. Mardinoglu, C. Zhang, K. von Feilitzen, J. Mulder, E. Sjostedt, A. Hober, P. Oksvold, M. Zwahlen, F. Ponten, C. Lindskog, A. Sivertsson, L. Fagerberg, and P. Brodin. 2019. A genome-wide transcriptomic analysis of protein-coding genes in human blood cells. *Science*. 366.

Uhlig, H.H. 2013. Monogenic diseases associated with intestinal inflammation: implications for the understanding of inflammatory bowel disease. *Gut*. 62:1795-1805.

Uhlig, H.H., and F. Powrie. 2018. Translating Immunology into Therapeutic Concepts for Inflammatory Bowel Disease. *Annu Rev Immunol*. 36:755-781.

Uhlig, H.H., and T. Schwerd. 2016. From Genes to Mechanisms: The Expanding Spectrum of Monogenic Disorders Associated with Inflammatory Bowel Disease. *Inflamm Bowel Dis*. 22:202-212.

Ungaro, R., S. Mehandru, P.B. Allen, L. Peyrin-Biroulet, and J.F. Colombel. 2017. Ulcerative colitis. *Lancet*. 389:1756-1770.

Van den Bossche, J., J. Baardman, N.A. Otto, S. van der Velden, A.E. Neele, S.M. van den Berg, R. Luque-Martin, H.J. Chen, M.C. Boshuizen, M. Ahmed, M.A. Hoeksema, A.F.

de Vos, and M.P. de Winther. 2016. Mitochondrial Dysfunction Prevents Repolarization of Inflammatory Macrophages. *Cell Rep*. 17:684-696.
Van Gassen, S., B. Callebaut, M.J. Van Helden, B.N. Lambrecht, P. Demeester, T. Dhaene, and Y. Saeys. 2015. FlowSOM: Using self-organizing maps for visualization and interpretation of cytometry data. *Cytometry A*. 87:636-645.
Vanier, M.T. 2010. Niemann-Pick disease type C. *Orphanet J Rare Dis*. 5:16.
Vanlandingham, P.A., and B.P. Ceresa. 2009. Rab7 regulates late endocytic trafficking downstream of multivesicular body biogenesis and cargo sequestration. *J Biol Chem*. 284:12110-12124.
Veenbergen, S., P. Li, H.C. Raatgeep, D.J. Lindenbergh-Kortleve, Y. Simons-Oosterhuis, A. Farrel, L.M.M. Costes, M.E. Joosse, L.A. van Berkel, L.F. de Ruiter, M.A. van Leeuwen, D. Winter, S.M. Holland, A.F. Freeman, Y. Wakabayashi, J. Zhu, L. de Ridder, G.J. Driessen, J.C. Escher, W.J. Leonard, and J.N. Samsom. 2019. IL-10 signaling in dendritic cells controls IL-1beta-mediated IFNgamma secretion by human CD4(+) T cells: relevance to inflammatory bowel disease. *Mucosal Immunol*. 12:1201-1211.
Verstockt, B., K.G. Smith, and J.C. Lee. 2018. Genome-wide association studies in Crohn's disease: Past, present and future. *Clin Transl Immunology*. 7:e1001.
Vicary, G.W., Y. Vergne, A. Santiago-Cornier, L.R. Young, and J. Roman. 2016. Pulmonary Fibrosis in Hermansky-Pudlak Syndrome. *Ann Am Thorac Soc*. 13:1839-1846.
Villani, A.C., M. Lemire, G. Fortin, E. Louis, M.S. Silverberg, C. Collette, N. Baba, C. Libioulle, J. Belaiche, A. Bitton, D. Gaudet, A. Cohen, D. Langelier, P.R. Fortin, J.E. Wither, M. Sarfati, P. Rutgeerts, J.D. Rioux, S. Vermeire, T.J. Hudson, and D. Franchimont. 2009. Common variants in the NLRP3 region contribute to Crohn's disease susceptibility. *Nat Genet*. 41:71-76.
Wang, C., Z. Liu, and X. Huang. 2012. Rab32 is important for autophagy and lipid storage in Drosophila. *PLoS One*. 7:e32086.
Wang, S., Z.Y. Tsun, R.L. Wolfson, K. Shen, G.A. Wyant, M.E. Plovanich, E.D. Yuan, T.D. Jones, L. Chantranupong, W. Comb, T. Wang, L. Bar-Peled, R. Zoncu, C. Straub, C. Kim, J. Park, B.L. Sabatini, and D.M. Sabatini. 2015. Metabolism. Lysosomal amino acid transporter SLC38A9 signals arginine sufficiency to mTORC1. *Science*. 347:188-194.
Wang, Y., A.W. Mohsen, S.J. Mihalik, E.S. Goetzman, and J. Vockley. 2010. Evidence for physical association of mitochondrial fatty acid oxidation and oxidative phosphorylation complexes. *J Biol Chem*. 285:29834-29841.
Waschbusch, D., N. Hubel, E. Ossendorf, E. Lobbestael, V. Baekelandt, A.J. Lindsay, M.W. McCaffrey, A.R. Khan, and A. Barnekow. 2019. Rab32 interacts with SNX6 and affects retromer-dependent Golgi trafficking. *PLoS One*. 14:e0208889.
Waschbusch, D., H. Michels, S. Strassheim, E. Ossendorf, D. Kessler, C.J. Gloeckner, and A. Barnekow. 2014. LRRK2 transport is regulated by its novel interacting partner Rab32. *PLoS One*. 9:e111632.
Wenham, M., S. Grieve, M. Cummins, M.L. Jones, S. Booth, R. Kilner, P.J. Ancliff, G.M. Griffiths, and A.D. Mumford. 2010. Two patients with Hermansky Pudlak syndrome type 2 and novel mutations in AP3B1. *Haematologica*. 95:333-337.
West, N.R., A.N. Hegazy, B.M.J. Owens, S.J. Bullers, B. Linggi, S. Buonocore, M. Coccia, D. Gortz, S. This, K. Stockenhuber, J. Pott, M. Friedrich, G. Ryzhakov, F. Baribaud, C. Brodmerkel, C. Cieluch, N. Rahman, G. Muller-Newen, R.J. Owens, A.A. Kuhl, K.J. Maloy, S.E. Plevy, I.B.D.C.I. Oxford, S. Keshav, S.P.L. Travis, and F. Powrie. 2017. Oncostatin M drives intestinal inflammation and predicts response to tumor necrosis

factor-neutralizing therapy in patients with inflammatory bowel disease. *Nat Med*. 23:579-589.
Westphal, A., W. Cheng, J. Yu, G. Grassl, M. Krautkramer, O. Holst, N. Foger, and K.H. Lee. 2017. Lysosomal trafficking regulator Lyst links membrane trafficking to toll-like receptor-mediated inflammatory responses. *J Exp Med*. 214:227-244.
Wolfson, R.L., L. Chantranupong, R.A. Saxton, K. Shen, S.M. Scaria, J.R. Cantor, and D.M. Sabatini. 2016. Sestrin2 is a leucine sensor for the mTORC1 pathway. *Science*. 351:43-48.
Wong, Y.C., D. Ysselstein, and D. Krainc. 2018. Mitochondria-lysosome contacts regulate mitochondrial fission via RAB7 GTP hydrolysis. *Nature*. 554:382-386.
Xie, X., Q. Ni, D. Zhou, and Y. Wan. 2018. Rab32-related antimicrobial pathway is involved in the progression of dextran sodium sulfate-induced colitis. *FEBS Open Bio*. 8:1658-1668.
Yang, D., X. Chen, J. Wang, Q. Lou, Y. Lou, L. Li, H. Wang, J. Chen, M. Wu, X. Song, and Y. Qian. 2019. Dysregulated Lung Commensal Bacteria Drive Interleukin-17B Production to Promote Pulmonary Fibrosis through Their Outer Membrane Vesicles. *Immunity*. 50:692-706 e697.
Yogalingam, G., E.J. Bonten, D. van de Vlekkert, H. Hu, S. Moshiach, S.A. Connell, and A. d'Azzo. 2008. Neuraminidase 1 is a negative regulator of lysosomal exocytosis. *Dev Cell*. 15:74-86.
Yokoyama, T., and B.R. Gochuico. 2021. Hermansky-Pudlak syndrome pulmonary fibrosis: a rare inherited interstitial lung disease. *Eur Respir Rev*. 30.
Yoshiyama, S., C. Miki, T. Araki, Y. Morimoto, Y. Okita, and M. Kusunoki. 2009. Complicated granulomatous colitis in a Japanese patient with Hermansky-Pudlak syndrome, successfully treated with infliximab. *Clin J Gastroenterol*. 2:51-54.
Young, L.R., M.T. Borchers, H.L. Allen, R.S. Gibbons, and F.X. McCormack. 2006. Lung-restricted macrophage activation in the pearl mouse model of Hermansky-Pudlak syndrome. *J Immunol*. 176:4361-4368.
Young, L.R., P.M. Gulleman, C.W. Short, H. Tanjore, T. Sherrill, A. Qi, A.P. McBride, R. Zaynagetdinov, J.T. Benjamin, W.E. Lawson, S.V. Novitskiy, and T.S. Blackwell. 2016. Epithelial-macrophage interactions determine pulmonary fibrosis susceptibility in Hermansky-Pudlak syndrome. *JCI Insight*. 1:e88947.
Young, M.D., M.J. Wakefield, G.K. Smyth, and A. Oshlack. 2010. Gene ontology analysis for RNA-seq: accounting for selection bias. *Genome Biol*. 11:R14.
Yu, H.H., Y.H. Yang, and B.L. Chiang. 2020a. Chronic Granulomatous Disease: a Comprehensive Review. *Clin Rev Allergy Immunol*.
Yu, J., X. He, A. Wei, T. Liu, Q. Zhang, Y. Pan, Z. Hao, L. Yang, Y. Yuan, Z. Zhang, C. Zhang, C. Hao, Z. Liu, and W. Li. 2020b. HPS1 Regulates the Maturation of Large Dense Core Vesicles and Lysozyme Secretion in Paneth Cells. *Front Immunol*. 11:560110.
Zhang, F., H. Liu, S. Chen, H. Low, L. Sun, Y. Cui, T. Chu, Y. Li, X. Fu, Y. Yu, G. Yu, B. Shi, H. Tian, D. Liu, X. Yu, J. Li, N. Lu, F. Bao, C. Yuan, J. Liu, H. Liu, L. Zhang, Y. Sun, M. Chen, Q. Yang, H. Yang, R. Yang, L. Zhang, Q. Wang, H. Liu, F. Zuo, H. Zhang, C.C. Khor, M.L. Hibberd, S. Yang, J. Liu, and X. Zhang. 2011. Identification of two new loci at IL23R and RAB32 that influence susceptibility to leprosy. *Nat Genet*. 43:1247-1251.
Zhao, J., S. Benlekbir, and J.L. Rubinstein. 2015. Electron cryomicroscopy observation of rotational states in a eukaryotic V-ATPase. *Nature*. 521:241-245.

Zhong, M., B. Cui, J. Xiang, X. Wu, Q. Wen, Q. Li, and F. Zhang. 2020. Rapamycin is Effective for Upper but not for Lower Gastrointestinal Crohn's Disease-Related Stricture: A Pilot Study. *Front Pharmacol*. 11:617535.

Zhou, X., R.A. Franklin, M. Adler, J.B. Jacox, W. Bailis, J.A. Shyer, R.A. Flavell, A. Mayo, U. Alon, and R. Medzhitov. 2018a. Circuit Design Features of a Stable Two-Cell System. *Cell*. 172:744-757 e717.

Zhou, Y., C.H. He, E.L. Herzog, X. Peng, C.M. Lee, T.H. Nguyen, M. Gulati, B.R. Gochuico, W.A. Gahl, M.L. Slade, C.G. Lee, and J.A. Elias. 2015. Chitinase 3-like-1 and its receptors in Hermansky-Pudlak syndrome-associated lung disease. *J Clin Invest*. 125:3178-3192.

Zhou, Y., C.H. He, D.S. Yang, T. Nguyen, Y. Cao, S. Kamle, C.M. Lee, B.R. Gochuico, W.A. Gahl, B.S. Shea, C.G. Lee, and J.A. Elias. 2018b. Galectin-3 Interacts with the CHI3L1 Axis and Contributes to Hermansky-Pudlak Syndrome Lung Disease. *J Immunol*. 200:2140-2153.

Zhou, Y.D., X.Q. Cao, Z.H. Liu, Y.J. Cao, C.F. Liu, Y.L. Zhang, and Y. Xie. 2016. Rapamycin Inhibits Oxidized Low Density Lipoprotein Uptake in Human Umbilical Vein Endothelial Cells via mTOR/NF-kappaB/LOX-1 Pathway. *PLoS One*. 11:e0146777.

Zoncu, R., L. Bar-Peled, A. Efeyan, S. Wang, Y. Sancak, and D.M. Sabatini. 2011. mTORC1 senses lysosomal amino acids through an inside-out mechanism that requires the vacuolar H(+)-ATPase. *Science*. 334:678-683.